UAB
Universitat Autònoma de Barcelona

Harnessing public neoantigens to develop TCR gene-engineered T-cell therapies

Anna Yuste Estevanez

ADVERTIMENT. L'accés als continguts d'aquesta tesi queda condicionat a l'acceptació de les condicions d'ús establertes per la següent llicència Creative Commons: https://creativecommons.org/licenses/?lang=ca

ADVERTENCIA. El acceso a los contenidos de esta tesis queda condicionado a la aceptación de las condiciones de uso establecidas por la siguiente licencia Creative Commons: https://creativecommons.org/licenses/?lang=es

WARNING. The access to the contents of this doctoral thesis it is limited to the acceptance of the use conditions set by the following Creative Commons license: https://creativecommons.org/licenses/?lang=en

Universitat Autònoma de Barcelona
Departament de Biologia Cel·lular, Fisiologia i Immunologia
Programa de doctorat en Immunologia avançada

Harnessing public neoantigens to develop TCR gene-engineered T-cell therapies

Anna Yuste Estevanez
Doctoral Thesis
Barcelona, 2024

Thesis director: Alena Gros i Josep Tabernero

Abbreviations

AA	Amino acid
ACT	Adoptive T-cell Transfer
APCs	Antigen-Presenting Cells
APM	Antigen Processing Machinery
B2M	β-2-Microglobulin
BLCA	Bladder urothelial carcinoma
BRCA	Breast invasive adenocarcinoma
CAR	Chimeric Antigen Receptor
CAR-T	CAR-Transduced T-cell
CCLE	Cancer Cell Line Encyclopedia
CD	Cluster of Differentiation
CDRs	Complementarity Determining Regions
CEA	Carcinoembryonic Antigen
CEF PP	Peptide pool of CMV, EBV, and Flu HLA-I epitopes
CESC	Cervical Squamous cell Carcinoma and Endocervical Adenocarcinoma
cfDNA	Cell-free DNA
CMV	Cytomegalovirus
COAD	Colon adenocarcinoma
CRS	Cytokine Release Syndrome
CTLA-4	Cytotoxic T-Lymphocyte Antigen 4
CTLs	Cytotoxic T Lymphocytes
D	Diversity gene segment
DCs	Dendritic Cells
EBV	Epstein-Barr Virus
EL	Eluted Ligands
ELISPOT	Enzyme-Linked ImmunoSpot Assay
ER	Endoplasmic Reticulum
ERAP	ER-Associated Aminopeptidases
FACS	Fluorescence-activated cell sorting
FDA	Food And Drug Administration
FDR	False Discovery Rate
GM-CSF	Granulocyte-macrophage colony-stimulating factor
gp100	Glycoprotein 100
HD	Healthy donor
HLA	Human Leukocyte Antigen

HPLC	High-Performance Liquid Chromatography peptides
HPV	Human Papillomavirus
HSTMG	Hotspot Tandem minigene
ICI	Immune checkpoint Inhibitor
IFN-γ	Interferon Gamma
IL-2	Interleukin-2
IVS	In Vitro Sensitization
IVT	In Vitro Transcribed
J	Joining gene segment
KO	Knockout
LC-MS/MS	Liquid Chromatography Coupled Tandem Mass Spectrometry
MAGE-A3	Melanoma-associated antigen 3
MART-1	Melanoma antigen recognized by T cells
ME	Minimal Epitope
MEP	Minimal Epitope Pool
MFI	Mean Fluorescence Intensity
MHC	Major Histocompatibility Complex
MS	Mass-spectrometry
NB	Non Binders
NGS	Next-Generation Sequencing
non-C	Non-canonical
NSMs	Non-synonymous Mutations
NY-ESO-1	New York esophageal squamous cell carcinoma 1
OVs	Oncolytic Virus
PAP	Prostatic Acid Phosphatase
PBLs	Peripheral Blood Lymphocytes
PBMCs	Peripheral Blood Mononuclear Cells Lymphocytes
PD-1	Programmed Death 1
PD-L1	PD-1 Ligand
pHLA-I	Peptide-HLA-I Complex
PLC	Peptide Loading Complex
PMEL	Premelanosome protein
PRM-MS	Parallel Reaction Monitoring mass spectrometry
PSA	Prostatic Acid Phosphatase
REP	Rapid Expansion Protocol
RNP	Ribonucleoprotein
SB	Strong Binders
scTCR-seq	Single-cell T-cell receptor sequencing

sgRNA	Single Guide RNA
SNVs	Single Nucleotide Variants
TAA	Tumor-associated antigen
TAP	Antigen Processing Proteins
T-biAbs	T-cell engaging bi-specific antibodies
TCGA	Tumor Cancer Genome Atlas
TCL	Tumor Cell Lines
TCR	T-Cell Receptor
TCR-T	TCR-engineered T cells
TCRtd	TCR transduced PBLs
Tg	Transgenic
TILs	Tumor-Infiltrating Lymphocytes
TPM	Transcripts Per Million
TSA	Tumor-specific antigen
TYR	Tyrosinase
UCEC	Uterine Corpus Endometrial Carcinoma
V	Variable gene segment
VAF	Variant allele frequency
WB	Weak Binders
WES	Whole-Exome Sequencing
WT1	Wilms' Tumor Protein
ZSG	ZsGreen protein

Index

Abbreviations **2**

Summary **10**

Introduction **13**

1. The immune system and Cancer 14
2. Antigen recognition by T cells 16
   - 2.1. HLA-I molecules and presentation pathway 17
     - 2.1.1. Structure of classical HLA-I molecules 18
     - 2.1.2. Conventional HLA-I antigen presentation pathway 19
   - 2.2. Tumor antigens 22
     - 2.2.1. Antigens of low tumor-specificity 23
     - 2.2.2. Antigens of high tumor-specificity 24
       - 2.2.2.1. Neoantigens 25
   - 2.3. Cancer Immunity cycle 27
3. Cancer immunotherapies 29
   - 3.1. IL-2 30
   - 3.2. Immune checkpoint inhibitors 30
   - 3.3. Bi-specific antibodies 30
   - 3.4. Oncolytic viruses 31
   - 3.5. Vaccines 31
   - 3.6. Adoptive T-cell transfer 32
4. Types of adoptive T-cell transfer 33
   - 4.1. ACT of tumor-infiltrating lymphocytes 33
   - 4.2. ACT of CAR-engineered T cells 35
   - 4.3. ACT of TCR-engineered T cells 36
5. Discovery of therapeutic TCR candidates for TCR-T ACT 39
   - 5.1. Defining the epitope-HLA pair 39
     - 5.1.1. *In silico* HLA-I binding predictors 40

5.1.2. Mass spectrometry-based immunopeptidomics 41
5.2. Isolation of epitope-specific T cells 43
5.2.1. Sources of reactive T cells 43
5.2.1.1. Mouse models 43
5.2.1.2. Human TILs or PBLs 44
5.2.2. Enrichment strategies for antigen-specific T-cell populations 45
5.2.2.1. Biomarker-based isolation 45
5.2.2.2. pHLA-I multimers 46
5.2.2.3. *In vitro* sensitization (IVS) 47
5.3. Determination of TCR sequence 48
5.4. Preclinical characterization of candidate TCRs 51
6. Reactive T cells and isolated TCRs targeting public neoantigens 52
Hypothesis and Objectives 56
Materials and methods 59
Patient samples 60
Establishment of patient-derived tumor cell line (TCL) 60
PBMC isolation 60
Whole exome and RNA sequencing 60
Tandem Minigenes construction, cloning, in vitro transcription of RNA and electroporation 61
Generation of autologous B cells 63
CRISPR/Cas9 Knockout 64
Flow cytometric analysis and fluorescence-activated cell sorting 64
Protein analysis 65
Purification of HLA-I peptides 67
LC-MS/MS acquisition 67
Mass spectrometry data analysis of HLA-I peptides 68
HLA-I typing and prediction of binding to selected HLA alleles 69
Peptide synthesis and peptide pulsing 69

Validation of HLA-I peptides with isotope-labeled peptides 70

In vitro sensitization (IVS) 71

Co-culture assays: IFN-γ enzyme-linked immunospot (ELISPOT) and detection of activation marker 4-1BB using flow cytometry 73

Dextramer generation and staining 73

Enrichment of antigen-specific T cells 74

Rapid expansion protocol (REP) 74

HLA-I expression and restriction 74

TCR sequencing and PBL transduction 75

Correlation and statistical analyses 76

Data analysis and visualization 76

Results 78

1. Design of an immunopeptidomics-based strategy to identify public neoantigens 79

1.1. Selection of recurrent mutations in cancer driver genes for the construction of Hotspot Tandem Minigenes (HSTMG) 79

1.2. Prioritization of the most frequent HLA-I alleles in the European Caucasian population 81

1.3. Evaluation of the different cell types for the detection of HSTMG-derived peptides by immunopeptidomics 82

1.3.1. Use of B cells as antigen-presenting cells to identify neoepitopes presented on HLA-I 82

1.3.1.1. MS-based immunopeptidomics of patient-derived B cells displayed poor resolution for the identification of candidate neoantigens 87

1.3.2. Exploiting HLA-I ligandome of HLA-I monoallelic cells for the identification of candidate neoantigens 90

1.3.2.1. Generation of an epithelial tumor cell line negative for B2M expression through CRISPR/Cas9 94

1.3.2.2. Generation of transient HLA-I monoallelic tumor cells expressing HSTMG 95

1.3.2.3. Optimizing the conditions for HLA-I ligandome screening by immunopeptidomics 97

1.4. Identification of HSTMG-derived peptides presented on HLA-I monoallelic tumor cells 101

1.4.1. Identification of public neoantigens presented by highly prevalent HLA-I alleles 103

1.5. Applying targeted mass spectrometry for validation of selected mutant peptide-HLA combinations 105

1.5.1. Removing false identifications from shotgun mass spectrometry screenings 106

1.5.2. Generation of a curated list of validated neoantigen-HLA pairs 107

1.5.3. Exploiting increased sensitivity of targeted mass spectrometry for the identification of additional peptide-HLA pairs 109

1.5.3.1. Prospective identification of HLA-I ligands by targeted mass spectrometry 110

1.5.4. Candidate public neoantigens identified through shotgun and targeted mass spectrometry screenings 111

1.6. Comparison of empirically identified HLA-I mutant peptides to the performance of an HLA-I binding prediction algorithm 112

1.7. Assessment of hotspot-derived neoantigen processing and presentation in patient-derived tumor cell lines 114

2. Isolation and characterization of TCRs reactive against hotspot mutations for their potential use to develop off-the-shelf T-cell therapies 118

2.1. Detection of T-cell responses against hotspot-derived neoantigens in the peripheral blood of a breast cancer patient using in vitro sensitization 118

2.1.1. IVS of PBL with $PIK3CA_{p.E545K}$ minimal epitope elicited an HLA-A*11:01 restricted T-cell response 122

2.1.2. Sensitization with MEP-1 induced de novo T-cell responses against $TP53_{p.R248Q}$ neoepitope restricted to HLA-A*11:01 123

2.1.3. Sensitization with MEP-2 induced de novo T-cell responses against $PIK3CA_{p.R88Q}$ restricted to HLA-C*04:01 127

2.2. Isolation of neoantigen-specific TCRs from enriched $CD8^+$ reactive T cells by TCR sequencing 129

2.3. The identified reactive TCRs recognize tumor cells in vitro and display variable functional avidity for their cognate antigens 133

2.3.1. Exploring the co-occurrence of hotspot mutation and HLA-I restriction elements, leading to the presentation of public neoantigens targeted by reactive TCRs in cancer patients 137

Discussion..... 142

Immunopeptidomics of HLA-I monoallelic cells combined with IVS led to the identification of TCRs targeting public neoantigens..... 143

B cells were not the optimal cell source for the identification of hotspot-derived neoepitope-HLA pairs..... 145

Factors influencing additional detection of neoantigens in transient HLA-I monoallelic cells..... 147

The confirmation of two candidate public neoantigens' presentation in patient-derived TCL was inconclusive..... 151

Exploring Hurdles: residual HLA-I expression in B2M KO cells and limitations in peptide capture via untargeted MS 152

IVS of unfractionated PBLs from a cancer patient could have expanded naïve and memory T-cell responses..... 154

Sensitization of PBLs with MEPs hamper detection of the entire neoantigen-specific T-cell repertoire 156

HLA-I dextramer staining and measurement of 4-1BB upregulation were not equivalent readouts for the identification of reactive T cells 157

Influence of donor TCR repertoire sampling on the detection of T-cell responses via IVS 159

Sensitization with minimal epitopes resulted in the expansion of single dominant TCRs 160

Preliminary insights into the anti-tumor potential of the discovered candidate therapeutic TCRs 161

HLA-I and hotspot mutation co-occurrence in cancer: implications for TCR-engineered T-cell therapies..... 163

Development of TCR-engineered T-cell products using the discovered off-the-shelf therapeutic TCR candidates..... 164

Conclusions 167

References..... 169

Appendix..... 197

Summary

Tumors accumulate genetic alterations, some of which may generate "non-self" epitopes recognized by T cells, known as neoantigens. These antigens can arise from private mutations unique to each individual or from shared mutations in hotspot regions of driver genes that occur in multiple cancer patients. When prevalent HLA alleles present epitopes from shared neoantigens, they become public neoantigens. These are ideal targets for cancer immunotherapies for multiple reasons. First, they are exquisitely tumor-specific, vital for sustaining the malignant phenotype, and have a higher likelihood of being clonal or expressed by most cancer cells. Second, due to their high conservation, they offer the possibility of developing off-the-shelf TCR T-cell-based therapies, broadening the applicability of adoptive T-cell therapy to multiple patients. However, despite the identification of hundreds of cancer driver mutations, only a small fraction of immunogenic public neoantigens and reactive TCRs have been identified.

In this thesis, we used a mass spectrometry-based (MS-based) HLA-I immunopeptidomics approach to discover hotspot-derived mutant peptides presented on highly prevalent HLA-I alleles. In addition, we aimed to detect and characterize T-cell receptors (TCRs) targeting these peptides, which could be used to develop novel off-the-shelf TCR-based T-cell therapies targeting public neoantigens.

We developed an HLA-I monoallelic cell platform to identify public neoantigens arising from 35 recurrent mutations across 13 cancer driver genes and 12 highly prevalent HLA-I alleles in the Caucasian population. We first constructed four hotspot tandem minigene (HSTMG) constructs encoding these mutations and B2M_HLA chimeras encompassing the prioritized alleles. Next, we generated a B2M null tumor cell line using CRISPR/Cas9, lacking cell surface HLA-I expression. B2M KO tumor cells were then co-electroporated with *in vitro* transcribed RNA encoding one B2M_HLA chimera and one of the four HSTMGs to generate HLA-I monoallelic cells expressing recurrent mutations. Last, shotgun MS-based immunopeptidomics was performed on cells expressing a total of 37 HSTMG-B2M_HLA combinations to identify naturally processed and presented HLA-I peptides, which were then validated using parallel reaction monitoring mass spectrometry. Using this strategy, we detected 49 mutant peptide-HLA pairs derived from 23 shared cancer neoantigens presented across 10 HLA-I alleles.

Moreover, our method, based on transient HLA-I monoallelic cells, captured 19 previously reported epitopes and, more importantly, 33 novel candidate public neoantigen-HLA pairs.

To determine whether some of the putative public neoantigens could be recognized by T cells, we carried out *in vitro* sensitization experiments using peripheral blood lymphocytes from a breast cancer patient. This strategy raised two HLA-A*11:01-restricted T-cell reactivities specific for $PIK3CA_{p.E545K}$ and $TP53_{p.R248Q}$, as well as an HLA-C*04:01-restricted response targeting $PIK3CA_{p.R88Q}$. By sequencing the TCRs of these reactive T cells, we identified three neoantigen-specific TCRs, each displaying specific recognition of the neoantigen compared to the wild-type counterpart. Interestingly, the three reactive TCRs recognized their target when processed and presented by tumor cells *in vitro,* underscoring their potential to develop off-the-shelf T-cell therapies.

In summary, we identified a diverse array of candidate public neoantigens through comprehensive MS-based immunopeptidomics screening of HLA-I monoallelic cells. These findings expand the number of shared actionable targets for cancer immunotherapy. Furthermore, the discovered TCRs reactive to public neoantigens pave the way for T-cell-based therapies applicable to multiple cancer patients.

Introduction

1. The immune system and Cancer

Tumorigenesis is a complex, multistep process that can occur in most normal tissues and is characterized by the gradual accumulation of genetic and epigenetic alterations. These changes promote the transformation of normal cells to malignant cells over time.

In the human body, with over 10^{14} cells, billions of cells mutate daily, which can disrupt their normal behavior. If a mutation gives a particular cell a selective advantage, it may replicate faster and survive better than its counterparts, eventually becoming the founder of a malignant clone (1). While that initial cell is presumed to mark cancer initiation, its progeny must acquire many additional mutations and epigenetic changes over time to fully develop a tumor.

In 2000, the hallmarks of cancer were introduced as a collection of functional capabilities acquired by normal human cells during malignant transformation that are thought to be critical for the initiation of malignant tumors (2). Since then, additional features have been uncovered by advances in understanding cancer pathogenesis. In 2011, Hanahan and Weinberg added genome instability and tumor-promoting inflammation along with cellular metabolic deregulation and immune evasion as novel features, which are now recognized as central cancer hallmarks (3,4) (Figure 1).

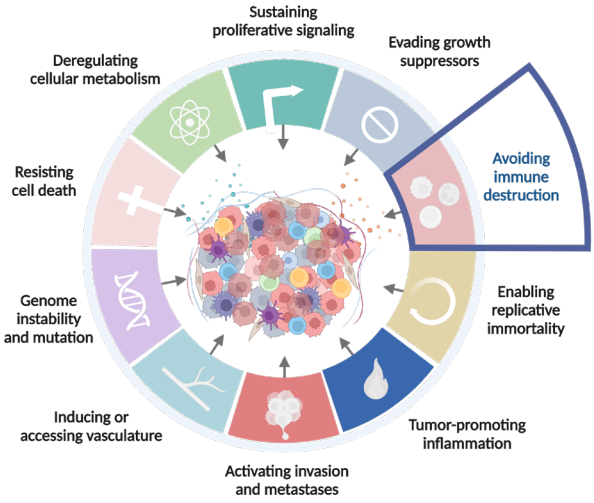


Figure 1. Current validated Hallmarks of Cancer. The eight core hallmarks of cancer and two enabling factors. Image adapted from Hannahan, 2022. Image created with BioRender.com.

The notion that the immune system has a pivotal role in preventing neoplastic cell progression to tumors was proposed over a century ago (5). After decades of debate, there has been widespread agreement that immune cells interact with cancer cells and influence tumor development through a process known as cancer immunosurveillance (6,7). This concept suggests that the immune system continuously monitors cells and tissues and plays a critical role in detecting and eliminating most nascent tumors.

Cancer immunosurveillance and its dependence on lymphocytes was evidenced by experiments in mice with selectively inactivated recombinase activating gene-2 (8). Those animals, lacking lymphocytes, developed chemically induced tumors faster and more frequently than genetically matched wild-type control. This is because of the absence of lymphocytes that play a protective role against tumor development.

In addition to mice studies, epidemiologic studies of immunosuppressed transplant recipients and immunocompromised human individuals revealed significantly increased risks of cancer, many of which were of viral origin (9–13). This provided well-founded evidence for the existence of human cancer immunosurveillance and its central role in controlling tumor growth. However, the question of why tumorigenesis could occur in individuals with intact immunosurveillance remained unanswered. Several studies showed that tumors arising in mice with specific immunodeficiencies were more immunogenic than those in immunocompetent mice (8,14–17). These findings led to the concept of cancer immunoediting, suggesting that the immune system not only defends against cancer but also shapes emerging tumors (9,18).

Cancer immunoediting is a conceptual framework to understand the dynamic process through which the immune system influences and shapes cancer development (9,18) (Figure 2). It is divided into three phases: elimination, equilibrium, and escape. In the elimination phase, the immune system successfully eradicates the nascent tumor, completing the editing process without progression to subsequent phases. If the immune system fails to eliminate all cancer cells, surviving cells and the immune system enter the equilibrium phase, in which the immune system can suppress but not eliminate tumors. Eventually, surviving tumor cells that evade immune detection enter the escape phase. In this phase, tumors accumulate genetic and epigenetic

changes that allow them to grow uncontrollably, leading to the formation of clinically detectable tumors (9,10). The concept of cancer immunoediting has gained widespread acceptance and it is believed to occur during immunotherapy in human cancer patients (19).

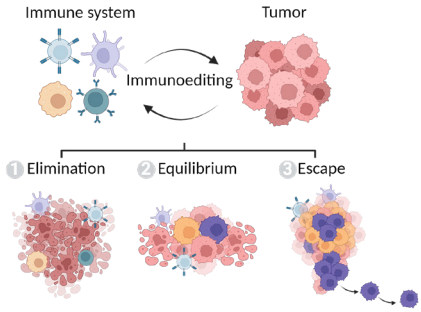


Figure 2. The cancer immunoediting process. Cancer immunoediting is a conceptual framework that integrates the dynamic process by which the immune system controls cancer. It comprises three phases. The first phase is elimination, in which the immune system response successfully destroys the emerging tumor. The second phase is equilibrium, in which the immune system can control tumor growth, but the tumor is not eradicated. Further immunologic shaping of the tumor (resistant tumor clones) and the establishment of a suppressive microenvironment leads to the escape phase. During this phase, cancer becomes a clinically visible disease and spreads to other organs, forming metastatic tumor lesions. Image adapted from Gubin & Vesely, 2022. Image created with Biorender.com.

2. Antigen recognition by T cells

Through their T-cell receptors (TCR), conventional T lymphocytes recognize peptides bound to the major histocompatibility complex (MHC) on the surface of target cells (20). The recognized peptide sequences are called "epitopes", while their originating proteins are called "antigens." In the context of cancer, these proteins are known as tumor antigens.

T cells are classified as CD8 or CD4 based on the surface expression of proteins known as cluster differentiation (CD) markers. These two subsets have distinct physiological roles and recognize cognate epitopes differently. $CD8^+$ T cells can target short peptides (8-12 amino acids) typically derived from cytoplasmic proteins by proteasomal digestion, which are then presented on MHC-I (21). In contrast, $CD4^+$ T cells recognize longer peptides presented on MHC-II, mainly derived from endosomal and ingested proteins via lysosomal digestion. The distinction between antigen-processing pathways for loading peptides into MHC-I and MHC-II molecules is not absolute. Specific subsets of professional antigen-presenting cells

(APCs), particularly dendritic cells (DCs), can present peptides derived from the phagocytosis of infected or malignant cells in the context of MHC-I, through a process known as cross-presentation (22).

While MHC-I is ubiquitously expressed, the constitutive expression of MHC class-II molecules is restricted to APCs. However, they can be expressed on endothelial and some epithelial cells under inflammatory conditions. Moreover, stress or inflammation can induce the expression of MHC-II on tumor cells or other cell types (23).

Following antigen recognition, TCR-associated molecules signal through their intracellular domains to activate distinct programs within the lymphocyte (24). In the case of $CD8^+$ cytotoxic T cells (CTLs), this activation ultimately results in the destruction of target cells (25), whereas $CD4^+$ T cells will primarily activate other immune cells and contribute to the amplification of a robust immune response. Nevertheless, $CD4^+$ T cells can directly mediate tumor cell killing when MHC-II is expressed in malignant cells (26).

2.1. HLA-I molecules and presentation pathway

Human MHC-I molecules, known as human leukocyte antigen class I (HLA-I), are a family of surface proteins involved in immune recognition and regulation. These molecules are broadly categorized as classical and non-classical variants, differing in the level of genetic polymorphism, cellular expression patterns, and functions.

Non-classical molecules encoded by the HLA-E, HLA-F, and HLA-G genes are crucial for maintaining immune tolerance in normal physiological conditions. In the context of cancer, upregulated expression of HLA-G, as well as HLA-E in multiple tumor types, has been reported to exert inhibitory effects (27,28).

Classical HLA-I molecules are the products of HLA-A, HLA-B, and HLA-C genes, which are highly polymorphic and ubiquitously expressed on nearly all nucleated cells except germ cells and placental trophoblasts. These molecules play a central role in antigen presentation to cytotoxic $CD8^+$ T cells, which monitor the internal state of cells (29).

2.1.1. Structure of classical HLA-I molecules

HLA-I molecules expressed on the cell surface are composed of three subunits: a polymorphic α-chain, an invariant β-2-microglobulin (β2M) chain, and a peptide antigen. Structurally, the α-chain is comprised of α1, α2, and α3 domains. The first two domains constitute the peptide-binding groove, also known as peptide binding cleft, while domain α3 anchors the complex to the cell membrane and interacts with CD8 co-receptor of T cells. Moreover, β2M forms a non-covalent association with the α-chain, contributing to the stability and function of the HLA-I molecule (Figure 3).

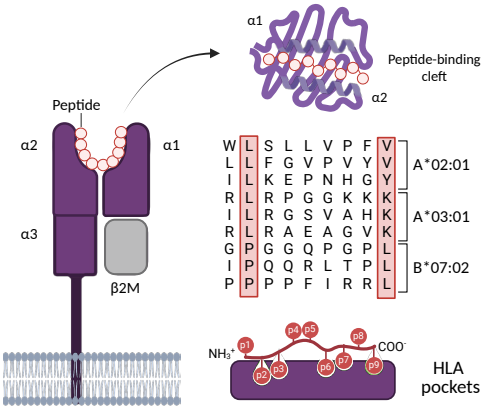


Figure 3. Structure of HLA-I molecules. The pHLA-I complex consists of a polymorphic α-chain, an invariant β-2-microglobulin chain, and the loaded peptide, depicted on the left. A schematic representation of the peptides bound to the peptide-binding groove is shown on the right. The 3D structure of the peptide-binding groove (top), potential peptide sequences bound to the HLA-I specified allele (middle), and the HLA-I pockets (bottom). The anchor residues at positions P2 and P9 are highlighted in red. Image created with Biorender.com.

The HLA-I α-chain is encoded by the HLA-A, HLA-B, and HLA-C genes, known to be the most polymorphic genes in the human genome, with more than 8,000 HLA alleles reported for each gene (https://www.ebi.ac.uk/ipd/imgt/hla/about/statistics/). The prevalence of each HLA allele varies among populations, reflecting their distinct evolutionary paths and genetic backgrounds. Previous studies suggest that alleles with higher peptide-binding promiscuity, such as HLA-A*02:01, the most frequent HLA-A allele in the Caucasian population, have been favored by natural selection (30). Although the promiscuity of these alleles may facilitate the presentation of a broader range of pathogen-derived epitopes, this property also compromised the generation of T-cell responses to other epitopes.

Indeed, some of these alleles have also been associated with increased risks of autoimmune disorders (31), Hodgkin's lymphoma (32) and adverse treatment outcomes in cancer patients (33).

Polymorphisms in HLA-I genes predominantly occur in the peptide-binding groove, defining the pockets of each HLA allele that influence peptide-binding (34). Consequently, each HLA allele restricts the peptide sequences presented to the immune system. The presented peptides, also known as HLA-I ligands, are inserted into the peptide binding groove and restricted in length (8-12 amino acids) and amino acid composition, which is determined mainly by the HLA pockets (35).

Specifically, the B and F pockets exert the most stringent control over peptide binding, as they preferentially interact with specific amino acids. Due to this constrained interaction, peptide sequences presented by a particular HLA-I allele exhibit a conserved binding motif with reduced amino acid diversity at positions two and nine, considered the anchor residues of HLA-I ligands. HLA-I alleles with similar presentation requirements may bind and present overlapping sets of peptides, forming groups known as supertypes (36).

Because individuals can be heterozygous for the three loci, each cell can express up to six different HLA-I molecules, resulting in a diverse peptide repertoire presented to T cells. Therefore, the widespread application of effective T-cell-based therapies is complex and requires a high degree of personalization.

2.1.2. Conventional HLA-I antigen presentation pathway

The HLA-I molecules play a critical role in the presentation of small protein fragments from the proteome on the plasma membrane of the cells. This enables T-cell recognition of infected and aberrant cells, such as those found in cancer. The process of antigen processing and presentation involves several steps, including peptide generation, transport, and loading of the epitopes onto the HLA class I molecules in the endoplasmic reticulum (ER), all of which must occur under specific conditions (37).

Under physiological conditions, HLA-I ligands are usually derived from proteasomal degradation of ubiquitinated mature proteins, cytosolic proteins, or defective ribosomal products (21).

However, proteins from intracellular pathogens in infected cells, or mutant proteins in cancer cells, may also undergo proteasomal processing.

The proteasome is a multicataliytic proteinase complex constitutively expressed and abundantly located in the nucleus and cytoplasm. It consists of two main subcomplexes: the 19S regulatory particle and the 20S core particle. The 20S particle acts as the catalytic unit for protein degradation and is composed of two outer α-rings and two inner β-rings, each consisting of seven structurally similar subunits (α1-7 and β1-7). Within the β-rings, three catalytic subunits β1, β2, and β5 will degrade proteins into small peptide fragments by proteolysis (38). Proteasomes presenting these three catalytic subunits are named standard proteasomes, present in most tissues at basal state.

In some contexts, the constitutive subunits can be replaced by the inducible subunits β1i, β2i, and β5i with modified catalytic capacities upon interferon-gamma (IFN-γ) stimuli (39). Proteasomes with the three inducible subunits are named immunoproteasomes, expressed in basal conditions in lymphoid tissues. Additionally, intermediate proteasomes, presenting different combinations of standard and inducible subunits, have also been described to be constitutively expressed in certain cells (40). The predominant proteasome present in a cell will generate slightly different pools of peptides from the processed proteins due to the different catalytic activities of their combination of β-subunits (41) (Figure 4).

After proteasomal processing, peptides can be further processed by cytoplasmic peptidases, which differ depending on the cell type and may have different processing specificities. These peptides are then transported into the ER by adenosine triphosphate-dependent transporters (TAP1 and TAP2). Once in the ER, ER-associated aminopeptidases (ERAP1 and ERAP2) can further truncate peptides to generate shorter peptides that fit into the HLA-I peptide binding groove.

In parallel, both β2M and HLA-I alpha chains are translated and inserted into the ER, forming a heterodimer facilitated by chaperones. Tapasin along with other chaperone molecules such as calreticulin and the thioloxidoreductase ERp57, facilitates peptide loading of class I molecules in the ER by bridging HLA class I molecules to TAP. Together, these molecules form the peptide loading complex (PLC), stabilizing the empty HLA class I dimer until the assembly of the peptide

(37). Once stably assembled, the peptide-HLA-I complex (pHLA-I) is transported through the ER and the Golgi network to the cell surface, where it can be recognized by the specific TCR of $CD8^+$ T cells (Figure 4).

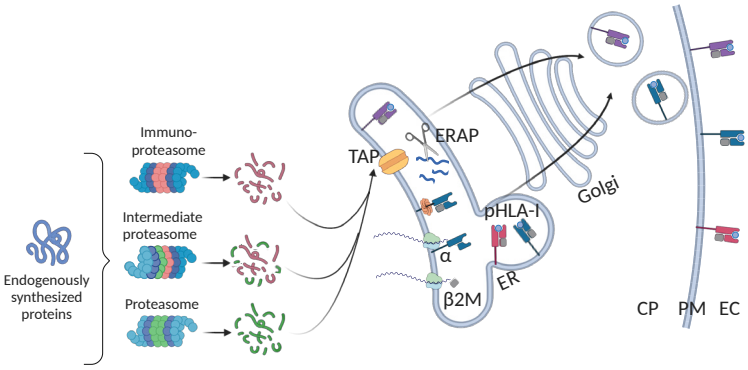


Figure 4. Conventional HLA-I antigen processing and presentation pathway. Endogenously synthesized proteins are degraded in the proteasome, immunoproteasome, or intermediate proteasome. The peptides produced are transported to the ER via TAP. Once there, ERAP further trims the peptides to generate shorter peptides that fit into the HLA-I peptide-binding groove. HLA-I α and β2m chains are translated and introduced into the ER where they are recruited to a multiprotein complex called PLC, enabling peptide loading. The pHLA-I complex traffics via Golgi to the cell surface. Endoplasmic reticulum (ER), ER-associated aminopeptidases (ERAP), transporter-associated with antigen processing proteins (TAP), ribosome (RB), HLA-I α chain (α), β-2-microglobulin (β2m), HLA-I peptide complex (pHLA-I), peptide-loading complex (PLC), cytoplasm (CP), plasma membrane (PM), extracellular (EC). Image created with Biorender.com.

Although all intracellular proteins have the potential to be presented on HLA-I, only a fraction reaches the plasma membrane for immune detection. Once on the surface, $CD8^+$ T cells will be able to recognize pHLA-I complexes resulting from abnormal proteins from those resulting from self-proteins, thanks to mechanisms of both central and peripheral tolerance.

The diverse repertoire of TCRs generated during T-cell development provides the capacity to recognize a wide range of antigens. However, this diversity requires stringent selection processes to prevent autoimmunity. Central tolerance in the thymus involves positive selection for T cells that recognize self-HLA molecules, followed by negative selection to eliminate strongly self-reactive T cells (42). While this process removes many self-reactive T cells or generates regulatory T cells, some may escape to the periphery, where peripheral tolerance mechanisms further regulate them (43). Despite these controls, spontaneous T-cell responses recognizing

normal self-proteins occur in autoimmune diseases. Such reactivities have also been reported in cancer patients, indicating that a fraction of T cells recognizing normal self-antigens evade immunological tolerance processes.

2.2. Tumor antigens

Tumor antigens refer to proteins expressed by tumor cells that can trigger a T-cell response when presented on HLA molecules. Given that T cells capable of targeting tumor antigens play a crucial role in tumor immunity, research efforts have been directed toward identifying T-cell responses and their corresponding antigenic targets for therapeutic intervention.

Although the immune system's ability to recognize and destroy cancer cells was widely acknowledged, it was not until the early 1990s when the molecular nature of antigens expressed by human tumors and recognized by cytotoxic T lymphocytes was unraveled (44).

Tumor antigens derived from canonical proteins have traditionally been grouped according to their tumoral specificity into two main categories: 1) low tumor-specificity antigens, also known as tumor-associated antigens (TAA), which are primarily distinguished by their expression in normal cells, albeit at reduced levels, and 2) high tumor-specificity antigens, also named as tumor-specific antigens (TSA) which are typically expressed exclusively in malignant cells (45) (Figure 5).

In the last decades, advancements in technology and bioinformatic tools have facilitated the identification of an additional source of tumor antigens, known as non-canonical (non-C) or cryptic antigens. These non-C antigens arise from aberrant transcription, translation, or post-translational modifications from coding, transposable elements, or non-coding genome regions (46). During periods of cellular stress, these aberrant events can be favored, suggesting that they may be enriched in tumors. The resulting non-C antigens may be of low tumor specificity when also generated in healthy cells. However, mutant non-C antigens can also arise uniquely in tumor cells, considering that 99% of cancer-specific mutations occur in non-coding regions (47). This mutant non-C would be antigens of high tumor-specificity as these mutations occur exclusively in cancer cells (Figure 5).

Although spontaneous T-cell responses to some non-C antigens have been observed in cancer patients (reviewed by 48), to what extent these type of antigens plays a major role in immune surveillance and whether the non-mutated are tumor-specific remains unclear. Recently, results from our laboratory showed that despite non-C antigens were frequently presented by tumor cells, recall T-cell responses in patients were not detected. Nonetheless, *in vitro* priming led to the identification of T cells targeting three non-C antigens and those preferentially recognized tumor cells over healthy cells, supporting their therapeutic potential (49).

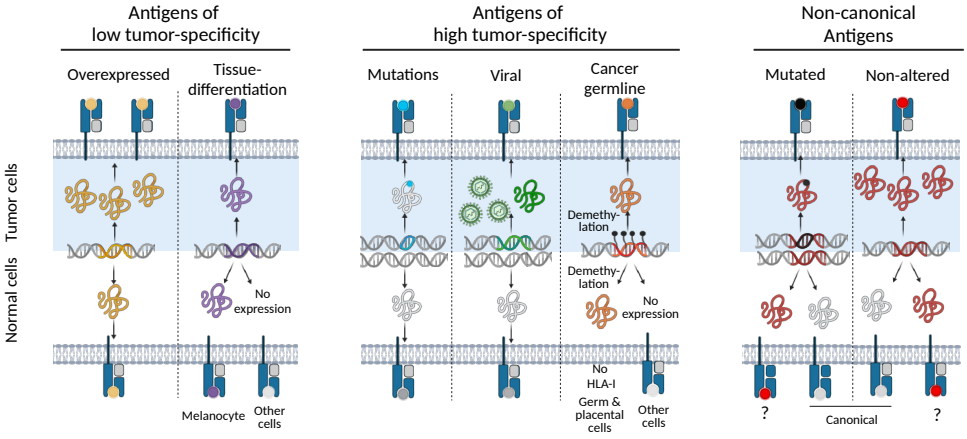


Figure 5. Classification of human tumor antigens. Expression and HLA-I presentation in tumor (top) and normal cells (bottom) of canonical antigens with low or high tumoral specificity (left) or from non-canonical antigens (right) are depicted. For canonical antigens, low tumoral specificity antigens include antigens derived from overexpressed proteins in tumor cells compared to normal cells and proteins involved in differentiating the specific tissue from which each tumor originates. Antigens of high tumor specificity include antigens derived from tumor-specific mutations, viral proteins, and cancer germline antigens. The latter are exclusively expressed in germline and tumor cells by epigenetic regulation. However, they are not presented on the cell surface of germline cells due to the lack of HLA-I molecules. For non-canonical antigens (non-C), low and high tumor-specific antigens can be generated. Low tumor-specific non-C include aberrant proteins resulting from aberrant transcription, translation, or post-translational modifications of coding or non-coding regions of the genome. Compared to healthy cells, tumors are more likely to produce abnormal proteins due to cellular stress. High tumor-specific non-C antigens result from the same aberrant processes occurring in genomic regions with somatic mutations found only in tumor cells. Adapted from Coulie et al., 2014. Image created with Biorender.com.

2.2.1. Antigens of low tumor-specificity

This category consists of antigens encoded by normal self-genes, which are highly expressed in tumors but also in healthy cells. Specifically, it comprises both antigens derived from proteins overexpressed in tumors and differentiation antigens.

Overexpressed antigens originate from genes constitutively expressed in several normal tissues presenting a higher level of expression in tumors (Figure 5). T-cell responses targeting ERBB2 and Wilm's tumor protein (WT1), which are antigens overexpressed in epithelial tumors like ovarian and breast carcinomas and in leukemic cells, respectively, have been observed in patients (50,51).

Differentiation antigens are proteins derived from genes expressed in tumor cells and in the differentiated normal tissue from which the tumor originated (Figure 5). In the literature, spontaneous anti-tumor T-cell responses targeting differentiation antigens derived from proteins such as tyrosinase (TYR), melanoma antigen recognized by T cells 1 (MART-1), and glycoprotein 100 (gp100) have been extensively documented in patients with melanoma (52–54). Furthermore, the prostate-specific antigen (PSA) and prostatic acid phosphatase (PAP), which are uniquely expressed in the prostate have been associated with spontaneous T-cell responses (55,56).

The identification of naturally occurring T-cell responses against these antigens in patients indicates that central tolerance towards low tumor-specific antigens is incomplete. Nevertheless, the expected affinity of TCRs targeting these antigens is low, given that high-affinity TCRs against normal cellular proteins are typically eliminated during negative selection in the thymus (57).

2.2.2. Antigens of high tumor-specificity

This group includes antigens encoded by proteins that are exclusively expressed in tumor cells, which can be derived from viral proteins, cancer germline antigens, and somatic mutations generating neoantigens.

A subset of cancers arises from viral infections, leading to the expression of viral proteins with oncogenic properties (Figure 5). These virus-derived antigens can be shared among patients with tumors of the same type. For example, human papillomavirus (HPV) is associated with a subset of head and neck, cervix, and anal cancers that express oncoproteins (E6 and E7) which can be recognized by T cells (58). Similar trends are observed in other virus-induced solid cancers, such as Merkel cell carcinomas resulting from polyomavirus infection (59), and nasopharyngeal carcinomas triggered by Epstein-Barr virus (EBV) infection (60).

Because of their foreign nature, there is no central tolerance to these viral antigens. Consequently, T cells targeting them are not eliminated in the thymus and can be detected and isolated from patient tumors or peripheral blood, often possessing high-affinity TCRs (57).

On the other hand, cancer-germline antigens originate from non-mutated self-genes normally expressed only during fetal development. In most normal adult tissues, except for germ cells and placental trophoblasts, these genes are typically epigenetically silenced. However, these cell types lack HLA-I expression, resulting in the absence of epitope presentation on the cell surface HLA of normal adult cells (61) (Figure 5). Through DNA demethylation, these genes can be reactivated in various tumor types, leading to their expression. Consequently, naturally occurring T-cell responses targeting cancer-germline antigens are frequently observed across various cancers (44,62).

2.2.2.1. Neoantigens

During carcinogenesis, somatic mutations occur in different genes, generating mutated proteins, known as neoantigens. At the DNA level, various types of changes, such as single nucleotide variants (SNVs), nucleotide insertions or deletions (indels), and gene fusions, can lead to the creation of new antigenic peptides. This can happen by altering amino acids, shifting the reading frame, extending the coding sequence beyond the normal stop codon, or by generating new DNA arrangements (63). These antigens arise exclusively in tumor cells due to unrepaired genomic alterations, rendering them immunogenic as they are interpreted as non-self-proteins.

Given that mutagenesis is a stochastic process that can affect the entire human genome, the likelihood of a single somatic alteration occurring in multiple patients is extremely low. This, coupled with the requirement that a mutated protein must undergo processing in the proteasome and be presented by one of the patient's HLA alleles to be detected by T cells, effectively results in most neoantigens being "private" as they will be unique to individual patients (Figure 6).

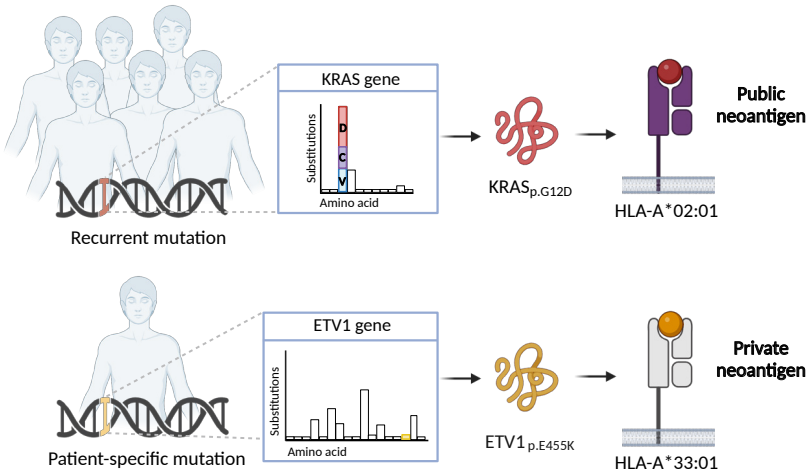


Figure 6. Types of neoantigens. Genetic mutations result in changes in the amino acid sequences of proteins. Mutations in hotspot regions of oncogenes, such as the KRAS gene, occur in multiple cancer patients (top). Mutations in other protein-coding genes, exemplified by the ETV1 gene, can occur exclusively in a single cancer patient (bottom). The resulting mutated proteins would be degraded by the proteasome, and the generated peptides may be processed and presented by HLA on the cell surface. Neoepitopes derived from shared neoantigens (e.g., $KRAS_{p.G12D}$) presented on highly prevalent HLA-I alleles (e.g., HLA-A*02:01) are considered public neoantigens, which can be found in multiple cancer patients. Conversely, mutant proteins resulting from patient-specific mutations (e.g., $ETV1_{p.E455K}$) can produce peptides presented by specific HLA-I alleles of the patient (e.g., HLA-A*33:01), considered private neoantigens. Image created with Biorender.com.

However, not all somatic mutations occur randomly. Mutations that alter the normal protein function of tumor suppressors (i.e., TP53) or oncogenes (i.e., KRAS) can reoccur systematically across many patients (64). Indeed, these recurrent mutations typically arise in tightly constrained hotspot regions within proteins, where only a single or limited number of amino acid residues can be substituted causing an altered protein function. A classic example is mutations affecting codons 12, 13, and 61 of the *KRAS* gene, with codon 12 being the most frequent site of mutations. In this hotspot region, single nucleotide changes can cause glycine to aspartic acid conversion, referred to as $KRAS_{p.G12D}$, which occurs in more than 40% of patients affected by pancreatic cancer (65). This single substitution leads to a constitutively active KRAS protein, which changes the normal behavior of the cell (66).

It is known that mutant proteins resulting from recurrent mutations in hotspot regions of key tumor suppressors or oncogenes can promote cellular transformation (67,68). These mutations are expected to happen in the early stages of carcinogenesis,

and that is why these genes are also named as "drivers" since they help to promote the malignant transformation of a cell (69). Because these mutations might be essential for maintaining the malignant phenotype of tumor cells, they tend to be conserved within cells of the same tumor lesion and across metastases (70).

Hence, neoantigens resulting from hotspot driver mutations are likely clonal and shared across different cancer patients. Moreover, if an epitope derived from a shared neoantigen binds to a relatively common HLA allele, it could potentially generate an ideal "public" neoantigen that can be found in multiple cancer patients (71)(Figure 6).

On the contrary, private neoantigens are typically the consequence of passenger mutations accumulated in tumor cells due to replicative defects during expansion but have no impact on tumor fitness. Therefore, the presence and expression of private neoantigens may vary within tumors and between malignant lesions within the same patient, challenging their therapeutical targeting.

Spontaneous T-cell responses targeting private (72,73) and shared (74–76) neoantigens have been detected in patients affected by different cancer types. Because T cells targeting them are not subjected to central tolerance, they are more frequently detected in the periphery, and often possess high-affinity TCRs since such receptors have not been depleted (77).

2.3. Cancer Immunity cycle

To elicit a potent immune response capable of efficiently killing tumor cells, a sequence of carefully orchestrated events must be initiated and consecutively followed until complete tumor rejection occurs (78). This coordinated process is commonly referred to as the cancer immunity cycle.

The first step involves the release of tumor antigens expressed in tumor cells, which are subsequently captured by DCs. These DCs will process the antigens and present them on HLA molecules (Figure 7).

Subsequently, these APCs migrate to lymph nodes, where they present the antigens to naïve T cells, resulting in the priming and activation of effector T cells that respond to tumor-specific antigens (Figure 7). In this second phase of the cycle, DCs assume a critical role. Through a process called "licensing" mediated by CD4

T cells, DCs become pre-activated, enabling them to cross-present antigens and express co-stimulatory molecules. These are two key features to effectively present antigens to $CD8^+$ T cells and induce an effector response rather than a tolerogenic response (79,80).

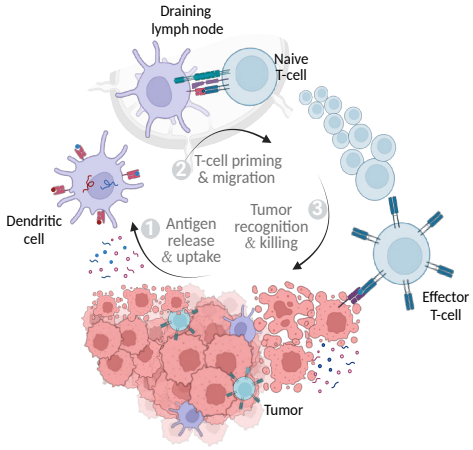


Figure 7. Cancer immunity cycle. (1) The first step involves the release of tumor antigens, which are then captured by DCs, processed, and cross-presented on HLA-I. (2) Next, these APCs migrate to lymph nodes where they interact with naïve $CD8^+$ T cells. This interaction leads to the priming and the activation of effector T cells that recognize tumor-specific antigens. The stimulated T cells proliferate and differentiate into effector $CD8^+$ T cells, then exit the lymph nodes and migrate to the tumor. (3) Activated effector T cells specifically recognize and kill tumor cells presenting their cognate antigen on HLA-I. This triggers the release of more tumor antigens, increasing the immune response's breadth and depth in subsequent cycles. Adapted from Chen & Mellman, 2013. Image created with Biorender.com.

Finally, the activated effector $CD8^+$ T cells exit lymph nodes and migrate to tumors, where they can identify their corresponding antigen presented on HLA-I molecules by tumor cells and lyse them (Figure 7). As a result of cell death, more tumor antigens will be released and other $CD8^+$ T cells can be primed to different tumor antigens. This process known as antigen spreading, has the potential to enhance the immune response by gaining breadth and depth in subsequent rounds of the cycle.

In cancer patients, tumors arise because of the breakdown of this immunity cycle. Every stage of the cycle can be influenced by immune-modulatory mechanisms that enable tumor cells to evade immune surveillance. Therefore, the goal of cancer immunotherapy is to stimulate the antitumor response by initiating or re-initiating the cycle of cancer immunity.

3. Cancer immunotherapies

Cancer immunotherapies have changed the landscape of oncology, achieving unprecedented success in moving from bench to bedside. Over the past 50 years, there has been remarkable activity in this area of immunology research, resulting in the development of several modalities aimed at harnessing the immune system to identify and eliminate cancer cells (Figure 8). Many of these immunotherapeutic approaches have focused on T lymphocytes and their ability to generate antigen-specific cytotoxicity as a key component in engaging the immune system to fight cancer.

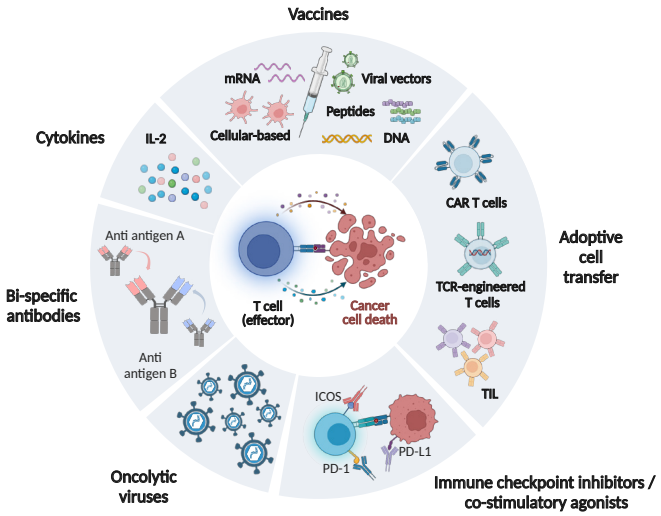


Figure 8. Types of cancer immunotherapies. Schematic overview of various cancer immunotherapy modalities developed to mobilize the immune system to destroy cancer cells. Most of these strategies focus on T lymphocytes and their ability for antigen-directed cytotoxicity. They can aim to reinvigorate naturally occurring tumor-reactive T cells or generate *de novo* T-cell responses. Image created with Biorender.com.

Immunotherapies can be categorized into two main groups based on whether the T cells' antigen-specificity is known before treatment. Those approaches without prior knowledge of the specific target antigen are the administration of interleukin-2 (IL-2), immune checkpoint inhibitors, oncolytic viruses, or adoptive cell transfer (ACT) of unselected tumor-infiltrating lymphocytes (TILs). On the contrary, those approaches with a defined target antigen include bi-specific antibodies, therapeutic vaccines, ACT of neoantigen-specific TILs, and ACT of chimeric antigen receptor (CAR) T cells or with TCR-engineered T cells.

3.1. IL-2

The first successful immunotherapy used in clinical trials was the systemic administration of IL-2 (81), discovered in 1976 as a T-cell growth factor (82). Ten years later, studies showed that high doses of recombinant human IL-2, causing early but reversible toxicities in some cases, led to tumor regression in patients with melanoma and renal cancer (83,84). High-dose IL-2 was approved by the U.S. Food and Drug Administration (FDA) in 1992 and 1998 for the treatment of metastatic renal cell carcinoma and metastatic melanoma, respectively (81). Although promising results were observed in treating patients affected by these cancers, responses were rarely seen in patients with other metastatic tumor types.

3.2. Immune checkpoint inhibitors

In the tumor microenvironment, persistent antigen exposure leads to T-cell exhaustion, a state characterized by the continuous expression of inhibitory immune checkpoint receptors such as Programmed Death- 1 (PD-1) and Cytotoxic T-Lymphocyte Antigen 4 (CTLA-4) among others (85). Immune checkpoint inhibitor (ICI) therapies have exploited the targeted blockade of these receptors and their ligands to reinvigorate the anti-tumor immune response (Figure 8).

Currently, nine FDA-approved ICIs agents are covering more than 50 cancer indications (86). Most ICIs agents used for the treatment of metastatic cancer patients are monoclonal antibodies that block CTLA-4, PD-1, or its major ligand PDL-1 (86,87). While ICI monotherapy has achieved remarkable success, particularly in melanoma, there is a need to improve the efficacy of this treatment across different tumor types (88). Compensatory upregulation of additional checkpoint molecules is a primary mechanism of resistance to this treatment. Thus, several strategies targeting both inhibitory (such as LAG-3, TIM-3) and activating molecules (such as ICOS, OX40) are being tested in clinical trials (89).

3.3. Bi-specific antibodies

Bi-specific antibodies simultaneously bind two different antigens, typically one on tumor cells and the other on immune cells, to mediate the formation of an immunological synapse with tumors and facilitate tumor cell killing (Figure 8).

T-cell-engaging bi-specific antibodies (T-biAbs) activate T cells through an anti-CD3 antibody fragment, triggering the activation of the TCR complex signaling cascade and bypassing the HLA restriction requirement of the TCR.

In 2014, the FDA approved the first T-biAb, Blinatumomab (targeting CD3 and CD19), for the treatment of Philadelphia chromosome-negative relapsed or refractory B cell precursor acute lymphoblastic leukemia. Its approval was based on positive results from a clinical trial in which 43% of the treated patients achieved a complete regression (90). Although T-biAbs have shown efficacy in hematologic malignancies, responses in solid tumors remain limited. Thus far, no T-biAbs have been approved for treating solid tumors.

3.4. Oncolytic viruses

Oncolytic viruses (OVs) selectively infect and replicate within cancerous cells rather than healthy ones. These viruses kill tumors by direct cell lysis, which is considered a type of immunological cell death, as it causes the release of damage-associated molecular patterns, which alert the immune system of the presence of abnormal cells. The tumor antigens released upon cell destruction can activate anti-tumor T-cell responses, thereby enhancing the immune system's ability to target and eliminate tumor cells.

Currently, there are four OVs approved for the treatment of several malignancies such as nasopharyngeal carcinoma (91), invasive bladder cancer (92) malignant glioma (93), and melanoma (94,95). Although these agents have been widely used as monotherapy, some clinical trials have evaluated their effectiveness in combination with chemotherapy or other immunotherapies such as immune checkpoint blockade (96,97) or ACT with CAR transduced T cells (98,99) in distinct solid tumors.

3.5. Vaccines

Therapeutic cancer vaccines aim to boost T-cell responses against growing tumors through active immunization, enhancing pre-existing $CD8^+$ and $CD4^+$ T-cell responses and activating naïve T cells by effectively presenting tumor antigens on activated APCs (100). Several strategies have been used to deliver target antigens to patients (Figure 8). These include the direct administration of peptides (both short or long), RNA or DNA (delivered directly or via viral particles) along with adjuvants

or the administration of pre-loaded DCs with the antigens of interest, or whole tumor lysate (101).

Several clinical trials have explored therapeutic vaccines targeting melanoma-differentiation antigens like gp-100 (102), cancer-germline antigens like New York esophageal squamous cell carcinoma 1 (NY-ESO-1) (103), overexpressed antigens such as ERBB2 (104) or mutant and wildtype peptides derived from TP53 (105).

In 2012, the first autologous therapeutic vaccine consisting of pre-loaded APCs with the fusion protein resulting from granulocyte-macrophage colony-stimulating factor (GM-CSF) and PAP was approved for the treatment of metastatic prostate cancer (106). Although this vaccine effectively generated anti-tumor responses, other vaccines delivering other antigens of low tumor specificity have generally failed to elicit clinically effective anti-tumor responses (107).

In recent years, personalized therapeutic cancer vaccines tailored to each patient's tumor have also been explored. However, results from clinical trials treating cancer patients with such vaccines, either alone or in combination with immune checkpoint inhibitors, have shown variable clinical efficacy (108–110). Nonetheless, therapeutic vaccines using various adjuvants and delivery approaches continue to be actively explored in clinical trials, alone or in combination with ICIs (111).

3.6. Adoptive T-cell transfer

ACT is a form of immunotherapy that involves the isolation and *ex vivo* expansion of large numbers of T lymphocytes for reinfusion into the patient (as shown in Figures 8 and 9). The effectiveness of this treatment is determined by the ability of the infused T-cell product to recognize and eliminate cancer cells. Currently, ACT can use T cells that naturally exhibit anti-tumor activity, such as TILs, or genetically engineered T cells that have been modified to express TCRs or CARs that target specific tumor antigens.

ACT offers several advantages over other immunotherapeutic approaches. For example, *ex vivo* expansion allows T cells to escape the immunosuppressive environment within tumors, which can inhibit T-cell activation and proliferation. The lymphodepletion preparative regimen, typically administered before ACT, eliminates endogenous regulatory T cells and other lymphocytes, thus facilitating access to

growth-promoting cytokines for the transferred cells. This pre-conditioning of the patient creates a favorable environment that enhances the anti-tumor capabilities of the transferred T cells. In addition, the growth and survival of infused T cells can be further supported by the administration of IL-2 after cell transfer.

4. Types of adoptive T-cell transfer

4.1. ACT of tumor-infiltrating lymphocytes

The adoptive transfer of *ex vivo* expanded TILs isolated from the patient's tumor (Figure 9) has been demonstrated as an effective approach for cancer treatment.

In 1988, a clinical trial using ACT of *ex vivo* expanded autologous TILs and administration of IL-2, showed that 11 of 20 treated patients with metastatic melanoma achieved an objective response. This was the first demonstration that autologous TILs could induce regression of large established tumors in patients with metastatic melanoma (112). Since then, ACT of autologous TILs has been used to treat numerous patients with metastatic melanoma and other epithelial cancers (113). However, in contrast to the 50% response rate observed in metastatic melanoma patients, objective responses have been limited in other tumor types.

Retrospective analyses of TIL products from responders and non-responders revealed that successful TIL-ACT was associated with the expansion of T cells targeting differentiation and cancer germline antigens, but mainly neoantigens (114–116). These studies suggested selecting and expanding tumor-specific T cells before ACT may be critical for its efficacy. Indeed, ACT of TIL products enriched for neoantigen recognition has shown potent anti-tumor efficacy, resulting in complete responses in certain patients with epithelial tumors other than melanoma (73,76,117).

Overall, the clinical experience with this T-cell therapy provides convincing evidence that it can achieve durable tumor regression in metastatic melanoma and in certain patients with other epithelial cancers when the T-cell product is enriched for neoantigen-specific T cells. Indeed, in 2024, the FDA has approved Lifileucel, the first autologous TIL cellular therapy for treating adult patients with unresectable or metastatic melanoma on the basis of an open-label Phase II trial showing a 30% overall response rate in the treated patients (118).

However, the widespread use of TIL-ACT is constrained by several factors. First, the need for a tumor biopsy to obtain autologous TILs restricts its applicability to patients with accessible tumors. Second, in order to improve the chances of a successful TIL-ACT, it is necessary to enrich for neoantigen-specific TILs, which are highly personalized products, primarily targeting private neoantigens in most cases. The requirement of such tailored products for each patient treatment, coupled with the high cost of the overall strategy, limits the generalizability of neoantigen-enriched TIL-ACT (119).

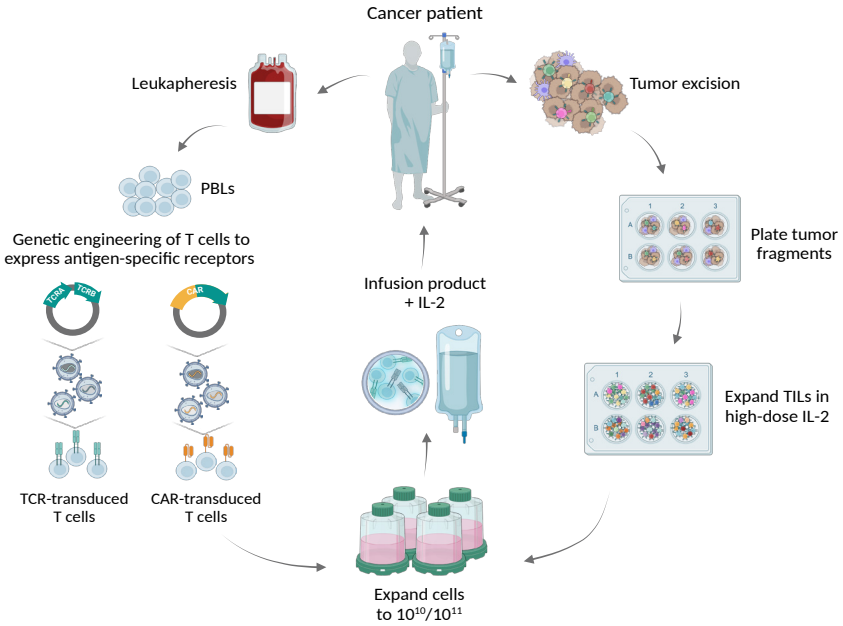


Figure 9. ACT of TILs or genetically engineered T cells. Autologous lymphocytes are expanded to high numbers and infused back into patients in the presence of IL-2 and after lymphodepleting chemotherapy. Two main types of ACT are currently in use: (1) ACT with TILs involves the ex vivo expansion of TILs isolated from tumor biopsies or resections (right). In this process, the tumor tissue is split into fragments and cultured in T-cell media containing high doses of IL-2 to promote the growth of TILs. (2) ACT with genetically engineered T cells (left), which consist of isolating autologous PBLs and transducing them, usually with viral vectors encoding the receptors of interest (TCR or CAR) targeting specific tumor antigens. Image created with Biorender.com.

4.2. ACT of CAR-engineered T cells

One strategy for directing T lymphocytes to recognize and eliminate tumor cells expressing a specific target antigen is to genetically engineer them to express a CAR (Figure 9). CARs are synthetic receptors composed of the variable region of the binding domains of monoclonal antibodies, a hinge, a transmembrane domain, and intracellular T-cell signaling domains (120). These chimeric receptors enable CAR-engineered T cells (CAR-T) to recognize natively folded proteins on the surface of cancer cells independently of HLA molecules. Recognition of tumor antigens via CAR also triggers T-cell activation through the signaling of the intracellular domains of these receptors, promoting T-cell-mediated cytotoxicity against tumors (121).

In contrast to TIL-ACT, CAR-T ACT can be considered a less invasive strategy because it only requires the collection of autologous T cells for CAR transfer. The design of chimeric receptors targeting shared antigens, which are present in multiple cancer patients, makes CAR-T ACT a more accessible therapeutic option for multiple cancer patients. However, the widespread applicability of CAR-T for cancer treatment is limited by the requirement of the target antigen expression on the tumor cell surface. Only 30% of proteins encoded in the human exome are estimated to be expressed on the cell membrane (122,123). Therefore, most mutations in the exome of tumor cells are more likely to affect genes encoding intracellular proteins. Consequently, the capacity of CAR-T cells to target neoantigens would be limited. Instead, targeting tumor-associated antigens has been the preferred option for CAR-T-cell approaches.

In 2017, the FDA approved anti-CD19 CAR-T cells for the treatment of B cell lymphomas and leukemias due to the impressive tumor regressions reported in the treated patients (124–126). Beyond the unprecedented success of anti-CD19 CAR-T and anti-BCMA CAR-T-cell therapy in multiple myeloma (127), the clinical efficacy of CAR-T cells in the treatment of solid malignancies has been very low. This limited efficacy in solid tumors may be explained by several challenges that remain to be addressed, including restricted trafficking and infiltration into the tumor site, antigen escape and heterogeneity, and susceptibility to the immunosuppressive microenvironment (120).

4.3. ACT of TCR-engineered T cells

Generating TCR-engineered T cells (TCR-T) requires introducing specific TCRs capable of recognizing tumor antigens into autologous T cells for use in ACT (Figure 9). Hence, metastatic patients affected by different cancer types expressing the targeted antigens and the HLA-I allele could benefit from these therapies.

TCR-T ACT can be considered a less invasive strategy than TIL-ACT because it only requires the collection of autologous T cells for TCR transfer once the expression of the antigen and HLA have been confirmed. Even though the HLA restriction of TCRs could represent a limitation compared to CARs, their ability to target epitopes derived from proteins in any subcellular compartment allows them to target peptides from any tumor antigen, including neoantigens. Moreover, whilst CAR receptors have a higher affinity for their targets (128,129) compared to TCRs (130), they require a much higher antigen density, in the order of thousands of molecules (131,132), compared to the tens of molecules required to trigger TCR recognition (133,134). Thus, TCR-T may induce more potent anti-tumor responses to a wider variety of tumor antigens present in solid tumors.

To maximize the widespread applicability of TCR-T ACT, off-the-shelf TCRs with pre-characterized specificity to shared tumor antigens and restricted to prevalent HLA alleles in the Caucasian population, have been explored. The proof-of-concept that TCR-T ACT could induce tumor regression was obtained in 2006 when melanoma patients were treated with engineered T cells recognizing the melanoma-associated antigen MART-1 (135). Since then, several clinical trials have exploited the use of TCR-engineered T cells with different receptors targeting epitopes derived from antigens of low and high tumor specificity (Table 1).

Table 1. Clinical trials using TCR-engineered T cells for ACT.

Type of tumor antigen	Antigen	HLA allele	T-cell source of the TCR	Affinity-enhanced TCR	Cancer patients treated	Overall response rate	TCR-related adverse events	References
Differentiation antigens	MART-1	A*02:01	TILs	No	Melanoma	13%	Not observed	135 ; 136
			TILs	No	Melanoma	30%	Toxicity in melanocytes from skin, eye and inner ear	136
	gp100		Tg A*02:01 mouse	No	Melanoma	19%		136
	TYR		TILs	No	Melanoma	33%	Toxicity in melanocytes from skin	137
	CEA		Tg A*02:01 mouse	Yes	Colorectal	33%	Toxicity in colonic epithelial cells	138
Overexpressed antigens	WT-1	A*24:02	HD PBLs	No	MDS/AML	0%	Not observed	139
		A*02:01	HD PBLs	No	prophylactic post-HST AML	NED	Not observed	140
Cancer germnline	NY-ESO-1	A*02:01	TILs	Yes	Melanoma	55%	Not observed	141 ; 142
					Synovial cell sarcoma	61% & 50%	Not observed & CRS	
	MAGE-A3/A9/A12	A*02:01	Tg A*02:01 mouse	Yes	Various	56%	Toxicity in neurons MAGE-A12^{+}	143
	MAGE-A3	A*01:01	TILs	Yes	Various	0%	Toxicity in cardiomyocites titin^{+}	144
	MAGE-A3 /A6	DPB1* 04:01	Patient PBLs	No	Various	24%	Prolonged fever	145
	MAGE-A4	A*24:02	HD PBLs	No	ESCA	0%	Not observed	146
	MAGE-A4	A*02:01	HD PBLs	Yes	Various	36%	CRS	147
	MAGE-A10	A*02:01	N.D.	Yes	NSCLC	11%	Not observed	148
Viral antigens	HPV-E6	A*02:01	TILs	No	HPV-16^{+} tumors	17%	Not observed	149
	HPV-E7	A*02:01	CILs	No		50%	Not observed	150
Neoantigens	Private	Various	Autolg. PBLs	No	Various	0%	CRS & encephalopathy	151
	$KRAS_{p.G12D}$	C*08:02	TILs	No	Pancreatic	(1/2)	CRS	152
	$TP53_{p.R175H}$	A*02:01	TILs	No	Breast	(1/1)	CRS	153

HD PBLs: Healthy donor peripheral blood lymphocytes; Tg A*02:01 mouse: transgenic HLA-A*02:01 mouse; N.D.: Not defined; Autolg. PBLs: Autologous PBLs; CILs: cervix infiltrating lymphocytes; Patient PBLs: peripheral blood lymphocytes from cancer patient; MDS: Myeloid dysplastic syndrome; HST: Hematolopoetic stem cell transplantation; AML: acute myeloid leukemia; ESCA: esophageal carcinoma; NSCL: Non-small cell lung cancer; NED: No evaluable disease; CRS: cytokine release syndrome.

The trials are categorized by the targeted tumor antigen, including the antigen's name and the corresponding HLA restriction element. Additionally, it annotates the source of T cells from which the TCRs were isolated and any modifications made to enhance their target affinity. Information on the types of tumors from patients treated with autologous TCR-T cells bearing these TCRs, the observed overall response rate, adverse events attributed to the TCR-T cells, and the reference to publications reporting these clinical trials are included.

So far, TCRs targeting cancer germline antigens have been the most exploited receptors for TCR-T ACT. Two clinical trials using genetically engineered T cells with distinct affinity-enhanced TCRs targeting melanoma-associated antigen 3 (MAGE-A3) showed objective cancer regressions but also lethal toxicities. In one study, patients unexpectedly developed severe neurological toxicities, while in the other, patients experienced cardiovascular toxicity. These adverse events resulted from the cross-recognition of the highly homologous peptides in MAGE-A12 or titin, expressed in neurons and cardiomyocytes, respectively (Table 1). These reports underscore the need to evaluate potential TCR toxicities before clinical application, especially when using affinity-enhanced TCRs.

The development of TCR-T ACT targeting neoantigens has been hindered because most neoantigens are unique to each patient. However, a recent approach aimed at simultaneously targeting different private neoantigens has been explored. In this study, patients were treated with a pool of TCR-T cells consisting of three different neoantigen-specific TCR-T populations, each targeting a different private neoantigen (151). Although safe, this approach did not show objective responses in any of the 16 patients treated (Table 1).

On the other hand, case reports of patients treated with TCR-T targeting public neoantigens proved the safety and potency of this strategy for cancer treatment. In one trial, two pancreatic cancer patients were treated with autologous T cells independently transduced with two different TCRs. Both receptors were restricted to HLA-C*08:02, each targeting a neoepitope (9-mer or 10-mer) derived from the $KRAS_{p.G12D}$ neoantigen (Table 1). These TCRs were obtained from a colorectal cancer patient who achieved an objective response upon TIL-ACT (76). One of the two treated pancreatic cancer patients experienced a partial response lasting for more than 6 months following the infusion of TCR-T cells (152).

In a second trial, a metastatic breast cancer patient was treated with TCR-T with a single TCR targeting a neoepitope derived from $TP53_{p.R175H}$ neoantigen presented on HLA-A*02:01 (Table 1). The TCR used for the generation of these cells was obtained from a colorectal cancer patient (75). The treated breast cancer patient, initially experienced cytokine release syndrome (CRS) that resolved after the administration of intravenous steroids. Even though the patient experienced a partial response that lasted for 6 months, she progressed with new metastatic lesions (153).

Overall, the use of TCR-T ACT, particularly of those targeting public neoantigens, represents a promising strategy that has significantly expanded the spectrum of tumors that can be treated with ACT, such as pancreatic cancers (152).

5. Discovery of therapeutic TCR candidates for TCR-T ACT

Building on the promising results achieved with TCR-T cells targeting public neoantigens, the discovery and characterization of novel TCRs recognizing these epitopes could expand the receptors available for therapeutic use.

Two different immunological strategies aimed at isolating reactive T cells and defining their cognate antigens can be used to discover therapeutic TCR candidates targeting public neoantigens. On the one hand, such TCRs can be identified retrospectively from T-cell reactive populations of cancer patients by forward immunology. This strategy starts with the observed T-cell response and works backward to determine the target antigen. In contrast, reverse immunology starts with the antigen and then searches for reactive T cells against a predefined target (154,155).

Given that T cells recognizing public neoantigens are rarely found in patients, reverse immunology strategies are preferred for prospective and high-throughput identification of TCRs targeting them. The successful identification of therapeutic TCR candidates by reverse immunology involves three critical steps. First, define the minimal epitope derived from the antigen of interest that can be presented on HLA-I molecules. Second, screening for T-cell populations reactive to the selected epitope-HLA combinations. Third, identification of the sequences of TCR therapeutic candidates through TCR sequencing of the isolated reactive populations. Finally, the specificity, safety, and efficacy profiles of the discovered TCRs need to be confirmed before their clinical application.

5.1. Defining the epitope-HLA pair

To identify HLA-I-restricted TCRs that target public neoantigens, defining the sequence of the presented epitopes and the HLA-I allele that presents them can significantly aid in directing the identification of TCRs towards specific pairs.

HLA-I binding predictors and mass spectrometry-based immunopeptidomics can be used to identify the sequence of these public candidate neoantigens and their corresponding HLA-I alleles. Although these approaches identify candidate epitopes, they do not ensure immunogenicity.

To better predict immunogenic neoantigens, several machine-learning algorithms have been trained with experimentally determined immunogenic antigens (156–158). Nonetheless, T-cell assays are ultimately required to confirm the immunogenicity of such predicted neoantigens.

5.1.1. *In silico* HLA-I binding predictors

Over the past years, advances in the field of computational biology have led to the development of several HLA-I epitope prediction algorithms. By focusing on biochemical properties of peptides, each software defines the minimal epitope derived from the antigen of interest that can ultimately reach HLA-I presentation. While some algorithms focus on specific steps of the HLA-I presentation pathway, such as proteasome processing (159), others integrate several steps of the presentation pathway and output a score for peptide binding capacity to specific HLA-I alleles (reviewed by 160). Among the algorithms currently available, NetMHCPan is one of the most widely used (161). This machine-learning algorithm is trained using databases of experimentally determined presented peptides from binding affinity assays and mass spectrometry eluted ligands.

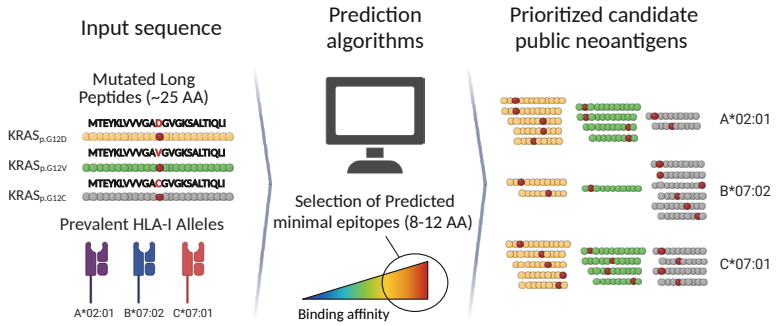


Figure 10. HLA-I binding prediction algorithms to infer public neoantigen candidates. As input, long mutated peptides (~25AA) representing the sequences of shared neoantigens of interest and prevalent HLA-I alleles are fed to the HLA binding prediction algorithm. A list of 8-12-mers predicted to bind to the specified HLA-I molecules is generated. The predicted candidate neoantigens are commonly prioritized based on the binding affinity ranking, synthesized, and tested in functional assays to determine their immunogenic potential. Image created with Biorender.com.

To predict which candidate minimal epitopes from shared neoantigens are more likely to bind to specific HLA-I alleles, the prediction tools are fed with a list of mutated long peptides and the HLA-I alleles of interest as input (Figure 10).

The algorithms output short peptides and a score representing the predicted likelihood of binding to the specified HLA-I alleles for each of them. Given that multiple minimal epitopes can be generated from the input sequence (8-mer to 12-mer, containing the mutant residue at various positions within the sequence), more than one is likely to be predicted to bind one or more alleles. To select candidate minimal epitopes for T-cell screening, they are commonly prioritized based on binding affinity ranking.

Whilst prioritization allows narrowing down the number of candidates to test, certain studies have shown that this selection introduces a bias and might exclude some epitopes actually presented in HLA-I (162,163) Although these predictors can have false positives and negatives, they have been used in numerous studies and have successfully predicted immunogenic peptide-HLA pairs from different shared neoantigens (164–167).

5.1.2. Mass spectrometry-based immunopeptidomics

The presented epitopes derived from shared neoantigens can be discovered by directly examining endogenous peptides displayed by HLA molecules on the cell surface. The repertoire of peptides presented on the HLA-I of cells is known as the immunopeptidome or ligandome (168). In 1994, a minimal epitope recognized by several human CTL clones, derived from the melanoma-associated antigen premelanosome protein (PMEL), was identified through a laborious process involving mass spectrometry (169). Since then, substantial progress in mass spectrometry technology and bioinformatics tools has facilitated a more comprehensive and sensitive exploration of the tumor ligandome. Immunopeptidomics is currently being applied to a wide range of cell sources, including fresh tumor tissues (170), tumor cell lines (171), tumor-derived organoids (172), and genetically modified cells (173).

To identify minimal epitopes derived from shared neoantigens that are naturally presented on HLA-I, the first step is the lysis of large amounts of the starting material (Figure 11). The cell source must express the shared neoantigen and a prevalent HLA-I to reveal presented public neoantigens, either naturally on tumor cells or by introducing them into cells through genetic engineering. Next, the HLA-I complexes are immunoprecipitated and peptides are eluted and purified.

The HLA-I bound peptides are separated and analyzed by liquid chromatography coupled tandem mass spectrometry (LC-MS/MS), typically in discovery mode (untargeted). The amino acid sequence is usually inferred by matching the mass spectrum into customized databases containing the reference proteome and the antigen of interest. When using tumor cells as starting material, personalized databases are frequently created by integrating next-generation sequencing (NGS) data from patient tumors with the reference proteome to identify peptides derived from private tumor-specific mutations.

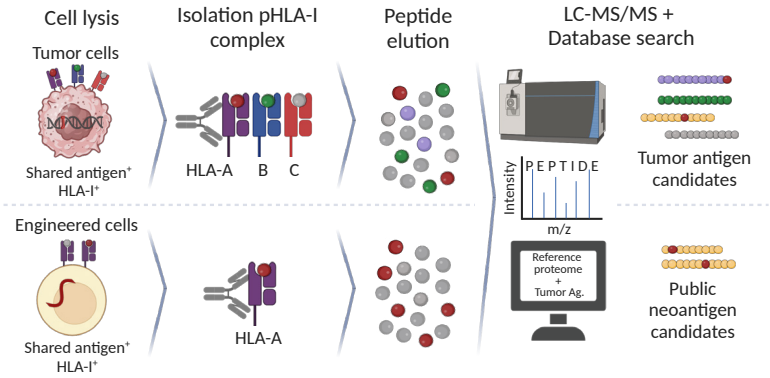


Figure 11. MS-based immunopeptidomics strategy to identify naturally presented HLA-I public neoantigens. Tumor cell lines expressing a shared neoantigen and a prevalent HLA-I allele or engineered cells to express a shared neoantigen together with a single prevalent HLA-I allele, are lysed and homogenized. Following the isolation of pHLA-I complexes by affinity chromatography, the peptides bound to HLA-I molecules are eluted, purified, and analyzed by LC-MS/MS. Next, the amino acid sequence is usually inferred by searching each experimental MS2 spectra to a database containing the reference proteome and the antigens of interest. When working with tumor cells, the database typically contains all tumor-specific AA sequences previously identified by WES or RNAseq. When using engineered cells, the database contains only the AA sequences of the introduced tumor antigens. The candidate public neoantigens identified can be synthesized and tested in functional assays to determine their immunogenic potential. Image created with Biorender.com.

Unlike prediction algorithms, the candidate epitopes identified through mass spectrometry-based (MS-based) immunopeptidomics are truly presented on HLA-I molecules. Still, as mentioned above, the immunogenic potential of these HLA-I ligands needs to be confirmed.

Although identifying neoantigens among the HLA-I ligands remains difficult, immunopeptidomics has successfully detected immunogenic epitopes derived from private (170,174) and shared neoantigens (175) from human tumors. However, the need for tumors to express both the HLA-I alleles and the shared neoantigen of interest makes immunopeptidomics from tumors an impractical approach for rapidly

identifying public neoantigens in a high-throughput manner.

In the last years, the generation of HLA-I monoallelic cells has enabled the study of presented epitopes in a single HLA-I allele of interest (176,177). These cells offer a flexible tool for interrogating the presentation of epitopes derived from the antigens introduced. Indeed, recent immunopeptidomics studies on HLA-I monoallelic cells engineered to express shared neoantigens have enabled the identification of multiple public neoantigens (178–182).

5.2. Isolation of epitope-specific T cells

Once the candidate epitope and HLA-I presenting allele are identified, the next step is to assess their capacity to elicit a T-cell response. Reactive T cells specific to the combinations of interests can be obtained from transgenic mouse models, humans' TIL, or peripheral blood lymphocytes (PBL). Although it is feasible to directly isolate reactive T cells from these sources, enrichment strategies are typically required to capture such infrequent populations.

5.2.1. Sources of reactive T cells

5.2.1.1. Mouse models

T-cell populations with the capacity to recognize epitopes derived from tumor antigens of interest can be obtained after immunization of different transgenic (Tg) mouse models.

Tg mouse models expressing human HLA-I molecules enable the obtention of reactive murine T cells restricted to such HLA-I alleles. Following immunization with a human antigen, murine T cells reactive to epitopes derived from this antigen can be isolated. The use of HLA transgenic mice immunized with tumor antigens has enabled the obtention of murine TCRs targeting carcinoembryonic antigen (CEA) (138) as well as MAGE-A3 (136,143), both of which have shown anti-tumor potential in human clinical trials. Moreover, murine TCRs targeting public neoantigens derived from hotspot mutations in the KRAS gene PIK3CA gene have also been obtained by immunization of these models (180,183).

While TCRs from Tg mouse models can target specific human antigens, their murine origin can be a drawback for clinical use. It has been observed that these

TCRs include immunogenic epitopes that can induce antibody production in treated patients (184) thus, potentially impairing the efficacy of TCR-T cells with such receptors.

To avoid generating TCRs with mouse sequences, humanized mice expressing the entire human TCRαβ genomic loci have been crossed with HLA Tg animals to generate TCR humanized mice (185,186). In these mice, the human TCR is restricted to a particular HLA allele, allowing the generation of fully human TCRs following immunization with tumor antigens. For instance, TCRs against MAGE-A1 (187) or NY-ESO-1 (188) have been obtained from these models and have shown higher functional avidities compared to human TCRs with the same specificity.

5.2.1.2. Human TILs or PBLs

Reactive T cells targeting epitopes derived from tumor antigens can be obtained from the TIL and PBL repertoire of cancer patients expressing the relevant antigen-HLA combination.

Multiple studies have isolated T-cell populations from TILs of patients affected by different cancer types and retrospectively identified their targets (72,189,190), including in some cases public neoantigens (74,75,191). The TIL repertoire contains a higher frequency of antigen-specific T cells because of clonal expansion triggered by antigen encounter in tumor cells. Thus, the TIL repertoire of patients represents a valuable source for directly identifying T-cell responses to the epitopes of interest.

Additionally, reactive T cells to specific epitope-HLA combinations can be directly identified in the blood of cancer patients. Although possible, the large diversity of the T-cell repertoire makes it challenging to detect and isolate such infrequent T-cell reactive populations without prior enrichment.

Despite TILs and PBLs from cancer patients expressing the desired antigen in their tumors are promising sources for capturing antigen-specific T cells, isolating reactive T cells is not always feasible, even using antigen-specific enrichment strategies (192). Alternatively, reactive T cells can be obtained from the naïve repertoire of healthy donor (HD) PBLs. However, effectively isolating these populations requires *in vitro* priming to the antigen and further stimulation to expand reactive T cells.

5.2.2. Enrichment strategies for antigen-specific T-cell populations

Considering the challenges posed by the large diversity of the T-cell repertoire and the need to efficiently isolate neoantigen-specific T cells for capturing reactive TCRs, various strategies have been explored to enrich antigen-specific T cells. These strategies are surface biomarker-based isolation, pHLA-I multimers, and *in vitro* sensitization (IVS) (Figure 12).

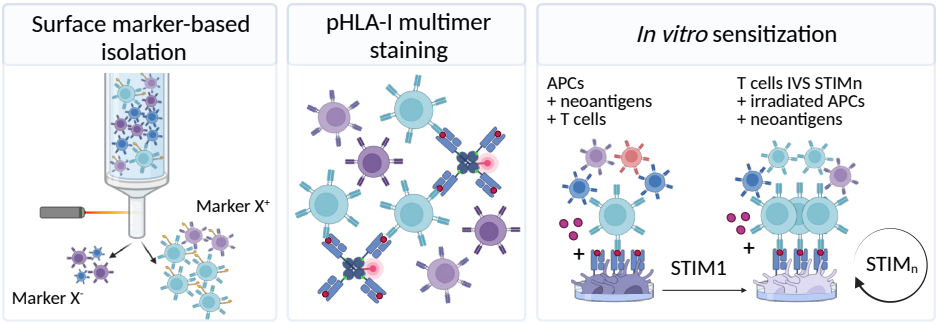


Figure 12. Enrichment strategies to identify public neoantigen-specific T lymphocytes. Three strategies can enrich infrequent neoantigen-specific T cells from different sources. One strategy consists of isolating T-cell subsets from TILs or PBLs of cancer patients based on the expression of surface markers associated with tumor recognition to enrich for neoantigen-specific or tumor-reactive T lymphocytes with undetermined specificity (left). Another strategy uses pHLA-I multimers that can be used to FACS pure neoantigen-specific T cells from different T-cell sources targeting specific epitope-HLA combinations (middle). Last, *in vitro* sensitization consists of the stimulation and expansion of T cells with antigens of interest to generate *de novo* T-cell responses from the naïve compartment when using PBLs from HD or to increase the frequency of infrequent naturally occurring T-cell reactivities from TILs or PBLs of cancer patients (right). Image created with Biorender.com.

5.2.2.1. Biomarker-based isolation

Following the recognition of their targets, T cells upregulate co-stimulatory and co-inhibitory molecules, leading to a different phenotype of antigen-experienced T cells. The isolation of T cells expressing these biomarkers using fluorescence-activated cell sorting (FACS) and subsequent expansion is a strategy to enrich tumor antigen-specific T cells in cancer patients (Figure 12). Isolating TILs with high levels of PD-1 (193–195) or co-expressing PD-1 and the ATPase CD39 (196) or CD39 and the tissue-resident marker CD103 (197) has successfully enriched for tumor-reactive T cells across various cancer types. Similarly, isolating circulating T cells expressing high levels of PD-1 (198,199) has enabled the identification of antigen-specific T cells recognizing tumors from the PBL repertoire of cancer patients.

Isolating T cells with high levels of these markers from PBLs or TILs in patients with the relevant HLA and shared neoantigen can enrich T cells with the desired reactivity. However, biomarker-based isolation alone does not guarantee sufficient enrichment for specific epitope-HLA combinations.

5.2.2.2. pHLA-I multimers

The pHLA-I multimers, which are complexes formed by peptide and HLA-I monomers, enable the specific detection and isolation of pure $CD8^+$ T-cell populations with TCRs that recognize a predefined minimal epitope presented in a particular HLA-I allele (Figure 12).

Typically, pHLA-I multimers are composed of peptide-loaded HLA-I monomers bound to a streptavidin molecule conjugated to a fluorophore. While the common structure involves four HLA-I monomers forming the multimer, various geometries have been designed to enhance TCR interaction. For example, pHLA-I dextramers, where multiple pHLA-I complexes are linked to a dextran backbone, increase multimer valency and improve the detection of T cells with low-affinity TCRs (200).

To facilitate the assessment of diverse epitopes with a given HLA-I multimer, methods such as UV-induced (201) or temperature-induced (202) peptide exchange have been employed. The development of empty stable HLA-I monomers has significantly advanced the flexible creation of custom reagents for T-cell analysis (203). Moreover, the wide variety of available fluorochromes enables the creation of pHLA-I multimers with different HLA-I monomers loaded with distinct peptides, each linked to a different dye. This enables the potential detection of multiple T-cell specificities to different epitope-HLA combinations in a single sample by fluorochrome-based combinatorial encoding using flow cytometry (204,205).

Fluorophore-conjugated multimers have enabled the isolation of reactive T cells to predefined epitope-HLA combinations from TILs and peripheral blood mononuclear cells (PBMCs) in cancer patients through FACS (206,207). Notably, the high sensitivity of pHLA-I multimers has enabled the isolation of reactive T cells to a public neoantigen directly from HD PBLs without prior *in vitro* stimulation (175).

In recent years, the development of pHLA-I multimers linked to DNA barcodes (208) has increased the high-throughput capacity of this technique, facilitating the isolation and subsequent TCR sequencing of multiple antigen-specific T-cell populations at the same time (209).

5.2.2.3. *In vitro* sensitization (IVS)

Antigen-driven *ex vivo* expansion of T cells can be achieved through IVS. This method stimulates antigen-specific T cells from different sources, using APCs and cytokines to promote T-cell expansion over multiple stimulation rounds (Figure 12). IVS can generate *de novo* T-cell responses from the naïve repertoire of PBLs from healthy donors (210) or expand pre-existing T-cell responses in cancer patients (211). Additionally, IVS is used to amplify reactive T-cell populations from transgenic mice post-immunization (180).

There is no standardized method for antigen-specific T-cell sensitization; different sources of APCs, initial T-cell populations, and cytokines can be used. While the first approaches employed tumor cell lines as APCs (212) nowadays, most of the studies use autologous monocyte-derived DCs (192,213,214). Nonetheless, a wide variety of cells, in some cases with modifications to enhance their stimulatory potential, can also be used as APCs (77,215–217).

The typical approach for expanding T cells specific to a predefined epitope-HLA is peptide pulsing of minimal epitopes in donors with the relevant HLA-I allele, either individually (178,179,218) or as peptide pools (181,219). Alternatively, pulsing APCs with long peptides (220–222) or electroporating them with RNA encoding the antigen of interest (211,216,223,224) also enables the expansion of reactive T cells with or without prior definition of the minimal epitope and HLA-I allele.

On the T-cell population side, different sources of T cells have been used for sensitization, including TILs (216,225) or PBLs from cancer patients or HD. When using peripheral blood, some protocols used unfractionated PBMCs (220–222), only CD8+ T cells (179,214) or pre-enriched memory or naïve T-cell subsets expressing specific surface-markers for cancer patients or healthy donors, respectively (75,210,211,226).

T-cell sensitization with antigen-expressing APCs is conducted in the presence of different cytokines cocktails, usually including combinations of IL-2, IL-7, IL-15, IL-12 or IL-21 (221,226). These cytokines are added in the first round of stimulation and replenished in subsequent re-stimulations. APCs are often irradiated in restimulation rounds to prevent proliferation and competition with sensitized T cells. Although variable, at least two consecutive rounds of stimulation, each lasting about 12 days, are generally applied to increase the detection of *de novo* T-cell responses, especially after priming naïve T cells from HD.

After expansion, reactive T cells can be further enriched before TCR sequencing using various methods. One approach involves FACS of T cells that upregulate functional markers such as CD137 (also known as 4-1BB) after functional screenings for antigen recognition. This marker can be useful to capture multiple T-cell reactive populations when IVS has been carried out with pools of epitopes or with antigens for which the epitope-HLA have not been defined. Alternatively, pHLA-I multimers with specific HLA-I and epitopes allow for FACS sorting of pure reactive T-cell populations before TCR sequencing.

5.3. Determination of TCR sequence

Following the isolation of reactive T cells, the next critical step is the sequencing of their TCR. Human T-cell receptors that interact with HLA-I molecules are formed by disulfide-linked α/β heterodimers, with each chain (α and β) comprising a constant and variable domain.

During T-cell development in the thymus, both chains undergo genetic recombination of the variable (V), diversity (D), and joining (J) gene segments for TRB, or solely V and J segments for TRA. With approximately 50V, 2D, and 13J segments for TRB and 70V and 60J segments for TRA, the recombination of these segments alone generates a vast diversity of α and β chains (227). Additionally, random nucleotide additions or deletions in the junctions after segment rearrangement further contribute to the huge diversity in the T-cell receptor repertoire (227). The resulting products from the VDJ or VJ rearrangement and junctional diversity form the variable domains of each TCR chain.

Each variable domain of a TCR chain contains three complementarity-determining regions (CDRs): CDR1, CDR2, and CDR3. CDR1 and CDR2, originating from V segments, engage with HLA-I, whereas CDR3, resulting from the junction of VDJ or VJ segments, exhibits the greatest variability and directly interacts with epitopes within the binding groove (227). Therefore, CDR3 is the critical target region for TCR sequencing, as it determines the antigen specificity.

Bulk or single-cell TCR sequencing (scTCR-seq) are two strategies that can identify the sequences of the variable domains of both TCR chains. Bulk TCR sequencing can capture the diversity of a sample's TCR repertoire, but often it cannot pair α and β sequences, except when using the pairSEQ strategy (228).

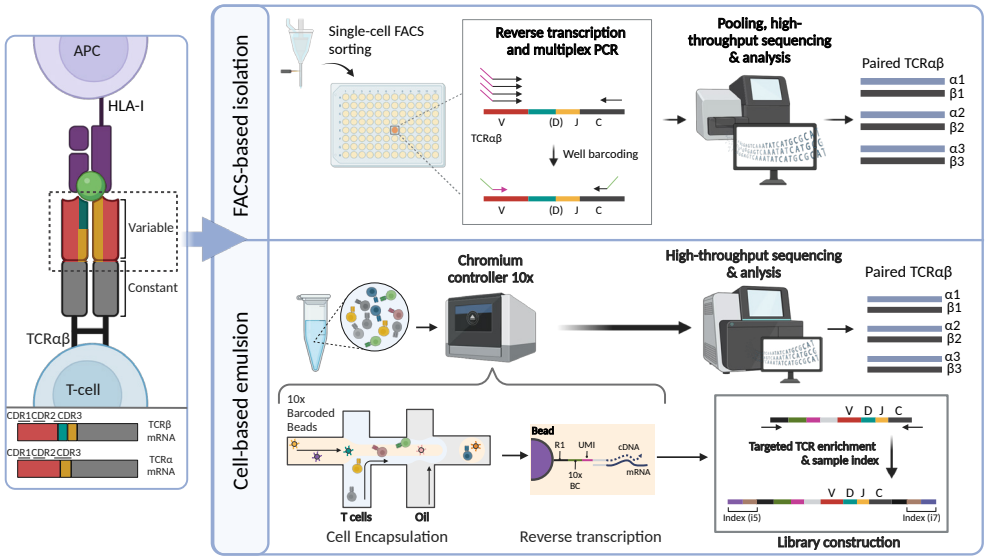


Figure 13. TCR single-cell sequencing (sc-TCR seq) approaches determining TCRαβ pairings. TCRs interacting with pHLA-I complexes are formed by an α and β chain, each consisting of a constant and variable domain (left). The variable domains of both chains include CDR1 and CDR2 (encoded by V segment of α or β) and the CDR3 (encoded by VJ or VDJ segments, incorporating junctional diversity) (bottom left). FACS-based isolation (top panel, right) and cell-based emulsion sc-TCR sequencing (bottom panel, right) are two strategies that can be used to obtain the sequences of both chains forming αβTCRs. To determine the TCR sequences using FACS-based isolation methods, single T cells are sorted by FACS into individual wells. Within each well, TCR transcripts undergo reverse transcription and amplification (reverse transcription and multiplex PCR). Transcripts are tagged with well-specific barcodes (well barcoding). Next, the amplified libraries are pooled and subjected to deep sequencing (pooling and high-throughput sequencing). TCRαβ pairings are computationally determined by analyzing which TCRα and TCRβ sequences share the same well barcode (paired TCRαβ).

Alternatively, the sequences of the TCRαβ can be identified using cell-based emulsion methods pioneered by 10x genomics. First, the chromium 10x controller encapsulates single T cells into oil droplets with 10x barcoded beads (Cell encapsulation). Within droplets and after cell lysis, mRNA is reverse transcribed to cDNA, resulting in barcoded cDNA (containing read 1 (R1), 10x cell barcode (BC), and unique molecular identifier (UMI)). Targeted enrichment of TCRs with specific primers is performed to generate TCR libraries, with sample indexes attached to both the 5' and 3' ends of each transcript. Next-generation sequencing of the libraries, followed by computational analysis using cellular barcodes, determines the TCRαβ pairings corresponding to individual T cells (paired TCRαβ). Adapted from Pai et al., 2021. Image created with BioRender.com.

In contrast, scTCR-seq strategies are currently available to identify the α and β TCR chains simultaneously. One approach involves isolating single T cells into individual wells via FACS sorting, followed by reverse transcription, amplification, and deep sequencing of the TCRα and TCRβ sequences (Figure 13). This strategy has led to the identification of several TCRs targeting hotspot-derived neoantigens of TP53 or KRAS genes from TILs (74,75) or in vitro sensitized PBLs (211,224) from different cancer patients.

Recently developed emulsion-based techniques have significantly advanced the throughput of scTCR-seq and transcriptomic profiling (229,230). This microfluidics technology, pioneered by 10x Genomics, encapsulates single cells in oil droplets with beads containing barcoded oligos, allowing unique molecular barcodes to be added to cDNA from each cell during reverse transcription (Figure 13). After amplification and deep sequencing, this strategy enables the determination of the TCRαβ pairings alongside the entire transcriptome of each cell. In recent reports, the 10x platform has facilitated the identification of TCRs targeting hotspot-derived neoantigens of KRAS, NRAS, and PIK3CA (178,223,231).

Once TCR sequences have been identified, the next step involves prioritizing the identified receptors for functional validation. Clonotypes with higher frequencies are typically selected for further characterization, particularly when sequencing TCRs from enriched T-cell populations. However, this frequency-based selection may overlook other candidate TCRs with lower enrichment levels. To assist in this selection process, various algorithms have emerged to predict TCRs interacting with epitopes, aiming to improve the selection of TCR candidates for downstream testing (232,233).

5.4. Preclinical characterization of candidate TCRs

The preclinical validation of candidate antigen-specific TCRs involves several steps to ensure their specificity, safety, and potency. Only those fulfilling these requirements can be considered for therapeutic use.

To confirm the epitope-HLA specificity of the TCR candidates, they are usually cloned and transferred into PBLs using methods such as lentiviral, retroviral vectors, or CRISPR/Cas9 (reviewed by 234). The TCR-transduced cells are then subjected to functional assays by coculture with APCs expressing the relevant HLA-epitope combination. Upon exposure to antigens, the activation level allows for evaluating the functionality and selecting the TCRs with the most potent reactivity. This is especially important when multiple candidates for a single epitope-HLA combination have been discovered. To further evaluate the potency of the TCRs (235) it is critical to confirm that the cognate target is recognized when processed and presented by endogenous proteins in tumors. Moreover, *in vivo* tumor regression studies in mouse models can assess a TCR candidate's ability to penetrate a tumor mass and cause a sustained anti-tumor response over time.

Additional properties such as TCR binding affinity are typically assessed during the preclinical characterization of therapeutic TCR candidates since it has been correlated with better anti-tumor efficacy in human clinical trials (135,136,150). TCR binding affinity refers to the strength of the interaction between the TCR and the peptide-HLA complex. The kinetics of this interaction can be measured using various approaches, such as the use of different structures of fluorescently labeled pHLA-I complexes (236,237) that measure the TCR-pHLA-I dissociation by flow cytometry. Another method uses two-dimensional structures of APCs presenting the pHLA-I complexes to study fluctuations in the cell membrane while interacting with the TCR (238). Additionally, surface plasmon resonance methods using recombinant soluble TCRs interacting with pHLA-I attached to a sensor surface (239) can measure TCR binding affinity.

On the other hand, an essential requirement before clinical application is to address potential toxicities caused by side effects that could compromise the safety of the therapeutic TCR. Various assays can be used to measure the promiscuity of TCRs in recognizing epitopes-HLA combinations other than the desired one (235).

A crucial aspect to evaluate is their potential cross-reactivity to self-peptides that closely resemble their target epitopes. Defining the TCR motif through amino acid position scanning coupled with in-silico searches of the human proteome (240,241) or screenings with yeast-display peptide-HLA libraries (242), can help to identify epitopes from proteins expressed in vital tissues that could induce unwanted TCR activation, leading to harmful toxicities.

6. Reactive T cells and isolated TCRs targeting public neoantigens

Efforts from various research groups over the last few decades have led to the discovery of HLA-I-restricted T cells targeting public neoantigens and the identification of their TCR sequences in some cases (Table 2). Although the safety and efficacy profiles of certain isolated TCRs have not been fully assessed, these receptors hold potential as promising therapeutic candidates for off-the-shelf TCR-based T-cell therapies.

An updated list in Table 2 summarizes the detection of reactive T cells and TCRs targeting public neoantigens, classified by their identification method as reported in the literature. Of note, many TCRs targeting public neoantigens have been discovered without predefining the minimal epitope-HLA restriction element. In most cases, these receptors were isolated from TILs of cancer patients without enrichment strategies. This highlights the higher frequency of antigen-reactive T cells in TILs than in other T-cell sources. Nonetheless, a few TCRs have also been discovered in the blood of patients or healthy donors through IVS without predefining the targeted epitope-HLA combination. As previously mentioned, two TCRs targeting $KRAS_{p.G12D}$ (152) and $TP53_{p.R175H}$ (153), isolated from patients, have already been used for TCR-T ACT and have shown encouraging responses in case reports. Furthermore, these receptors and other TCRs targeting a public neoantigen derived from $KRAS_{p.G12V}$ are currently being tested in clinical trials.

Strategies predefining the epitope-HLA target combinations by prediction algorithms or MS-based immunopeptidomics have also identified T cells targeting public neoantigens. While most of the TCRs discovered through these strategies are of human origin, murine TCRs have also been described.

In fact, the safety and efficacy of ACT of TCR-T cells bearing murine receptors targeting neoantigens derived from $KRAS_{p.G12D}$ and $KRAS_{p.G12V}$ are currently being investigated in clinical trials.

In recent years, screening HLA-I monoallelic cells using MS-based immunopeptidomics combined with IVS of HD PBLs has substantially expanded the list of experimentally validated immunogenic public neoantigens. One study focused on the KRAS gene (178) detected T cells recognizing 14 peptides presented on several prevalent HLA-I alleles from three distinct mutations. However, the TCR sequences for all these T cells have not been published (Table 2). This combined method has emerged as a potent strategy to identify new public neoantigens in a high-throughput and prospective manner.

Indeed, MS-based screenings on HLA-I monoallelic cells have enabled the identification of presented epitopes derived from different shared neoantigens, although reactive T cells have not yet been detected. Most of these studies primarily focused on identifying public neoantigens derived from different hotspot mutations in KRAS (178,179,182,252), but only a few have expanded their focus to other specific driver genes, such as NRAS (182,231) or PIK3CA (180,223). However, in a very recent report, Gurung and colleagues have exploited the high-throughput capacity of such an approach to identify HLA-I-presented epitopes derived from a broader selection of shared neoantigens. More specifically, they evaluated 36 shared neoantigens resulting from hotspot mutations in different driver genes across 12 highly prevalent HLA-I alleles in the Caucasian population (181).

Table 2. Summary of HLA-I-restricted T cells and TCRs targeting public neoantigens.

Predefined epitope-HLA	T-cell source	Shared neoantigen	HLA-I restriction	Reference	Used for TCR-T ACT
No	Cancer patient (TIL/PBL)	$KRAS_{p.G12D}$	C*08:02	76 ; 191	152 NCT06218914
			C*01:02	243	-
			A*11:01	211	
			A*02:01	244	
		$KRAS_{p.G12V}$	A*02:01	244	-
			A*11:01	211 ; 243	NCT04146298 NCT06105021
		$TP53_{p.Y220C}$	A*02:01	153	-
		$TP53_{p.Y220D}$			
		$TP53_{p.R175H}$		75 ; 224	153 NCT05877599
				245	
		$TP53_{p.R248W}$	A*68:01	75	-
		$CDK4_{p.R24C}$	A*02:01	246	-
		TGFBR2 fs		247	-
	Cancer patient (TIL/PBL) & HD PBLs	$NRAS_{p.Q61R}$	A*01:01	248	-
		$PIK3CA_{p.H1047L}$	A*03:01	223	-
Prediction algorithm	Cancer patient & HD PBLs	$BRAF_{p.V600E}$	A*02:01	249	-
			B*27:02	250	
	Tg mouse	$KRAS_{p.G12D}$	A*11:01	183	NCT03745326 NCT05438667
		$KRAS_{p.G12V}$		183 ; 251	NCT05438667 NCT03190941 NCT06043713
MS IP AML tumors	HD PBLs	NMP1fs	A*02:01	175	-
MS IP HLA-I monoallelic	Cancer patients (TIL)	$NRAS_{p.Q61K}$	A*01:01	231	-
	HD PBLs	$KRAS_{p.G12V}$	A*03:01	178 ; 179	-
			A*11:01		
			A*68:01	178	
			C*01:02		
		$KRAS_{p.G12D}$	A*03:01	178	-
			A*11:01		
			A*68:01		
			B*07:02		
			C*03:04		
			C*08:02		
		$KRAS_{p.G12R}$	B*07:02	179	-
			A*03:01	178	
			A*11:01		
			A*68:01		
			B*07:02		
		$FLT3_{p.D835Y}$	A*02:01	181	-
		$PIK3CA_{p.E545K}$	A*11:01		
	Tg mouse	$EGFR_{p.L858R}$	A*03:01	180	-
		$BRAF_{p.V600E}$			
		$KRAS_{p.G12V}$			
		$EGFR_{p.L858R}$	A*11:01		
		$BRAF_{p.V600E}$			
		$PIK3CA_{p.E545K}$			
		$KRAS_{p.G13D}$			

MS IP: Mass spectrometry-based immunopeptidomics; AML: Acute Myeloid Leukemia;TCR-T ACT: Adoptive T-cell transfer of TCR-engineered T cells.

The table groups T-cell populations and TCRs based on their specificity for public neoantigens. It outlines the method for predefining the epitope-HLA targeted combination and specifies the T cell source. The specific shared neoantigen and the corresponding HLA-I restriction element for the isolated reactive T-cell populations are identified. Cells highlighted in grey indicate reactive T cells restricted to specific public neoantigens and HLAs, which have been detected but whose TCR sequences have not been reported. References are provided for reports identifying the reactive HLA-I-restricted T-cell populations to epitopes derived from the listed shared neoantigens. TCRs used for ACT of TCR-T for cancer patient treatment are documented with the clinical trial codes or article references.

Although this thesis focuses on HLA-I-restricted TCRs, it is worth mentioning that several HLA-II-restricted TCRs recognizing public neoantigens presented in highly prevalent HLA-II alleles have also been described. These include TCRs targeting neoepitopes from various hotspot mutations of the KRAS gene (211,243,253–255) or the TP53 gene (74,75,153,224). Additionally, TCRs specific for other public neoantigens, such as those derived from $BRAF_{p.V600E}$ (256), $IDH1_{p.R132H}$ (257), or $PIK3CA_{p.H1047R}$ (253) have also been discovered. Despite none of these TCR candidates currently being investigated as therapeutic candidates for TCR-T ACT, they may be useful for treating HLA-II-expressing tumors or in combination with HLA-I restricted TCR-T to provide help, potentially mediating longer and more potent anti-tumor responses.

The improved sensitivity of DNA sequencing techniques, combined with comprehensive bioinformatic methods, has helped to identify recurring mutations in hotspot regions of cancer-wide driver genes as well as cancer-specific driver genes (258–260). Leveraging shared neoantigens from these mutations as T-cell targets presents a promising avenue for treating a broad range of cancer patients. Therefore, a comprehensive analysis of the presentation of neoepitopes derived from these recurrent mutations on multiple prevalent HLAs can vastly increase the actionable targets available for cancer treatment.

Hypothesis and Objectives

Effectively identifying and harnessing cancer antigens that induce potent immune recognition is critical for the success of cancer immunotherapy. While private neoantigen-targeted adoptive T-cell therapies have shown promising efficacy, such tailored products are expensive and limited to a single patient. Shared neoantigens presented on prevalent HLA-I alleles offer promising targets for T cells, potentially expanding the number of patients that can be treated. However, only a small fraction of shared immunogenic antigens has been reported thus far.

We hypothesize that:

1. Extensive mass spectrometry screenings of purified peptide-HLA complexes from cells expressing cancer driver genes and highly frequent HLA-I alleles may broaden the landscape of targetable public neoantigens.
2. Some of the identified candidate neoantigens are immunogenic and can be targeted therapeutically through the isolation of neoantigen-specific TCRs and the development of gene-engineered T-cell therapies.

The **overall objective** of this thesis is:

To identify hotspot-derived mutant peptides presented on highly frequent HLA-I alleles through immunopeptidomics and detect and characterize TCRs targeting them to develop novel off-the-shelf T-cell therapies targeting public neoantigens.

The **specific objectives** are the following:

1. Develop an immunopeptidomics-based method to study the presentation of peptides derived from shared mutations in driver genes on highly prevalent HLA-I alleles.
    1.1. Identify and prioritize the most frequent HLA-I alleles in the European Caucasian population, as well as recurrent alterations affecting cancer driver genes for the construction of hotspot tandem minigenes (HSTMG).
    1.2. Establish a high-throughput system to investigate the presentation of peptides derived from mutations of interest on specific HLA-I molecules via immunopeptidomics.

1.3. Examine and validate the presentation of mutant peptides derived from alterations in hotspot regions of key cancer genes.

2. Isolate and characterize reactive TCRs targeting hotspot mutations for their potential use as off-the-shelf T-cell therapies.

   2.1. Detect T-cell responses against hotspot-derived neoantigens in peripheral blood lymphocytes (PBL) from a cancer patient through *in vitro* sensitization.

   2.2. Clone and express candidate mutation-reactive TCRs in PBL via genetic modification.

   2.3. Study the avidity of TCR-transduced T cells for their cognate neoantigen as well as tumor recognition *in vitro*.

Materials and methods

Patient samples

Patient samples were obtained as part of a project PR(AG)23/2019 approved by the Institutional Review Board at Vall d'Hebron Hospital and/or Hospital Universitari Bellvitge. All patients signed the corresponding informed consent. Buffy coats from healthy donor (HD) blood were supplied by the Blood and Tissue Banc of Catalonia (BST, www.bst.cat).

Establishment of patient-derived tumor cell line (TCL)

A small fragment (2-4 mm^3) of tumor biopsies or surgically resected tumor was cultured in RPMI 1640 plus (Lonza) containing 10% FBS Hyclone (GE Healthcare), 100 U/mL penicillin (Lonza), 100 µg/mL streptomycin (Lonza) and 25 mM HEPES (Thermo Fisher Scientific) at 37°C in 5% CO_2 humidified incubators. The culture medium was replaced once a month until the first cell colonies were identified and selected and then further expanded in T2 media containing RPMI 1640 plus (Lonza), 10%-20% FBS (Gibco), depending on the TCL, 100 U/mL penicillin (Lonza), 100 µg/mL streptomycin (Lonza) and 25 mM HEPES (Thermo Fisher Scientific) or cryopreserved until used. TCL cultures were regularly tested for mycoplasma and authenticated by identifying patient-specific somatic mutations and HLA molecules using exome sequencing.

PBMC isolation

Peripheral blood mononuclear cells (PBMC) were separated by centrifugation in a Ficoll density gradient (Lymphoprep, Stem cell) from leukapheresis or from whole blood. Cell aliquots were cryopreserved with FCS/DMSO 10% for later expansion of B cells or IVS or kept as dry pellets at -80ºC for DNA extraction for whole exome sequencing (WES) or Next-generation sequencing (NGS).

Whole exome and RNA sequencing

To identify the tumor-specific non-synonymous somatic mutations (NSM), genomic DNA was purified from either tumoral cell pellets or from the patient-derived TCL and from matched PBMC as a source of germline DNA using Allprep DNA/RNA mini kit (Qiagen, Germany). WES libraries were generated at the company Macrogen by exome capture of approximately 20,000 coding genes using "SureSelect human All exon V6" kit (Agilent Technologies) and paired-end sequenced on a HiSeq sequencer (Illumina). The average sequencing depth ranged from 100-150 for each of the individual libraries generated. Alignments of WES to the reference human genome

build hg19 were performed using novoalign MPI from Novocraft (http://www.novocraft.com/). Duplicates were marked using Picard's MarkDuplicates tool (picard/releases/tag/1.127). Insertion and deletion (indel) realignment and base recalibration were performed according to GATK best-practices (https://www.broadinstitute.org/gatk/). SAMtools was used to create tumor and normal pileup files.

mRNA sequencing libraries were prepared from total RNA obtained from either tumor biopsy or patient-derived TCL using TruSeq RNA library prep kit (Macrogen). The RNA sequences were aligned to the human genome using STAR (PMID: 23104886), and the Transcripts per Kilobase Million (TPM) were calculated with feature Counts (PMID: 24227677).

Four independent mutation callers software packages (Varscan, SomaticSniper, Mutect and Strelka) were used to call somatic NSM from WES data of patients according to the following criteria: minimum coverage of 10 reads, minimum 4 variant reads, greater than 7% Variant allele frequency (VAF) and called by 2 or more callers for SNVs or one for indels and annotated as coding mutation in two of the three annotation data sets (RefGene, UCSC, Ensmbl). The genomic coordinates from variant call format files containing tumor-specific mutations were converted from hg19 to hg38 assemblies.

Tandem Minigenes construction, cloning, in vitro transcription of RNA and electroporation

The four tandem minigenes encoding for hotspot mutations (HSTMG) were constructed as previously described (116) generating HSTMG-1 to HSTMG-4. Briefly, for each non-synonymous variant of interest, we constructed a "minigene", consisting of the mutant amino acid flanked by 12 amino acids of the wild-type protein sequence. Up to 25 minigenes, including some derived from private mutations of cancer patients, were concatenated to generate an HSTMG construct. Fused to the 3' terminus of the concatenated minigenes a BamHI site was included for downstream cloning. Immediately after the restriction site, a P2A sequence and ZsGreen protein were added to act as a reporter of the transfection efficiency of these constructs.

For each of the HSTMG1-4, we also generated constructs encoding the same minigenes with the wild-type sequence, resulting in the generation of HSTMG1-4 WT plasmids. All HSTMG constructs, mutant and wild-type forms, were codon optimized and subcloned cloned into pcDNA3.1+ using HindIII and EcoRI.

B2M_HLA chimeras were constructed as previously reported (261) with some modifications. Briefly, the human B2M coding sequence, including the leader peptide, was

directly fused in the 3' terminus to a short tandem GS linker (15AA in total) followed by the sequence of the HLA-I allele of interest without the signal peptide. Allele sequences were obtained from IPD-IMGT/HLA. Alternatively, the HLA-I sequences of interest, including the signal peptide, from IPD-IMGT/HLA were selected for further cloning. B2M_HLA chimeras or the alpha chain of HLA-I alleles were codon optimized and subcloned cloned into pcDNA3.1+ containing a Kozak motif upstream of the start codon either using BamHI and EcoRI or HindIII and NotI, respectively.

Sequences for full-length PIK3CA and TP53 wild-type proteins were obtained from NCBI. To generate mutant full-length proteins, the codons corresponding to the residues of interest were manually mutated to introduce the desired amino acid. After codon optimization full-length proteins, either mutant or wild-type, were cloned into pcDNA3.1+v2, which already includes the P2A and ZsGreen sequences, with HindIII and BamHI.

Oligonucleotides encoding for all the constructs described were supplied by GenScript Biotech (Rijswijk, Netherlands). For in vitro transcription (IVT) of RNA the plasmids were linearized beforehand with Not-I (New England Biolabs) followed by phenol-chloroform extraction and precipitation with sodium acetate and ethanol. Next, 1 μg of linear DNA was used as a template to generate RNA by IVT using HiScribe# T7 ARCA mRNA Kit with tailing (New England) following manufacturer's instructions. RNA was precipitated using $LiCl_2$, resuspended at 1 μg/μL in molecular grade H_2O, and stored at -80º until use.

For co-culture experiments, from 0.5-5x10^6 B cells or TCL were harvested and resuspended in 100μl of Opti-MEM media (Gibco) and transferred into a sterile 0.2 cm cuvette (VWR electroporation cuvettes). From 6 to 9 μg of RNA encoding for the sequence of interest were added for electroporation. For the B cells to be used for MS-based immunopeptidomics, 1.5x10^7 cells were resuspended in 150 μl Opti-MEM and electroporated with 12 μg of RNA encoding for HSTMG1-3 into sterile 0.2 cm cuvette. To generate transfectants with B2M KO cells, 2x10^7 tumor cells were resuspended in 150 μl Opti-MEM and electroporated with 12 μg of RNA encoding for B2M_HLA chimera and/or 18 μg of RNA encoding for HSTMG1-4 into sterile 0.2 cm cuvette. For the generation of B2M transfectants to be used for MS-based immunopeptidomics, several electroporations were performed until generating 6-8x10^7 total cells per combination.

The electroporation conditions applied to all the cells used in the subsequent experiments, were 150 V, 20 ms, and 1 pulse using an ECM 830 BTX-Electroporator. After electroporation, cells were resuspended in their corresponding pre-warmed specific media containing DNAse (Pulmozyme, Roche). TCL and B cells for co-

culture experiments were cultured in tissue-treated 6 well plates or 5ml polystyrene tubes, respectively. For B2M KO transfectants and B cells to be used in MS-based immunopeptidomics experiments, cells were cultured in in tissue-treated p150 or 24 well plates, respectively.

After 20h culture at 37°C and 5% CO_2 cells were harvested, washed with PBS, and used in co-culture assays. For B2M KO transfectants and HSTMG-expressing B cells, transfection efficiency was assessed by flow cytometry. The efficiency of transfection for HSTMG and the B2M_HLA chimeras was measured by flow cytometry taking advantage of the ZsGreen (ZSG) reporter in the HSTMG or measuring HLA class I expression using a Pan-HLA-I antibody (HLA-ABC antibody, Table 3) respectively. Only transfected cell preparations in which >65% of cells express both markers were preserved and snap-frozen to generate pellets for HLA-I elution.

Generation of autologous B cells

To generate autologous antigen-presenting cells (APC), B cells were isolated from cryopreserved PBMC by positive selection using $CD19^+$ microbeads (Miltenyi Biotec). These primary B cells were expanded through CD40-CD40L stimulation by culturing cells for 4-5 days with irradiated NIH3T3 feeder cells constitutively expressing CD40L at 37ºC in 5% CO_2 in B cell medium (Iscove's IMDM media (Gibco) containing 10% human AB serum (Biowest), 100 U/mL penicillin (Lonza), 100ug/mL streptomycin (Lonza), 2mM L-Glutamine (Lonza) and supplemented with 200 U/mL IL-4 (Prepotech)). Up to three rounds of stimulation and expansion were performed consecutively. At day 5-6, B cells were either used for generation of snap-frozen pellets for HLA-I immunopeptidomics, used in co-culture experiments or cryopreserved until use. When used after cryopreservation, B cells were thawed in B cell medium containing DNAse (Pulmozyme, Roche) 20h before use in co-culture assays.

For some experiments, immortalized B cells were used as targets. Briefly, $CD19^+$ cells were cultured with irradiated NIH3T3 feeder cells constitutively expressing CD40L in immortalized B cell medium (Iscove's IMDM media (Gibco) containing 10% FBS, 100 U/mL penicillin (Lonza), 100ug/mL streptomycin (Lonza) and supplemented with IL-21 (25 ng/mL ,Prepotech)). On day 5, B cells were transferred onto retronectin-coated plates and transduced with concentrated supernatants containing retroviruses carrying a plasmid encoding the Bcl6-T2A-BclXL-P2A-tNGFR construct. From the day of transduction, B cells were stimulated every five days with irradiated NIH3T3 cells and fresh immortal B cell medium containing IL-21 (25ng/mL). The immortalized phenotype was monitored by flow cytometry using the anti-NGFR-APC (Clone:

ME20.4; BioLegend; Dilution: 1:1000) to measure the NGFR reporter present in the plasmid used for transformation and anti-CD19-PECy7 antibody (Clone: SJ25C1; Biolegend; Dilution: 1:1000). B cells, either freshly stimulated or after cryopreservation, were employed for co-culture experiments. When used after cryopreservation, B cells were thawed in immortalized B cell medium containing DNAse (Pulmozyme, Roche) at least 20h before use.

CRISPR/Cas9 Knockout

Single guide RNA (sgRNA) targeting the human B2M gene were designed with three online tools (ccTOP, CHOPCHOP, Synthego CRISPR designer tool). The selected sgRNA combined the best scores in terms of predicted knockout (KO) efficiency and reduced off-targets by the three tools. The sgRNA was obtained from Synthego.

To inactivate the B2M gene in tumor cells, the whole ribonucleoprotein (RNP) complex was electroporated. To allow formation of the RNP complex, 100μM of sgRNA and 62μM of Cas9 (IDT) were incubated in presence of PBS for 20min RT. Tumor cells used for transfection were harvested, washed and resuspended in supplemented nucleofection solution (P3 primary cells solution; Lonza). Tumor cells were mixed with the RNP complex solution and then transferred to 0.2cm electroporation cuvettes and electroporated at 150V, 20ms, 1 pulse (BTX Square electroporator). Immediately after electroporation, cells were transferred to pre-warmed T2 media.

To obtain a pure population of B2M KO cells, four days after electroporation cells were stained for HLA class I with Pan-HLA-I antibody (HLA-ABC antibody, Table 3) and sorted by flow cytometry selecting HLA-I negative cells. The negative fraction was expanded in culture with T2 media until establishing the B2M KO cell line. Negative HLA-I surface expression was regularly tested by flow cytometry.

Flow cytometric analysis and fluorescence-activated cell sorting

To measure cell surface expression of HLA-I in tumoral cells, or induction of T-cell responses after IVS through HLA dextramer staining or co-culture assays several human-specific antibodies were employed in different extracellular panels. A list of antibodies used, and their applications are given in Table 3.

In all experiments, cells were stained for 30min at 4ºC, washed and resuspended in staining buffer containing either PI (1:1000) or DAPI (1:1000) and acquired in BD FACSCanto™ or BD FACSCelesta™.

Table 3. List of antibodies employed for phenotyping and fluorescence-activated cell sorting (FACS).

Target	Clone	Conjugate	Supplier and catalog number	Applications
HLA-ABC	APC	W6/32	BioLegend, 311410	HLA-I phenotyping & FACS
B2M	APC	2M2	BioLegend, 316311	HLA-I phenotyping
HLA-A2	APC	BB7.2	Invitrogen, 17-9876-42	HLA-I phenotyping
HLA-A3	PE	GAP.A3	BD Biosciences, 566605	HLA-I phenotyping
HLA-B	PE	YTH 76.3.rMAb	BD Biosciences, 567211	HLA-I phenotyping
HLA-B7	PE	BB7.1	BioLegend, 372403	HLA-I phenotyping
HLA-C	PE	DT-9	BD Biosciences, 566372	HLA-I phenotyping
B2M	PE	BBM.1	Santa Cruz, sc-13565	Dextramer folding
CD3	APC-H7	SK7	BD Biosciences, 557851	Co-culture; Dextramer staining & FACS
CD4	BV510	SK3	BioLegend, 344534	Dextramer staining & FACS
CD4	PE	RPA-T4	BD Biosciences, 555347	Co-culture
CD8	PECy7	SK1	BD Biosciences, 557746	Co-culture; Dextramer staining & FACS
4-1BB	APC	4B4-1	BioLegend, 550890	Co-culture & FACS
OX40	PE-CF954	ACT35	BD Biosciences, 563662	Co-culture
moTCR-β	PE	H57-597	Invitrogen, 11-5961_85	Co-culture

Protein analysis

Cell samples from $5x10^6$ cells were homogenized in basal complete homogeneization buffer (50mM TrisHCl pH 7.5, 150mM NaCl, 1mM EDTA and 1% Triton) supplemented with 50X Complete Proteinase Inhibitor (Roche) and Complete Phosphatase Inhibitor cocktail 3 (Sigma Aldrich) by three rounds of incubation for 10min on ice and vortex. The homogenate was centrifuged at 15000 rpm for 15 min at 4 °C and the amount of proteins in the supernatant was quantified using a commercially available Pierce BCA protein assay (Thermofisher).

For analysis of B2M and HLA-I on B2M KO cells, 60ug of total protein per sample were loaded in 15% acrylamide SDS-PAGE gel whereas for analysis of the catalytic subunits of the proteasome and TAP proteins in B2M KO cells, 20ug of total protein per sample were loaded in 12% acrylamide SDS-PAGE gel. Immunoblot analysis were performed according to standard procedures. Membranes were incubated with the primary antibodies described in Table 4 overnight at 4ºC and then washed three times with TBS-Tween and incubated for 1h with the corresponding secondary antibodies. Membranes were incubated in ECL Prime Western blotting detection Reagents (Cytiva RPN2232) for 2min and analyzed using iBright 1500 CL (Thermofisher).

Table 4. Antibodies used for immunoblotting analysis.

Antibody	Isotype	Reference	Dilution
Anti-Human B2M (EP2978Y)	Rabbit, IgG	Abcam, ab75853	1:5000
Human MHC-I W6/32	Mouse, IgG2a	Santa Cruz, sc-32235	1:500
Anti-human/mouse B-Actin	Mouse, IgG1	Santa Cruz, sc-47778	1:2000
Anti-Human 20S proteasome B1 subunit (PSMB6)	Mouse, IgG1	Enzo Life Science, BML-PW8140	1:1000
Anti-Human 20S proteasome B2 subunit (PSMB7)	Mouse, IgG1	Enzo Life Science, BML-PW9300	1:1000
Anti-Human 20S proteasome B5 subunit (PSMB5)	Rabbit, Polyclonal IgG	Abcam, ab3330	1:1000
Anti-Human 20S proteasome B1i subunit (LMP2)	Rabbit, Polyclonal IgG	Abcam, ab3328	1:1000
Anti-Human 20S proteasome B2i subunit (MECL-1)	Goat, Polyclonal IgG	Invitrogen, PA5-19146	1:1000
Anti-Human 20S proteasome B5i subunit (LMP7)	Mouse, IgG1	Santa Cruz, sc-365699	1:1000
Anti-Human TAP1	Rabbit, Polyclonal IgG	Proteintech, 11114-1-AP	1:1000
Anti-Human TAP2	Rabbit, IgG	Cell Signaling, 25657	1:1000
Anti-human/mouse B-Actin	Mouse, IgG1	Santa Cruz, sc-47778	1:2000
anti-mouse HRP	Mouse, IgG	Cell signaling, #7076	1:5000
Anti-rabbit HRP	Rabbit, IgG	Cell signaling, #7074	1:5000
Anti-goat HRP	Goat, IgG	Thermofisher, 31402	1:5000

Purification of HLA-I peptides

Purified anti-HLA-I clone W6/32 (ATCC® HB95) antibodies were cross-linked to protein-A Sepharose 4B conjugated beads (Invitrogen) with dimethyl pimelimidate dihydrochloride (Sigma-Aldrich) in 0.2 M Sodium Borate buffer pH 9 (Applichem). Stable cross-link of W6/32 to Sepharose beads was assessed by SDS-PAGE and Coomassie staining before use for HLA-I purification.

Snap-frozen pellets of $1.5x10^7$ electroporated B cells, $6x10^7$ to $8x10^7$ B2M KO transfectants or $1x10^8$ to $3x10^8$ patient-derived TCL were thawed and lysed with PBS containing 0.6% CHAPS (Applichem) and Protease inhibitor Cocktail Complete (Roche). The cell lysates were sonicated (Misonix 3000) and cleared by centrifugation for 1 h at 15000g to obtain the soluble fraction containing the pHLA-I complexes.

HLA-I affinity chromatography was performed using a 96-well single-use micro-plate with 3 µm glass fiber and 10 µm polypropylene membranes (Agilent) as previously described (262). Ultra-Micro SpinColumn C18 (Harvard Apparatus) were used for peptide purification and concentration following manufacturer instructions. Peptides were eluted with 500 µl of 32,5% ACN in 0.1% TFA and preserved immediately with liquid N_2. HLA-I alpha chain and B2M were recovered from C18 tips using 80%ACN 0.1% TFA. Before LC-MS/MS acquisition, peptide samples were lyophilized and the efficiency of the pull-down protocol of HLA-I was measured by immunoblot analysis of B2M protein from the 80% ACN 0.1% TFA eluate fraction.

LC-MS/MS acquisition

Purified HLA-I peptides were diluted in 3%ACN, 1% FA. Samples were analyzed using a Orbitrap Eclipse™ mass spectrometer (Thermo Fisher Scientific, San Jose, CA, USA) coupled to an EASY-nLC 1200 (Thermo Fisher Scientific (Proxeon), Odense, Denmark). A 45% of each of the generated samples was injected and analyzed in a single run. Peptides were loaded directly onto the analytical column and were separated by reversed-phase chromatography using a 50-cm column with an inner diameter of 75 µm, packed with 2 µm C18 particles spectrometer (Thermo Scientific, San Jose, CA, USA). Chromatographic gradients started at 95% buffer A (0.1% FA in water) and 5% buffer B (0.1% FA in 80% ACN) with a flow rate of 300 nl/min and gradually increased to 25% buffer B in 79 min, and then to 40% buffer B in 11 min. After each analysis, the column was washed for 10 min with 100% buffer B.

The mass spectrometer was operated in positive ionization mode with nanospray voltage set at 2.4 kV and source temperature at 305°C. The acquisition was performed in data-dependent acquisition mode and full MS scans at resolution of 120,000 were used over a mass range of 400-650 m/z with detection in the Orbitrap mass analyzer. Auto gain control (AGC) was set to 1E6 and injection time to 50 msec. In each cycle of data-dependent acquisition analysis, following each survey scan, the most intense ions above a threshold ion count of 5000 were selected for fragmentation with a dynamic exclusion of 10 sec. Fragment ion spectra were produced via collision-induced dissociation at a normalized collision energy of 35% and they were acquired in the Orbitrap mass analyzer at 30,000 resolution. The quadrupole isolation window was set to 1.4 m/z, AGC was set to 15E4, and the maximum injection time to 150 msec. The maximum cycle time was set to 3 seconds.

Mass spectrometry data analysis of HLA-I peptides

To identify HLA-I ligands derived from HSTMG constructs, PEAKS Xpro software (Bioinformatics Solutions, Inc) was used to interpret mass-spectra obtained from liquid chromatography-tandem mass spectrometry (LC-MS/MS) acquisition of purified HLA-I peptides from B cells or B2M KO transfectants.

All spectra from the different samples were searched using a custom database containing the human proteome (Swissprot, downloaded 21/05/2021, 20395 entries) and the full sequence of the HSTMGs (HSTMG1-3 for B cells and HSTMG1-4 for B2M KO transfectants). Additionally, the database applied to for B2M KO transfectants included all the identified NSM from VHIO-08 TCL as independent 25-mer minigenes (2427 entries). Moreover, a customized list of common contaminants in immunopeptidomics (CRAP and MaxQuant, 338 entries) was used to filter out peptide spectrum matches (PSMs) to these sequences. All database searches were performed under a no-enzyme and an unspecific digestion mode, with oxidized methionine and cysteinylation as variable modifications. A precursor mass tolerance of ± 5 ppm and a fragment ion of 0.02Da were used for HLA-peptide datasets. PSMs were automatically designated and assigned to each sample and the False Discovery Rate (FDR) was estimated with decoy-fusion by PEAKS Xpro.

Unique PSM with the highest -10lgP were retained for each sample. To count unique peptide sequences per sample, identifications with variable modifications were counted only once. All identified matches to HSTMG constructs were categorized into mutated (peptide sequence containing the mutant amino acid), wild-type (peptide sequence containing the reference sequence) or artificial junction (peptide sequence

derived from the junction of two minigenes). Additionally, peptides mapping to P2A or ZsGreen reporter of HSTMG plasmids were identified. Peptides not mapping to HSTMG sequences were categorized as endogenous. The detected HLA-I mutant ligands were further classified as shared (when originating from recurrent alterations on driver genes) or patient-specific neoantigens (when originating from private mutations of cancer patients included in HSTMGs). All the analyses were performed with R studio and the FDR was set at 1%.

HLA-I typing and prediction of binding to selected HLA alleles

HLA-I typing from patients was inferred from the WES data using the PHLAT algorithm (PMID 29858810). For patients VHIO-133, VHIO-153 and MBM, the HLA-I genotype was determined at high-resolution by NGS at the EFIS accredited HLA laboratory of BST.

Eluted ligand likelihood (ELL) percentile rank scores for binding to the HLA alleles were obtained for all unique peptides above eight amino acids eluted from B cells or HLA-I monoallelic cell lines using NetMHCpan 4.1. Additionally, NetMHCpan 4.1 was used to predict peptide binders in HLA molecules of interest, either from 25-mer minigenes or from the full-length HSTMG sequences. The threshold for binding was set to <2%-tile EL rank.

GibbsCluster 2.0 software was used to cluster all unique peptides of 9 amino acids eluted from B cells or monoallelic cell lines. The software was run with default settings to group peptides into one or up to six clusters for HLA-I monoallelic cells or B cells, respectively, based on their similarity. Subsequently, the resulting clusters were compared to the binding motif of the corresponding HLA-I obtained from NetMHCPan4.1 using naturally presented ligands (EL).

Peptide synthesis and peptide pulsing

The amino acid sequences of selected HLA-I ligands were purchased from Thermo Fisher Scientific as crude (PePotec grade 3) with one stable isotope-labeled amino acid and used for PRM validation (see Appendix Figure 6).

The same peptide sequences without modifications were purchased from JPT Peptide Technologies as high-performance liquid chromatography (HPLC)-purified peptides (>95% purity) and used for *in vitro* sensitization.

The HPLC CEF peptide pool (ProMix™), containing 32 epitopes from CMV, EBV and Flu, was used as a positive control for IVS.

The amino acid sequences of 25-mer peptides, each including one shared NSM of a driver gene encoded in HSTMGs were purchased from Genscript at crude grade and used for pulsing B cells employed in co-culture experiments.

Target cells used in co-cultures (either B cells or tumor cells) were harvested, washed, and resuspended at $2x10^6$ to $5x10^6$ cells/mL in their corresponding media with peptides at concentrations of 5μg/mL or 1 μg/mL for long peptides (25-mers) and minimal epitopes, respectively. Long peptides, which require the processing of cell proteases, were pulsed overnight while minimal epitopes were only pulsed for 2h. After pulsing, cells were washed with PBS and immediately used in co-culture assays.

Validation of HLA-I peptides with isotope-labeled peptides

For each selected peptide tested, an equivalent synthetic peptide isotope-labeled at one given amino acid was spiked into each sample and used as an internal standard for Parallel Reaction Monitoring (PRM) detection. The amount of internal standard peptide to be spiked in each sample was evaluated using dilution curves and the final concentration was chosen based on a good chromatographic signal and no trace detectable of potential unlabeled traces from the synthetic internal standard. For the 28 HSTMG-B2M_HLA combinations or VHIO-133 and EC-35035 patient-derived TCLs, a 45% of the sample (total of 6-$8x10^7$ transfected B2M KO cells or $1x10^8$ for TCL of EC-35035 and $3x10^8$ for TCL of VHIO-133) was analyzed by PRM using an Orbitrap Eclipse™ (Thermo Fisher Scientific) coupled to an EASY-nanoLC 1000 UPLC system (Thermo Fisher Scientific) with a 50 cm C18 chromatographic column.

The chromatographic gradient started at 95% buffer A (0.1% FA in water) and 5% buffer B (0.1% FA in 80% ACN) with a flow rate of 300 nL/min and going up to 25% buffer B and 75% A in 52 min and to 40% B and 60% A in 8 min. The Orbitrap Eclipse was set in positive ionization mode with an EASY-Spray nanosource at 2.4 kV and at a source temperature of 305 ºC.

A PRM method was used for data acquisition with a quadrupole isolation window set to 1.4 m/z and MS2 scans over a mass range of m/z 250-1800, with detection in the Orbitrap mass analyzer at a 240K resolution. MS2 fragmentation was performed using HCD fragmentation at normalized collision energy of 30%, the AGC was set at 100,000 and the maximum injection time at 502 ms. All data was acquired with XCalibur software.

For data analysis fragment ion chromatographic traces corresponding to the targeted precursor peptides were evaluated with Skyline software v.21.2. Verification of the endogenous peptides was based on: i) the number of detected traces, ii) co-elution of endogenous traces, iii) co-elution of endogenous and internal standard peptides, iv) correlation of the fragment ions relative intensities between endogenous and internal standard peptides and, v) expected retention time.

To verify the presentation of repeatedly identified peptides from $KRAS_{p.G12D}$, $KRAS_{p.G12V}$, and $BRAF_{p.V600E}$ in a particular B2M_HLA chimera, we established a threshold based on the relative ratio. This relative ratio was obtained employing the formula:

$$Relative\ ratio\ (\%) = \frac{Ratio\ \left(\frac{light}{heavy}\right)\ in\ B2M_HLAx}{Ratio\ \left(\frac{light}{heavy}\right)\ in\ B2M_HLAy}\ x\ 100$$

In each sample, the internal ratio of the intensity of the endogenous peptide (light) is compared to the intensity of the internal standard peptide (heavy) for a particular neoantigen. The B2M_HLA chimera with the highest internal ratio (B2M_HLAy), was used as the reference value for all the other B2M_HLA chimeras (B2M_HLAx).

Each neoantigen was considered as validated in (B2M_HLAx) chimeras when the relative ratio was above the established threshold of 20%. Of note, the reference (B2M_HLAy) for neoantigens $KRAS_{p.G12D}$, $KRAS_{p.G12V}$ and $BRAF_{p.V600E}$ were B2M_C*05:01, B2M_A*03:01 and B2M_A*11:01 and B2M_A*03:01. These references align with the HLA-I alleles previously reported as presenting each peptide (178,179,181,182).

In vitro sensitization (IVS)

Human Peripheral Blood Lymphocytes (PBLs) from a breast cancer patient were sensitized with two minimal epitope pools (MEPs) containing a variable number of peptides. These peptides were selected based on evidence from the LC-MS/MS experiments of being presented on at least one of the patient's HLA-I alleles of interest (HLA-A*11:01 and HLA-C*04:01). MEPs or single minimal epitope (ME) sensitization experiments were always replicated independently. Peptides were pulsed at a concentration of 1μg/ml per ME in all stimulation rounds. Additionally, PBLs were stimulated with the CEF peptide pool (CEF PP) (ProMix™) used as a positive control in each stimulation round.

The sensitization protocol we followed was based on (213,214), with some modifications. Before every stimulation round, PBMCs were pre-treated to mobilize and mature APCs in a two-step manner. Briefly, at day-2, $5x10^6$ bulk PBMCs were cultured with AIM V™ (Gibco®), 5% hAB serum (BST) supplemented with GM-CSF (1000 IU/mL, Prepotech) and IL-4 (500 IU/mL, Prepotech) in 24-well plates to mobilize precursors of DCs. At day-1, APCs in the culture were matured for 12h by replacing the media for AIM V™, 5% hAB serum supplemented with a combination of LPS (10ng/mL, Sigmaldrich), IFN-γ (100 IU/mL, Prepotech), GM-CSF (800 IU/mL) and IL-4 (50 IU/mL).

At day 0, pre-treated PBMCs were washed and resuspended in IVS T-cell medium (OpTmizer CTS (Gibco®), T-cell Expansion Supplement (Gibco®), 2% hAB serum (BST), 2mM L-Glutamine, 100U/ml penicillin and 100ug/ml streptomycin (Pen Strep, Gibco®)) supplemented with IL-21 (30ng/mL, Prepotech) and the corresponding ME, MEP or CEF PP. At day 3, half of the medium was partially replaced with fresh IVS T-cell medium supplemented with IL-7 (5ng/mL, Prepotech) and IL-15 (5ng/mL, R&D systems) to promote T-cell growth. Thereafter, fresh IVS T-cell medium was replaced every three days or when cells required splitting because of confluence until the end of the stimulation round (day 12-14). For restimulation rounds (STIM2, STIM3 and STIM4), T cells from the previous stimulation round were harvested and $1x10^6$ cells were restimulated for another twelve to fourteen days with pre-treated and irradiated autologous PBMCs (25Gy), at a ratio 1:4. Peptide mixtures and concentrations were maintained for re-stimulation rounds. Cells underwent up to four consecutive rounds of stimulation.

The expansion of antigen-specific T cells was tested after each stimulation round. Briefly, sensitized T cells were tested by analyzing 4-1BB expression by flow cytometry after co-culture with autologous B cells pulsed with the corresponding peptide pools used for sensitization (MEP or CEF PP) as described below (Co-culture assays). Additionally, ME-specific HLA dextramer staining was used to evaluate the presence of antigen-specific T cells after sensitization. Positive T cells were FACS sorted by 4-1BB expression or dextramer binding (see enrichment of antigen-specific T cells). Antigen-specific enriched T cells were then expanded for 14 days in a rapid expansion protocol.

Co-culture assays: IFN-γ enzyme-linked immunospot (ELISPOT) and detection of activation marker 4-1BB using flow cytometry

T cells were thawed in T-cell medium supplemented with $3x10^3$ IU/mL IL-2 (Proleukin) and DNAse (Pulmozyme, Roche) three to four days before co-culture with the target cells, or immediately used upon the end of an IVS round. Co-cultures were performed in the absence of exogenously added cytokines. After 20h co-culture, cells were stained with a panel of human-specific antibodies to surface markers (Table 3) to identify T-cell responses. In parallel, IFN-γ secretion was measured by ELISPOT (MABtech technologies) using IFN-γ capture and detection antibodies following manufacturer instructions.

For all the assays, plate bound anti-CD3 (clone OKT3) (1μg/mL; Biolegend) was used as positive control. Media and/or autologous APC electroporated or pulsed with irrelevant HSTMG or peptides, respectively, were used as negative controls.

For the detection of T-cell responses, from $2x10^4$ to $5x10^4$ in vitro sensitized T cells, enriched populations of antigen-specific lymphocytes (see Enrichment of antigen-specific T cells) or TCR transduced PBLs (generated as detailed in section TCR sequencing and PBL transduction) were cocultured with $1.5x10^5$ to $2x10^5$ peptide-pulsed or $3x10^5$ to $4x10^5$ electroporated target cells (either B cells or tumor cells). T-cell reactivities were considered positive if the number of IFN-y positive spots was greater than double the amount of the irrelevant control condition and greater than 50 spots. Additionally, reactivities had to be consistent with 4-1BB upregulation. T-cell responses were always measured with HPLC-grade peptides. Due to sample availability limitations, most experiments before the enrichment for antigen-specific T cells were carried out only once. From then on, reactivities were confirmed in two independent experiments.

Dextramer generation and staining

U-Load Dextramers (Immudex) were loaded independently with an HLA monomer corresponding to one of the patient's HLA-I alleles (HLA-A*11:01, HLA-A*68:01, HLA-B*40:01 or HLA-C*04:01) and a peptide of interest at a time. easYmers HLA-I peptide monomers and loading of U-Load dextramers were prepared following manufacturer instructions. Flow cytometry-based quality control assay to monitor peptide loading efficiency was performed at least once for each of the peptide-HLA combinations evaluated.

Custom HLA dextramers conjugated to PE, were used to stain T cells in

combination with antibodies for evaluation of induced T-cell reactivities after IVS or FACS applications referenced in Table 3. Dextramer staining was also applied to identify the ME specifically recognized by the enriched T-cell populations among the MEPs used for sensitization. For all applications, T-cell recognition was considered positive when the percentage of dextramer-binding cells was double the percentage of cells binding to dextramers loaded with the irrelevant control peptides.

Enrichment of antigen-specific T cells

To enrich for antigen-specific T cells, in vitro sensitized T cells were co-cultured with peptide-pulsed autologous B cells for 20h or stained with U-Load dextramers loaded with the recognized peptide-HLA combination before sorting. $CD3^+CD8^+$ T cells expressing 4-1BB or $CD3^+CD8^+$ cells binding to custom HLA dextramers were sorted in BD FACS AriaII™ and expanded using a REP, explained below. Antibodies described in Table 3 for FACS or evaluation of IVS applications were employed.

Rapid expansion protocol (REP)

To expand enriched T-cell populations after FACS, we applied a 14-day REP. T cells were cultured in T25 flasks in T-cell medium (RPMI 1640 plus (Lonza):AIM-V (Gibco) medium containing 5% human AB serum (BST), 100 U/mL penicillin (Lonza), 100ug/mL streptomycin (Lonza), 2mM L-Glutamine (Lonza), 12.5mM Hepes (Thermo Fisher Scientific)) supplemented with 30 ng/ml anti-CD3 (OKT3, Biolegend) and $3x10^3$ IU/mL of interleukin IL-2 (Proleukin) in the presence of irradiated allogenic PBMC (50Gy) pooled from three healthy donors. After day 6, half of the medium was replaced with fresh T-cell medium containing IL-2 every other day. Cells were split when confluent, harvested on day 14 and used in co-culture assays or cryopreserved until use.

HLA-I expression and restriction

Cell-surface expression of HLA-I on tumor cells was determined by flow cytometry with Pan-HLA-I antibody (HLA-ABC antibody) or HLA-I allele-specific antibodies (Table 3) based on the HLA-I typing of VHIO-08 patient.

To determine the HLA-I restriction element of the immunogenic peptides, COS7 cells were transfected with plasmids encoding the individual HLA-I molecules using Lipofectamine 2000 (Life Technologies). After resting overnight, cells were harvested and pulsed with the corresponding peptides for 2h, washed, and used as targets in co-culture assays.

TCR sequencing and PBL transduction

For single-cell TCR sequencing, enriched antigen-specific T-cell populations were used. For sample multiplexing, cells were stained with TotalSeq-C hashtag antibodies (BioLegend) after FcR blockade with human TruStain FcX (BioLegend). Barcoded cells were separated using a Next GEM chip N on the 10x Chromium X, and libraries were prepared using the Chromium next GEM single cell 5' HT reagent kit v2 (dual index) with feature barcode technology for cell surface protein and immune receptor mapping (10x Genomics). Libraries were then pooled and sequenced on the Illumina NovaSeq 6000 sequencing platform (Illumina) according to the manufacturer's instructions for paired-end 150 bp (PE150) reads using v1.0 reagent kits (Novogene). Mapping, quantification, and clonotype definitions were performed using Cell Ranger multi-pipeline version 7.1.0 with reference vdj-GRCh38-alts-ensembl-7.0.0. Demultiplexing and downstream analyses were performed in R using Seurat version 5.0.1 and a dedicated pipeline.

To verify the most abundant clonotypes inferred from the single-cell data, we sequenced the beta chain of the TCRs present in our enriched populations. Genomic DNA was extracted from the target populations according to the Human TCRB Assay Sample Preparation Guidelines and submitted to the Adaptive Immunosequencing hsTCRB_v4b Service (UltraDeep) (Adaptive Biotechnologies). Processed samples were downloaded from the immunoSEQ analyzer and TCR frequencies were calculated from productive rearrangements in R.

The most enriched TCR-β sequences consistently identified by the two sequencing techniques were paired with the corresponding TCR-α sequences according to single-cell RNA sequencing and selected for further studies. TRB V-D-J encoding variable sequences and TRA V-J-encoding variable sequences were combined with the constant mouse sequences of the TRB and TRA chains (263), respectively. Mouse constant regions were modified, as previously described (264,265). The full-length TRB and TRA chains were cloned, in this orientation and separated by a furin SGSG P2A linker, into pMSGV1 retroviral vector (Twist Bioscience). The use of the modified mouse TCR constant regions promotes pairing of the introduced TCR and facilitates the identification of positively transduced human T cells by flow cytometry using an antibody specific for the mouse TCR-β chain (Table 3).

To generate transient retroviral rich supernatants, the retroviral vector pMSGV1 encoding the antigen-specific TCR and the envelope encoding plasmid RD114 were co-transfected into the retroviral packaging cell line HEK293GP (plated the day prior to transfection) using Lipofectamine 2000 (Life Technologies).

Retroviral supernatants were collected 48h after transfection, diluted 1:1 with DMEM media (Gibco), and then centrifuged onto Retronectin-coated (10ug/ml, Takara), non-tissue culture-treated 24-well plates at 2000g for 2h at 32ºC. Donor PBMC activated 2 days before with soluble anti-CD3 (OKT3, 50ng/ml) and IL-2 (300 IU/mL) in T-cell media, were harvested, added onto the retrovirus plates, and centrifuged for 10min at 300g. Three days after transduction, activated T cells were transferred to tissue culture-treated plates and further cultured in T-cell media containing IL-2 (300 IU/ml). Cells were typically assayed 10-14 days post-retroviral transduction.

Correlation and statistical analyses

Statistical analyses were conducted with GraphPad PRISM 8.2.1 software with a significance set at $p \leq 0.05$ (two-tailed). After testing for normality with Shapiro test, variables showed a non-normal distribution. Therefore, all the performed tests were non-parametric.

Spearman rank-order correlation test was applied to evaluate the correlation between % HLA-I$^+$ cells according to Pan-HLA-I (HLA-ABC antibody) staining and the number of total unique peptides recovered from B2M KO transfectants or the unique HSTMG-derived hits.

Fisher's exact test was applied to assess for association between recurrent mutations and HLA-I alleles in selected cohorts of cancer patients from TCGA. Baptista-Pike odds ratio was also computed in each analysis.

Data analysis and visualization

All flow cytometry data were analyzed with FlowJo software v10.9.0 (Tree Star). Mass spectrometry data was analyzed as specifically described with PEAKS Xpro and Skyline software. Data were plotted with GraphPad PRISM 8.2.1 software and R studio version 4.2.2 using ggplot2 package. Several repository data was downloaded for analysis purposes and refined as specified for each analysis below.

Gene expression and mutation analysis of genes involved in the antigen presentation machinery. NSM identified in the WES analysis of VHIO-08, VHIO-133 and EC-35035 were filtered for genes present in a curated gene set based on the Gene Ontology Antigen Processing and Presentation pathway (GO:0019882). Mutations called by at least two variant callers and with a VAF above 5% and a minimum of 4 mutated counts were retained. For the gene expression study, TPM for each gene was considered according to the analysis of total RNA sequencing from tumor cell lines.

TPM values were used to compare the expression of genes belonging to same gene set pathway between our patient-derived tumor cell lines and a panel of relevant cell lines from the Cancer Cell Line Encyclopedia (CCLE). We used the median TPM in CCLE cell lines from SALIVARY_GLAND or UPPER_AERODIGESTIVE_TRACT (n = 33), SKIN (n = 50) or ENDOMETRIUM (n = 29) origin, as reference for comparison with expressions in patient VHIO-08 (head and neck), VHIO-133 (melanoma) and VHIO-EC-35035 (endometrial), respectively.

Prioritization of HLA-I alleles and recurrent mutations affecting driver genes. For the selection of the most frequent HLA-I alleles in European Caucasian population, data from The Allele Net Database was downloaded (https://www.allelefrequencies.net/). Evaluation of the frequency of the selected HLA-I alleles in cancer patients was done with the HLA-I genotyping inferred from Optitype of individuals contained in The Cancer Genome Atlas (TCGA) Pan-Cancer Atlas study. The specific analysis conducted in each case are specified in section 1.2. To select for recurrent alterations in cancer driver genes data from Cancer Hotspots (https://www.cancerhotspots.org/#/home) a resource derived from (266,267) was downloaded and analyzed as specified (results section 1.1).

Co-occurrence of hotspot mutations in driver genes and HLA-I alleles in cancer patients. Mutations detected in PIK3CA or TP53 genes for cancer patients included in TCGA Pan-Cancer Atlas study were downloaded from cBioPortal (https://www.cbioportal.org/). HLA-I genotyping of cancer patients from the specified study was inferred with Optitype and downloaded (https://gdc.cancer.gov/about-data/publications/panimmune). Cohorts presenting the highest prevalence of the mutations of interest were selected to evaluate the association between HLA-I alleles and these alterations employing a Fisher's exact test.

Results

1. Design of an immunopeptidomics-based strategy to identify public neoantigens

Our first goal was to develop an immunopeptidomics-based approach to identify public neoantigens derived from shared mutations in cancer driver genes. We focused on detecting peptides derived from selected mutations in hotspot regions of genes such as *TP53* and *KRAS*, presented by the most prevalent HLA-I alleles. In the future, this approach could be applied to other types of tumor antigens and a more extensive selection of HLA alleles.

To achieve this, we initially chose the most common HLA-I alleles in the European Caucasian population. We then defined the selected list of mutations in cancer driver genes that we intended to investigate. We also assessed the best cell source for identifying peptides through immunopeptidomics and used this platform to discover and validate putative neoantigens derived from recurrent cancer mutations using mass spectrometry.

1.1. Selection of recurrent mutations in cancer driver genes for the construction of Hotspot Tandem Minigenes (HSTMG)

As a first step, we explored several cancer sequencing data repositories (Cancer Gene Census, Cancer Hotspots, My Cancer Genome, cBioportal, and IntOGene) as a means to detect and prioritize the shared mutations present in common tumor suppressors genes and oncogenes. We selected a total of 13 cancer driver genes based on: (1) harboring mutations across many types of cancer (i.e., *TP53*, *KRAS*, *PIK3CA*, *BRAF*, *PTEN*, *NRAS*, *SMAD4*, and *AKT1*) (Figure 14A) or (2) having a high prevalence in a restricted group of tumor types (i.e., *ERBB2*, *KIT*, *GNAQ*, *GNA11*, and *POLE*) such as breast, gastrointestinal, uveal melanoma or endometrial cancer. Within these genes, we prioritized 35 missense variants mapping in hotspot regions (Figure 14B).

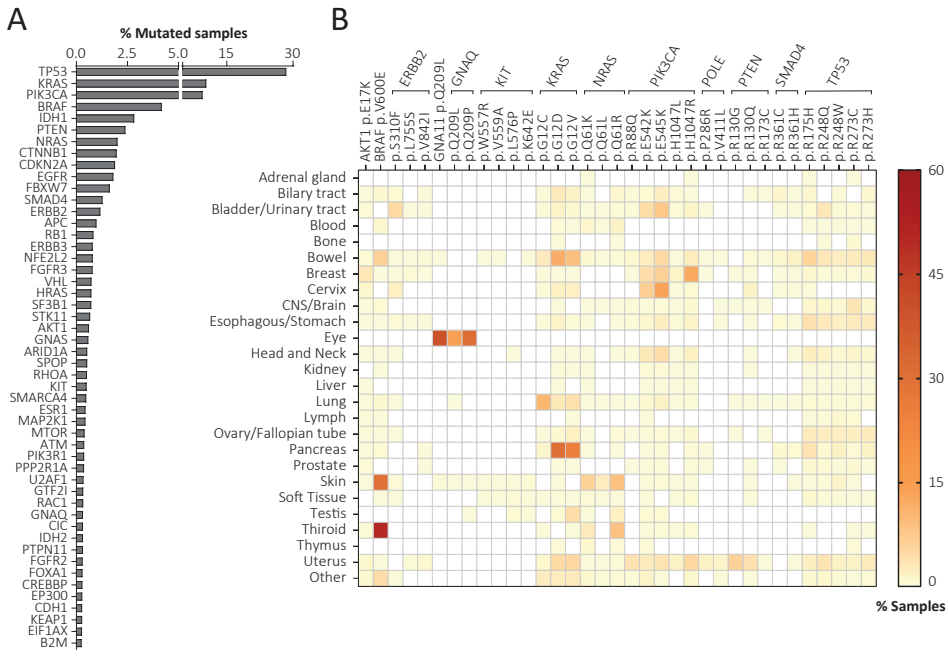


Figure 14. Selection of the most relevant recurrent alterations affecting cancer driver genes from repository data. Data were obtained from the website Cancer Hotspots, a resource derived from Chang et al. 2016, 2018. A) The percentage of tumor samples across all cancer types containing mutations in the top 50 most highly mutated genes are plotted. Only single residue type of mutation was considered for this analysis. B) Heat map displaying the frequency of the 35 selected hotspot mutations in 13 driver genes by anatomical location. Frequency was calculated as the number of samples presenting the specified mutation relative to the total number of samples analyzed per anatomical location.

For each of the selected hotspot mutations we synthesized 25-mer minigenes encoding for one non-synonymous mutation (NSM) flanked by 12 amino acids (AA) of the wild-type sequence on each side. These minigenes were concatenated with other minigenes encoding for patient-specific mutations, to form a HSTMG containing up to 25 minigenes. A total of four constructs were generated to encompass all selected hotspot mutations. Specifically, HSTMG1 contained (n = 13), HSTMG2 (n = 15), and HSTMG (n = 6). As an exception, HSTMG4 contained only one hotspot mutation, but the rest of the minigenes encoded for patient-specific mutations. It is important to note that while minigenes encoding private mutations were also included in each of the HSTMG constructs, the resultant mutant neoantigens will not be discussed in this thesis, as they do not derive from the selected hotspot mutations in driver genes.

ZsGreen (ZSG) was incorporated into all HSTMG plasmids as a fluorescent reporter to monitor the transfection efficiency of these constructs. A P2A linker was added before ZSG to ensure proper separation from the minigenes, as explained in the Materials and Methods section related to tandem minigenes construction.

1.2. Prioritization of the most frequent HLA-I alleles in the European Caucasian population

Our study focused on discovering public neoantigens presented by the most frequent HLA-I alleles of the European Caucasian population, which could be leveraged to develop off-the-shelf TCR-engineered T-cell therapies or vaccines. To select these HLA-I alleles, we analyzed data from the Allele Frequency Net Database and chose five HLA-A alleles, three HLA-B, and four HLA-C alleles, all exceeding a 5% frequency in the population of interest (Figure 15A). We also included the allele HLA-C*08:02 to test the ability of our approach to identify previously reported peptides presented by this allele (76,178).

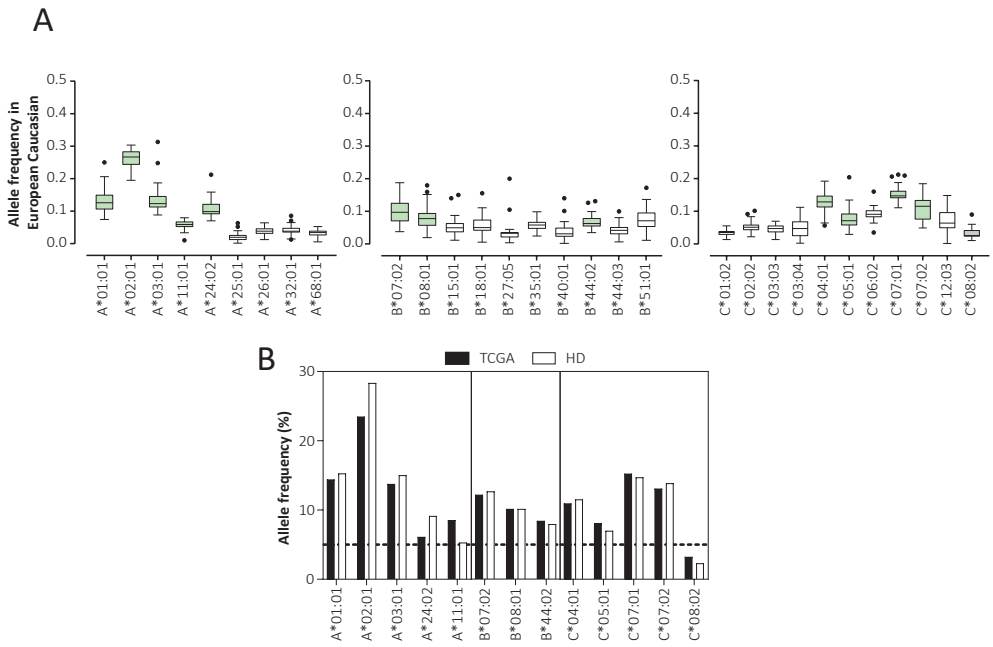


Figure 15. Prioritization of highly frequent HLA-I alleles. A) Allele frequency of the top ten most prevalent HLA-A, B, and C alleles in the European Caucasian population. Data were obtained from the website Allele Frequency Net Database, as of September 2023. Weighted frequency was calculated for alleles reported in at least 40 populations, each with a minimum size of 100 individuals. Highlighted in green are the 12 HLA-I alleles prioritized with a frequency above 5% in the indicated population. Highlighted in grey, HLA-C*08:02, selected for comparison purposes.

B) Percent allelic frequency of the selected HLA-I alleles in cancer patients. HLA-I genotyping of cancer patients from the TCGA Pan-Cancer Atlas study was inferred with Optitype and downloaded (https://gdc.cancer.gov/about-data/publications/panimmune). All TCGA cancer types were included, but the frequency of the HLA-I alleles of interest was calculated for the group of patients reporting EUR in their Genetic Ancestry Label (n = 8012). The allelic frequency of the 13 selected HLA-I alleles from cancer patients (TCGA) is compared to healthy donors (HD) of European Caucasian population (as calculated in panel A).

Since the selection of HLAs was based on healthy donor typing, we verified that cancer patients did not present a major bias in frequency for the prioritized alleles. To this end, we examined the occurrence of specific HLA-I alleles in patients categorized as having European genetic ancestry in the Tumor Cancer Genome Atlas (TCGA) Pan-Cancer dataset. We found that the allelic frequency of the HLA-I alleles we prioritized was similar in healthy donors and cancer patients (Figure 15B).

In total, we selected 13 different HLA-I alleles that are highly prevalent in the European Caucasian population and cancer patients.

1.3. Evaluation of the different cell types for the detection of HSTMG-derived peptides by immunopeptidomics

We reasoned that we could leverage HLA-I immunopeptidomics to discover novel mutant epitopes presented by antigen-presenting cells expressing both the selected hotspot mutations in the form of HSTMGs and the HLA-I of interest.

To optimize the detection of HSTMG-derived peptides, we evaluated two different sources of antigen-presenting cells: cells naturally expressing multiple HLA-I alleles or cells expressing a single HLA-I allele through exogenous overexpression, referred to as HLA-I monoallelic cells.

1.3.1. Use of B cells as antigen-presenting cells to identify neoepitopes presented on HLA-I

We first evaluated the potential of B lymphocytes, which are professional APCs, as a source for identifying candidate neoantigens derived from recurrent mutations. B cells are abundant and readily available in peripheral blood from healthy donors or cancer patients and can be expanded up to large numbers, providing significant advantages as a source for immunopeptidomics studies.

In addition, B cells express high levels of HLA class I gene products, facilitating the simultaneous evaluation of neoantigen candidates from up to six different HLA-I alleles. For all these reasons, we designed an MS-based immunopeptidomics strategy for using patient-derived B cells, depicted in Figure 16.

Briefly, the strategy entailed identifying PBMCs from donors expressing prevalent HLA-I alleles of interest, expanding their B cells to high numbers, and then transfecting them with HSTMGs to express the mutations of interest via electroporation of in vitro transcribed (IVT) HSTMG RNA. Finally, we used these modified B cells to perform HLA-I immunopeptidomics to identify the mutated peptides presented on HLA-I.

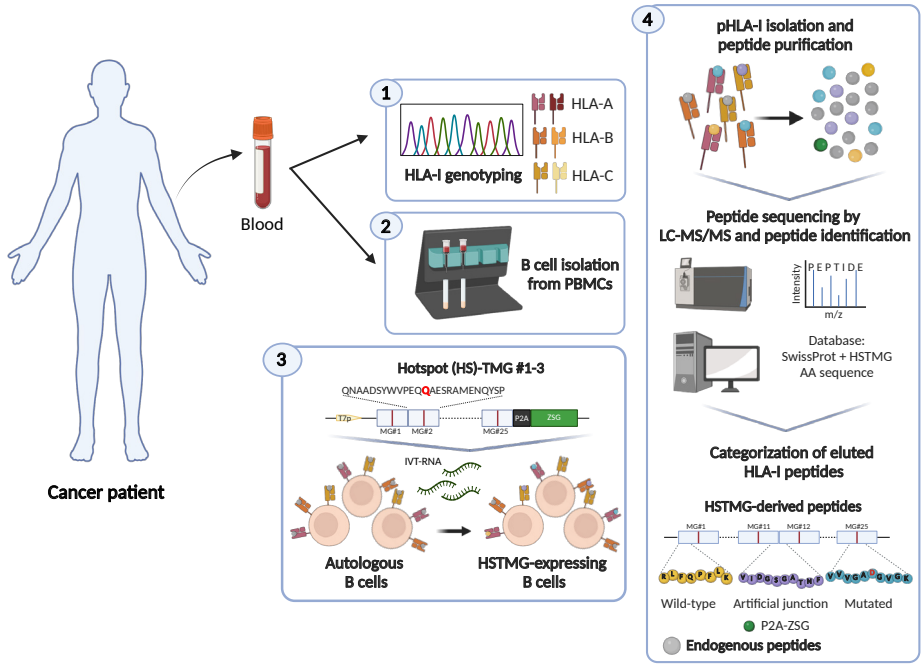


Figure 16. Experimental strategy to identify HSTMG-derived peptides by HLA-I immunopeptidomics of B cells. Blood samples were obtained from VHIO cancer patients and DNA was extracted from PBMCs. (1) HLA-I genotyping from genomic DNA extracted from PBMCs was obtained either from WES or NGS. (2) B cells from patients containing at least one HLA-I of interest were isolated by CD19 selection from PBMCs and in-vitro expanded to $5x10^7$-$1x10^8$ cells. (3) HSTMG-expressing B cells were obtained through independent electroporation of IVT RNA from HSTMG1-3 constructs. (4) HLA-I immunopeptidomics was performed using HSTMG transfected B cells to identify the peptides presented on HLA-I molecules. The peptide sequences that came from the constructs were identified using a customized database including the human proteome (SwissProt) as well as the HSTMG AA sequences and then categorized based on where they mapped in the HSTMG constructs into wild-type, artificial junction, mutated or as P2A-ZSG. Peptides that did not map to the HSTMG construct were categorized as endogenous. Image created with Biorender.com.

First, we selected patients with highly prevalent HLA-I alleles. We extracted DNA from PBMCs to perform HLA-I genotyping (Figure 16.1). Based on these results, we chose to work with B cells from four cancer patient donors carrying at least one of the HLA-I alleles of interest for our work (Table 5). B cells from selected patients were purified from PBMCs using anti-CD19 magnetic beads and expanded in vitro up to $5x10^7$-$1x10^8$ cells (Figure 16.2).

Table 5. Relevant patient characteristics included in the immunopeptidomics experiments using B cells.

Patient ID	Tumor type	Shared somatic variant	HLA-I typing
VHIO-08	Head and Neck (H&N)	$PIK3CA_{p.E542K}$	**A*02:01** **A*03:01** **B*07:02** B*18:01 **C*05:01** **C*07:02**
VHIO-09	Head and Neck (H&N)	None	**A*24:02** A*29:02 B*14:02 B*44:03 C*02:02 C*16:01
VHIO-153	Pancreatic	$KRAS_{p.G12D}$	**A*03:01** A*26:01 **B*07:02** B*18:01 **C*07:02** C*16:02
MBM	Lung	$KRAS_{p.G13C}$*	**A*11:01** A*32:01 B*14:01 B*55:01 C*03:03 C*08:02

Patient identification, tumor type, the shared somatic variant detected by WES or targeted sequencing in each patient tumor, and HLA-I typing of their PBMCs. The somatic variant (*) was not encoded in the three HSTMGs used for the study. HLA-I alleles highlighted in bold represent those with an allelic frequency above 5% in the European Caucasian population. The underlined alleles were of interest for comparison with previous reports.

To test whether HSTMG-derived peptides were expressed, processed, and presented on the HLA-I molecules of B cells and could be detected through immunopeptidomics, each of the patient-derived B cells were independently electroporated with IVT RNA-derived from HSTMG1, HSTMG2, and HSTMG3 (Figure 16.3). After 20 hours of culture, cells were harvested and analyzed by flow cytometry to monitor transfection efficiency by the expression of the ZSG reporter. Next, we immunoprecipitated the pHLA-I from the B cells and eluted and analyzed the peptides bound to HLA-I molecules by LC-MS/MS. The amino acid sequences corresponding to each acquired mass spectrum data set were inferred by database search using a customized database comprising the reference human proteome and the AA sequences of the three HSTMGs.

The identified peptides were classified as mutated, wild-type or artificial junction depending on whether the peptides mapped to regions in the HSTMG containing a mutation, not containing a mutation, or to the junction between two different concatenated minigenes, respectively. Additionally, HSTMG-derived peptides mapping to the P2A linker or ZSG reporter were categorized as P2A-ZSG. Those peptides mapping to the human proteome, but not to HSTMG sequences, were categorized as endogenous, as they arise from proteins natively expressed by B cells (Figure 16.4).

The three HSTMGs were electroporated into B cells from each of the four selected patients, resulting in a total of 12 HSTMG-B cell combinations. The average number of unique total peptides recovered from each sample ranged from 2921 for MBM patient to 4744 for VHIO-09 (Figure 17A). The eluted peptide sequence features were typical of HLA-I ligands, in terms of length distribution (predominantly 8-12AA, Figure 17B) and the proportion of peptides predicted to bind to patient-specific HLA-I alleles (Figure 17C). Unsupervised clustering analysis of the identified peptides from each patient was carried out using GibbsCluster 2.0 software to align the input peptides and group them based on their amino acid sequences. For each patient studied, we observed that the eluted peptides grouped into clusters displaying motifs similar to the consensus motifs of the patient's HLA-A and HLA-B alleles as defined by NetMHCPan4.1-EL (Figure 17D). Only patient VHIO-153 showed a pattern resembling peptides binding to HLA-C*16:02, suggesting that B cells do not express high levels of HLA-C.

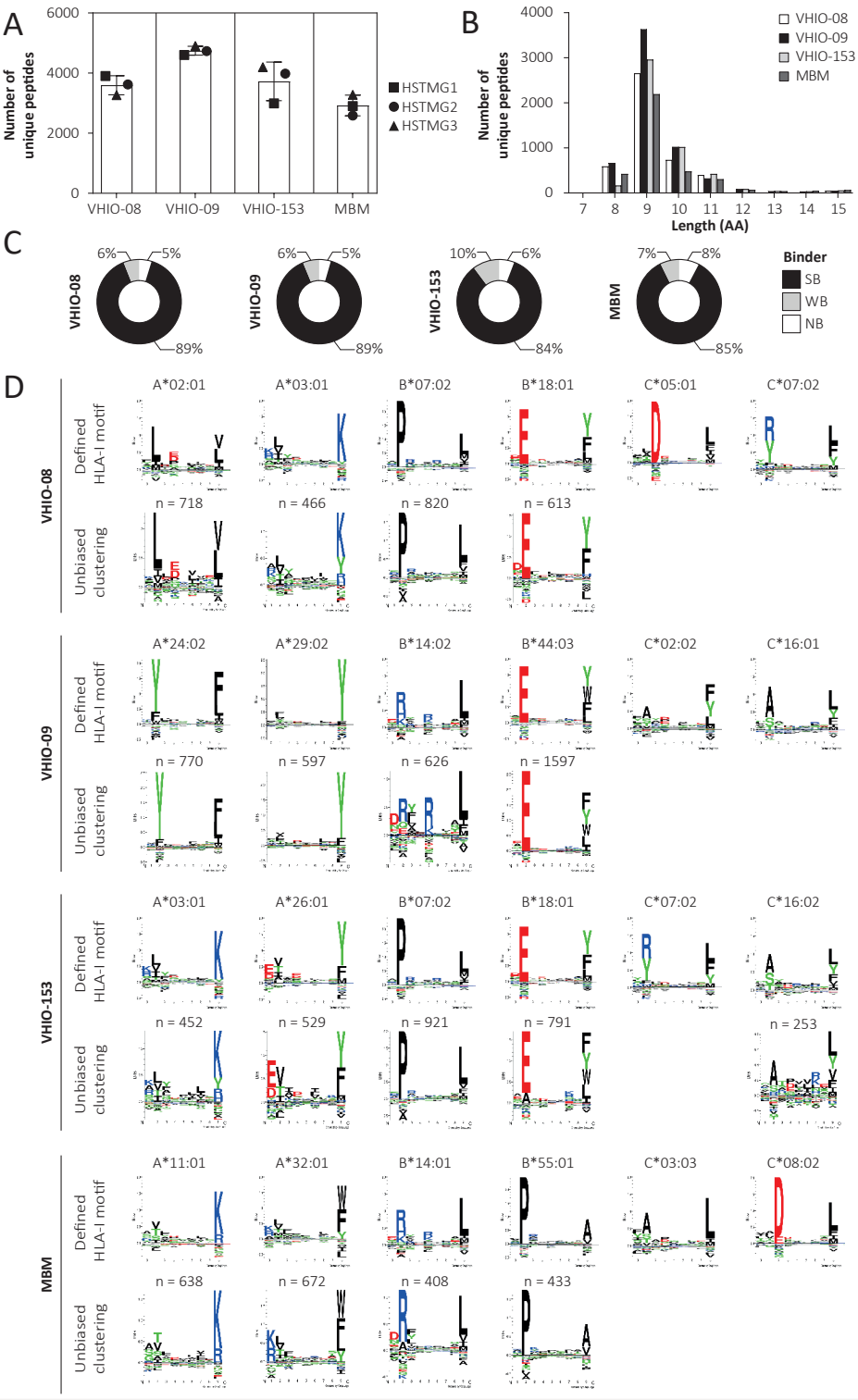


Figure 17. Peptides eluted from HSTMG-expressing B cells display typical HLA-I peptide features.

A) Number of unique peptides eluted from HLA-I and identified by database search for B cells derived from four cancer patients at 1% FDR using PEAKS Xpro. B) Peptide length distribution of the total unique HLA-I peptide sequences identified for each of the patient-derived B cells considering all HSTMG1-3. Only peptides <15AA are depicted. C) Percentage of peptides predicted to bind to corresponding HLA-I molecules of each patient according to the Eluted Ligand (EL) likelihood rank of NetMHCPan 4.1. Peptides ranging from 8 to 15 AA length, considering all HSTMG1-3 combinations per patient, were classified as strong binders (SB, %-tile EL rank <0.5), weak binders (WB, %-tile EL rank 0.5-2) and non-binders (NB, %-tile EL rank >2). For each peptide, the minimal predicted %-tile EL rank across all the patient's HLA-I molecules was considered. D) Comparison of HLA-I binding motif for the patient's HLA-I alleles defined by NetMHCPan4.1-EL (top row) to the groups defined by unbiased clustering (bottom row). All unique 9-mers identified for B cells from each patient were selected for the analysis. The optimal solution according to GibbsCluster2.0 analyzed by default settings is depicted. The number of sequences per group is indicated (n=).

Collectively, these analyses indicated that the majority of identified sequences were consistent with peptides eluted from HLA-I molecules, rather than arising from contaminants or originating from misidentifications.

1.3.1.1. MS-based immunopeptidomics of patient-derived B cells displayed poor resolution for the identification of candidate neoantigens

Next, we investigated whether HSTMG-derived peptides could be detected in the repertoire of HLA-I ligands eluted from the electroporated B cells. As expected, we found that most of the identified peptides were derived from endogenous proteins expressed by B cells. Forty-eight peptides were derived from the HSTMGs studied. One limitation was that peptides mapping to the wild-type sequence of the mutated minigenes encoded by the HSTMG also mapped to the corresponding endogenous protein, as both were included in the customized database used to analyze the proteomics data. Although we were unable to unequivocally distinguish whether these peptides arise from wild-type sequences of the introduced HSTMG construct or the native protein potentially expressed by B cells, these were considered as HSTMG wild-type peptides for the purpose of our study.

The number of total HSTMG-derived peptides diverged largely between the four patients. Patients VHIO-09 and VHIO-153 presented the largest number of peptides, which coincided with the high transfection efficiency of HSTMG constructs (Figure 18A).

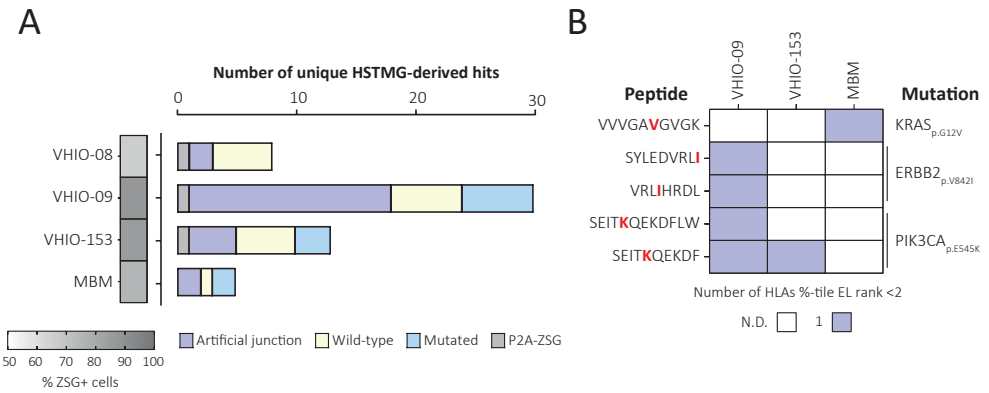


Figure 18. HLA-I eluted peptides from transfected B cells contained several HSTMG-derived peptides. A) The bars show the number of unique HSTMG1-3 derived peptides identified, classified by categories and per patient. The mean intensity of ZsGreen (ZSG) fluorescence measured by flow cytometry is shown in the left bar as an indicator of the level of HSTMG expression. B) Unique mutant HSTMG-derived peptides identified in each patient. Cells filled in blue indicate peptides detected in B cells derived from a particular patient, while blank cells indicate that none were detected (N.D.). For each presented peptide, the number of HLA-I alleles from the patient for which it can be considered as a binder according to NetMHCPan 4.1 (%-tile EL rank <2) is specified in the corresponding cell as pale blue (n = 1). The specific peptide sequence (left) and the mutation from which they derive (right) are annotated. The mutated AA is highlighted in red.

Regarding the categories of peptides originating from HSTMGs, artificial junction peptides were the most abundant in the four patients (Figure 18A). Moreover, peptides derived from the P2A linker and the ZSG reporter were also recovered from the HLA-I molecules of three of the four patients studied (Figure 18A).

Among the 48 HSTMG-derived peptides, we detected 10 mutated peptides, five derived from shared mutations in driver genes (Figure 18B; for peptides derived from patient-specific mutations, see Appendix Figure 1). These mutated peptides were detected in B cells from all individuals except for VHIO-08. Notably, all the identified neoantigens were predicted to bind to at least one of the HLA-I alleles from the corresponding patient B cells where they were identified (Figure 18B).

Because we used cancer patient-derived B cells, we also had the unique opportunity to investigate the presentation of hotspot mutations present in the patient's tumor as determined by WES (Table 5) by their autologous HLAs. This analysis was limited to the $PIK3CA_{p.E542K}$ mutation in VHIO-08 and $KRAS_{p.G12D}$ mutation in VHIO-153, since these were the only shared mutations identified by

tumor WES that were included in our HSTMGs. Nonetheless, mutant peptides derived from these recurrent mutations were not detected by immunopeptidomics following electroporation into their respective B cells.

To determine whether B cells were the optimal cell type to elute HSTMG-derived peptides, we tested their ability to present previously reported mutated peptides originating from recurrent mutations encoded by our constructs. By using our method with the HSTMG-electroporated B cells from the four patients analyzed, we could potentially identify 16 mutated peptides documented by July 2021 presented in different HLA-A, B, and C alleles. However, only one of the 16 peptides was detected in the B cells of MBM patient, a peptide derived from $KRAS_{p.G12V}$ presented by HLA-A*11:01. The remaining 15 mutated peptides reported to bind to HLA-I alleles, expressed by B cells of at least one of the four studied patients, such as HLA-A*03:01, HLA-B*07:02 and HLA-C*08:02, were not identified (Table 6).

Table 6. Reported neoepitopes expected to be detected on HLA-I alleles of HSTMG-expressing B cells.

				HSTMG-expressing B cells		
Peptide sequence	**Shared neoantigen**	**HLA-I allele**	**Reference**	**VHIO-08**	**VHIO-153**	**MBM**
LAT**E**KSRWS	$BRAF_{p.V600E}$	A*02:01	249	✕		
LAT**E**KSRWSG				✕		
KLVVVGA**D**GV	$KRAS_{p.G12D}$	A*02:01	244	✕		
VVVGA**D**GVGK		A*03:01	182	✕	✕	
VVGA**D**GVGK				✕	✕	
VVVGA**D**GVGK		A*11:01	183			✕
VVGA**D**GVGK			179			✕
GA**D**GVGKSAL		B*07:02	179	✕	✕	
GA**D**GVGKSAL		C*08:02	76			✕
GA**D**GVGKSA						✕
KLVVVGA**V**GV	$KRAS_{p.G12V}$	A*02:01	244	✕		
VVVGA**V**GVGK		A*03:01	252	✕	✕	
VVGA**V**GVGK				✕	✕	
VVVGA**V**GVGK		A*11:01	183			■
VVGA**V**GVGK						✕
HMTEVVR**H**C	$TP53_{p.R175H}$	A*02:01	75	✕		

Peptide sequence with the mutant AA highlighted in red, shared neoantigen from which they derive, HLA-I presenting allele, and reference of the first report detecting the peptide-HLA pairs are listed. Three patients presenting HLA-I alleles where these peptides should have been detected using the HSTMG-expressing B cells are annotated.

Cells filled in black indicate the detection of the peptide in the patient, crossed cells for the expected peptides not identified in the patient, and empty cells for peptides not expected to be detected based on lack of evidence in the literature. Only reports before July 2021, when this analysis was performed, are listed.

These results indicated that although HLA-I immunopeptidomics of HSTMG-expressing B cells from cancer patients led to the detection of some neoantigens, it appeared less robust to discover novel peptides, as it failed to capture the majority of shared neoantigens reported in the literature.

1.3.2. Exploiting HLA-I ligandome of HLA-I monoallelic cells for the identification of candidate neoantigens

Based on the results mentioned above, we opted to evaluate our protocol on a distinct type of antigen-presenting cells. Guided by prior literature, we reasoned that performing immunopeptidomics on cells expressing one HLA-I allele instead of several could lead to more sensitive detection of peptides and more accurate assignation of the eluted peptides to the unique HLA-I allele tested. Thus, we decided to engineer cells derived from a tumor cell line (TCL) to express only one HLA-I allele at a time.

We preselected a TCL derived from a head and neck cancer patient VHIO-08. Given that tumor cell lines can evolve to limit antigen presentation as a result of immunoediting, we sequenced VHIO-08 TCL via WES and RNA sequencing to ensure that this cell line did not present any major alteration in the antigen presentation pathway. This TCL harbored 2485 NSM as detected by WES. Importantly, VHIO-08 TCL carried somatic mutations in HLA-A and B genes, as well as one hotspot mutation in the PIK3CA gene, which was encoded in our HSTMGs (Table 7).

Table 7. Characteristics of patient-derived tumor cell line VHIO-08.

Patient ID	Tumor type	Tumor specific NSM	Shared somatic variant	HLA-I typing
VHIO-08	Hypopharingeal carcinoma (H&N)	2485	$PIK3CA_{p.E542K}$	A*02:01[a] A*03:01[b] B*07:02[b] B*18:01[c] C*05:01 C*07:02

Patient identification, tumor type, number of tumor-specific NSM, and shared somatic variant detected by WES of tumor DNA are annotated. HLA-I typing of tumor cells inferred from WES and the genetic alterations detected are specified: (a) Loss of HLA-A*02:01 (b) Missense mutations (c) Nonsense mutations.

Next, we evaluated the status of genes involved in the antigen processing and presentation machinery (APM) based on a curated gene set founded on Gene Ontology. As a reference, we compared our data with the corresponding transcriptomic data of tumor cell lines of similar origin in the Cancer Cell Line Encyclopedia (CCLE) database. VHIO-08 TCL did not show alterations in genes encoding key elements involved in the HLA-I presenting pathway such as TAP, ERAP or the catalytic subunits of the proteasome (Figure 19A). Despite some gene mutations related to antigen presentation (Figure 19B), we had extensive evidence in our laboratory that this cell line could express, process, and present known antigens in HLA-I, which were recognized by the patient's TILs (Appendix Figure 2).

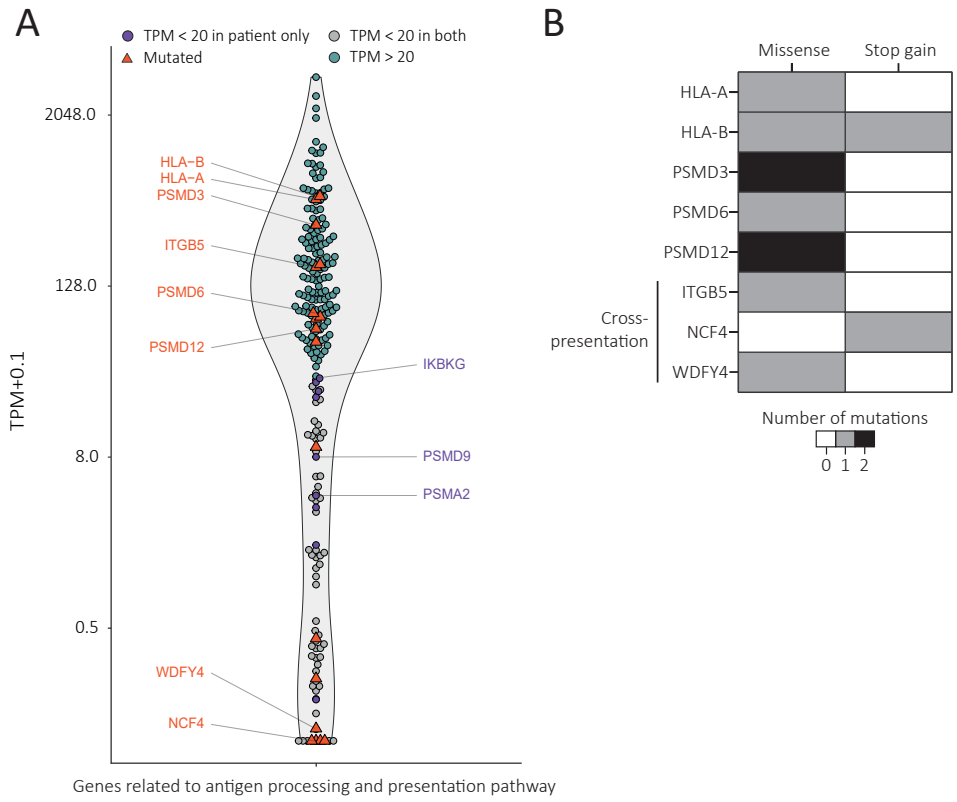


Figure 19. Gene expression and mutation analysis of antigen presentation pathway genes in VHIO-08 TCL. A) Expression levels of the 234 genes included in a curated gene set based on the Gene Ontology Antigen Processing and Presentation pathway in VHIO-08 TCL.

Expression level is plotted as Transcripts Per Million (TPM+0.1) and compared to the median expression levels of these genes in tumor cell lines of similar origin (n= 33) from the Cancer Cell Line Encyclopedia (CCLE) data repository. Gene expression levels are represented as dots for non-mutated and triangles for mutated genes; green dots indicate genes with higher expression (TPM > 20) and purple with lower expression (TPM < 20), specifically in VHIO-08 but not in the corresponding CCLE biorepository (median TPM CCLE). Grey dots denote low expression (TPM < 20) in VHIO-08 TCL and CCLE cell lines. Genes of interest directly related to the HLA-I presentation pathway, poorly expressed genes (TPM < 20) in VHIO-08 patient only, or mutated genes are labeled. B) Mutations in genes related to the HLA-I processing pathway in VHIO-08 TCL. Heat map summarizing the number and categories of mutations in genes coding for proteins involved in the HLA-I processing pathway or cross-presentation, as detected by WES of VHIO-08 TCL. Cell colors indicate the number of mutations.

Once we had selected VHIO-08 TCL as our working model, we designed the strategy depicted in Figure 20 to discover novel HLA-I mutant peptides arising from recurrent driver mutations in cancer. Our goal was to engineer VHIO-08 TCL to eliminate all the native cell surface HLA-I expression and presentation from the cell line. Afterward, we planned to reintroduce specific HLA-I alleles together with the candidate antigens of interest. Finally, we leverage immunopeptidomics to identify the peptides arising from the antigen of interest presented on the expressed HLA-I.

To this end, we genetically modified VHIO-08 TCL to obtain a B2M negative cell line through CRISPR/Cas9 inactivation of the β2-microglobulin gene (Figure 20.1). As β2M is required for the surface expression of HLA-I molecules, B2M gene inactivation results in a lack of HLA class I expression on the cell membrane (268). The resulting B2M KO cells were used for the generation of transient monoallelic cells via co-electroporation of one HSTMG1-4, consisting of the concatenated 25-mers harboring recurrent mutations of interest, and one B2M_HLA chimera, each encoding for one of the HLA-I alleles of interest (Figure 20.2). Next, HSTMG-expressing HLA-I monoallelic tumor cells were lysed to isolate the pHLA-I complexes by affinity chromatography, and the purified peptides were analyzed by LC-MS/MS shotgun mass spectrometry (shotgun MS) (Figure 20.3, left and middle panels). A customized database, including the entire human proteome and the HSTMG AA sequences, was used to identify the peptide sequences of the HLA-I ligands. As explained in section 1.3.1, HSTMG-derived peptides were categorized as mutant, wild-type, artificial junction, or P2A-ZSG, depending on where their sequences mapped to in the HSTMG constructs.

Last, selected mutant peptides identified in each HSTMG-B2M_HLA chimera combination were validated through Parallel Reaction Monitoring mass spectrometry (PRM-MS) using isotope-labeled peptide versions (Figure 20.3, right panel).

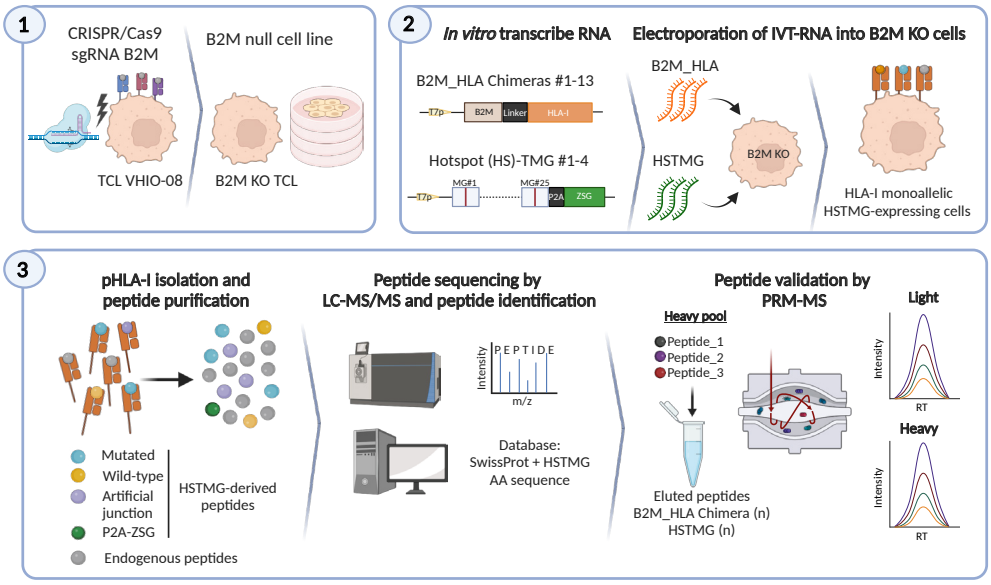


Figure 20. Strategy for identifying and validating HSTMG-derived peptides through HLA-I immunopeptidomics using monoallelic tumor cells. (1) B2M KO recipient cells were generated by CRISPR/Cas9 KO of B2M on VHIO-08 TCL. The resultant B2M null cell line was *in vitro* expanded up to high numbers. (2) To generate cells expressing an HLA-I and HSTMG of interest, IVT RNA from one HSTMG construct and one B2M_HLA chimera encoding for one of the 13 prioritized HLA-I alleles for our study were co-electroporated into B2M KO recipient cells to obtain HLA-I monoallelic HSTMG-expressing cells. After 20h of culture, the transfection efficiency of both constructs was measured through flow cytometry, and cells were collected and snap-frozen. (3) Surface pHLA-I complexes from transfectants were immunoprecipitated; the peptides were isolated, purified, and then analyzed by liquid chromatography coupled to mass spectrometry (LC-MS/MS). The peptide sequences arising from the constructs were identified using a customized database including the human proteome (SwissProt) as well as the HSTMG AA sequences, and then categorized based on where they mapped in the HSTMG constructs into wild-type, artificial junction, mutated, P2A-ZSG or as endogenous peptides if they did not map to the HSTMG construct. Selected HSTMG-derived mutant peptides were validated using pools of isotope-labeled peptide versions (heavy pool) that were spiked into HLA-I eluted peptides from transfectants (consisting of a specific B2M_HLA chimera (n) and HSTMG (n) combination) for which LC-MS/MS identified at least one mutant peptide. In the corresponding HLA-I preparations for peptide validation, endogenous peptides (light) and isotope-labeled peptides (heavy) were monitored through PRM-MS. Image created with Biorender.com.

The establishment of this strategy and the results derived from each step are summarized in the following sections.

1.3.2.1. Generation of an epithelial tumor cell line negative for B2M expression through CRISPR/Cas9

To obtain the B2M null VHIO-08 tumor cells, we introduced the ribonucleoprotein complex, consisting of Cas9 and a specific single guide RNA (sgRNA) for B2M, via electroporation. Four days later, approximately 40% of the tumor cells were found to be HLA-I negative by cell surface flow cytometry (Figure 21A). To enrich for HLA-I negative cells, we selected the HLA-I negative population through cell sorting and obtained a 96% pure HLA-I negative population. These cells were expanded in culture until VHIO-08 B2M knockout TCL was established. The final resulting TCL (referred to as B2M KO cells) was HLA-I negative by cell surface flow cytometry (Figure 21B), although the endogenous HLA-I molecules were still expressed in the cells (Figure 21C).

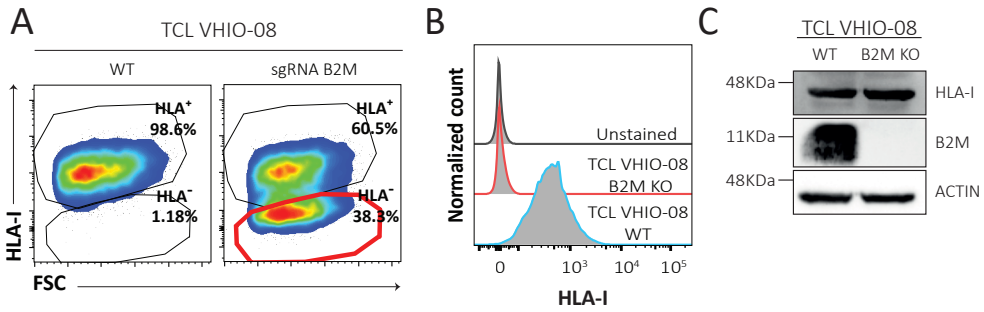


Figure 21. Generation of surface HLA class I negative tumoral cells by knocking out the B2M gene in VHIO-08 TCL. A) Flow cytometry plots showing HLA-I expression using a Pan-HLA-I antibody on VHIO-08 TCL at basal levels (WT) or four days after electroporation of the CRISPR/Cas9 + sgRNA B2M (sgRNA B2M) constructs. HLA-I negative cells were sorted (red gate) and expanded in culture to establish the B2M KO TCL. B) Flow cytometry evaluation of cell surface HLA-I expression using a Pan-HLA-I antibody on the established B2M KO TCL compared to the parental TCL (WT). The background autofluorescence (unstained) of B2M KO TCL is shown. C) Immunoblot analysis of B2M, HLA, and ACTIN in TCL VHIO-08 WT and B2M KO.

Next, we characterized the proteasome of the B2M KO cells since it is known that the activity of specific catalytic subunits can shape the repertoire of presented peptides (41). Western blot analysis revealed that the proteasome's three constitutive catalytic subunits (β1, β2, β5) were expressed by both the parental and B2M KO cells. In contrast, the inducible subunits (β1i, β2i, β5i) were expressed in B cells and hardly detectable in tumor cells.

We also detected the TAP1 and TAP2 proteins in B2M KO cells, suggesting that the translocation of degraded cytosolic peptides to the endoplasmic reticulum was preserved (Figure 22).

The results above indicated that we had generated a B2M KO cell model lacking cell surface HLA-I expression and with constitutive expression of a standard proteasome from a patient-derived TCL. This B2M KO cell model constituted the basis for establishing our HLA-I monoallelic platform and leveraging it for public neoantigen discovery.

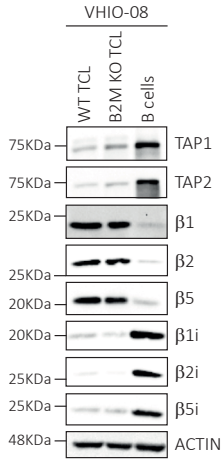


Figure 22. Characterization of the catalytic subunits of the proteasome and TAP proteins on B2M KO TCL. Immunoblot analysis of the constitutive β1, β2, β5 and the inducible subunits β1i, β2i, and β5i together with TAP1, TAP2, and ACTIN proteins in TCL VHIO-08 WT and B2M KO as well as in B cells derived from the same patient.

1.3.2.2. Generation of transient HLA-I monoallelic tumor cells expressing HSTMG

For the generation of HLA-I monoallelic cells, we first designed 13 B2M_HLA chimeras to cover each of the prioritized HLA-I alleles, as previously reported (261). Briefly, these constructs encoded the B2M protein linked via a short GS linker to the sequence of an HLA-I allele without the signal peptide, ensuring that only the HLA-I allele of interest was folded with β2M and loaded with intracellular peptides. This way, pHLA-I complexes on the cell surface of B2M KO recipient cells were expected to exclusively derive from the specific B2M_HLA allele expressed but not the endogenous alleles.

To analyze mutant peptides presented on each selected HLA-I allele at a time, we generated RNA from constructs encoding the 13 different B2M_HLA chimeras and the four HSTMG by IVT to further co-electroporate B2M_HLA-HSTMG combinations individually into B2M KO recipient cells. This system enabled us to study the presentation of the mutations selectively encoded in the HSTMG in transient HLA-I monoallelic cells.

To determine the optimal RNA quantity for achieving the highest percentage of transfected cells and expression level, considering the mean fluorescence intensity (MFI), while maintaining viability, increasing amounts of B2M_A*02:01 RNA or HSTMG1 RNA were electroporated into $2x10^7$ tumor cells. Cell surface expression was monitored using an anti-human Pan-HLA-I antibody and ZSG expression was evaluated as a surrogate for HSTMG expression. As observed in Figure 23, 12 μg of B2M_A*02:01 construct was enough to achieve the highest percentage of HLA-I positive cells with the least impact on cell viability (Figure 23A), while 18 μg appeared optimal in the case of the HSTMG construct (Figure 23B).

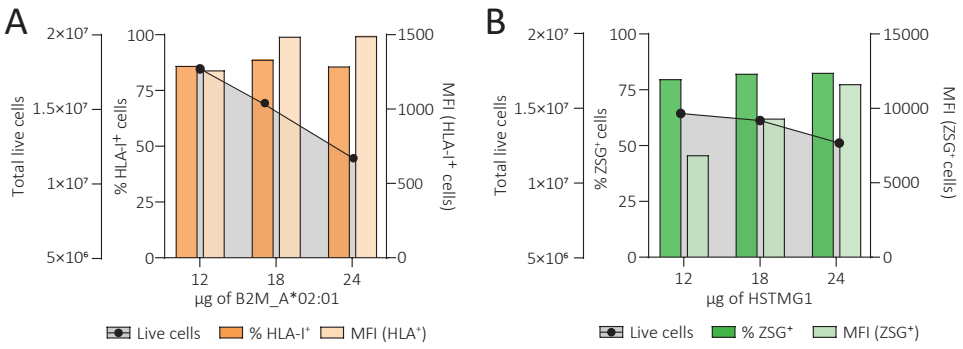


Figure 23. Evaluation of the optimal RNA quantity of HSTMG and B2M_HLA chimera for electroporation into B2M KO cells. Cells were transfected with increasing amounts of B2M_HLA chimera or HSTMG RNA. After 20h culture, the number of live cells was assessed via trypan blue staining using a Neubauer chamber while HLA-I and control gene ZSG expression was measured by flow cytometry. A) Cell surface expression of HLA-I was measured by staining with the Pan-HLA-I antibody to evaluate the transfection efficiency of B2M_A*02:01, as a representative construct of the B2M_HLA chimeras. B) The expression of ZSG was used to assess the transfection efficiency of HSTMG1, a representative example of the efficiency of the HSTMG RNA. The black dots, lines, and shaded areas indicated the number of total live cells (outer y-axis) while the bars indicated the % of positive cells (left y-axis) and mean fluorescence intensity (MFI) (right y-axis) for each marker as evaluated by flow cytometry. Data are representative of at least three independent experiments.

1.3.2.3. Optimizing the conditions for HLA-I ligandome screening by immunopeptidomics

After fixing the RNA quantity for each construct, we generated single or double transfectants using two different B2M_HLA chimeras, each combined with HSTMG1 to study the expression of the constructs as well as the HLA-I ligandome of electroporated B2M KO cells via immunopeptidomics.

Cell pellets with two different quantities of electroporated cells (i.e. $2x10^7$ and $6x10^7$ total cells) were generated in parallel to evaluate the best condition for identifying the highest number of HSTMG-derived peptides. As controls, we used two pellets of $6x10^7$ cells that were either not electroporated or transfected with HSTMG1 alone. These controls, both lacking exogenous expression of a B2M_HLA chimera, also enabled us to test the presence of residual HLA-I expression and presentation by the B2M KO cells.

As observed in Figure 24A, expression of ZSG or HLA-I was exclusively detected in tumor cells that were electroporated with the corresponding constructs (i.e., ZSG in HSTMG1-transfected cells and HLA-I in B2M_HLA chimera electroporated cells). Of note, equivalent levels of expression of B2M_HLA chimeras were observed when the cells were electroporated with the B2M_HLA construct alone or combined with HSTMG1 (Figure 24A). Based on these results, we decided to set a minimum transfection efficiency threshold of 65% for each of the constructs to proceed with LC-MS/MS in double transfectants.

Following immunopeptidomics via shotgun MS analysis of the single and double transfectants, we recovered from 1887 to 5895 peptides in all the conditions in which a B2M_HLA chimera was electroporated alone or combined with HSTMG1. The number of recovered peptides increased with the number of transfected cells used (Figure 24A). Notably, more peptides were recovered from B2M_A*02:01 transfectants than from B2M_A*03:01 (Figure 24A).

As expected, we did not detect peptides in B2M KO cells that had not been electroporated. However, despite the lack of surface HLA-I expression in B2M KO cells electroporated with HSTMG1 alone (Figure 24A), 465 peptides were identified. Of note, none of the peptides were derived from the construct introduced.

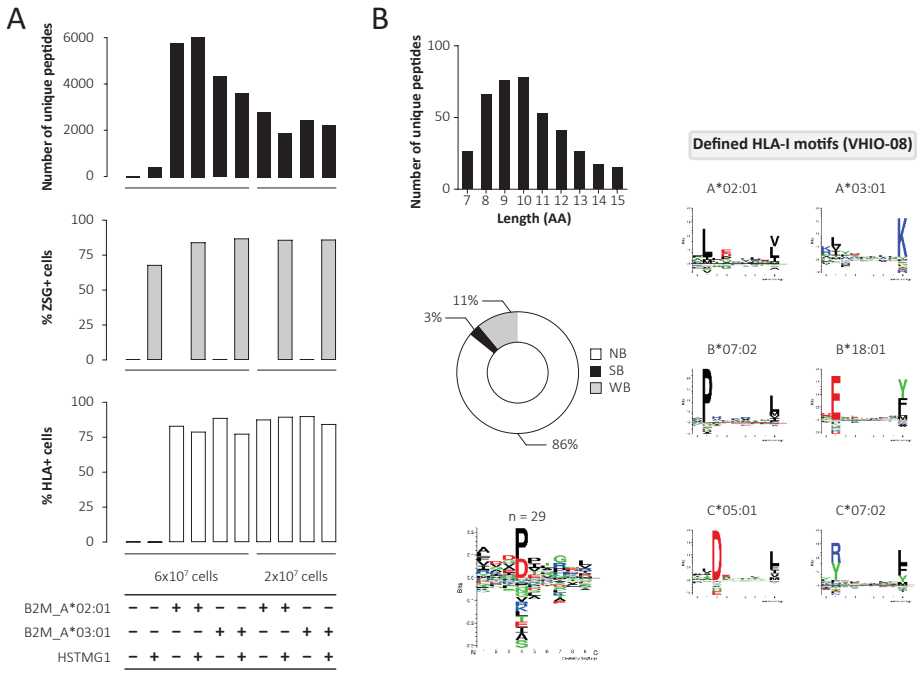


Figure 24. Transfection efficiency of single and double transfectants and immunopeptidomics analysis of HLA-I peptides of HSTMG1-single transfectant. A) Number of unique peptides eluted from HLA-I and identified by database search for each transfectant generated at 1% FDR using PEAKS Xpro (top). Transfection efficiency of HSTMG1 measured by ZSG reporter (middle) and of B2M_HLA chimeras measured by Pan-HLA-I staining (bottom) on single or double transfectants 20h post-electroporation. Constructs electroporated into the B2M KO cells are specified below. Results from cell preparations consisting of $2x10^7$ and $6x10^7$ cells are plotted. B) Characteristics of peptides recovered from single transfectant with HSTMG1. Length distribution of unique peptides (top left panel). Only peptides <15AA are plotted. Percentage of unique peptides (8-15AA) predicted to bind to endogenous HLA-I alleles of the recipient B2M KO cells (middle left panel). Peptides are classified as strong binders (SB) (%-tile EL rank <0.5), weak binders (WB) (%-tile EL rank 0.5-2), or not binders (NB) (%-tile EL rank >2) considering the minimal predicted %-tile EL rank for VHIO-08 HLA's. Single motif generated by unbiased grouping of 9-mer peptides using GibbsCluster 2.0 (bottom left panel). Defined HLA-I binding motifs of VHIO-08 patient HLA-I alleles according to NetMHCPan4.1-EL are depicted (right panel).

The peptides recovered from the HSTMG1 single transfectant did not follow the typical length distribution of peptides eluted from HLA-I (Figure 24B). They were not predicted as binders for any of the six endogenous HLA-I alleles, did not cluster in a group with conserved anchor residues according to GibbsCluster2.0, nor resembled any of the binding motifs of the HLA-I alleles from VHIO-08 patient (Figure 24B). Altogether, these results suggested that these peptides were derived from a contamination rather than classical HLA-I bound peptides.

Next, we analyzed the peptides recovered from single (only B2M_HLA chimera) or double transfectants (B2M_HLA chimera + HSTMG). The identified peptides displayed the typical features of HLA-I ligands, including length distribution (Figure 25A), regardless of the number of cells from which they were eluted. Moreover, approximately 80% of the recovered peptides from each transfectant were predicted as binders of the specific HLA-I allele introduced (Figure 25B). In addition, unsupervised clustering analysis of the peptides identified from each transfectant consistently clustered in a group that recapitulated the anchor motifs expected for HLA-A*02:01 or HLA-A*03:01 (Figure 25C). Overall, these results indicated that HLA-I ligands from B2M KO cells transfected with B2M_HLA chimeras displayed the expected characteristics for the HLA-I allele introduced.

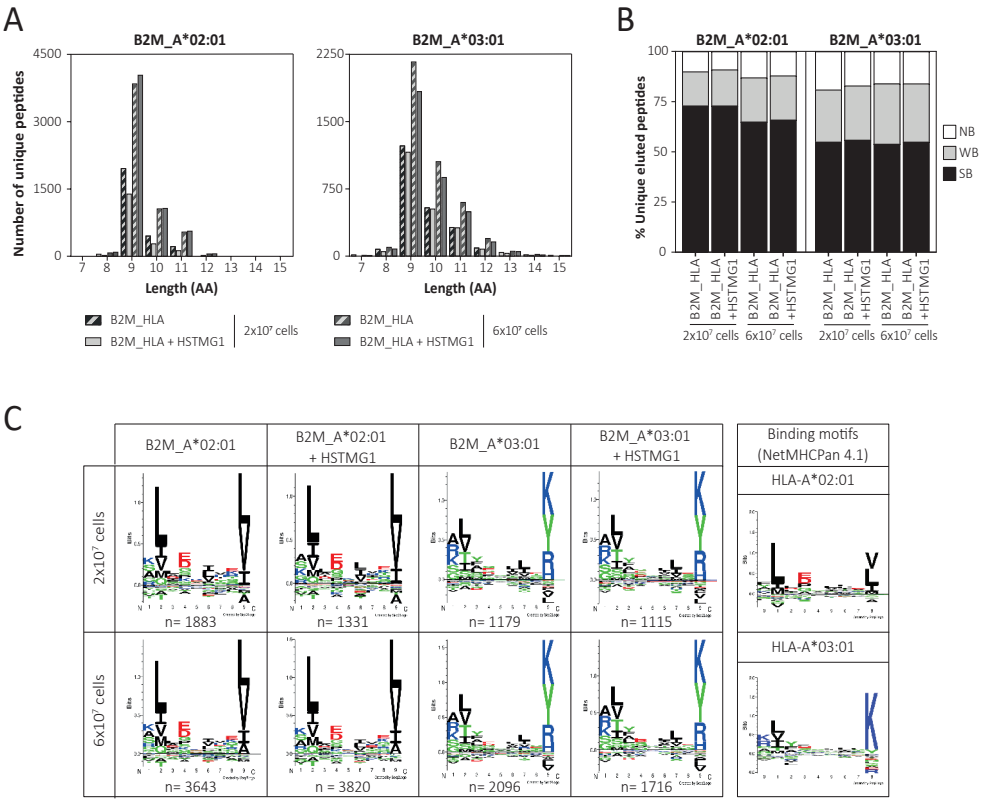


Figure 25. Peptides presented by B2M_HLA chimeras in electroporated B2M KO TCL display the expected HLA-I characteristics. A) Peptide length distribution of the total unique HLA-I peptide sequences identified for transfectants with B2M_A*02:01 or B2M_A*03:01 chimeras alone or in combination with HSTMG1 for the two cell quantities tested. Dashed bars show results from single transfectants with B2M_HLA chimeras. Solid bars represent results from double transfectants with B2M_HLA chimeras and HSTMG1. Only peptides <15AA are plotted.

B) The percentage of unique peptides ranging from 8 to 15 AA predicted to bind to the introduced B2M_HLA chimera either alone or in combination with HSTMG1 for the two cell quantities tested according to NetMHCPan4.1. Peptides were classified as strong binders (SB, %-tile EL rank <0.5), weak binders (WB, %-tile EL rank 0.5-2), and non-binders (NB, %-tile EL rank >2). C) Comparison of HLA-I binding motif from the introduced B2M_HLA chimeras to the consensus motif defined by NetMHCPan4.1-EL. Unique 9-mers identified in each of the generated single or double transfectants were used for the analysis. The optimal solution, according to GibbsCluster2.0, analyzed by default settings when allowing for a single group, is depicted. The number of peptide sequences (n=) is indicated in each case.

Further, these data also supported that the endogenous HLA-I alleles of the B2M KO cells were not able to stabilize and present peptides in the absence of the native B2M expression.

We then focused on identifying peptides derived from HSTMG1. As expected, detection of HSTMG-derived peptides was only possible when both constructs were co-electroporated. Notably, the number of total HSTMG-derived peptides identified was higher in cell preparations containing $6x10^7$ transfectants compared to $2x10^7$ cells. Specifically, we detected 24 and 27 HSTMG-derived peptides for B2M_A*02:01 and B2M_A*03:01, respectively, from $6x10^7$ transfected cells, compared to 13 and 12 HSTMG-derived peptides when using $2x10^7$ transfected cells (Figure 26). More details about the specific number of mutant ligands and their sequences are given in sections 1.4 and Appendix. Based on the enhanced capability to capture HSTMG-derived peptides in single HLA-I alleles, we found that the optimal number of cells to generate novel double transfectants by this approach was $6x10^7$ cells.

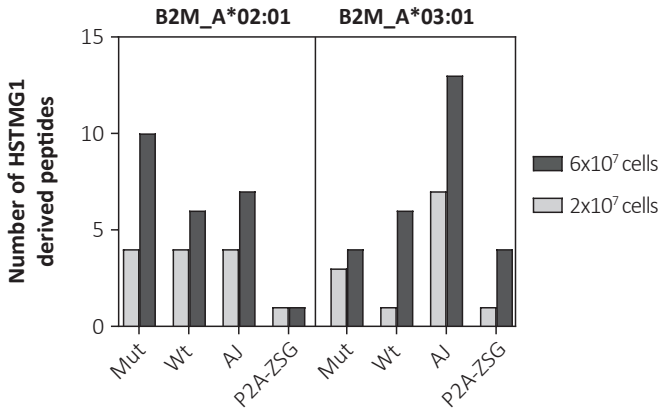


Figure 26. Greater cell numbers of double transfectants enabled the detection of more HSTMG-derived peptides via immunopeptidomics. Comparison of the number of HSTMG1-derived peptides identified per category (mutated (Mut), wild-type (Wt), artificial junction (AJ) and P2A-ZSG) in double transfectants for the two cell quantities evaluated.

All mutant and wild-type peptides mapping to the HSTMG1 construct were considered for this analysis, irrespective of whether they mapped to minigenes encoding for shared or private mutations included in the HSTMG1 construct. The specific category of hits derived from HSTMG1 is annotated for B2M_A*02:01 and B2M_A*03:01 combinations.

Overall, our data established the B2M KO cells transiently expressing a B2M_HLA chimera and antigen of interest as a flexible RNA-based HLA-I monoallelic platform to discover novel epitopes via immunopeptidomics.

1.4. Identification of HSTMG-derived peptides presented on HLA-I monoallelic tumor cells

To comprehensively investigate the presentation of neoantigens across various HLA-I alleles, we generated 40 transfectants carrying a combination of one of four HSTMG and one of 13 B2M_HLA chimeras. Thereafter, we immunoprecipitated pHLA-I complexes and analyzed the HLA-I ligands from each generated transfectant through shotgun MS.

The mean total number of unique peptides recovered from each of the B2M_HLA chimeras analyzed when combined with the three different HSTMG constructs ranged from 1055 peptides for B2M_C*04:01 to 7053 peptides for B2M_A*11:01 (Figure 27A, left panel). For B2M_A*03:01, which was also combined with HSTMG4, the total number of unique peptides was within the above-mentioned range. Importantly, all peptides recovered from the different HLA-A, HLA-B, and HLA-C chimeras displayed the expected HLA-I characteristics in terms of peptide length distribution, HLA-I binding affinity and recapitulated the expected HLA-I binding motifs for each of the introduced alleles (Appendix Figure 3).

The number of unique peptides retrieved varied significantly and was correlated with the percentage of HLA-I$^+$ cells obtained following transfection of the 13 different B2M_HLA chimeras (Figure 27A, left panel, and 27B $r = 0.6007$; $p<0.0001$). It is unclear whether this variability is due to a potential differential binding of the Pan-HLA-I antibody to HLA-I alleles or to differences in the stability and/or transfection efficiency among the B2M_HLA chimera constructs used.

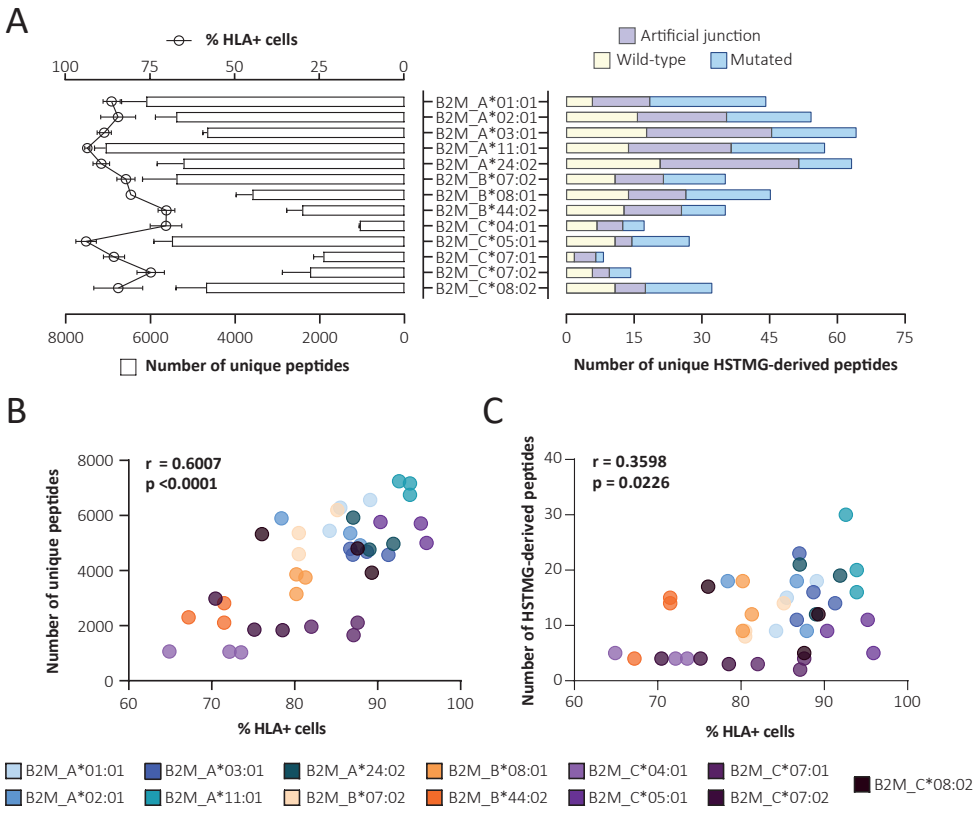


Figure 27. Characterization of HSTMG-derived peptides presented by B2M_HLA chimeras electroporated into B2M KO TCL. A) Number of total unique peptides identified by LC-MS/MS from B2M KO cells transfected with the B2M_HLA chimera and percentage of Pan-HLA-I expression measured by flow cytometry for each B2M_HLA chimera analyzed (left). Mean and SD are plotted for each chimera considering the three HSTMG studied (HSTMG1-3) except for B2M_A*03:01(*), for which an extra HSTMG was evaluated (HSTMG1-4). The total number of unique HSTMG-derived peptides classified per category is shown (right). All peptides mapping to the HSTMG constructs were considered for this analysis, irrespective of whether they mapped to shared or private minigenes encoding for mutations included in the HSTMG constructs. Peptide sequences mapping to P2A-ZSG are not shown. B) Correlation analysis between the total number of unique peptides identified for each B2M_HLA chimera and % HLA-I$^+$ cells. Each dot represents a single transfectant where a B2M_HLA and one HSTMG construct were combined. C) Correlation analysis between the total number of unique HSTMG-derived peptides to % HLA-I$^+$ cells. Only HSTMG-derived hits that can be unequivocally attributed to the introduced HSTMGs, excluding wild-type peptides, are considered for each transfectant. The p-value and Spearman's rho (r) for each analysis are annotated in the corresponding graph.

A highly variable number of HSTMG-derived hits were identified in each chimera, ranging from 9 to 70 total unique sequences. Mutated and artificial junction were the most abundant categories. Nonetheless, we detected peptides derived from minigenes encoded throughout the entire construct sequences for all HSTMG

studied, indicating that tumor cells effectively processed the entire polypeptide.

Importantly, at least one mutant peptide derived from the 97 mutations (35 hotspot drivers and 62 patient-specific) encoded in the four HSTMG was captured by shotgun MS from each B2M_HLA chimera (Figure 27A, right panel). Moreover, the number of peptides unequivocally derived from HSTMGs, excluding wild-type peptides, showed a correlation with the percentage of HLA-I^{+} cells obtained following transfection of the 13 different B2M_HLA chimeras ($r = 0.3598$; $p = 0.0226$) (Figure 27C), but not with the expression of ZSG ($r = 0.1370$; $p = 0.3992$) (not shown).

Overall, 124 mutant peptides were identified across 13 HLA-I alleles: 49 from hotspot mutations in driver genes representing 84 peptide-HLA pairs (Figure 28), and 75 peptides derived from patient-specific mutations representing 96 peptide-HLA pairs (Appendix Figure 4).

1.4.1. Identification of public neoantigens presented by highly prevalent HLA-I alleles

The 49 mutated HLA-I ligands detected were derived from 22 different recurrent mutations encoded in the HSTMGs. A total of 84 peptide-HLA pairs were detected; while some of the 49 identified neoepitopes were presented by multiple B2M_HLA chimeras, others were restricted by a single B2M_HLA chimera. Among these pairs, B2M_A*01:01 emerged as the top presenter for mutant ligands. Notably, at least one hotspot-derived neoantigen was identified for each B2M_HLA chimera studied, except for B2M_C*07:01 (Figure 28).

By using HLA-I monoallelic cells, we captured 19 out of the 29 previously reported public neoantigens encoded in our HSTMG constructs, indicating our strategy was capable of detecting relevant neoantigens. One such neoantigen was a 10-mer derived from $KRAS_{p.G12D}$ presented in HLA-C*08:02 (76). Another relevant example is the detection of a 9-mer derived from $PIK3CA_{p.H1047L}$ presented in HLA-A*03:01 (223). More importantly, we also discovered many novel putative neoantigen-HLA pairs.

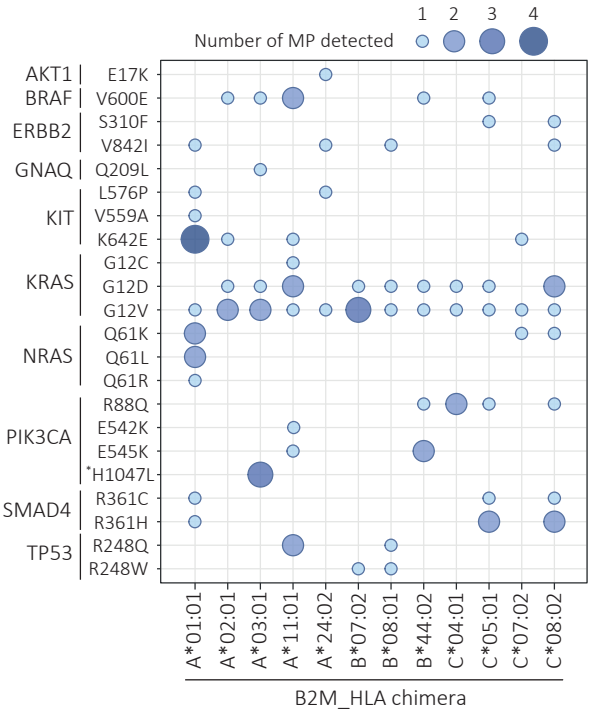


Figure 28. HLA-I immunopeptidomics of HLA-I monoallelic tumor cells detected more than 80 mutant peptide-HLA pairs derived from 22 shared cancer neoantigens presented by 12 HLA-I alleles. The number of mutated peptides (MP) detected by HLA-I immunopeptidomics is displayed for each of the B2M_HLA chimeras studied. The specific gene, position, and specific AA change are specified. The PIK3CA$_{p.H1047L}$ labeled as (*) was encoded in HSTMG4, which was studied only in combination with B2M_A*03:01.

With few exceptions, the peptides mapping to hotspot-derived neoantigens were identified in samples transfected with the specific constructs encoding the corresponding recurrent mutation, suggesting that those peptide sequences were correctly identified (Appendix Figure 5). It is worth noting that although B2M KO cells harbored the PIK3CA$_{p.E542K}$ variant (Table 7), the mutant peptide was only detected in the B2M_A*11:01 and HSTMG2 transfectant and not in other HSTMG-B2M_HLA chimera combinations. This indicated that the peptide identification was due to the introduced RNA of HSTMG2, which encoded this recurrent mutation, rather than the expression of the endogenous mutant protein of the tumor cell line. Moreover, the peptide was exclusively presented by the B2M_A*11:01 chimera (Figure 28).

Altogether, these results showed that this method, based on HLA-I monoallelic tumor cells and shotgun MS, appeared more sensitive at detecting mutated peptides than the B cell strategy (see section 1.3.1.2). Importantly, immunopeptidomics of HLA-I monoallelic cells led to the detection of a considerable number of novel candidate mutant peptide-HLA pairs that had not been previously reported in the literature. Nonetheless, given that we set a 1% False discovery rate (FDR) as a threshold to identify the HLA-I ligands by mass spectrometry, a small fraction of these could be miss-identifications. Moreover, against all odds, three peptide sequences derived from $BRAF_{p.V600E}$ (KIGDFGLATEK), $KRAS_{p.G12D}$ (GADGVGKSAL) and $KRAS_{p.G12V}$ (VVVGAVGVGK) were consistently identified when HSTMG1 or HSTMG2 were electroporated in B2M KO cells, regardless of the specific B2M_HLA chimera expressed. This raised concerns that these could represent false positives. To generate a more curated list of mutant peptide-HLA pairs presented with high confidence, we sought to perform PRM-MS.

1.5. Applying targeted mass spectrometry for validation of selected mutant peptide-HLA combinations

This thesis focused exclusively on identifying mutant peptides derived from hotspot mutations in driver genes across 12 prevalent HLA-I alleles and HLA-C*08:02, which did not meet the 5% frequency threshold in the European Caucasian population. From now on, all results refer to the 74 peptide-HLA pairs detected in these 12 prevalent HLA-I alleles.

We used PRM-MS to validate the selected mutant hotspot-derived neoantigens. This method is used routinely in the field of proteomics and immunopeptidomics, providing high selectivity and high sensitivity for confident target peptide confirmation. To this end, we generated new snap-frozen pellets of B2M KO cells expressing the combinations that led to at least one identified mutant peptide by shotgun MS (in total 28 HSTMG-B2M_HLA chimera combinations) and purified the HLA-I peptides.

In parallel, we purchased the individual isotope-labeled peptide versions of the sequences of interest (a total of 48 peptides). We generated pools of the labeled peptide versions and spiked these into each corresponding sample, and both the heavy (isotope-labeled) and light (endogenous) peptides were monitored through

PRM-MS. Only those ligands for which both peptide versions were detected were considered as validated for a particular HSTMG-B2M_HLA combination.

1.5.1. Removing false identifications from shotgun mass spectrometry screenings

As mentioned in section 1.4.1, we noticed that three peptides were repeatedly identified in several B2M_HLA chimera HSTMG1/HSTMG2 combinations. Of note, these peptides had been previously reported to be exclusively presented in HLA-A*03:01, HLA-B*07:02, and HLA-C*05:01 alleles (178,180,181). Given that these HLA-I alleles were present in the original VHIO-08 TCL used for the obtention of B2M KO cells and that these were not cloned, we wondered whether we were dealing with an incomplete knockout of the B2M gene in VHIO-08 TCL. A small remanent of B2M competent cells could explain the repeated detection of these peptides from cells carrying different B2M_HLA chimeras and HSTMG1/HSTMG2 combinations, as a result of presentation by endogenous HLA-I alleles. Consistent with this hypothesis, when re-stained with more specific anti-HLA-I antibodies, we found that B2M KO tumor cells showed residual level of HLA-A*03:01 (0.4%) and HLA-C (0.8%) expression (Figure 29A).

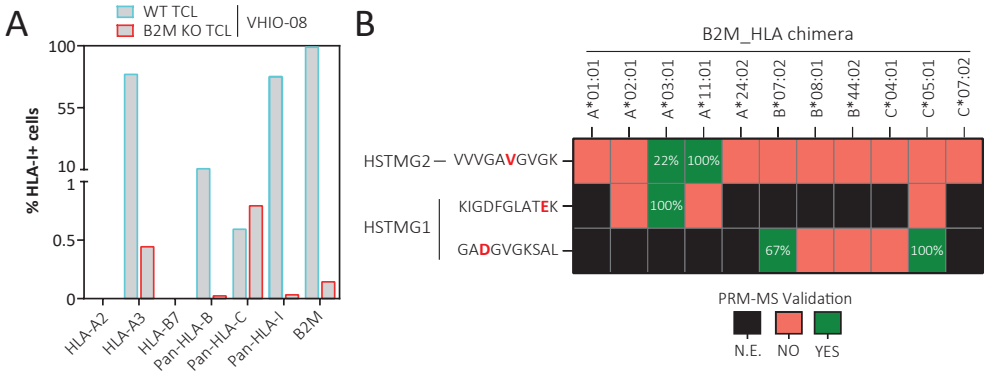


Figure 29. Residual HLA-I and B2M cell surface expression in B2M KO cells and PRM-MS validation of peptides detected using multiple B2M_HLA chimeras. A) Percentage of B2M KO and parental VHIO-08 WT TCL expressing surface HLA-I and B2M. Expression was assessed with allele-specific antibodies for VHIO-08 HLA-I (HLA-A2, HLA-A3, HLA-B7) and the Pan-HLA-B, Pan-HLA-C, Pan-HLA class I or B2M antibodies. B) Checkers plot showing the mutant peptides (hits) repeatedly detected by shotgun MS and confirmed by PRM-MS in various B2M_HLA chimera transfectants. The peptide sequence with the mutant AA highlighted in red, the HSTMG transfectant from which each peptide was derived and the specific B2M_HLA chimera are shown in the rows and columns, respectively.

Black squares indicate peptides that were not evaluated (N.E.) by PRM-MS. Red squares indicate peptides not validated according to PRM-MS (No), while green cells indicate peptides validated according to PRM-MS (Yes). The relative ratio light/heavy of validated peptides is annotated within the corresponding square.

To account for the interference from the residual expression of the endogenous HLA-I, even if very low, we introduced an additional validation filter for these three neoantigens. Given the low percentage of cells with residual HLA-I expression (lower than 1%) and the high transfection efficiency of B2M_HLA chimeras (over 65%), we anticipated that peptide presentation by residual HLA-I would result in lower peptide intensity. To differentiate between presentation by residual or transfected HLA-I alleles, we analyzed the relative ratio of light/heavy peptides in each transfectant. We considered these three neoantigens as validated in a specific B2M_HLA chimera only when the relative ratio of light/heavy peptide was above 20% of the highest ratio for that peptide (see materials and methods for more detail).

Using this more stringent criterion, only five peptide-HLA pairs were validated. More specifically, they were only validated by PRM-MS when presented in the expected B2M_HLA chimeras based on prior literature (178,180,181) (Figure 29B).

1.5.2. Generation of a curated list of validated neoantigen-HLA pairs

After removing the false positive peptide identifications resulting from residual B2M expression, we focused on validating the remaining 54 peptide-HLA pairs identified across 11 B2M_HLA chimeras. We decided to exclude five public neoantigens from our PRM-MS experiments (ILDTAGREEY from $NRAS_{p.Q61R}$ in B2M_A*01:01; VVVGADGVGK derived from $KRAS_{p.G12D}$ and ALHGGWTTK derived from $PIK3CA_{p.H1047L}$ in B2M_A*03:01; VVVGADGVGK and VVGADGVGK both derived from $KRAS_{p.G12D}$ in B2M_A*11:01) as they had previously been reported and validated by different mass spectrometry techniques (181,182,223,231). Of the remaining 49 peptide-HLA pairs, 38 were validated by PRM-MS. Of note, for B2M_A*24:02 and B2M_C*05:01 chimeras, all the identified peptide sequences via shotgun MS were effectively validated using PRM-MS (Figure 30A).

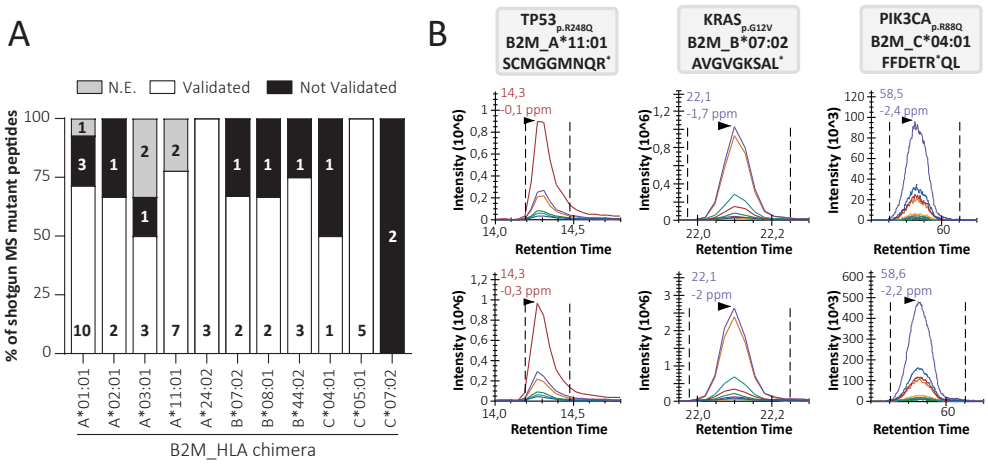


Figure 30. Targeted mass spectrometry guided validation of 38 peptide-HLA combinations detected by shotgun MS. A) Percentage of mutant peptides identified by shotgun MS and validated or not by PRM-MS. For some B2M_HLA chimeras, peptides already described in the literature were not evaluated (N.E.) by PRM-MS. Peptide-HLA pairs validated using the relative light/heavy ratio (Figure 16B) were not considered. The specific number of peptides for each group is annotated. B) Co-elution profile of transitions of endogenous (top) and isotope-labeled (bottom) peptides using Skyline software for three shared neoantigens detected in B2M_A*11:01, B*07:02 or B2M_C*04:01 chimeras. The isotope-labeled amino acids of the peptides monitored by PRM-MS are indicated by (*).

Among all validated candidates, the following exemplify three neoantigens consistently identified using shotgun MS and PRM-MS methods: SCMGGMNQR derived from $TP53_{p.R248Q}$, presented by B2M_A*11:01; AVGVGKSAL derived from $KRAS_{p.G12V}$, presented by B2M_B*07:02 and FFDETRQL derived from $PIK3CA_{p.R88Q}$, presented by B2M_C*04:01 (Figure 30B). These neoantigens represent promising candidates identified by our method for the development of cancer immunotherapies that could apply to multiple cancer patients.

Overall, PRM-MS led to the validation of 43 peptide-HLA pairs identified by shotgun MS. This included five peptide-HLA pairs mentioned in the previous section and the 38 peptide-HLA presented pairs in this section. Our results underscore the potential of this flexible RNA-based strategy, coupling expression of a selected HLA-I allele and antigen of interest and HLA-I immunopeptidomics, for discovering novel neoantigen-HLA pairs.

1.5.3. Exploiting increased sensitivity of targeted mass spectrometry for the identification of additional peptide-HLA pairs

PRM-MS is more sensitive than shotgun MS at identifying HLA-I peptides. Because of this, we decided to use this technique to investigate whether we could capture additional peptides derived from hotspot mutations encoded in our HSTMGs that were not detected through shotgun MS.

We first investigated six previously reported peptide-HLA combinations which theoretically could have been detected in our study but shotgun MS missed (75,178,182,218,252). By spiking the isotope-labeled peptides into the HLA-I preparations from selected HSTMG-B2M_HLA combinations and monitoring by PRM-MS the signals of the light and heavy versions, we identified four of the six selected neoantigens in the corresponding HLA-I alleles reported (Table 8). Notably, the two remaining neoantigens that were not validated, derived from $TP53_{p.R248Q}$ and $TP53_{p.R248W}$ mutations, were not originally described using mass spectrometry techniques (218). Nonetheless, this experiment evidenced the well-known limited sensitivity of shotgun MS and suggested that we may have missed peptide-HLA pairs of interest.

Table 8. Monitoring previously reported neoantigens that were not captured in the shotgun MS screening of HLA-I monoallelic tumor cells using targeted MS.

Peptide sequence	Shared neoantigen	HLA-I allele	Reference	Tested combination	Detected by PRM-MS
VVVGA**C**GVGK	$KRAS_{p.G12C}$	A*03:01	178	B2M_A*03:01 + HSTMG3	YES
VVGA**V**GVGK	$KRAS_{p.G12V}$	A*03:01	252	B2M_A*03:01 + HSTMG2	YES
		A*11:01	183	B2M_A*11:01 + HSTMG2	YES
HMTEVVR**H**C	$TP53_{p.R175H}$	A*02:01	75	B2M_A*02:01 + HSTMG1	YES
GMN**Q**RPILTI	$TP53_{p.R248Q}$	A*02:01	218	B2M_A*02:01 + HSTMG1	NO
GMN**W**RPILTI	$TP53_{p.R248W}$	A*02:01	218	B2M_A*02:01 + HSTMG2	NO

Peptide sequence with the mutant AA highlighted in red, shared neoantigen from which they derive, HLA-I presenting allele and the reference to the first report detecting the peptide-HLA pair are listed. The tested transfectants expressing the corresponding B2M_HLA chimera and HSTMG construct encoding for the mutation evaluated in each case and detection by PRM-MS in the corresponding transfectants is specified.

1.5.3.1. Prospective identification of HLA-I ligands by targeted mass spectrometry

When analyzing the peptides identified in our screenings, we noticed that most of the HLA-I ligands detected in the cells electroporated with B2M_A*03:01 chimera were also detected in cells electroporated with the B2M_A*11:01 chimera. The high overlap in peptide identification could be explained by the similarity between their HLA-I allele binding motifs (Figure 31A). Nevertheless, perhaps due to the limited sensitivity of shotgun MS, some peptides uniquely detected when transfecting with B2M_A*11:01 scored as potential binders to HLA-A*03:01 according to NetMHCPan4.1, and vice versa, but were not identified in those chimeras. For instance, we initially detected two mutant peptides derived from different PIK3CA mutations by shotgun MS uniquely in HLA-I preparations with the B2M_A*11:01 chimera. By monitoring these peptides in HLA-I preparations with B2M_A*03:01 using PRM-MS, which is more sensitive, we were also able to detect presentation of the HLA-I ligand STRDPLSEITK, derived from PIK3CA$_{p.E545K}$, by B2M_A*03:01 (Figure 31B).

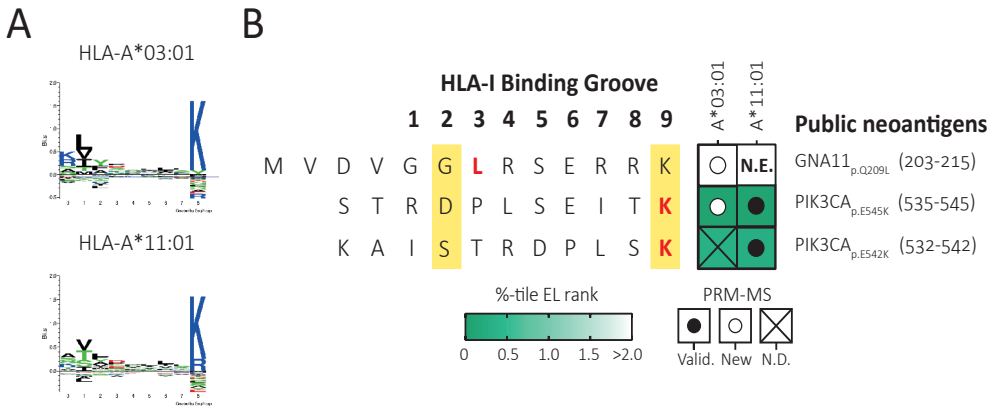


Figure 31. PRM-MS identified two additional peptide-HLA pairs. A) HLA-I binding motifs of HLA-A*03:01 and HLA-A*11:01 as defined by NetMHCPan4.1-EL are shown. B) The sequence of mutant peptides studied by PRM-MS aligned with the HLA-I binding groove. The amino acid sequences are aligned based on the consensus lysine (K) in position 9 of the peptide binding groove; anchor residues (P2 and P9) are highlighted in yellow. A heat map displaying the predicted binding affinity (%-tile EL rank) of each neoantigen for HLA-A*03:01 or HLA-A*11:01 alleles according to NetMHCPan4.1 is shown in the right panel. Peptides detected by shotgun MS and validated by PRM-MS (Valid.) in a specific B2M_HLA are labeled as black dots inside each corresponding cell. Peptides not identified by shotgun MS but detected by PRM-MS (New) in a B2M_HLA chimera are labeled as white dots.

Crossed cells represent peptides not identified by shotgun MS in a particular B2M_HLA chimera but monitored by PRM-MS for which the endogenous peptide was not detected (N.D.) and thus not validated in the specific HLA-I allele. Peptides not evaluated by PRM-MS in a specific B2M_HLA chimera are also indicated (N.E.). The recurrent mutations and coordinates in the protein of each public antigen are annotated.

We also checked for the presentation of a mutant ligand derived from $GNA11_{p.Q209L}$ in B2M_A*03:01. This experiment was prompted since, although GNA11 and GNAQ genes are highly homologous in their hotspot regions, we only detected a peptide derived from $GNAQ_{p.Q209L}$ presented by B2M_A*03:01 by shotgun MS. Indeed, targeted mass spectrometry identified this same public neoantigen derived from $GNA11_{p.Q209L}$ in B2M_A*03:01 (i.e. MVDVGGLRSERRK) (Figure 31B).

Overall, two additional mutant peptide-HLA pairs were uniquely identified through PRM-MS using this approach, along with four previously reported neoantigens that were originally missed by shotgun MS, as discussed in the previous section (Figure 32A, shown in orange). Altogether, PRM-MS identified mutant peptides in specific HSTMG-B2M_HLA combinations that would have been overlooked using only shotgun MS screenings.

1.5.4. Candidate public neoantigens identified through shotgun and targeted mass spectrometry screenings

Using our HLA-I monoallelic cell method, we identified and validated a total of 49 peptide-HLA pairs from 28 HSTMG-B2M_HLA chimera combinations studied (Figure 32A; Appendix Figure 6 and Appendix Table 1). The detected mutant peptides were derived from 23 out of the 35 hotspot mutations encoded by the HSTMG constructs. Despite 16 of the identified peptide-HLA pairs had been reported by other authors, we detected 33 novel peptide-HLA pairs by using our HLA-I monoallelic tumor cell system that, to our knowledge, had not been previously described (Figure 32B).

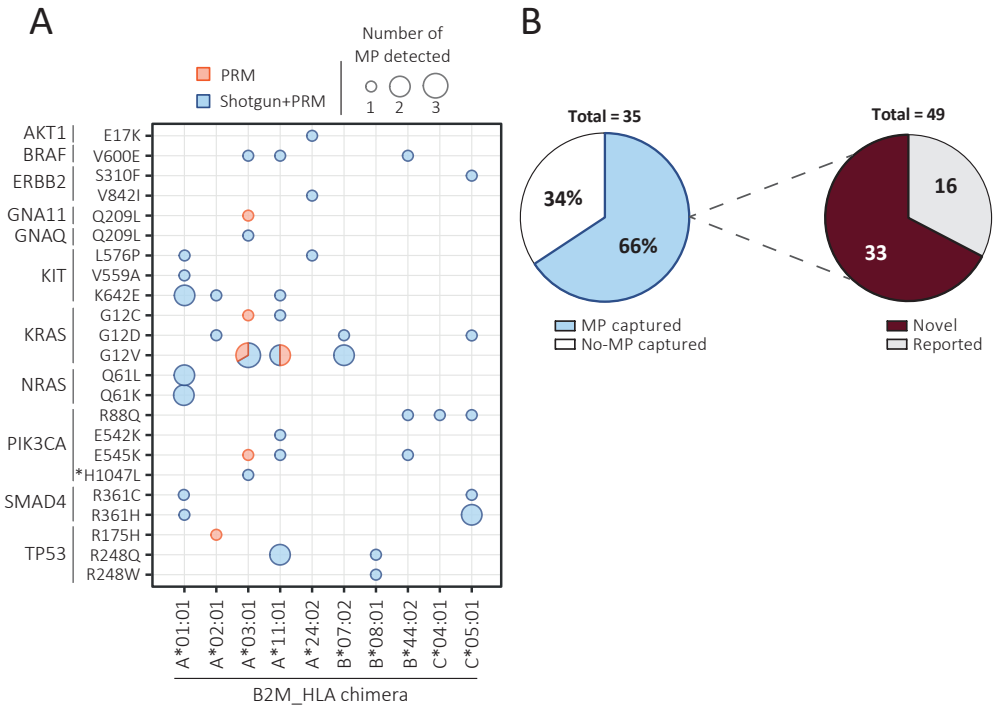


Figure 32. Forty-nine shared candidate neoantigens-HLA pairs were validated by PRM-MS. A) The number of mutated peptides (MP) detected only by PRM-MS (orange) or detected by shotgun and validated by PRM-MS (blue) are shown for the B2M_HLA chimeras analyzed, which includes only those chimeras where PRM-MS has validated at least one peptide. The name of the driver gene, the position, and the specific AA change are specified. The mutation labeled with (*) was encoded in HSTMG4, which was exclusively combined with B2M_A*03:01. B) Pie chart showing the percentage of shared mutations (n=35) encoded in HSTMG1-4, giving rise to at least one presented mutant peptide and validated by PRM-MS (MP captured) for the 12 B2M_HLA chimeras included in PRM-MS validations (left). Pie chart showing the number of peptide-HLA complexes validated by PRM-MS previously reported in the literature (reported) or, to our knowledge, identified for the first time (novel) (right). Only shared mutations encoded in HSTMG presenting at least one mutant peptide were considered for this analysis.

1.6. Comparison of empirically identified HLA-I mutant peptides to the performance of an HLA-I binding prediction algorithm

HLA-I binding prediction algorithms are routinely used to prioritize candidate neoantigens for the development of personalized vaccines or the identification of antigen-reactive TIL or TCRs (192,269).

As opposed to our approach to discover public neoantigens, which explored the presentation of any candidate peptide derived from the HSTMG constructs by 12 prevalent HLA-I alleles, other studies typically exploit HLA-I binding prediction algorithms to preselect a few mutant peptides that are investigated through targeted mass spectrometry (178).

To investigate whether our approach was advantageous, potentially capturing peptides that HLA-I binding prediction algorithms would have overlooked, we aimed to compare the experimentally identified mutant peptide-HLA pairs with those predicted by *in silico* HLA-I binding prediction algorithms. To this end, we employed the widely used NetMHCPan4.1 algorithm to predict peptides derived from the selected recurrent mutations that could bind to the evaluated HLA-I alleles.

To identify predicted mutant HLA-I binders, we uploaded the sequences of all 25-mers encoding the 35 hotspot mutations onto the NetMHCPan4.1 website. Mutant peptides with a %-tile EL rank <2 scores for binding with any of the 12 HLA-I alleles evaluated with PRM-MS were considered binders (only 8-14AA were considered as per default settings in NetMHCPan4.1). This analysis predicted 353 peptide-HLA combinations, with HLA-A*01:01 being the allele with the highest candidate mutant ligands (Figure 33, middle panel).

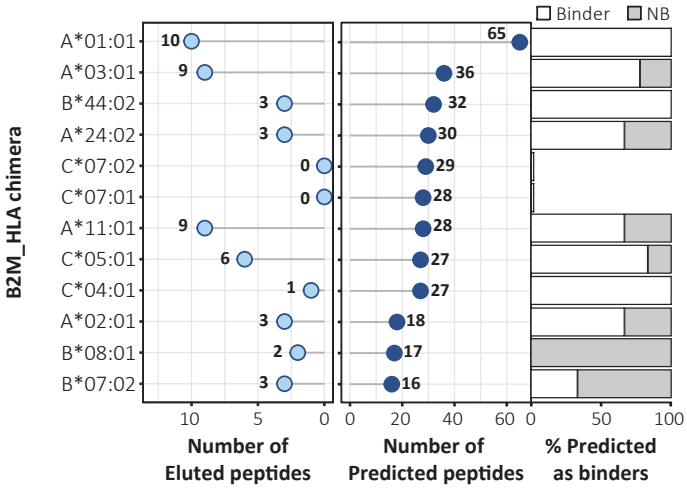


Figure 33. Comparison of experimentally eluted and identified mutant peptides to peptides predicted as binders by the NetMHCPan4.1 algorithm. The left and center plots show the number of experimentally identified peptides (labeled as eluted) vs predicted peptides for each HLA-I allele tested. Peptides derived from a total of 35 shared mutations encoded in the HSTMGs evaluated are represented. Mutant peptides within the 25-mers were considered binders if they were in the 8-14 AA range and had a %-tile EL rank <2 according to NetMHCPan4.1.

Bars in the right panel represent the percentage of peptides experimentally identified and validated in the mass spectrometry screenings that were considered binders (Binders; %-tile EL rank<2) or non-binders (NB; %-tile EL rank >2) by NetMHCPan4.1.

Importantly, almost 25% of the peptide-HLA combinations experimentally identified and validated by our method were not predicted to bind to the specific HLA-I allele restricting their presentation, as empirically determined using our method (Figure 33, left panel). The frequency of misclassified peptides was higher for some HLA-I alleles, including HLA-B*07:02 and HLA-B*08:01, for which most of the experimentally determined presented peptides were classified as non-binders by the HLA-I binding affinity algorithm (Figure 33, right panel). These results are particularly interesting because HLA-I binding algorithms are currently the most commonly used tool for generating peptide vaccines for cancer treatment. At least using this specific HLA-I binding prediction algorithm, peptides that were shown to be empirically processed and presented by specific HLA-I alleles were classified as non-binders. Consequently, these peptides would not have been prioritized for patient treatment.

Our method, based on MS screenings using HLA-I monoallelic tumor cells, enabled high-throughput mining for mutated peptides presented on frequent HLA-I alleles while limiting the bias for peptides prioritized based on HLA-I binding prediction algorithms.

1.7. Assessment of hotspot-derived neoantigen processing and presentation in patient-derived tumor cell lines

Next, we wanted to evaluate the reliability of our approach in identifying naturally processed and presented public neoantigens in a more physiological setting by tumor cells harboring the relevant variant and HLA-I allele. To this end, we evaluated the presentation capacity of two selected mutant peptide candidates, validated in our transfectants of B2M KO cells, $BRAF_{p.V600E}$ and $PIK3CA_{p.R88Q}$ presented by HLA-A*11:01 and HLA-C*05:01, in two patient-derived TCL. We selected VHIO-133 melanoma TCL and EC-35035 endometrial TCL, harboring the $BRAF_{p.V600E}$ and $PIK3CA_{p.R88Q}$ variants, respectively, as assessed by WES and RNA sequencing (Table 9).

Through HLA-I genotyping, these cell lines were also found to present the corresponding restriction elements, HLA-A*11:01 or HLA-C*05:01. Thus, we expanded the cell lines, performed immunopeptidomics and PRM-MS analysis to evaluate the spontaneous presentation of these peptides by the tumor cells.

Table 9. Features of patient-derived tumor cell lines used in PRM-MS exploratory experiments testing the spontaneous presentation of selected public neoantigens.

Patient ID	Tumor type	Shared somatic variant	(%-tile) Gene expression	Gene TPM	tVAF (DNA)	tVAF (RNA)	HLA-I typing
VHIO-133	Melanoma	$BRAF_{p.V600E}$	73.4	12.2	99.4	100	**A*11:01** A*30:02 B*18:01 B*35:01 C*04:01 C*05:01
EC-35035	Endometrial cancer, POLE	$PIK3CA_{p.R88Q}$	79	43.4	52	40	A*02:01 B*07:02 B*44:02 **C*05:01** C*07:02

Patient identification, tumor type, the detected shared somatic variant and the expression levels determined by WES and RNA sequencing of tumor DNA. The percentile (%-tile) gene expression, transcripts per million (TPM) and tumor variant allele frequency (tVAF) at DNA and RNA level are shown. HLA-I typing of the TCLs is indicated with the relevant HLA-I alleles presenting selected neoantigens in bold and underlined.

Although the two TCL expressed HLA-I molecules on the cell surface, as assessed with a Pan-HLA-I antibody (Figure 34A), we did not detect the corresponding interrogated peptides in these TCLs (Figure 34B).

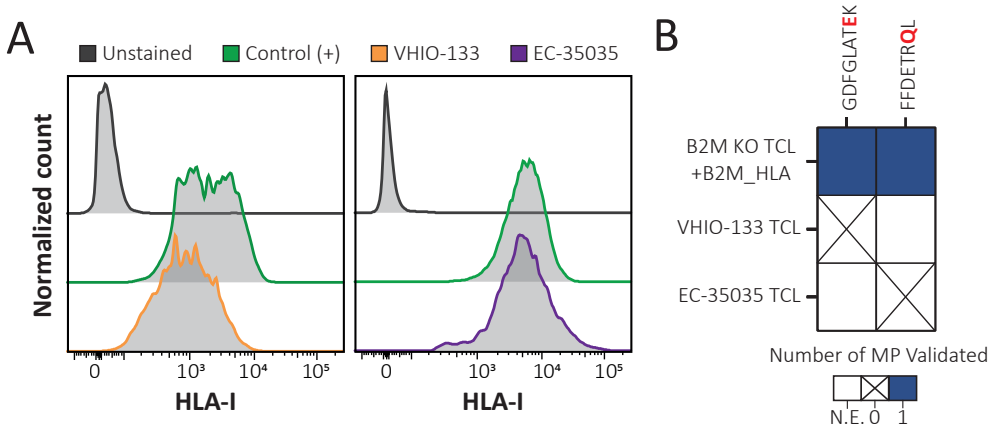


Figure 34. HLA-I cell surface expression and PRM-MS detection of two candidate shared neoantigens in patient-derived TCL. A) HLA-I surface expression of patient TCLs VHIO-133 and EC-35035 measured by flow cytometry using a Pan-HLA-I antibody. An unrelated patient-derived TCL (NCI-1913) was used as a positive control. The left and right plots show the background autofluorescence (unstained) of VHIO-133 and EC-35035 controls.

B) PRM-MS detection of peptide candidates GDFGLATEK (derived from $BRAF_{p.V600E}$) and FFDETRQL (derived from $PIK3CA_{p.R88Q}$) for the two-patient derived TCL compared to B2M KO cells transfected with B2M_A*03:01 or B2M_C*05:01 chimeras, respectively. Blue cells indicate mutant peptides (MP) that were detected through our method and validated by PRM-MS, and crossed cells indicate peptides that PRM-MS did not validate in the corresponding patient-derived TCL. White cells indicate peptides that were not evaluated (N.E.) by PRM-MS.

Based on these results, we suspected that these TCLs could present alterations of the APM, as this can directly impact the HLA-I ligandome of cells. Therefore, somatic mutations or an abnormal expression level of antigen processing and presentation-related genes in these tumor cells were evaluated and compared with data from other tumor cell lines of the same origin from the CCLE repository. For VHIO-133 TCL, we found a reduced expression of TAP1, and TAP2 which are important players for HLA-I presentation (Figure 35A), compared to other tumor cell lines derived from skin of the CCLE repository.

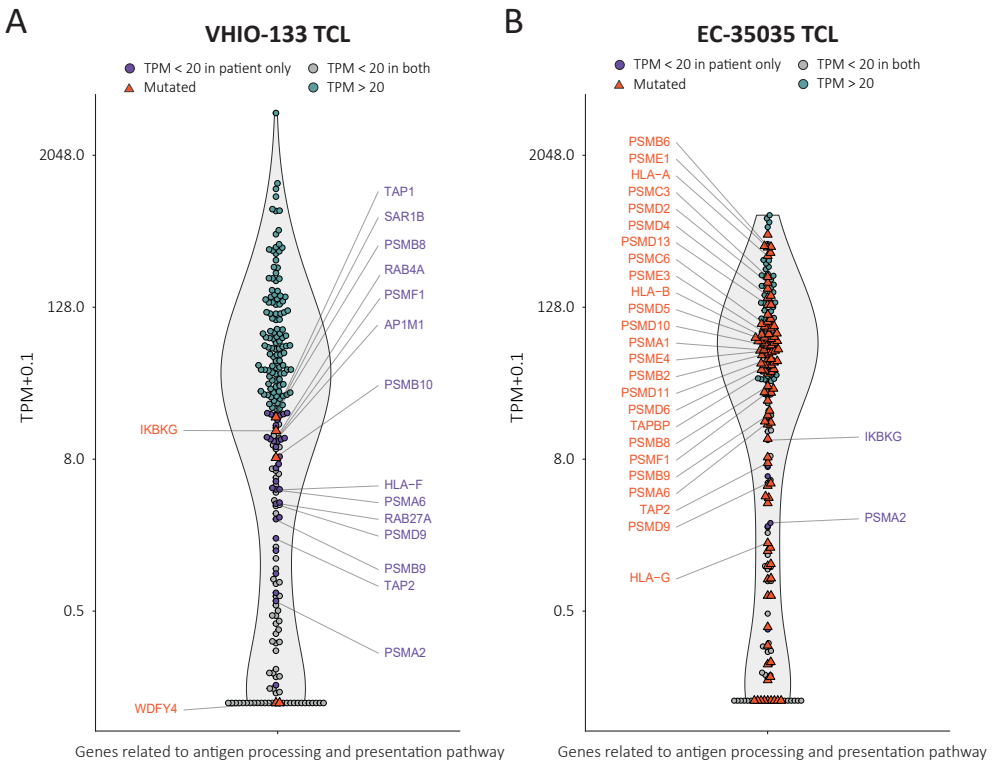


Figure 35. Characterization of alterations in the antigen presentation pathway of VHIO-133 and EC-35035 TCL. Expression levels of 234 genes included in a curated gene set based on the Gene Ontology Antigen Processing and Presentation pathway in VHIO-133 and EC-35035 TCL.

Expression level is plotted as Transcripts Per Million (TPM+0.1) and compared to the median expression levels of these genes in tumor cell lines originating from A) skin (n= 50) for VHIO-133 or B) endometrium (n=29) from the CCLE data repository. Gene expression levels are represented as dots for non-mutated and triangles for mutated genes; green dots indicate genes with higher expression (TPM > 20) and in purple with lower expression (TPM < 20) specifically in VHIO-133 or EC-35035 TCL but not in the corresponding CCLE biorepository (median TPM CCLE). Grey dots denote low expression (TPM < 20) in both VHIO-133 and EC-35035 TCL and CCLE cell lines. Genes of interest directly related to the HLA-I presentation pathway, poorly expressed genes (TPM< 20) in VHIO-133 or EC-35035 only, or mutated genes are labeled.

In the case of EC-35035 TCL, we observed several somatic non-synonymous or stop-gain mutations in many different genes related to this pathway. Of note, TAP2 as well as PSMB6, the gene encoding for the β1 catalytic subunit of the proteasome, both presented several non-synonymous mutations (Figure 35B). The alterations observed in each case could impact the pool of peptides that can be processed and presented by these patient-derived TCLs, potentially explaining the lack of presentation of the interrogated peptides.

Altogether, these results suggested that antigen presentation could be influenced by factors other than expression of the recurrent mutation and the HLA-I allele. Whether the public neoantigens identified through our approach are naturally processed and presented by patient-derived tumor cells warrants further exploration with a broader panel of tumor samples.

2. Isolation and characterization of TCRs reactive against hotspot mutations for their potential use to develop off-the-shelf T-cell therapies

After identifying peptides derived from hotspot driver mutations presented by specific HLA-I alleles, we aimed to detect T cells capable of targeting them. This could lead to the identification of TCRs that could be used for off-the-shelf T-cell therapies for cancer patients.

We explored IVS of PBLs, entailing subsequent antigen-specific stimulation with specific peptides, to potentially drive antigen-specific stimulation and capture TCRs reactive to different candidate public neoantigens across multiple HLA-I alleles within a single donor.

2.1. Detection of T-cell responses against hotspot-derived neoantigens in the peripheral blood of a breast cancer patient using *in vitro* sensitization

We sought to explore IVS for expanding neoantigen-specific circulating $CD8^+$ T cells obtained from the metastatic breast cancer patient GOI-01. We selected this patient because: 1) the tumor harbored the recurrent mutation $PIK3CA_{p.E545K}$ as detected by tumor DNA WES (Table 10) and 2) the patient was HLA-A*11:01$^+$, which, according to our HLA-I immunopeptidomics screenings, presented one mutated peptide derived from $PIK3CA_{p.E545K}$ hotspot mutation. In addition, this patient presented the highly prevalent allele HLA-C*04:01, which was also of interest, given its relatively high frequency in the Caucasian population and for which we had identified some candidate neoantigens through immunopeptidomics.

Table 10. Features of GOI-01 patient relevant to the IVS experiment.

Patient ID	Tumor type	Shared somatic variant	Recognized private neoantigens
GOI-01	Breast cancer	$PIK3CA_{p.E545K}$	**$KIAA1524_{p.S57I}$** $PLXNB3_{p.D252Y}$ $RPS6KL1_{p.K536fs}$

Patient identification, tumor type and shared somatic variant detected through WES of tumor DNA. In addition, the three recognized private neoantigens identified in a previous high throughput personalized screening of enriched subsets of GOI-01 PBLs performed in our laboratory are listed.

The neoantigen arising from the mutation highlighted in bold, recognized by enriched CD8+ PBL subsets, was included in MEP-2 for the IVS experiment.

Thus, we exploited IVS to expand potentially pre-existing T-cell responses against PIK3CA$_{p.E545K}$ from GOI-01 PBL and to induce de novo responses to other public neoantigens presented in these two HLA-I alleles. To this end, we generated two personalized minimal epitope pools (MEPs) (MEP-1 and MEP-2) containing candidate public neoantigens identified through our immunopeptidomics screenings on either of the two HLA-I alleles of interest. MEP-1 and MEP-2 shared ten candidate public neoantigens presented by HLA-A*11:01 or HLA-C*04:01 (Table 11). Additionally, MEP-2 contained four neoantigens, three derived from KRAS$_{p.G12C}$ and KRAS$_{p.G12V}$ recurrent mutations that had previously been shown to induce de novo responses from HLA-A*11:01+ HD PBLs (178,179). Furthermore, it included a mutant peptide derived from a private neoantigen, KIAA1524$_{p.S57I}$ restricted to HLA-B*40:01 (Table 10 and Table 11), recognized by CD8+ PBL-enriched subsets of GOI-01 using a high-throughput personalized screening performed in our laboratory (Appendix Figure 7). This peptide served as an internal control to investigate whether our IVS protocol could enrich for a known CD8+ T-cell reactivity present in the blood.

Table 11. Minimal epitope pools (MEP) used for the IVS experiment with GOI-01 PBLs.

						Pools for IVS	
Minimal epitope ID	**Peptide sequence**	**Length**	**Neoantigen**	**Presented by**	**PRM-MS Validated**	**MEP-1**	**MEP-2**
ME_1	SSCMGGMN**Q**R	10-mer	TP53$_{p.R248Q}$	A*11:01	YES		
ME_2	SCMGGMN**Q**R	9-mer			YES		
ME_3	KIGDFGLAT**E**K	11-mer	BRAF$_{p.V600E}$		NO		
ME_4	GDFGLAT**E**K	9-mer			YES		
ME_5	STRDPLSEIT**K**	11-mer	PIK3CA$_{p.E545K}$		YES		
ME_6	ALMSEL**E**VLSY	11-mer	KIT$_{p.K642E}$		YES		
ME_7	KAISTRDPLS**K**	11-mer	PIK3CA$_{p.E542K}$		YES		
ME_8	GA**D**GVGKSAL	10-mer	KRAS$_{p.G12D}$	C*04:01	NO		
ME_9	FFDETR**Q**LC	9-mer	PIK3CA$_{p.R88Q}$		NO		
ME_10	FFDETR**Q**L	8-mer			YES		
ME_11	VVVGA**C**GVGK	10-mer	KRAS$_{p.G12C}$	A*11:01	YES		
ME_12	VVVGA**V**GVGK	10-mer	KRAS$_{p.G12V}$		YES		
ME_13	VVGA**V**GVGK	9-mer			YES		
ME_14	SECL**I**CLVEL	10-mer	KIAA1524$_{p.S57I}$	B*40:01	N.E.		

The minimal epitope identification, the peptide sequence with the mutant AA highlighted in red, its length, and the neoantigen from which it originated are annotated. Peptide sequences (ME1-13) were identified by shotgun MS as presented by HLA-A*11:01 or HLA-C*04:01 and validated by PRM-MS in the corresponding HSTMG-B2M_HLA transfectants. The private neoantigen from GOI-01 binding to HLA-B*40:01, which was not evaluated (N.E.) in our PRM-MS studies, was included as a control. Peptides contained in MEPs are marked in pale blue or dark blue for MEP-1 and MEP-2, respectively, in the last two columns.

Although we were interested in raising T-cell responses to public neoantigens restricted to the prevalent alleles HLA-A*11:01 or HLA-C*04:01 from GOI-01, we were concerned that other HLA-I alleles with similar HLA-I binding motifs (Figure 36A) could also present the candidate public neoantigens. In silico predictions confirmed that the candidate neoantigens contained in MEP-1 and MEP-2 could potentially bind to other HLA-I alleles present in the patient (Figure 36B). This, together with the potential competition among peptides from a pool for binding to one same HLA-I, could limit the amount of peptide presented on the allele of interest. Therefore, for the HLA-A*11:01-PIK3CA$_{p.E545K}$ minimal epitope (ME), we chose to perform IVS individually to maximize the possibility of detecting a T-cell response to this specific peptide.

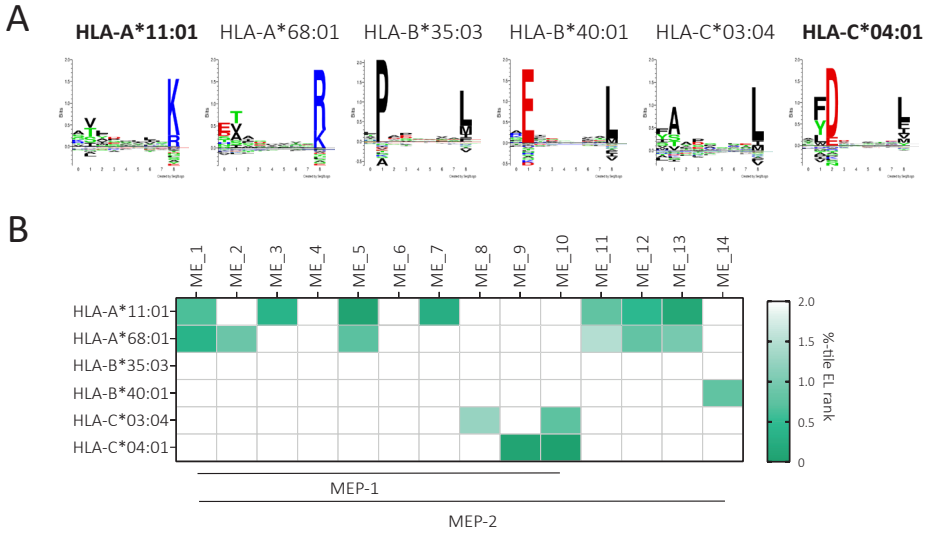


Figure 36. Patient GOI-01 HLA-I genotype and binding affinity prediction of the epitopes included in the corresponding MEPs to the patient's HLA-I alleles. A) HLA-I genotyping according to GOI-01 PBMC WES data. Reference consensus binding motifs generated by NetMHCPan4.1-EL for each HLA-I allele are shown. B) Heat map displaying the predicted HLA-I binding affinity (%-tile EL rank) according to NetMHCPan4.1 of the minimal epitopes (ME) contained in MEP-1 and MEP-2 for each patient HLA-I alleles. The specific ID of each ME is specified.

In addition, CEF peptide pool (PP), consisting of minimal epitopes from cytomegalovirus (CMV), EBV and Influenza virus (Flu) binding to prevalent HLA-I alleles, was used as a positive control for detecting HLA-I responses.

We conducted multiple rounds of stimulation on two independent replicates per condition using an IVS protocol based on prior literature with some modifications to enhance the activation and expansion of specific T-cell responses. After each stimulation round, we assessed the frequency of peptide-reactive T cells by measuring the upregulation of the 4-1BB activation marker following co-culture with autologous peptide-pulsed B cells using flow cytometry. Alternatively, we used peptide-loaded HLA-I dextramer staining to identify expanded T-cell reactivities. If any reactivity was detected by these readouts, the identified 4-1BB$^+$ or HLA dextramer$^+$ T cells were isolated and expanded ex vivo. Finally, the TCRs of the resulting peptide-reactive enriched populations were sequenced and cloned for further characterization (Figure 37).

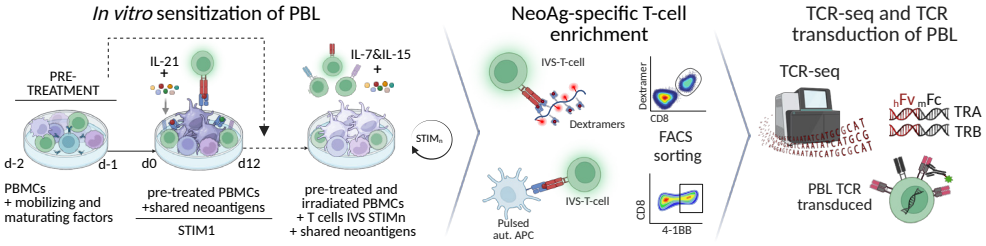


Figure 37. Schematic representation of the strategy for enriching and isolating T cells and TCRs targeting shared neoantigens through in vitro sensitization. Cancer patient peripheral blood lymphocytes (PBL) were *in vitro* sensitized via four consecutive rounds of stimulation with HPLC (High-Performance Liquid Chromatography) grade peptides representing selected HLA-I ligands identified through immunopeptidomics. Briefly, before every stimulation round PBMCs were pre-treated with mobilizing (IL-4 and GM-CSF) and maturating factors (including IFN-γ and LPS, among others). The first stimulation round (STIM1) started with the pre-treated PBMCs pulsed with the corresponding shared neoantigens cultured in the presence of IL-21 to promote the induction of naïve T-cell responses. For re-stimulation, T cells from the previous stimulation round (T cells IVS STIMn) were cultured with pre-treated and irradiated PBMCs in the presence of IL-7 and IL-15 with the pool of shared neoantigens used in the previous stimulation (STIMn). Further details of the specific IVS protocol are provided in the Materials and Methods section. After each stimulation round, the expansion of neoantigen-specific T cells was evaluated. When detected, reactive in vitro sensitized T cells (IVS-T-cell) were enriched through FACS sorting based on custom HLA dextramer positivity or CD8$^+$ 4-1BB$^+$ expression after 20h co-culture with autologous B cells pulsed with the specific peptides and expanded for 14 days in a REP (NeoAg-specific T-cell enrichment). Following bulk and single-cell TCR sequencing, the most frequent TCRαβ pairs were cloned into a retroviral vector to transduce PBL (PBL TCRtd).

The TCR constructs contained mouse constant regions, enabling the detection of the TCRtd lymphocytes by using antibodies specific to the mouse constant region (TCRtd$^+$). The resulting PBL TCR transduced cells were used to characterize TCR reactivity.

2.1.1. IVS of PBL with PIK3CA$_{p.E545K}$ minimal epitope elicited an HLA-A*11:01 restricted T-cell response

We investigated whether we could raise a T-cell response from PBL to the HLA-A*11:01 restricted PIK3CA$_{p.E545K}$ peptide by IVS in cancer patient GOI-01. As previously mentioned, this mutant peptide was included in both MEP-1 and MEP-2 used for stimulation. Additionally, two replicates independently stimulated with the PIK3CA$_{p.E545K}$ minimal epitope were included.

After the first sensitization round, there was no evidence of T-cell recognition of this public neoantigen. However, after the second round of stimulation, approximately 1% of the CD8$^+$ T-cell population bound to dextramers loaded with HLA-A*11:01-PIK3CA$_{p.E545K}$ minimal epitope (Figure 38A, top panel). This reactivity was only detected in one of the replicates in which PBLs were sensitized exclusively with this ME. Remarkably, neither upregulation of 4-1BB nor HLA dextramer staining detected any additional reactivity to this neoantigen in the conditions stimulated with MEPs.

Next, CD8$^+$ lymphocytes binding to the dextramer were enriched using FACS and the sorted cells were expanded using a rapid expansion protocol (REP). This strategy led to the enrichment of the reactive population, increasing its frequency fifty-fold from around 1% after IVS, to up to 50% after sorting and expanding them ex vivo (Figure 38A).

Co-culture assays with autologous B cells confirmed recognition of the shared neoantigen derived from PIK3CA$_{p.E545K}$ by the resulting peptide reactive T cells. B cells were either pulsed with the ME used for sensitization, the 25-mer peptide encoding for the hotspot mutation, or electroporated with RNA derived from HSTMG1 encoding for PIK3CA$_{p.E545K}$ minigene. Enriched T cells were co-cultured with the different B cells and T-cell reactivity was evaluated by measuring 4-1BB upregulation and IFN-γ secretion captured by ELISPOT. HLA-A*11:01_PIK3CA$_{p.E545K}$ dextramer-sorted T cells recognized the mutant peptide. The reactivity was mutation-specific, as T cells did not recognize the wild-type counterpart.

Of note, T-cell recognition of HSTMG1-expressing B cells was barely detectable compared to peptide-pulsed B cells, suggesting impaired processing of these constructs by these cells (Figure 38B).

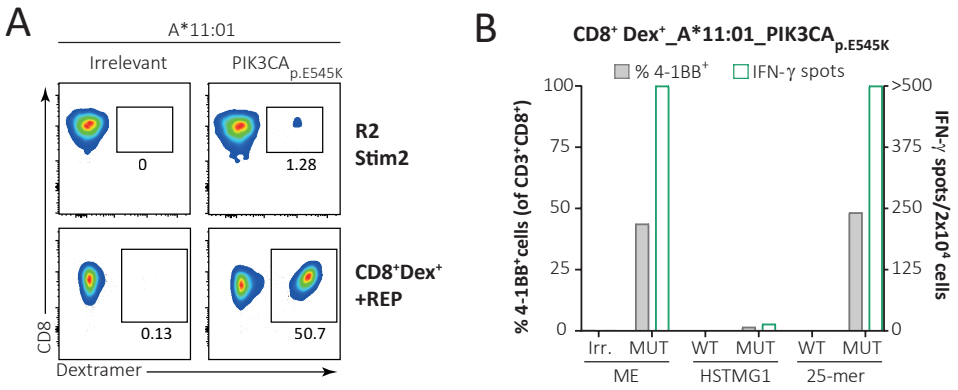


Figure 38. Detection, enrichment, and target recognition of a T-cell population sensitized with an HLA-A*11:01-PIK3CA$_{p.E545K}$ neoantigen. A) Flow cytometry plots showing CD8$^+$ T cells stained by HLA-A*11:01 dextramers loaded with PIK3CA$_{p.E545K}$ neoepitope or an irrelevant peptide. The top panel shows the T-cell staining of replicate-2 (R2) after two rounds of sensitization with the PIK3CA$_{p.E545K}$ neoepitope. The bottom panels show dextramer$^+$ CD8$^+$ HLA-A*11:01-PIK3CA$_{p.E545K}$ T cells stained after enrichment by FACS sorting and expansion by REP (CD8$^+$Dex$^+$ + REP). B) Functional assessment of neoantigen recognition by enriched dextramer$^+$ CD8$^+$ T cells (CD8$^+$ Dex$^+$_A*11:01_PIK3CA$_{p.E545K}$). GOI-01 ex vivo expanded B cells were pulsed with either an irrelevant (Irr.) or the relevant mutated (MUT) PIK3CA$_{p.E545K}$ minimal epitope (ME) peptides, wild-type (WT) and MUT long 25-mer peptides, or electroporated with HSTMG1 RNA encoding the relevant neoantigen or its WT counterpart. The number of IFN-γ spots measured by ELISPOT and the frequency of 4-1BB$^+$ cells gated on CD3$^+$CD8$^+$ after 20h co-culture with B cells are plotted. Data are representative of at least two independent experiments.

In summary, we successfully detected and expanded a T-cell population reactive against PIK3CA$_{p.E545K}$. The reactivity was only detected in one of the replicates where T cells were exclusively sensitized with the specific mutant peptide, but not the peptide pools. This suggests that the frequency of the reactivity in the blood may be low, giving rise to spurious enrichment, or that there may be competition for binding to HLA-I between different peptides in the pool.

2.1.2. Sensitization with MEP-1 induced *de novo* T-cell responses against TP53$_{p.R248Q}$ neoepitope restricted to HLA-A*11:01

We next evaluated the induction of *de novo* T-cell responses to candidate public neoantigens presented by HLA-A*11:01 or HLA-C*04:01 by IVS with MEPs.

After the first two stimulation rounds, we did not detect any reactivity to MEP-1 in the sensitized PBLs. However, after the third round of stimulation, we observed a low-frequent 4-1BB$^+$ CD8$^+$ T-cell population when co-cultured with B cells pulsed with MEP-1. Subsequently, we conducted a fourth round of stimulation, which further expanded the reactive population from 5% to 10% of 4-1BB$^+$ expressing T cells (Figure 39A).

To enrich for MEP-1-specific lymphocytes, we sorted CD8$^+$ 4-1BB$^+$ T cells by FACS after co-culture with MEP-1 pulsed autologous B cells (Figure 39B) and expanded them ex vivo. This strategy led to the enrichment of the reactive population, to 25% for T cells enriched after the third round of stimulation, and to 50% for T cells enriched after the fourth round of stimulation (Figure 39C). Notably, enriched T cells (referred to as CD8$^+$ 4-1BB$^+$ vs MEP-1 Stim3 or Stim4) recognized their target neoantigen(s) equally well when presented by HSTMG1-expressing B cells, which encoded for 8 out of the 10 ME contained in MEP-1, than when presented by MEP-1 pulsed B cells (Figure 39C). Importantly, MEP-1 enriched lymphocytes displayed specific recognition of the mutant form but not the wild-type counterpart of the neoantigen(s) encoded in HSTMG1 (Figure 39C).

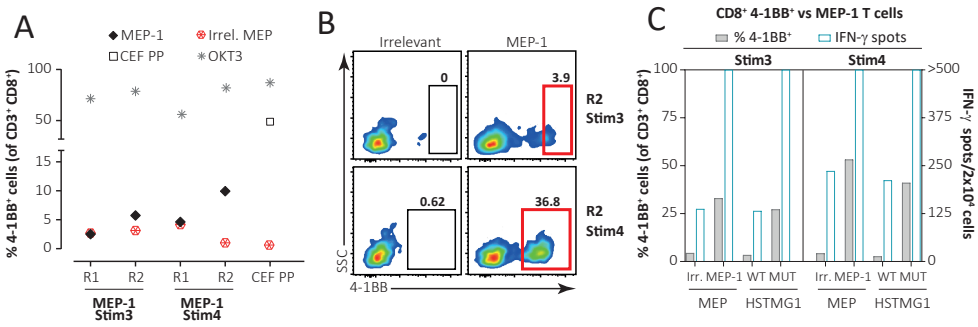


Figure 39. Sensitization of GOI-01 PBL with MEP-1 elicited T-cell reactivities after several rounds of stimulation. A) Induced T-cell reactivities were assessed in replicate following three (Stim3) or four (Stim4) consecutive rounds of stimulation with MEP-1 or CEF PP. The frequency of 4-1BB$^+$ cells gated on CD3$^+$CD8$^+$ cells is shown for each sensitized replicate (R1 or R2) after 20h co-culture with B cells pulsed with the corresponding peptide pools. B cells pulsed with an Irrelevant MEP and anti-CD3 (OKT3) activated T cells are shown as negative and positive controls, respectively. The T-cell reactivity induced by CEF PP at Stim4 for the single stimulated replicate is plotted. B) Plots show gates applied for 4-1BB$^+$ sorting of CD8$^+$ in vitro sensitized PBLs reactive to MEP-1 from replicate 2 (R2) of two different stimulation rounds (Stim3 and Stim4). Cells were sorted after 20h co-culture with autologous B cells pulsed with MEP-1. Autologous B cells pulsed with an irrelevant MEP were used as a negative control for T-cell activation. Gates applied for sorting are shown in red. Following sorting, cells were expanded for 14 days using a REP.

C) Reactivity of enriched CD8$^+$4-1BB$^+$ vs MEP-1 T cells from Stim3 or Stim4 to MEP-1. Number of IFN-γ spots detected by ELISPOT and frequency of 4-1BB$^+$ cells gated on CD3$^+$CD8$^+$ lymphocytes after 20h co-culture with B cells pulsed with MEP-1 or an irrelevant MEP (Irr.) are shown. B cells electroporated with HSTMG1 RNA, coding for the wild-type (WT) or mutant (MUT) form of 8 of the 10 MEP-1 neoantigens were also used as targets. Data are representative of at least two independent experiments.

To determine the specific neoantigen(s) recognized, we stained with fluorescently labeled HLA dextramers individually loaded with the minimal epitopes contained in MEP-1. Based on the immunopeptidomics results, HLA-A*11:01 dextramers were loaded with ME-1 to ME-7 separately, while HLA-C*04:01 dextramers were loaded with ME-8 to ME-10 (Table 11). HLA-A*68:01 dextramers loaded with the same peptides as HLA-A*11:01 were also tested because of the similarity of the binding motifs between these two alleles.

Most of the HLA-A*11:01 and HLA-C*04:01 monomers loaded with their corresponding peptides folded properly, as experimentally assessed according to the manufacturer's specifications (Figure 40A). However, the HLA-A*11:01 dextramer loaded with the 10-mer and 9-mer derived from $TP53_{p.R248Q}$ and the HLA-C*04:01 dextramer bound to the 9-mer derived from $PIK3CA_{p.R88Q}$ did not fold correctly. Unexpectedly, we could not determine the specific public neoantigen recognized by enriched CD8$^+$ 4-1BB$^+$ vs MEP-1 lymphocytes using this approach, since the T cells did not stain positive with any of the HLA dextramers evaluated (Figure 40B).

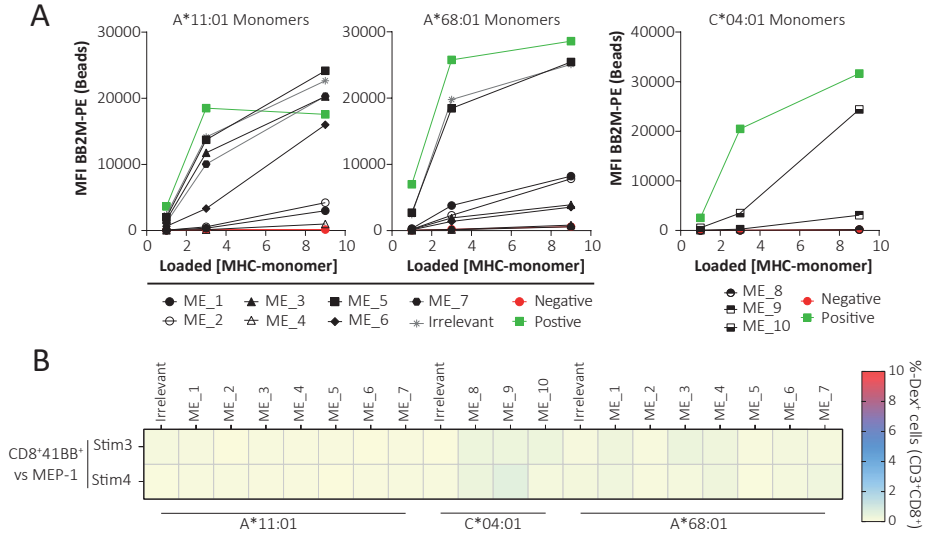


Figure 40. Dextramer staining failed to identify the mutant epitope(s) recognized by MEP-1 reactive CD8$^+$ lymphocytes.

A) Representative plots of the folding performance of the monomers loaded with the ME peptides contained in MEP-1 following manufacturer instructions. Monomers with properly folded control peptides and empty monomers were used as positive and negative controls, respectively. For HLA-A*11:01 and HLA-A*68:01, two irrelevant peptides (not actually used in the PBLs IVS experiments) were also included. B) Heat map summarizing staining of two enriched MEP-1 reactive T-cell populations ($CD8^+4\text{-}1BB^+$ vs MEP-1 from Stim3 or Stim4) with HLA-A*11:01, A*68:01 or C*04:01 dextramers individually loaded with ME (from panel A) contained in MEP-1. One irrelevant ME was used as a negative control for each group of HLA dextramers (A*11:01, C*04:01, and A*68:01). The frequency of HLA dextramer-positive T cells gated on $CD3^+CD8^+$ T cells is shown. Data from (A-B) are representative of at least two independent experiments.

Nevertheless, by individually testing the recognition of each of the ME included in MEP-1 in co-culture assays we found that both MEP-1- reactive T-cell populations recognized a 9-mer derived from $TP53_{p.R248Q}$ (Figure 41A). Next, we determined HLA-A*11:01 as the restriction element for the $TP53_{p.R248Q}$ reactivity present in the MEP-1 reactive populations after co-culture with COS-7 cells individually transduced with GOI-01 HLA-I alleles and pulsed with the $TP53_{p.R248Q}$ minimal epitope recognized (Figure 41B).

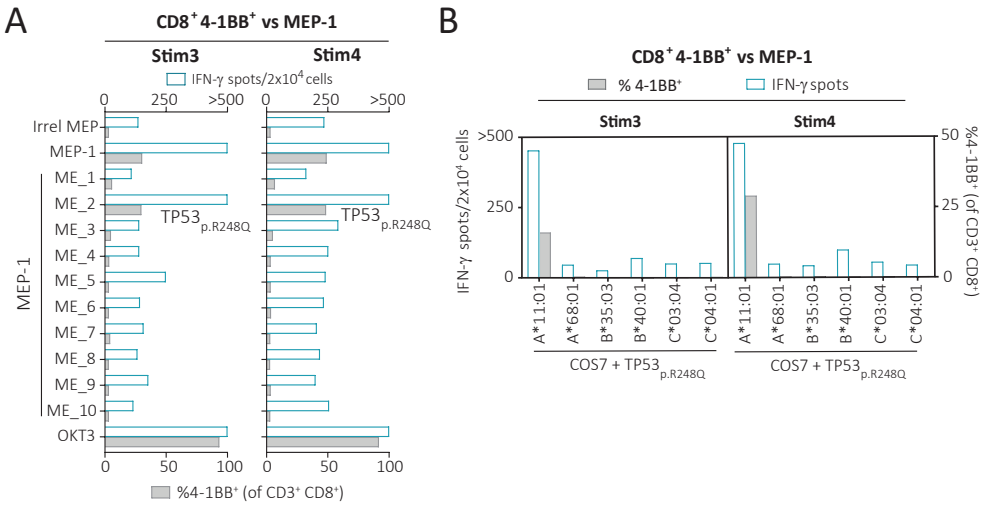


Figure 41. Enriched MEP-1-reactive T-cell populations both recognize a neoantigen derived from $TP53_{p.R248Q}$. A) Reactivity of enriched MEP-1 lymphocytes to the indicated MEP or the individual mutant ME contained in the pool. The number of IFN-γ spots and frequency of $4\text{-}1BB^+$ cells gated on $CD3^+CD8^+$ T cells from Stim3 and Stim4 enriched populations after 20h coculture with autologous B cells pulsed with the specified epitopes are plotted. The specific mutated protein and amino acid change of the recognized target are annotated. Autologous B cells pulsed with an irrelevant MEP and anti-CD3 (OKT3) were used as negative and positive controls, respectively. B) Restriction element was evaluated by coculturing enriched MEP-1 reactive populations with COS-7 cells individually expressing one of the patient's HLA-I alleles and pulsed with the $TP53_{p.R248Q}$ 9-mer specifically recognized by these lymphocytes.

The number of IFN-γ spots and frequency of 4-1BB$^+$ cells gated on CD3$^+$CD8$^+$ T cells from Stim3 and Stim4 enriched populations after 20h coculture is shown. Data from (A-B) are representative of at least two independent experiments.

Overall, IVS with MEP-1 effectively induced a de novo T-cell response to an HLA-A*11:01-restricted TP53$_{p.R248Q}$ neoantigen from PBL of metastatic cancer patient GOI-01 after three or four rounds of stimulation.

2.1.3. Sensitization with MEP-2 induced *de novo* T-cell responses against PIK3CA$_{p.R88Q}$ restricted to HLA-C*04:01

To identify additional T-cell reactivities induced by IVS to other candidate public neoantigens, we focused on PBLs sensitized with MEP-2.

The initial assessment of reactivities to MEP-2 following the first three stimulations yielded negative results in both stimulated replicates. Yet, after the fourth round of stimulation, one of the stimulated replicates showed 10% of 4-1BB$^+$ T cells when co-cultured with B cells pulsed with MEP-2 (Figure 42A). We enriched MEP-2-specific lymphocytes by sorting of CD8$^+$ 4-1BB$^+$ T cells by FACS after co-culture with autologous B cells pulsed with MEP-2 (Figure 42B) and expanded them ex vivo. However, the expanded population (termed as CD8$^+$ 4-1BB$^+$ vs MEP-2) did not recognize MEP-2 nor HSTMG1 in the co-culture assays (Figure 42C).

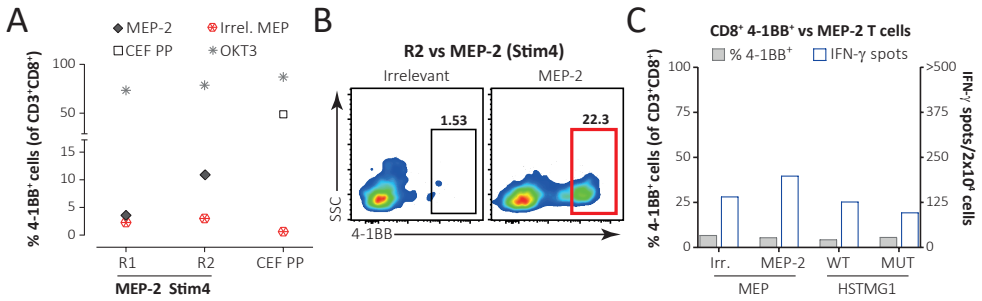


Figure 42. Sensitization of GOI-01 PBL with MEP-2 elicited T-cell reactivities after four rounds of stimulation. A) Induced T-cell reactivities were assessed in replicates following four (Stim4) consecutive rounds of stimulation with MEP-2 or CEF PP. The frequency of 4-1BB$^+$ cells gated on CD3$^+$CD8$^+$ cells is shown for each sensitized replicate (R1 or R2) after 20h co-culture with B cells pulsed with the corresponding peptide pools. B cells pulsed with an Irrelevant MEP and anti-CD3 (OKT3) activated T cells are shown as negative and positive controls, respectively. The T-cell reactivity induced by CEF PP at Stim4 for the single stimulated replicate is plotted. B) Plots depicting the gates used for 4-1BB$^+$ sorting of CD8$^+$ in vitro sensitized PBLs reactive to MEP-2 from replicate 2 (R2) of Stim4. Cells were sorted after 20h co-culture with autologous B cells pulsed with MEP-2.

Autologous B cells pulsed with irrelevant MEP were used as a negative control for T-cell activation. Gates used for sorting are displayed in red. Following cell separation, cells were expanded for 14 days via a REP. C) Reactivity of enriched $CD8^+4\text{-}1BB^+$ vs MEP-2 lymphocytes to MEP-2. Number of IFN-γ spots measured by ELISPOT and frequency of $4\text{-}1BB^+$ cells gated on $CD3^+CD8^+$ lymphocytes after 20h co-culture with B cells pulsed with MEP-2 or an irrelevant (Irr.) MEP are shown. B cells electroporated with mutated (MUT) or wild-type (WT) HSTMG1 RNA, encoding 8 of the 14 neoantigens contained in MEP-2, were also used as targets. Data are representative of at least two independent experiments.

Nevertheless, we explored the recognition of candidate neoantigens contained in MEP-2 by independent HLA dextramer staining following the same strategy as for the MEP-1-reactive populations. Surprisingly, using this strategy, we identified $PIK3CA_{p.R88Q}$ as the specific public neoantigen recognized by the enriched $CD8^+$ $4\text{-}1BB^+$ vs MEP-2 lymphocytes when presented by HLA-C*04:01 (Figure 43). Of note, IVS failed to enrich for a pre-existing circulating T-cell response targeting the private neoantigen $KIAA1524_{p.S57I,}$ or KRAS neoantigens shown to frequently elicit de novo T-cell responses from PBLs of HD (178,179). This indicates some limitations in the protocol used for IVS. Nevertheless, IVS successfully enriched T-cell responses to viral epitopes contained in CEF PP, achieving 50% enrichment after four stimulation rounds (Figure 39A and Figure 42A). This suggests that our IVS protocol could effectively expand pre-existing circulating anti-viral T-cell responses.

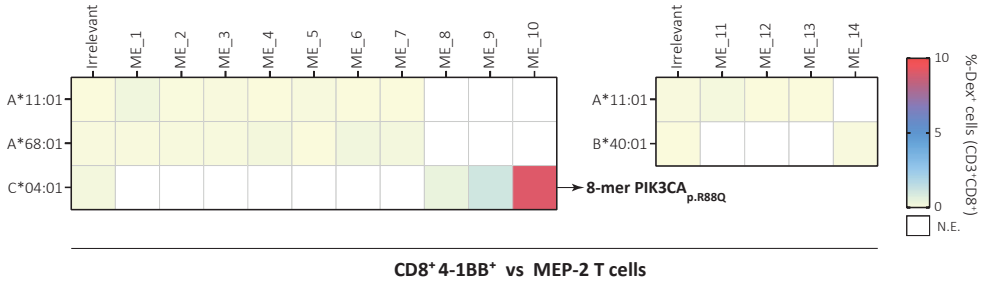


Figure 43. HLA dextramer staining determined $PIK3CA_{p.R88Q}$ 8-mer as the epitope recognized by MEP-2-reactive T cells. Heat map summarizing independent staining with HLA-A*11:01, A*68:01 or C*04:01-dextramers individually loaded with ME contained in MEP-2 for the $CD8^+4\text{-}1BB^+$ vs MEP-2 enriched T-cell population. The frequency of HLA dextramer-positive cells gated on $CD3^+CD8^+$ cells is plotted. KRAS neoantigens (ME_11 to ME_13) and $KIAA1524_{p.S57I}$ neoantigen (ME_14) contained in MEP-2, were independently evaluated with dextramers HLA-A*11:01 or B*40:01 loaded with the corresponding ME. For each of the dextramers, one irrelevant ME was used as a negative control. White cells indicate combinations that were not evaluated (N.E.). Data are representative of at least two independent experiments.

Overall, IVS with MEP-2 induced an additional de novo T-cell response targeting PIK3CA$_{p.R88Q}$ after four rounds of stimulation.

In total, using our IVS method we identified T cells targeting three different public neoantigens. The reactive T cells and their corresponding TCRs targeting public neoantigens, could be exploited to develop off-the-shelf TCR engineered-cell therapies to treat patients with tumors harboring the specific hotspot mutation.

2.2. Isolation of neoantigen-specific TCRs from enriched CD8$^+$ reactive T cells by TCR sequencing

In order to sequence and clone TCRs targeting the public neoantigens, we first sought to determine the frequency and specificity of the distinct TCR clonotypes in the three enriched T-cell populations resulting from the IVS experiments. We performed bulk TCRβ deep sequencing to study their clonality and complemented this with single-cell TCR sequencing to obtain both the TCRα and TCRβ sequences needed to clone and synthesize selected TCRs.

In the case of CD8$^+$ dextramer-sorted HLA-A*11:01_PIK3CA$_{p.E545K}$ T cells, a dominant TCRβ sequence was detected in 63.5% of the cells, followed by 22.2% and 4% of other beta chains (Figure 44A). For the CD8$^+$ 4-1BB$^+$ vs MEP-1 reactive T cells recognizing TP53$_{p.R248Q}$, we had two enriched populations from different rounds of stimulations: those sorted after the third stimulation (Stim3) and those sorted after the fourth stimulation (Stim4). Both populations shared the most dominant TCRβ chain, albeit enriched at different levels: 39.3% and 48.4% for Stim3 and Stim4 T-cell populations, respectively. Interestingly, the other top two- and three-ranking TCRβ sequences from Stim3 T cells differed from those in the population from Stim4 (Figure 44B). Of note, those TCRβ sequences from Stim3 population were not contained within the top 5 most enriched TCRβ sequences in Stim4 population. Finally, the MEP-2 reactive T-cell population recognizing PIK3CA$_{p.R88Q}$ did not contain a uniquely dominant TCRβ sequence. In contrast, the top three most enriched TCRβ chains were found at similar frequencies (i.e. 10.5%, 7.9%, and 7.5%, respectively) (Figure 44C).

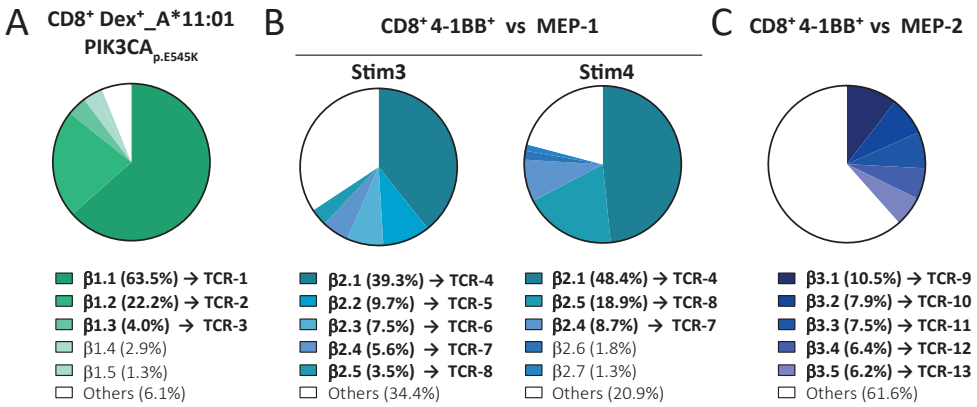


Figure 44. TCRβ deep sequencing identified multiple dominant sequences for some of the enriched in vitro sensitized PBLs. Pie charts showing the frequency of the top five most frequent TCRβ chains identified by TCRβ deep sequencing of the following T-cell populations: A) $CD8^+$ $Dextramer^+$ HLA-A*11:01_$PIK3CA_{p.E545K}$, B) $CD8^+$4-1BB$^+$ vs MEP-1 for Stim3 and Stim4 and C) $CD8^+$4-1BB$^+$ vs MEP-2 for Stim4. Only TCRβ chains highlighted in bold were selected for further testing. The ID given to each of the TCR clonotypes constructed is specified.

To investigate which of the dominant TCRs were mutation-reactive, we cloned the three most frequent TCRαβ pairs detected in $CD8^+$ dextramer sorted $PIK3CA_{p.E545K}$ population and the Stim4 MEP-1-reactive in vitro sensitized T cells. For the Stim3 MEP-1 reactive T cells and the MEP-2-reactive T cells, displaying lower levels of neoantigen reactivity, we selected the five most frequent TCRαβ pairs for testing. To clone the selected TCRαβ pairs, we fused the TRB V-D-J-encoding sequences and TRA V-J-encoding sequences to sequences encoding the mouse constant TRB and TRA chains, respectively in this order separated by a furin SGSG P2A linker cleavage site into pMSGV1 retroviral vector. This vector was subsequently used to generate viral supernatant and infect HD PBLs. We used the murine TRA and TRB constant regions to reduce mispairing with the endogenous TCR and to precisely track the TCR-transduced PBLs (TCRtd) cells using an anti-mouse TRB antibody.

To identify neoantigen-specific TCRs, TCRtd cells were co-cultured with immortalized autologous B cells pulsed with the ME recognized by the corresponding T-cell population of interest or electroporated with HSTMG1 RNA, which encoded for the three public neoantigens potentially recognized by the tested TCRs.

In some cases, we also performed HLA dextramer staining as an alternative method to detect the neoantigen-specific TCRs.

As shown in Figure 45A, all 13 TCRs were cloned and successfully transduced into PBLs, but not all recognized neoantigens. In fact, only one TCR detected in each of the enriched populations was found to be reactive against their respective public neoepitope tested in the form of a synthetic peptide. Moreover, they displayed variable avidity for their specific target as the TCRtd lymphocytes displayed variable levels of 4-1BB expression. All three were neoantigen-specific, as they showed preferential reactivity to the mutant but not to the wild-type peptides (Figure 45A).

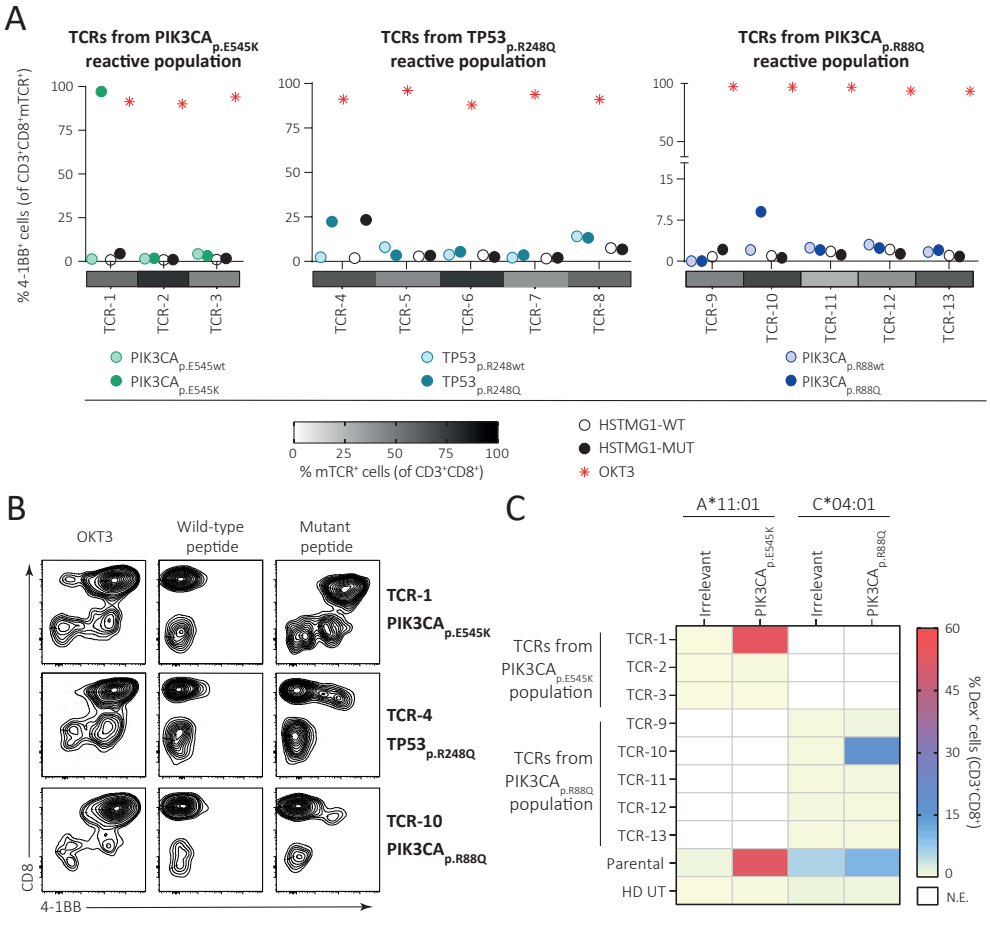


Figure 45. TCRs targeting PIK3CA$_{p.E545K}$, TP53$_{p.R248Q,}$ and PIK3CA$_{p.R88Q}$ display preferential recognition of the mutated epitopes. A) Reactivity of HD PBL transduced with the candidate TCRs selected for each *in vitro* sensitized PBL population.

The frequency of 4-1BB$^+$ cells gated on CD3$^+$CD8$^+$mTCR$^+$ lymphocytes after 20h co-culture with immortalized B cells pulsed with the mutated and wild-type minimal epitope of PIK3CA$_{p.E545K}$ (left), TP53$_{p.R248Q}$ (middle) and PIK3CA$_{p.R88Q}$ (right) is shown. B cells electroporated with the mutant (MUT) or wild-type (WT) HSTMG1 RNA, encoding for the three immunogenic neoantigens, were also used as targets. Anti-CD3 (OKT3) was used as a positive control for T-cell activation. The frequency of mTCR$^+$ cells gated on CD3$^+$CD8$^+$ T cells is also shown for each tested population. B) CD8 co-receptor activation dependence of PBLs transduced with antigen-specific TCRs. Flow cytometry plots show the expression of 4-1BB by CD8 (gated on CD3$^+$mTCR$^+$) after 20h co-culture with immortalized B cells pulsed with the corresponding peptides. Anti-CD3 (OKT3) and B cells pulsed with the corresponding wild-type peptides were used as positive and negative controls, respectively. Data from (A-B) are representative of at least two independent experiments. C) Heat map summarizing dextramer staining of HD PBL TCR transduced cells with the candidate TCRs identified from populations displaying PIK3CA$_{p.E545K}$ and PIK3CA$_{p.R88Q}$ recognition. The frequency of HLA dextramer-positive cells gated on CD3$^+$CD8$^+$ cells is plotted. Non-transduced PBLs from the same HD (HD UT) and parental T-cell populations for PIK3CA$_{p.E545K}$ (CD8$^+$Dex$^+$ HLA-A*11:01_PIK3CA$_{p.E545K}$) and PIK3CA$_{p.R88Q}$ (CD8$^+$4-1BB$^+$ vs MEP-2 from Stim4) were included as negative and positive controls, respectively. White cells indicate combinations that were not evaluated (N.E.).

Surprisingly, among the three identified neoantigen-specific TCRs, only the one targeting TP53$_{p.R248Q}$ was reactive to B cells electroporated with HSTMG1 RNA encoding for the three mutations (Figure 45A). This could result from deficient processing and presentation of some of these epitopes by B cells. Alternatively, this could indicate that the PIK3CA$_{p.E545K}$ and PIK3CA$_{p.R88Q}$ TCRs identified did not recognize the peptide naturally processed and presented. The latter seemed unlikely since these peptides were originally identified through HLA-I immunopeptidomics, following processing and presentation of the same HSTMG1 RNA electroporated into B2M KO tumor cells.

Of note, the upregulation of 4-1BB on both CD4$^+$ and CD8$^+$ TCRtd suggested that the TCR recognizing PIK3CA$_{p.E545K}$ could be co-receptor independent. In contrast, the other two identified TCRs required CD8 co-receptor expression to recognize their cognate epitopes (Figure 45B).

HLA dextramer staining did not capture additional reactive clonotypes for any of the two PIK3CA reactivities interrogated for which HLA dextramers were available. The neoantigen-specific TCRtd cells bound to HLA dextramers loaded with their corresponding targets as their respective polyclonal parental populations (Figure 45C).

Overall, the results above demonstrate the feasibility of isolating TCRs specifically targeting public neoantigens by IVS of T cells using patient peripheral blood as starting material. Nonetheless, we wanted to further investigate whether the isolated TCRs could recognize the neoantigens processed and presented by tumor cells.

2.3. The identified reactive TCRs recognize tumor cells *in vitro* and display variable functional avidity for their cognate antigens

We next investigated whether the isolated TCRs could recognize their targets when processed and presented by tumor cells.

None of the in-house patient-derived TCLs expressed $PIK3CA_{p.E545K}$ or $TP53_{p.R248Q}$ hotspot mutations and were HLA-A*11:01^{+}, the restriction allele for two of the neoantigen-specific TCRs. To overcome this difficulty, we selected the melanoma patient-derived VHIO-029 TCL, which naturally expressed HLA-A*11:01, and modified it to express the neoantigen of interest. We also used the B2M KO TCL transfected with B2M_A*11:01 chimera as a target, which was the source of tumor cells where these ME were detected, and modified them as VHIO-029 TCL to express the mutated antigens. B cells from two patients expressing HLA-A*11:01 (i.e. VHIO-029 and GOI-01) were also used to compare the ability of the TCRtd cells to recognize two different types of target cells that could potentially differ in their ability to process and present peptides on HLA-I.

Target cells (B cells and tumor cells) were modified to express these public neoantigens by electroporation of HSTMG1 RNA or by pulsing the ME recognized by the reactive TCRs. Since these ME were identified by electroporating the HSTMG1 encoding for a 25-mer minigene containing the mutation, we also wondered whether these ME would be naturally processed and presented from the full-length protein. Thus, target cells were additionally transfected with the full-length RNA encoding the mutant $PIK3CA_{p.E545K}$ or $TP53_{p.R248Q}$ proteins to investigate whether the neoepitope could also be processed and presented from the complete mutant protein.

As shown in Figure 46, TCRtd cells specific for PIK3CA$_{p.E545K}$ and TP53$_{p.R248Q}$ recognized the TCL better than B cells, regardless of whether the neoepitope was derived from HSTMG1, the full-length protein, or the ME (Figure 46A). As expected, these TCRs were mutation-specific, as demonstrated by the preferential recognition of the mutated epitopes. TCRs targeting PIK3CA$_{p.E545K}$ and TP53$_{p.R248Q}$ reacted to VHIO-29 TCL in the absence of forced exogenous HLA-I expression, demonstrating that both peptides were processed by the tumoral cells and presented by their endogenous HLA-A*11:01. Nonetheless, evaluating recognition of a tumor cell line expressing physiological levels of the native mutated proteins would still be of interest, given that protein overexpression obtained through RNA electroporation may not be representative.

Noteworthy, B cells seemed to ineffectively process the antigen upon transfection of the full-length protein or HSTMG1 RNA, resulting in reduced target recognition by TCRtd cells (Figure 46A). Nevertheless, the TCR targeting PIK3CA$_{p.E545K}$ equally recognized B cells and tumor cells when its cognate antigen was pulsed onto both target cells. This is in line with the results presented in section 2.1.1, where the enriched CD8$^+$ dextramer$^+$ HLA-A*11:01-PIK3CA$_{p.E545K}$ parental T-cell population did not recognize HSTMG1-expressing B cells equally well as B cells pulsed with the corresponding ME. This could be related to the differences in the expression of the constitutive and inducible proteasomal subunits in epithelial cells such as B2M KO TCL and B cells (Figure 22) as this could result in differences in antigen processing and presentation by these cells.

For the PIK3CA$_{p.R88Q}$ TCR, we took advantage of EC-35035, a patient-derived TCL endogenously expressing this hotspot mutation. Because EC-35035 did not carry the HLA-C*04:01, which was the restriction element for PIK3CA$_{p.R88Q}$ neoantigen, we decided to engineer the cells to express it by electroporating IVT RNA encoding the HLA-C*04:01 alpha chain into the TCL. This allowed us to test whether the antigen derived from PIK3CA$_{p.R88Q}$, this time presumably expressed at physiological levels, could be naturally expressed, processed, and presented on HLA-C*04:01. As shown in Figure 46B, we found that the TCRtd cells were not able to recognize EC-35035 TCL when the expression of the specific restriction HLA-I allele was forced.

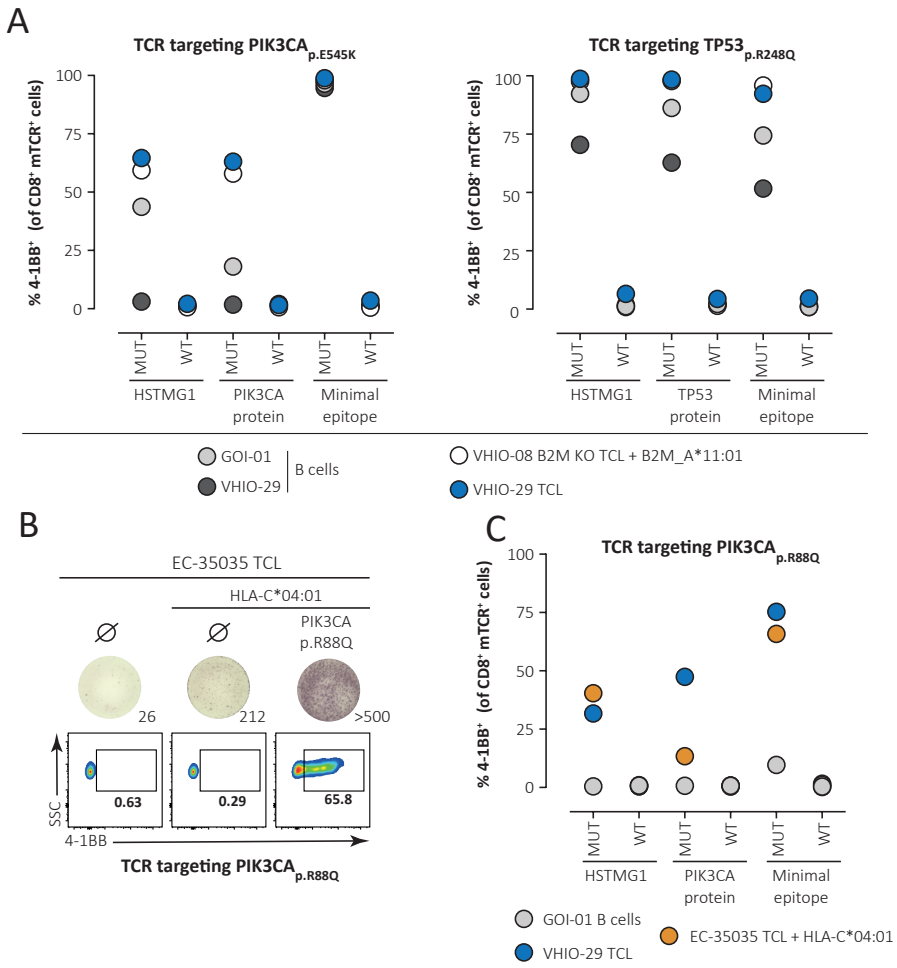


Figure 46. Tumor recognition by PBL TCR transduced (TCRtd) cells with the reactive TCRs for the three public neoantigens. A) Reactivity of PBLs transduced with TCR-1, recognizing PIK3CAp.E545K (left) or TCR-4, recognizing TP53p.R248Q (right) to VHIO-29 and VHIO-08 B2M KO + B2M_A*11:01 tumors or immortalized B cells from GOI-01 and VHIO-29. Target cells, either tumor cells or B cells, were electroporated with HSTMG1 or the full-length construct RNA, or pulsed with the mutant (MUT) ME. The wild-type (WT) versions of these constructs and the ME were used as controls. The frequency of 4-1BB+ cells gated on CD8+mTCR+ after 20h of co-culture with the specified targets is shown. B) Reactivity of PBLs transduced with TCR-10, recognizing PIK3CAp.R88Q, to EC-35035. Representative ELISPOT results (top) and flow cytometry plots (bottom) showing PBL TCRtd reactivity after 20h co-culture to the unmodified TCL (left), TCL transfected with HLA-C*04:01 (middle) or TCL transfected with HLA-C*04:01 and pulsed with PIK3CAp.R88Q minimal epitope (right). The frequency of 4-1BB+ cells gated on CD8+mTCR+ after 20h of co-culture with the specified targets is shown. C) Reactivity of PBLs transduced with the TCR recognizing PIK3CAp.R88Q to VHIO-29 TCL or GOI-01 immortalized B cells, and to EC-35035 TCL transfected with HLA-C*04:01. Target cells, either tumor cells or B cells, were electroporated with HSTMG1 or the full-length construct RNA, or pulsed with the mutant (MUT) ME. The wild-type (WT) versions of these constructs and the ME were used as controls. The frequency of 4-1BB+ cells gated on CD8+mTCR+ after 20h co-culture with the specified targets is shown. Data from (A-C) are representative of at least two independent replicates.

Nevertheless, TCRtd cells specific for PIK3CA$_{p.R88Q}$ recognized EC-35035 when the HLA-C*04:01 transfected cell line was pulsed with the minimal epitope (Figure 46B).

Next, we investigated whether the failure of the TCRtd cells to recognize EC-35035 was due to inefficient processing of the endogenous PIK3CA$_{p.R88Q}$ protein in this cell line. As for the previous experiments, we used VHIO-29 as an additional tumor naturally presenting HLA-C*04:01 and, as a control, GOI-01 B cells because this patient was also HLA-C*04:01^{+}. We found that TCRtd cells targeting PIK3CA$_{p.R88Q}$ recognized the neoepitope presented by the two TCL better than by B cells, irrespective of whether the neoepitope originated from the HSTMG1, the full-length protein, or via direct pulsing peptide onto the target cells (Figure 46C). The PIK3CA$_{p.R88Q}$ TCR recognized VHIO-29 TCL better than EC-35035 TCL when the neoantigen originated from the full-length protein (Figure 46C). The exact mechanism explaining such limited recognition in this cell line is still unknown and needs to be further investigated.

Notably, similar to what was observed for PIK3CA$_{p.E545K}$, B cells but not tumor cells showed defective neoantigen processing and/or presentation upon transfection of RNA encoding the full-length mutated protein or HSTMG1, as evidenced by the lack of recognition by TCRtd cells (Figure 46C). However, TCRtd cells also poorly recognized ME pulsed B cells, suggesting that the expression level of the HLA-C by B cells, may also hinder recognition of the neoantigen.

Lastly, we investigated the functional avidity of the TCR-transduced cells for their cognate targets. CD8^{+}TCRtd^{+} cells showed varying functional avidities for their antigens when co-cultured with antigen-presenting cells pulsed with serial dilutions of the corresponding wild-type or mutated peptides. The highest avidity was observed in PIK3CA$_{p.E545K}$ -specific TCR-transduced T cells, while PIK3CA$_{p.R88Q}$-specific TCR-engineered lymphocytes had the lowest avidity (Figure 47). Of note, TCRs reacting against the three public neoantigens showed highly specific recognition of the mutant forms. Even high concentrations of the wild-type counterparts failed to elicit activation of these TCRtd cells (Figure 47).

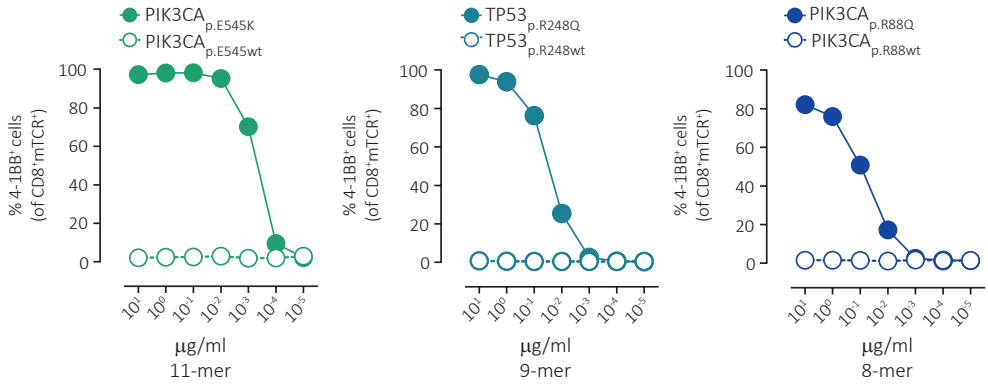


Figure 47. Differential functional avidity of TCR-engineered T cells targeting public neoantigens. Reactivity of PBLs transduced with the TCRs recognizing PIK3CA$_{p.E545K}$ (left), TP53$_{p.R248Q}$ (middle) or PIK3CA$_{p.R88Q}$ (right) to B cells or tumor cells pulsed with serial dilutions of the wild-type (PIK3CA$_{p.E545wt}$, TP53$_{p.R248wt}$ or PIK3CA$_{p.R88wt}$) or mutant (PIK3CA$_{p.E545K}$, TP53$_{p.R248Q}$ or PIK3CA$_{p.R88Q}$) peptides. For the PIK3CA$_{p.E545K}$-reactive TCR, GOI-01 immortalized B cells were used as target cells, whereas for TP53$_{p.R248Q}$ and PIK3CA$_{p.R88Q}$, VHIO-08 B2M KO + B2M_A*11:01 and HLA-C*04:01^{+} VHIO-29 tumor cells were used as targets, respectively. T-cell reactivity was evaluated by measuring the upregulation of 4-1BB expression on CD8^{+}mTCR^{+} cells after 20h.

Overall, the three TCRs recognized their respective targets when processed and presented on tumor cells modified to either express the respective HLA-I, the neoantigen, or both. Furthermore, these TCRs demonstrated specific recognition of the mutation with variable functional avidities. These findings represent a first step in the characterization of the TCRs, and thus far support the potential use of these TCRs targeting public neoantigens for off-the-shelf T-cell therapies. Particularly, the TCRs targeting PIK3CA$_{p.E545K}$ and TP53$_{p.R248Q}$ appeared more attractive, both displaying marked recognition of at least two different tumor cell lines expressing the full-length mutated protein.

2.3.1. Exploring the co-occurrence of hotspot mutation and HLA-I restriction elements, leading to the presentation of public neoantigens targeted by reactive TCRs in cancer patients

We explored the TCGA repository data to estimate the population of cancer patients who may benefit from off-the-shelf T-cell therapies using the three identified TCRs. We evaluated the prevalence of the targeted hotspot mutations across different cancer types and considered the frequency of the HLA-I allele in the overall cancer TCGA population.

The novel reactive TCRs reported here targeted three public neoantigens, two arising from PIK3CA and one derived from TP53, two of the most frequently mutated genes across all cancer types. Notably, the recurrent alterations generating these neoantigens were among the most common missense mutations for both genes in patients within the TCGA Pan-Cancer study registry. More specifically, E545K ranked first and the R88Q ranked fourth for the PIK3CA gene, while the R248Q ranked third for the TP53 gene (Figure 48A).

Regarding the HLA-I alleles presenting these neoantigens, HLA-A*11:01 and HLA-C*04:01 are also among the most prevalent alleles in cancer patients of Caucasian origin, with allelic frequencies of 8.5% and 10.9% in the TCGA Pan-Cancer study, respectively. Considering the widespread occurrence of these alterations and the HLA-I alleles, and by extrapolating incidence rates from 2022, it is estimated that approximately 93,530 patients from various cancer types could potentially benefit each year from off-the-shelf T-cell therapies exploiting these reactive TCRs (Table 12).

Table 12. Estimated population of cancer patients potentially benefiting from off-the-shelf TCR-based T-cell therapies per year using the identified TCRs.

				Mutation freq. (%)		Neoantigen freq. (%)[b]		Incidence of cancers carrying neoantigens[c]	
Shared neoantigen	**HLA-I**	**Top cancer**	**Freq. (%) HLA-I in TCGA[a]**	**All cancers**	**Top cancer**	**All cancers**	**Top cancer**	**All cancers**	**Top cancer**
$PIK3CA_{p.R88Q}$	C*04:01	Endometrial adenocarcinoma	10.96%	0.6	6.85	0.07	0.75	13,930	3,150
$PIK3CA_{p.E545K}$	A*11:01	Breast carcinoma	8.54%	2.7	5.98	0.23	0.51	45,770	11,730
$TP53_{p.R248Q}$	A*11:01	Colon adenocarcinoma	8.54%	2	3.1	0.17	0.26	33,830	4,940

Shared neoantigen and HLA-I restriction element of the TCRs targeting public neoantigens. The cancer type with the highest prevalence of each mutation (top cancer) and the mutation frequency for each shared neoantigen in the top and all cancers were obtained from the TCGA Pan-Cancer Atlas analysis. (a) Frequency was calculated within a population of individuals reporting EUR in their genetic ancestry label. (b) Frequency was obtained as the product of the HLA-I and mutation frequencies. (c) The estimated incidence of cancers carrying neoantigens is calculated based on the neoantigen frequency and the global incidence of cancer in 2022, as reported by the WHO (https://gco.iarc.who.int/today/en/fact-sheets-cancers).HLA-I frequencies refer to allelic frequencies, not phenotype, of a specific population of cancer patients slightly underestimating the target population expressing HLA-I of interest.

One potential limitation for the applicability of off-the-shelf T-cell therapies with the identified reactive TCRs is that the targeted peptide-HLA combinations might be negatively selected in tumors if, as indicated by our work, they are immunogenic and could potentially be immune edited at early stages of cancer development. If this were the case the mutation and the specific HLA-I allele presenting it would not co-occur as frequently as estimated. To address this, we evaluated the association of HLA-I alleles and mutations using TCGA data, particularly focusing on cancer types where each of the hotspot mutations was prevalent.

In the case of $PIK3CA_{p.E545K}$, cervical squamous cell carcinoma and endocervical adenocarcinoma (CESC) and breast invasive carcinoma (BRCA) were selected as the two cancer types having the highest number of patients presenting this alteration (Figure 48B). Then, we stratified patients from each cohort based on the presence or absence of this hotspot mutation. Within each group, we classified patients as HLA-A*11:01^{+} or HLA-A*11:01^{-} based on their HLA-I genotyping. We only focused on this HLA-I allele as this restriction element presented the public neoantigen targeted by the $PIK3CA_{p.E545K}$ reactive TCR. We did not observe a statistically significant difference in the likelihood of presenting the HLA-A*11:01 allele between patients presenting or not the hotspot mutation for any of the two analyzed cohorts (Figure 48C).

We followed the same strategy for $PIK3CA_{p.R88Q}$ and $TP53_{p.R248Q}$ mutations for which uterine corpus endometrial carcinoma (UCEC) and colon adenocarcinoma (COAD) or bladder urothelial carcinoma (BLCA) and COAD cohorts were interrogated (Figure 48B). Of note, we did not observe significant variations in the association of HLA-C*04:01 or HLA-A*11:01 HLA-I alleles and the hotspot mutations $PIK3CA_{p.R88Q}$ and $TP53_{p.R248Q}$ respectively, in the evaluated cohorts (Figure 48C).

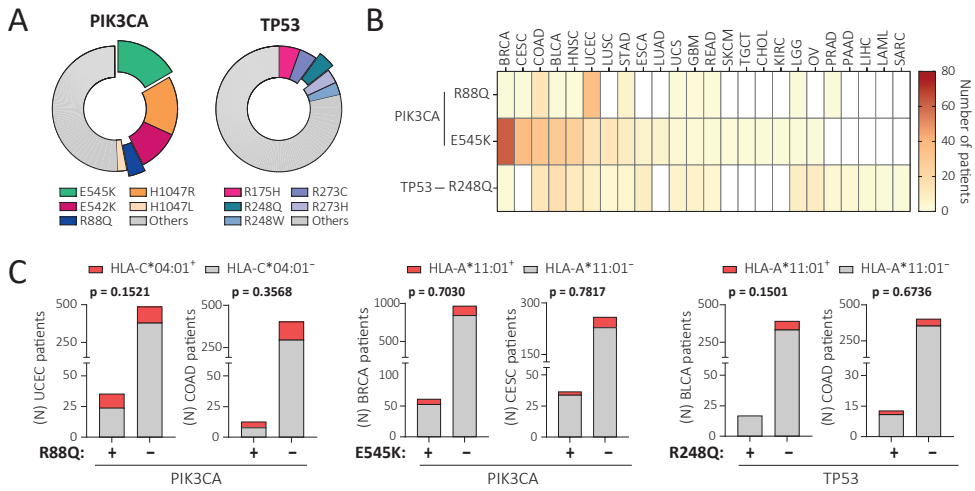


Figure 48. Co-occurrence of hotspot mutations and HLA-I restriction elements recognized by the three reactive TCRs in the TCGA cancer data repository. A) Pie charts showing the frequency of the most prevalent missense mutations in the PIK3CA and TP53 genes across cancer type collection from TCGA. The hotspot mutations generating the public neoantigens targeted by the identified TCRs are depicted as exploded sectors. B) Heat map summarizing the total cases (number of patients) per cancer type with specific hotspot mutations in the PIK3CA or TP53 genes from each TCGA cancer cohort. Abbreviations of tumor types found in Appendix. C) Assessment of non-random associations, using Fisher's exact test, between the presence of hotspot mutations and HLA-I restriction elements. Patients from two cancer cohorts with a high prevalence of the specific mutations were stratified based on the presence (+) or absence (-) of the hotspot mutations and the corresponding HLA-I restriction elements (HLA-A*11:01 or HLA-C*04:01 +/-). The number (N) of patients in each group per cohort is plotted. The corresponding p-value is shown in the graph. Data from (A-C) was obtained from Pan-Cancer Atlas TCGA study.

The absence of a discernible link between the recurrent alterations and the HLA-I restriction elements in the analyzed cohorts, suggests that there are no clear indications of a negative selection for HLA-I alleles in patients presenting the corresponding hotspot mutations. This was not completely unexpected since additional immune evasion mechanisms, including expression of immune checkpoints receptor-ligand interaction, contribute to dampen immune attack, even enabling the growth of cancers with high mutation and neoantigen burden. Nonetheless, we acknowledge that our analysis was a simplified approach that only relied on the presence or absence of mutations and HLA-I alleles. Other factors, such as mutations in the APM or alterations in the RNA expression of the interrogated mutations, were not taken into consideration and could have a major impact on the resulting associations between these factors.

Overall, TCRs targeting $PIK3CA_{p.E545K}$, $PIK3CA_{p.R88Q}$, and $TP53_{p.R248Q}$ might be promising for the development of off-the-shelf T-cell therapies helpful in treating multiple cancer patients harboring different types of metastatic solid tumors. Nevertheless, the frequency of patients with each specific combination of HLA-I and mutation is still relatively low in cancer types with the highest prevalence of the selected mutations (0.51%, 0.75% and 0.26%, respectively, Table 12). In this sense, accumulating many TCRs targeting several hotspot mutations will prove critical to broadening this off-the-shelf TCR approach to more patients.

Discussion

In this thesis, we aimed to discover mutant peptides derived from hotspot mutations in cancer driver genes presented on highly frequent HLA-I alleles in the Caucasian population and to detect and characterize TCRs targeting them. These neoantigen-specific TCRs could then be used to develop off-the-shelf T-cell therapies targeting public neoantigens.

By immunopeptidomics-based analysis on the HLA-I ligandome of HLA-I monoallelic tumor cells and using IVS to expand and isolate neoantigen-specific TCRs, we were able to identify and validate several candidate public neoantigens and to demonstrate that some of them were immunogenic. HLA-I monoallelic tumor cell MS-based screenings demonstrated high sensitivity in detecting not only previously reported but also novel mutant peptides from hotspot driver mutations across prevalent HLA-I alleles. Moreover, we identified neoantigen-specific TCRs for three public neoantigens, two of them derived from different mutations in hotspot regions of the *PIK3CA* gene and one from the *TP53* gene. Importantly, these TCRs showed preferential recognition of their targets when they were processed and presented by tumor cells as compared to APCs.

In summary, we have described a rapid and flexible method for the systematic identification of actionable targets that can be exploited in cancer immunotherapies. More importantly, the identified neoantigen-specific TCRs hold great promise for developing off-the-shelf T-cell therapies to treat cancer patients with different tumor malignancies.

Immunopeptidomics of HLA-I monoallelic cells combined with IVS led to the identification of TCRs targeting public neoantigens

To identify TCRs with the capacity to target candidate hotspot-derived neoantigens when presented by highly prevalent HLA-I alleles, we followed a three-step approach. First, we used immunopeptidomics on HLA-I monoallelic tumor cells to identify the candidate public neoantigens. Second, we evaluated whether they could be recognized by T cells by performing IVS of PBLs from a cancer patient. Finally, the TCRs targeting these candidate public neoantigens were identified by TCR sequencing techniques.

By employing immunopeptidomics analysis of transient HLA-I monoallelic cells expressing HSTMGs, we identified and validated 49 HLA-I ligands across 10 HLA-I alleles prevalent in the Caucasian population (Figure 32A). As many other studies assessing neoantigen presentation through MS-based immunopeptidomics methods (178–181), we used constructs encoding for concatenated minigenes carrying the mutations of interest. There is a concern in the field about how representative these constructs are compared to full-length mutant proteins in terms of the final epitope presented and the density of HLA-I presentation. This concern stems from potential changes introduced by the concatenation compared to the natural amino acid context surrounding the presented epitopes. These natural amino acid contexts play an important role in guiding the processing of such HLA-I ligands (176,270,271). Additionally, the resulting artificial polypeptide of these constructs may be unstable and more easily degraded, potentially leading to an increased presentation density in HLA-I (272). Despite these differences with native proteins, studies have identified conserved neoantigens using both constructs and full-length mutant proteins in MS-based immunopeptidomics studies (181). Importantly, these constructs reflect presented epitopes from mutant proteins that are physiologically expressed in patient-derived tumor cell lines. Therefore, the use of concatenated minigene constructs, such as our HSTMG, can accurately reflect neoepitopes that are naturally processed and presented in tumor cells.

Alternative strategies, such as HLA-I binding predictor algorithms, could have been used for the prioritization of candidate neoantigens derived from the selected hotspot mutations in the HLA-I alleles of interest. However, these predictors often generate large lists of candidate neoepitopes, making the downstream evaluation of the immunogenic potential for all of them challenging. Although MS-based immunopeptidomics methods can miss some peptides due to inherent technical limitations that will be discussed later, it is currently the only strategy that unbiasedly identifies peptides naturally processed and presented in the HLA-I ligandome.

Importantly, our strategy captured neoantigens that had been previously described not only by MS-based techniques (178–182,223) but also by other unrelated MS-based techniques, including functional assays to determine the antigens targeted by TILs of cancer patients (75,76,183,244,248). These results support the robustness of our experimental approach for detecting candidate public neoantigens.

For the identification of TCRs recognizing the peptide-HLA combinations captured in our MS-based immunopeptidomics screening, we used IVS as an enrichment strategy to expand and isolate antigen-specific T cells. While other enrichment strategies, such as pHLA-I multimers, could have directly isolated multiple neoantigen-specific T cells from a single sample (192,273), we chose IVS because of its demonstrated effectiveness in isolating TCRs targeting public neoantigens. This method has proven successful in both healthy donors (178,179,181,223) and cancer patients (211,224,243).

The IVS of PBLs from a breast cancer patient using selected neoepitopes led to the identification of three different TCRs targeting public neoantigens. This serves as a proof of concept that the candidate public neoantigens identified by our MS-based immunopeptidomics method can be immunogenic. Further experiments are needed to assess the immunogenic potential of the remaining candidates. Overall, the identification of these TCRs targeting public neoantigens paves the way for developing TCR-engineered T cells with such TCRs for ACT in cancer patients.

B cells were not the optimal cell source for the identification of hotspot-derived neoepitope-HLA pairs

In this thesis, we first decided to explore B cells as recipient cells to perform MS-based immunopeptidomics and identify HLA-I ligands originating from hotspot mutations. B cells offer several advantages for MS-based immunopeptidomics studies, as mentioned in Results section 1.3.1. Moreover, different immunopeptidomics protocols using transformed and primary B cells demonstrated that the HLA-I ligandome of B cells is a rich source of information and holds promise for identifying T-cell epitopes (274–276). Based on our optimizations and previous literature, our sensitive elution system can detect approximately 1500 peptides by eluting HLA-I ligands from as few as $1x10^7$ B cells (262). Therefore, we used $1.5x10^7$ HSTMG-expressing B cells for our MS-based screenings, as this cell quantity already had the potential to capture hotspot-derived epitopes. Although the total peptides per sample detected was within the expected range for the number of cells used (Figure 17A), only five shared neoantigens were detected in the four patients studied. Among all the previously reported public neoantigens, only one of the 16 expected peptides was captured using our method (Table 6).

This poor performance in capturing public neoantigens represented a significant limitation for our purpose.

The inability to detect certain neoantigens may be due to the varying expression of specific HLA-I alleles in B cells. Indeed, analysis of the HLA-I ligandome from transformed B cells using deconvolution software revealed that HLA-C alleles are less frequently observed, likely because they are often poorly expressed and have more overlapping binding specificities (277–279). This is consistent with our observation that MS-based immunopeptidomics from HSTMG-expressing B cells preferentially recovered HLA-I ligands from HLA-A and HLA-B alleles rather than from HLA-C in three of the four patients studied (Figure 17D).

Therefore, the low expression of HLA-C, as shown in previous studies on peripheral blood lymphocytes (280–282), could explain why the neoantigens derived from $KRAS_{p.G12D}$, previously reported to be presented on HLA-C*08:02 (76,178) were not detected using the B cell approach. Nevertheless, the failure to detect other reported neoantigens in HLA-A and HLA-B alleles remains unexplained. This may be related to the abundance of such peptides on the cell surface rather than the expression of the specific HLA-I allele.

Another limitation of this method is determining the specific HLA-I presenting allele for each peptide, especially when the identified HLA-I ligands can be considered as binders of multiple HLA-I alleles expressed in the antigen-presenting cells. This is because recipient B cells can express up to 6 different HLA-I alleles. In such cases, the co-occurrence of HLA-I alleles across different HLA-I peptidome datasets could have been used to accurately map the identified peptides to their corresponding alleles without needing prior knowledge of HLA-I binding specificity (278). Although this approach seems feasible, it requires a wide variety of samples for analysis, which becomes challenging when analyzing 12 different HLA-I, as in our work.

We reasoned that adjusting the amount of transfected RNA or increasing the total number of cells analyzed would not overcome the limitations we encountered. At that time, several reports using MS-based immunopeptidomics on HLA-I monoallelic cells showed increased sensitivity in detecting low abundant peptides in the HLA-I ligandome compared to multiallelic cells (176,177,283,284).

Moreover, the peptides identified were clearly assigned to a single HLA-I molecule. Considering this, we chose to explore HLA-I monoallelic cells as a source for our MS-based immunopeptidomics screenings.

Factors influencing additional detection of neoantigens in transient HLA-I monoallelic cells

Our MS-based immunopeptidomics screenings of transient HLA-I monoallelic cells led to the identification of both novel and previously reported candidate public neoantigens across several HLA-I alleles (Figure 32B). These results showed that HLA-I monoallelic cells were more suitable than B cells for the detection of HLA-I-presented shared neoantigens derived from selected mutations. Importantly, we were able to identify novel public neoantigens derived from hotspot mutations and HLA-I allele combinations previously interrogated in other MS-based immunopeptidomics approaches (178–182,223,231) highlighting the high performance of our method. Although our system, like most previously reported approaches, relies on the overexpression of the mutations and HLA-I alleles of interest in HLA-I negative cells, some particularities may explain the detection of additional peptides.

One factor that can explain the detection of more peptides in our system is the **high amount of HSTMG RNA** used (Figure 49). Many studies choose lentiviral or retroviral transduction to deliver constructs encoding for hotspot mutations in driver genes into HLA-I negative cells. The expression is regulated by strong promoters to achieve substantial overexpression of the mutations of interest (180–182,231). Nevertheless, the expression of these constructs might not reach the levels of RNA we introduce by electroporation. Previous immunopeptidomics studies have indicated that higher gene expression levels and/or RNA abundance are statistically associated with increased HLA-I presentation density (172,176,272). As a result, the high abundance of RNA in our system may facilitate the HLA-I presentation of neoantigens that would not be, or at least to a lesser extent, present in the HLA-I ligandome of a cell expressing the mutated gene from transduced constructs.

Another factor that could account for the detection of additional neoantigens is the differential **peptide stabilization in B2M_HLA chimeras** compared to native HLA-I molecules (Figure 49).

Most of the approaches for generating HLA-I monoallelic cells only introduce the α-chain of the HLA-I alleles of interest, using the endogenous β2M to form HLA-I complexes (178,180–182,223,231). The resulting pHLA-I complexes will be stabilized and folded as native HLA-I molecules. In contrast, we introduced B2M_HLA chimeric constructs encoding for the two molecules directly linked through a short GS linker (261,285). This linkage potentially increases the stability of the resulting empty HLA-I complexes.

The improved stability of these molecules may make it easier to load peptides into the ER that would not normally be loaded into native HLA-I molecules. This is because the resulting pHLA-I complex would not be sufficiently stable to reach the cell surface under normal circumstances. Previous MS-based immunopeptidomic studies on HLA-I monoallelic cells expressing chimeric HLA-I constructs, similar to our B2M_HLA chimeras, revealed that these molecules present peptides stable in native HLA-I molecules (179). Additionally, studies using our design of chimeric B2M_HLA constructs with mouse molecules demonstrated that the peptide-B2M_MHCI complexes displayed a stability comparable to peptide-MHC-I complexes (286). However, as this correlation has not yet been confirmed in B2M_HLA chimera constructs, it is still possible that the differential peptide stabilization, compared to native HLA-I, led to the identification of some additional neoantigens in our approach.

Another factor influencing the detection of neoantigens is the predominant type of **proteasomes** in the recipient cells (Figure 49). Our working model is based on an epithelial tumor cell line that prominently expresses the standard proteasome (Figure 22). This is a substantial difference from previous studies, which mainly used cell lines of hematopoietic origin (i.e., K562, C1R, 721.221) that are more likely to exhibit immunoproteasomes.

Although some studies have indicated that certain peptides are consistently produced across different types of proteasomes, with varying processing efficiencies (41,287), others are exclusively generated by the standard proteasome (288,289), the immunoproteasome (41,290) or intermediate proteasome (40,287).

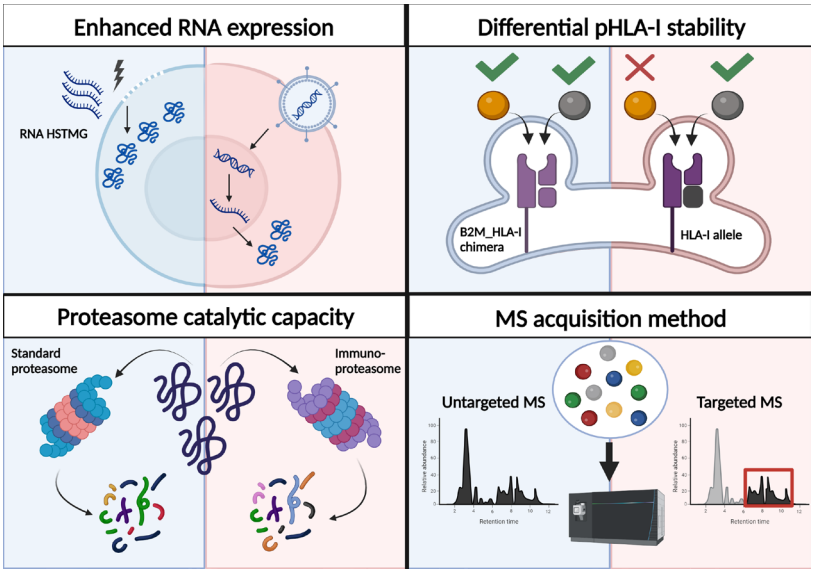


Figure 49. Schematic representation of factors influencing the detection of neoantigens in HLA-I transient monoallelic cells. 1) The electroporation of HLA-I monoallelic cells with large amounts of RNA may result in higher protein abundance and density of specific peptide-HLA complexes compared to the expression and presentation density obtained when transducing constructs with viral vectors. 2) In HLA-I monoallelic cells the conformational structure of B2M_HLA-I may facilitate the loading of peptides that are poor stabilizers of pHLA-I complexes compared to cells that use endogenous β2M with a transfected HLA-I allele 3) Processing a protein by proteasomes containing different catalytic subunits may generate different sets of epitopes for HLA-I presentation in different recipient cells. 4) Targeted MS may miss some peptides that would have been detected in an untargeted MS screen. Image created with Biorender.com.

In line with this, our approach detected and validated the $KRAS_{p.G12D}$ neoantigen presented by HLA-A*02:01. This neoantigen was previously identified in PANC-1 cells (244), which are of epithelial origin and likely express the standard proteasome, similar to our recipient cells. However, it also expresses some inducible proteasome subunits (291). In contrast, studies using HLA-I monoallelic cells derived from C1R or COS-7 did not detect the $KRAS_{p.G12D}$ neoantigen presented on HLA-A*02:01 (181,182).

Another example is the $KRAS_{p.G12V}$ neoantigen presented by HLA-B*07:02. Our approach captured this neoantigen, but it was not detected in HLA-I monoallelic cells generated with C1R (178,181) and A375 cells. The latter is a melanoma cell line with constitutive expression of some inducible proteasome subunits (292). There are other discrepancies in neoantigen identification when comparing our approach to studies using C1R or 721.221 cell lines.

Previous studies showed that 721.221 expresses the inducible subunits, suggesting that these cells might present immunoproteasomes (176,180).

Based on the differences observed, we believe that the distinct catalytic activities of the proteasomes in recipient cells influence the pool of presented peptides in the HLA-I ligandome, leading to the discovery of a unique set of neoantigens in our system.

Lastly, another factor contributing to identifying novel neoantigens is our use of **untargeted MS-based screenings** (Figure 49). Most MS-based immunopeptidomics approaches for discovering shared neoantigens using HLA-I monoallelic cells rely primarily on targeted mass spectrometry due to its high sensitivity in capturing low-abundant peptides (293,294).

However, targeted mass spectrometry requires prior knowledge of the sequences to be interrogated, limiting its applicability to predefined peptide candidates. For example, peptide candidates for targeted MS analysis are usually prioritized based on their binding affinity or stability to the HLA of interest. Both features have been correlated with neoepitope immunogenicity (295–297). Despite this, false positives and false negatives during the experimental determination of HLA-I ligands have been observed among peptides prioritized by binding affinity predictors (178,179,182). Similarly, targeted MS-based analysis of peptides prioritized based on the stability of pHLA-I complexes has encountered the same issue (181).

In our approach, we relied on untargeted MS to discover all potential peptides present in the HLA-I ligandome to avoid the bias introduced for predefined peptide features. Using shotgun MS-based analysis, we identified and later validated some shared neoepitopes that would not have been prioritized for interrogation using the binding affinity algorithm NetMHCPan4.1 (Figure 33). Thus, our approach may have helped to identify new neoepitopes that had not been previously investigated using targeted MS analysis, focusing on the binding affinity for prioritization of candidate neoantigens.

Overall, the combination of all these factors might explain the detection of additional candidate neoantigens when transient HLA-I monoallelic cells were used in comparison to previously reported approaches.

The confirmation of two candidate public neoantigens' presentation in patient-derived TCL was inconclusive

The main goal of MS-based immunopeptidomic studies employing monoallelic cells is to discover neoantigens that can be naturally processed and presented by tumor cells with physiological levels of expression of the hotspot mutation and the HLA-I allele. Nevertheless, most approaches to identifying these neoantigens rely on the overexpression of such mutations. This might raise the concern that peptides detected using these methods would not reach HLA-I presentation on tumor cells expressing natural levels of such mutations and, thereby, would never be targets of T cells mediating anti-tumor responses.

In our study, we were not able to confirm the natural processing and presentation of two candidate public neoantigens. These were detected by our MS-based immunopeptidomics screenings of HLA-I monoallelic cells but not in two patient-derived TCLs, naturally expressing the hotspot mutation and the HLA-I allele (Figure 34B). Although this could indicate that the natural levels of expression of such mutations are insufficient for the generation and HLA-I presentation of these neoantigens on tumor cells, it is important to consider that other factors, such as alterations in the APM found in both TCL (Figure 35) might affect their processing and presentation.

Although we could not evaluate the presentation of any other candidate in patient-derived TCL due to the lack of TCLs presenting both the relevant HLA-I allele and the hotspot mutation of interest, we did compare the neoantigens identified in our system to the ones already reported by other groups. In these studies, 10 of our identified peptides were found to be processed and presented by tumors with constitutive expression of the hotspot mutation from which these neoantigens were derived. This was the case for some $KRAS_{p.G12D,}$ $KRAS_{p.G12V,}$ and $KRAS_{p.G12C}$ neoantigens presented in HLA-A*02:01, HLA-A*03:01 and HLA-A*11:01. These were detected through MS-based immunopeptidomics on TCLs derived from pancreatic, lung, and colorectal cancer patients (178,179,181,182,244,252).

Additional examples are the 10-mers derived from $NRAS_{p.Q61L}$ or $NRAS_{p.Q61K}$ both presented in HLA-A*01:01 and validated in promyelocytic patient-derived TCLs (252) and in several melanoma tumors (231), respectively. Another example is the HLA-A*02:01-restricted neoantigen derived from $TP53_{p.R175H}$ validated in patient-derived TCLs from myeloma, ovarian, and endometrial tumors (298).

These results supported the notion that our MS-based immunopeptidomics method is a promising approach for identifying relevant public neoantigens, which could be used for developing novel T-cell therapies. Future efforts would be required to validate the natural presentation in patient-derived TCL of the other candidate neoantigens identified by our method.

Exploring Hurdles: residual HLA-I expression in B2M KO cells and limitations in peptide capture via untargeted MS

The generation of transient HLA-I monoallelic cells by co-electroporation of RNA encoding HSTMGs and B2M_HLA chimeras resulted in a sensitive method for the identification of several candidate public neoantigens, even when conducting untargeted MS-based screenings. Nevertheless, the experimental approach we followed presented some limitations that are worth mentioning.

One of such limitations while employing untargeted MS analysis is the misidentification of low-abundant peptides (299). Although we aimed to boost the HLA-I presentation of such peptides by electroporating high quantities of RNA, it is possible that certain neoepitopes may still be poorly represented in the HLA-I ligandome and therefore, might not be detected by shotgun MS. For instance, some peptides that were previously reported as well as some peptides predicted as binders for certain HLA-I alleles, were missed by untargeted MS but were captured with PRM-targeted MS (Table 8 and Figure 31). This might be because peptides with amino acid sequences suboptimal for MS-based analysis could not be captured by this technique. The preferential identification of peptides that are easily ionized and fragmented (300) and the inefficient detection of cysteinylated peptides due to modifications introduced during sample preparation (301) are well-known drawbacks of MS instruments.

Thus, the absence of evidence for peptide presentation through MS-based technologies cannot be considered evidence of absence, due to technical limitations associated with such techniques.

Another limitation of our method was the observation of residual HLA-I expression in the B2M KO recipient cells. In contrast to other methods employing HLA-I negative cells that lack expression of the endogenous HLA-I alleles, our B2M KO model retained the expression of the HLA-I alleles of the TCL. Even though after CRISPR/Cas9 knockout of the B2M gene, cells were sorted to enrich for HLA-I negative cells (Figure 21A), some carryover of HLA-I positive cells occurred, as some cell surface expression of HLA-A*03:01 and HLA-C was detected in B2M KO cells (Figure 29A). Despite only 1% of the cells expressing these alleles, this was sufficient for the repetitive identification of the same three peptides regardless of the introduced B2M_HLA chimera.

Although other approaches generating monoallelic cell lines with C1R and 721.221 as recipient cells, could have encountered the same problem, as some previous reports detected residual expression of HLA-B and/or HLA-C alleles in these cell lines (302–304), they did not confront this issue. In the case of the study using 721.221 as recipient cells for the generation of HLA-I monoallelic cells, this can be explained by the fact that they performed targeted MS analysis, and thus, their identifications could only be peptides predicted to bind to the alleles introduced (179). In contrast, in the study employing C1R as recipient cells and conducting untargeted MS analysis, they knocked out the HLA-C*04:01 before the generation of HLA-I monoallelic cells, which eliminated the potential residual endogenous expression of such HLA-I allele (181).

We are aware that we could have knocked out the HLA-I alleles or established clones from the B2M KO TCL to get rid of the residual HLA-I expression. Nevertheless, nearly all identified and validated novel HLA-I ligands in our approach were exclusively recovered when introducing a specific B2M_HLA chimera for which they are considered binders, according to *in silico* predictors. Consequently, there is high confidence in their accurate detection.

Thus, our method provides a rapid and flexible approach to interrogate for peptide presentation across any antigen and any HLA-I allele of interest. Through this approach, we have identified actionable targets to advance the development of novel cancer immunotherapies.

IVS of unfractionated PBLs from a cancer patient could have expanded naïve and memory T-cell responses

In contrast to certain studies that focus on enriching reactive T-cell populations from isolated memory subsets when sensitizing cancer patient PBLs (211,224) or naïve subset when sensitizing HD PBLs (210,226), we used unfractionated PBLs from a cancer patient. This strategy facilitated the detection of T-cell responses potentially originating from both the memory and naïve T-cell compartments.

The use of IL-21 during the initial stimulation round in our IVS protocol aims to facilitate the expansion of T cells within the naïve repertoire (226). Through the stimulation of PBLs with MEP-1 and MEP-2 in the presence of this cytokine, we succeeded in expanding two de novo reactivities against $PIK3CA_{p.R88Q}$ and $TP53_{p.R248Q}$. These two reactive T-cell populations likely expand from the naïve T-cell repertoire, as these mutations were not detected in the patient's tumor by WES.

Conversely, the expansion of virus-specific T cells upon stimulation of PBLs with CEF PP suggests the efficacy of our IVS protocol in potentially expanding T-cell populations from the memory compartment. CEF encompasses 32 epitopes derived from Cytomegalovirus, Epstein-Barr virus, and Influenza virus, known to bind to the most prevalent HLA-I alleles. Given the widespread prevalence of these viruses, it is assumed that individuals have encountered them at some point in their lives. Hence, stimulation of PBLs with CEF PP likely expanded antigen-experienced $CD8^+$ T-cells specific for some of these peptides from the T-cell memory compartment of the patient (305,306).

Due to the lack of phenotypical characterization of the expanded populations with CD45RA/RO and CD62L markers, which are typically used to distinguish naïve and memory T cells (307), we are unable to classify the expanded T-cell population reactive against $PIK3CA_{p.E545K}$.

However, given that the hotspot mutation was detected in the patient's tumor via WES, it is tempting to speculate that the identified reactive T cells following IVS may originate from the memory compartment. This idea is supported by studies that conducted IVS of independent PBL subsets from cancer patients. Specifically, these studies sorted T-cell subsets based on CD45RA/RO and CD62L into four independent groups (i.e. naive, central memory, effector memory, and terminally differentiated effector memory). Each subset was independently stimulated with KRAS or TP53 neoantigens corresponding to mutations found in the patient's tumor. Through this strategy, these studies showed that the reactive T cells consistently originated from the memory compartment in cancer patients (211,224,243).

Despite the observations made by these studies, we believe that the $PIK3CA_{p.E545K}$ population likely originated from the naïve compartment due to different reasons. First, previous work from our laboratory did not detect recall responses to $PIK3CA_{p.E545K}$ neoantigen in high-throughput immunological screenings on subsets of $CD8^+$ PBLs from this patient (Appendix Figure 7). As antigen-experienced cells, memory T cells have a low activation threshold, potentially allowing for their direct detection from PBLs through functional immunogenic assays without prior stimulation (308). Nevertheless, since only specific biomarker-based enriched subsets of $CD8^+$ PBLs were tested, we cannot rule out the possibility that the reactive population was overlooked.

Second, we hypothesize that there is a defective in vivo priming to some tumor antigens, which results in ineffective activation of T-cell responses in patients. In line with this, recent studies have demonstrated the induction of T-cell responses in cancer patients whose tumors expressed KRAS hotspot mutations upon therapeutic vaccination with the corresponding tumor-specific KRAS neoantigens (309).

Last, further evidence supporting the notion that reactive T cells to $PIK3CA_{p.E545K}$ could have expanded from the naïve pool is the isolation of neoantigen-specific responses from HD PBLs. Indeed, the use of the same epitope derived from $PIK3CA_{p.E545K}$ that we used for IVS of PBLs from the breast cancer patient induced the expansion and isolation of $CD8^+$ PBLs from HLA-A*11:01$^+$ HDs upon IVS (181).

Taking all this into account and considering that our IVS protocol relied on unfractionated PBLs, it is plausible that T cells were primed in vitro to the antigen and expanded from the naïve T-cell repertoire.

Sensitization of PBLs with MEPs hamper detection of the entire neoantigen-specific T-cell repertoire

In this work, we explored the sensitization of PBLs using minimal epitopes derived from hotspot driver mutations, presented in one of the patients' HLA-I alleles based on our MS-based immunopeptidomics screenings. The use of the three immunogenic peptides in MEPs for PBL sensitization did not result in the simultaneous detection of the three neoantigen-specific T-cell responses, as observed in our IVS experiments. These findings contrast with previous publications detecting similar T-cell responses upon PBMC stimulation with either single or extensive peptide pools (219).

We hypothesized that competition for HLA-I binding might explain the inconsistent T-cell expansion observed with MEPs. The inclusion of seven and ten neoepitopes in MEP-1 and MEP-2, respectively, all binding to HLA-A*11:01, may have caused competition for presentation. Moreover, since several peptides within the pool display high-affinity binding for the allele, an uncontrolled preferential presentation of a particular ligand and a reduced presentation of others may have occurred. Such reduced HLA-I presentation could have hampered $PIK3CA_{p.E545K}$-specific T-cell expansion when using MEPs as opposed to when stimulating PBLs with the single peptide (Table 11 and Figure 38A).

The lack of detection of additional T-cell responses to other hotspot-derived neoantigens, such as KRAS neoepitopes presented by HLA-A*11:01 contained in MEP-2, may also be due to peptide competition. Previous studies have successfully sensitized PBLs from multiple HLA-A*11:01$^+$ HD to the same KRAS epitopes (178,179). Thus, despite using PBLs from a cancer patient, which has a different TCR repertoire, we expected at least one T-cell response to KRAS peptides. Contrary to previous reports, we did not add peptides separately during sensitization, which could have led to competition for binding, ultimately resulting in the absence of expanded T-cell populations.

This underscores the importance of performing independent stimulation to favor the expansion of neoantigen-specific T cells.

On the other hand, it has been described that in the presence of multiple HLA-I ligands, immunodominant epitopes cause the preferential expansion of specific reactive T-cell populations (310). However, when we stimulated with MEP-1, it resulted in the expansion of a $TP53_{p.R248Q}$-specific T-cell population, while MEP-2 stimulation expanded the $PIK3CA_{p.R88Q}$-specific T-cell population. Even though both peptides were present in MEP-1 and MEP-2 (Table 11), they led to the expansion of different reactivities. This indicates that neither of these neoepitopes was immunodominant because if they were, we would have expected expansion of the same population when PBLs were stimulated with these MEPs.

Overall, stimulation with MEPs caused an underrepresentation of the neoantigen-specific T-cell repertoire, as not all the raised T-cell responses were consistently captured when the three neoantigens were used in combination to sensitize PBLs.

HLA-I dextramer staining and measurement of 4-1BB upregulation were not equivalent readouts for the identification of reactive T cells

To detect T-cell populations targeting shared neoantigens upon IVS, we used both HLA-I dextramer staining and measurement of 4-1BB activation marker as readouts. These two different strategies enabled the detection of varied reactivities at different time points.

The dextramer technology we used is a flexible platform that enables the interrogation of several peptides in different HLA-I restriction elements. While staining with HLA-A*11:01-dextramers loaded with $PIK3CA_{p.E545K}$ enabled the detection of reactive T cells (Figure 38A), the measurement of 4-1BB upregulation after co-culture with peptide-pulsed autologous B cells failed to identify them. Although discrepancies between binding to pMHC-I multimers and functional activity have already been reported (200,311,312), further experiments with enriched dextramer-binding T cells proved that the isolated T cells were functional as they secreted IFN-γ and upregulated 4-1BB upon recognition of their target (Figure 38B).

Hence, HLA-I dextramers, compared to 4-1BB measurement, were more sensitive in detecting this low-frequent T-cell population.

Despite their increased sensitivity in the above-mentioned example, other factors can negatively impact the identification of certain T-cell reactivities by pMHC-I multimers. One key aspect is the effective loading of the peptides into the HLA-I monomers. We specifically used empty stable monomers and later loaded them with the desired neoepitopes. The incomplete complex formation during peptide loading can potentially lead to false-negative results. For instance, the likely reason HLA-I dextramers failed to capture the $TP53_{p.R248Q}$-reactive T-cell population, which was effectively detected by 4-1BB measurement, was the improper complex formation between this neoepitope and HLA-A*11:01 monomers (Figure 40A). We assume the low predicted binding affinity of this peptide to the HLA-I allele, above the common 500nM threshold, may hinder HLA-I complex formation (313,314). Nevertheless, our data shows that this standard threshold of binding cannot be used to determine misfolding.

Table 13. The folding of monomers is not always consistent with predicted binding.

Minimal epitope ID	Peptide sequence	Neoantigen	HLA-I allele	nM affinity	Folding monomers
ME_1	SSCMGGMN**Q**R	$TP53_{p.R248Q}$	A*11:01	149.04	NO
ME_2	SCMGGMN**Q**R			6878.8	NO
ME_3	KIGDFGLAT**E**K	$BRAF_{p.V600E}$		102.32	YES
ME_4	GDFGLAT**E**K			4822.77	NO
ME_5	STRDPLSEIT**K**	$PIK3CA_{p.E545K}$		93.97	YES
ME_6	ALMSEL**E**VLSY	$KIT_{p.K642E}$		1358.27	YES
ME_7	KAISTRDPLS**K**	$PIK3CA_{p.E542K}$		318.81	YES
ME_8	GA**D**GVGKSAL	$KRAS_{p.G12D}$	C*04:01	20365.9	NO
ME_9	FFDETR**Q**LC	$PIK3CA_{p.R88Q}$		1733.39	NO
ME_10	FFDETR**Q**L			362.46	YES

Minimal epitopes contained in MEP-1 used for sensitization of GOI-01 PBLs are shown. The specific presenting allele identified via shotgun MS screenings of HLA-I monoallelic cells and predicted affinity (nM) by NetMHCPan4.1 are specified. Cells highlighted in green indicate predicted stable complexes (<500nM), red cells indicate unstable complexes (>500nM). The experimental assessment of monomer folding (YES/NO) is also shown.

We observed a proper folding of HLA-A*11:01 monomers with $KIT_{p.K642E}$ neoepitope despite having a predicted binding affinity above the 500nM threshold (Table 13). On the contrary, the 10-mer neoepitope derived from $TP53_{p.R248Q}$ did not fold HLA-A*11:01 monomers even though the predicted binding affinity was below the threshold (Table 13). This highlights the importance of empirically evaluating the effective loading of peptides in monomers before employing HLA-I dextramers for T-cell identification.

Overall, our data indicates that while HLA-I dextramer staining and measurement of the 4-1BB may be equivalent for identifying some antigen-specific T-cell populations, in certain cases, both techniques should be considered complementary readouts for T-cell detection.

Influence of donor TCR repertoire sampling on the detection of T-cell responses via IVS

The vast diversity within the TCR repertoire (315) potentially allows for the expansion of different clonotypes reactive to several peptide-HLA combinations when PBLs are stimulated with multiple peptides. However, it is important to consider that we have only evaluated a fraction of the patient's broad TCR repertoire, and this sampling may impact the final TCRs identified.

Given the large number of distinct T-cell clones within the total repertoire (316), it can be assumed that the initial number of PBL used for IVS had a low representation of the entire pool of antigen-specific T cells. Additionally, we divided the PBL repertoire into multiple wells for sensitization with different MEPs. This random allocation of cells into various stimulation conditions may have unintentionally biased each replicate toward a different representation of each T-cell population. Consequently, an increased representation of a specific T-cell population may have caused those specific T-cells to expand preferentially in each condition. This provides an explanation for the limited expansion of neoantigen-specific T-cell populations from only one of the two stimulated replicates under each condition (Figure 39A and Figure 42A).

Another factor that affects the detection of neoantigen-specific T-cell responses is the fitness of the T cells carrying the reactive receptors. Circulating T cells expressing high levels of PD-1 have been found to contain tumor-reactive antigen-specific T cells (198,199). However, T cells with high levels of PD-1 have been associated with an "exhausted" state (317,318). This could mean that these cells can have impaired proliferation capacity. As a result, these neoantigen-specific T cells might be missed because other T cells with better fitness outcompete them.

This might explain why we were unable to detect KIAA1524$_{p.S571}$ neoantigen-specific T cells from PBLs stimulated with MEP-2 in our IVS experiments. Even though this reactivity was found in several CD8$^+$ PBL subsets expressing high levels of PD-1 in the patient circulating T cells, as shown in previous experiments performed in our laboratory (Appendix Figure 7).

Last, it is also possible that T cells reactive to other hotspot-derived neoepitopes contained in MEPs were absent in the entire T-cell repertoire of the patient. Screening multiple donors will be essential to detect T cells targeting the remaining neoepitopes contained in MEPs (Table 11) (213).

Sensitization with minimal epitopes resulted in the expansion of single dominant TCRs

The presence of multiple reactive TCRs to the same minimal epitope and HLA-I pair within a single patient has been observed in TILs (74,75,231,255) and in PBL post-IVS (211,224,243). This suggests the potential to capture several TCRs reactive to the same neoepitope-HLA pair from a single donor.

Although some clonotypes seemed to be more enriched than others in each of the T-cell reactive populations as observed by TCRβ deep sequencing (Figure 44), only one TCR per population, among the ones chosen for functional validation, showed reactivity. Our results align with previous reports that have shown the expansion of a single dominant TCR after sensitization with single minimal epitopes (178,179,223).

The rapid expansion protocol used to expand the sorted T-cell populations detected after IVS may lead to a reduction in clonotype diversity.

Although these populations were enriched in neoantigen-specific T cells, they likely contained some bystander T cells that could outcompete reactive cells during REP. This limitation is a known issue in the field and has been previously reported (319). To reduce the risk of missing additional reactive clonotypes during expansion, TCR sequencing could be carried out immediately after sorting. This could be done using DNA-barcoded multimers to unbiasedly identify expanded neoantigen-specific TCRs during IVS (178).

Moreover, it is possible that there are additional reactive TCRs that we have not explored in our study. This is because we only selected for functional validation TCRs with high frequency in each of the pre-enriched antigen-specific T-cell populations. To efficiently test many TCR candidates, TCR library screenings can be carried out (320). This approach not only enables the identification of multiple reactive TCRs to a specific antigen but also allows the concurrent detection of TCRs that are reactive to different peptide-HLA combinations.

It is also possible that only a single TCR reactive to each antigen was present in the patient's repertoire, that it expanded after IVS, and that our approach captured it. Because of this, further screenings of HD and cancer patients are necessary to identify additional therapeutic candidate TCRs that recognize the same and other peptide-HLA combinations.

Preliminary insights into the anti-tumor potential of the discovered candidate therapeutic TCRs

We identified three neoantigen-specific TCRs that could be potential off-the-shelf TCR therapeutic candidates. While the comprehensive characterization of their safety and potency needs to be addressed, experiments conducted in this thesis provide insights into their anti-tumor potential.

One crucial aspect to consider during preclinical testing of potential therapeutic TCRs is their ability to target tumor cells. Our data indicates that the three TCRs could identify their specific targets when resulting from the endogenous processing and presentation of overexpressed full-length mutant proteins in tumors (Figure 46A and 46C).

However, the assessment of the cytolytic potential of these TCRs in tumors with natural expression of the mutation and the corresponding HLA-I restriction element remains to be evaluated.

Additionally, we addressed the functional avidity of TCR-transduced T cells with the three TCRs, as it has been shown to correlate with the extent of tumor cell recognition (136,321,322). Among them, the TCR targeting the $PIK3CA_{p.E545K}$ neoantigen exhibited the highest functional avidity as it responded to progressively lower peptide concentrations (Figure 47). In addition, this TCR was the only suggestive to be coreceptor independent. The observation that bulk T cells transduced with the TCR specific for $PIK3CA_{p.E545K}$ neoantigen, either expressing the CD4 or CD8 co-receptor, could be activated when they encountered the neoantigen, suggests that this TCR can function in a co-receptor independent manner (Figure 45B). This property is important because it indirectly indicates that the receptor is likely to have a high affinity (136,223,323). Further experiments are necessary to confirm the ability of the $PIK3CA_{p.E545K}$ TCR to exert its antigen-specific effector functions independently of co-receptors.

Altogether, our initial findings underscore the $PIK3CA_{p.E545K}$ TCR as the most potent among the three receptors. However, the other two candidate TCRs, although of lower affinity, may still contribute to tumor control. Some studies have shown that T-cells carrying TCRs with moderate-affinity exhibited prolonged persistence and sustained anti-tumor responses compared to those with high-affinity receptors (76,324–326). It is possible that the varying persistence of T cells can be attributed to a rapid exhaustion of T cells carrying high-affinity TCRs. Recent studies using mouse models have demonstrated that $CD8^+$ TILs with higher affinity tend to become exhausted more quickly, while those with lower affinity retain a more progenitor-like profile (327). In accordance with this observation, cells with a central memory phenotype, exhibiting stem cell-like properties, have shown long-term persistence and superior anti-tumor responses in humans (328,329). Therefore, TCRs targeting $PIK3CA_{p.R88Q}$ and $TP53_{p.R248Q}$, potentially with lower affinity than the $PIK3CA_{p.E545K}$, remain promising candidates for ACT of TCR-T.

We acknowledge that essential aspects concerning the safety and potency of the identified TCRs still need to be assessed (235). Though there is still much work to be done to complete the preclinical characterization of these receptors, we believe that the discovered TCRs hold promising potential for the development of off-the-shelf T-cell therapies.

HLA-I and hotspot mutation co-occurrence in cancer: implications for TCR-engineered T-cell therapies

Given the identification of TCRs that target public neoantigens, we aimed to estimate the number of cancer patients who could benefit from TCR-T ACT using these TCRs. By analyzing the mutation frequencies of PIK3CA and TP53, as well as the prevalence of HLA-A*11:01 and HLA-C*04:01 alleles, we estimated that approximately 90,000 patients could benefit annually from T-cell therapies targeting these peptide-HLA pairs (Table 12).

Despite the potential of these TCRs to treat multiple patients, the negative selection of tumors harboring both the HLA-I alleles and mutations could limit their applicability. Therefore, we assessed deviations in the proportion of patients with the relevant HLA-I and the hotspot mutation in cancer-specific cohorts from the TCGA repository (Figure 48). Although we did not observe a background selection, we acknowledge that our analysis was a simplified approach, as we only considered the presence of the HLA-I and the mutation. Many other factors, such as mutations in APM or the level of RNA expression of the hotspot mutations, can impact the HLA-I presentation of the neoantigens targeted by these TCRs. Consequently, these factors should have been considered, as they might limit the use of TCR-based therapies with the identified TCRs.

A thorough study that considered these additional factors found evidence of immune editing in the TCGA cohort of colorectal cancer patients. This study specifically observed that tumors with alleles capable of presenting immunogenic neoantigens had a lower prevalence of certain hotspot mutations, including $PIK3CA_{p.R88Q}$ (158). This suggests that the effectiveness of TCR-T cells targeting the $PIK3CA_{p.R88Q}$ mutation in colorectal tumors may be limited by tumor immune edition.

Nevertheless, tumor editing involves a dynamic interaction between T cells and tumors. Thus, the infusion of TCR-engineered T cells may intensify the selective pressure of tumor clones with alterations in neoantigen presentation. For instance, tumors can avoid T-cell detection when they lose the HLA-I restriction element, which is responsible for presenting immunogenic neoantigens. This evasion of T-cell surveillance limits the efficacy of TCR-based therapies. Two case reports have shown that T cells with TCRs targeting public neoantigens failed to achieve long-lasting tumor rejection because of HLA-I loss in certain tumor lesions (76,153). This resistance mechanism has also been observed in patients treated with TCR-engineered T cells targeting viral proteins (150). These findings underscore the importance of closely monitoring tumor evolution during TCR-based therapy treatments.

Development of TCR-engineered T-cell products using the discovered off-the-shelf therapeutic TCR candidates

The candidate TCRs show promise for treating cancer because they can target public neoantigens. We will discuss the development of ACT of TCR-engineered T cells with the identified TCRs, although the preclinical characterization of these receptors has not yet been completed. To identify suitable candidate patients for these T-cell therapies, it is important to assess the hotspot mutation and the expression of the HLA-I restriction element. These factors can be detected from either peripheral blood samples or tumor biopsies.

Blood samples can identify eligible patients for ACT of TCR-T cells carrying the identified TCRs by analyzing circulating cell-free DNA and DNA extracted from PBMCs. Circulating cell-free DNA (cfDNA) comprises small DNA fragments released into the bloodstream by cells undergoing cell death or damage across various tissues, including tumor cells (330,331). In cancer patients, circulating tumor DNA represents a fraction of cfDNA originating from tumor cells. This tumor-derived genetic material serves as a valuable resource for identifying tumor mutations directly from blood plasma. Previous studies have shown that it is possible to detect hotspot mutations in PIK3CA and TP53 genes from cfDNA. These mutations were used as biomarkers to measure therapeutic efficacy and monitor residual disease (332–336). Therefore, cfDNA can be used to examine the presence of hotspot mutations in the tumor lesions of metastatic cancer patients.

Additionally, NGS of DNA from PBMCs can be used to determine the germline HLA-I genotype. This allows for the identification of the relevant HLA-I restriction element.

However, it is well known that tumors can downregulate or lose expression of HLA-I alleles through various mechanisms (337). As a result, the HLA-I genotyping of PBMCs may not always correspond with the expression of HLA-I in tumors. Instead, we suggest examining mutations that could potentially cause HLA-I loss using WES and confirming the expression of the relevant HLA-I allele through RNA sequencing analysis of tumor biopsies. In addition, hotspot mutations can be detected from tumor DNA through WES or by using a targeted sequencing panel for the genes of interest. Although more invasive, this strategy could better identify patients who would benefit from ACT of TCR-T cells.

Once the coexistence of the hotspot mutation and the relevant HLA-I allele is confirmed, blood samples will be required to obtain autologous T cells. These cells will be engineered to express the corresponding off-the-shelf TCR of interest for patient treatment (Figure 50). To avoid using viral vectors for TCR transfer and to prevent TCRαβ chain mispairing, an alternative genetic editing strategy using CRISPR/Cas9 can be used. Recent studies have shown that simultaneously knocking out the endogenous TCR and knocking in the TCR of interest into the same locus is a safe method to produce TCR-engineered T cells for treating cancer (151). After introducing the TCRs, cells can be selected and expanded to high numbers in a REP. Before infusing the expanded TCR-engineered T cells, lymphodepletion will be used on the patient to create space for the therapeutic cells. Additionally, administration of IL-2 will further promote *in vivo* T-cell growth (Figure 50).

Similar manufacturing procedures have been used to produce TCR-engineered T cells targeting different shared tumor antigens as the one we are proposing (135,136,138,139,141,150,152). These TCR-T cells have been used in clinical trials, demonstrating strong anti-tumor responses and highlighting their effectiveness in cancer treatment. While there is currently limited clinical experience with TCR-engineered T cells targeting public neoantigens, promising results from case reports (152,153) indicate that ACT using TCR-engineered T cells offers a promising treatment option for patients with metastatic epithelial cancers.

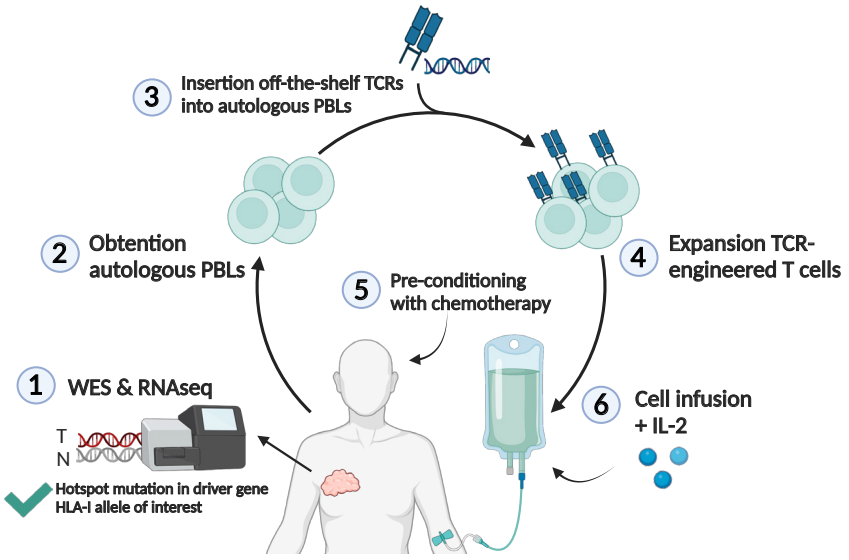


Figure 50. Schematic representation of the proposed ACT strategy using TCR-engineered T cells with the identified candidate off-the-shelf TCRs. DNA extracted from a tumor biopsy and PBLs would be used for 1) WES and RNA sequencing of tumors to identify hotspot mutations and HLA-I typing. 2) Collection of patients' blood to separate autologous PBLs 3) transduction of the adequate off-the-shelf TCR to the patient's T cells. Upon transduction, cells will be selected and 4) expanded to high numbers for patient treatment. 5) In parallel, the patient will receive pre-conditioning chemotherapy. Finally, 6) TCR-engineered T cells would be infused into patients followed by IL-2 to further support the growth and survival of the infused T cells. Image created with Biorender.com.

Identifying and harnessing cancer antigens that trigger a strong immune response is vital for the success of immunotherapies. Antigens originating from recurrent mutations in hotspot regions of driver genes are of particular interest, as they are conserved and highly expressed in tumor cells. Hence, treatments using T cells directed to these antigens have the potential to trigger tumor regression in different tumor lesions within a patient. Additionally, TCRs capable of recognizing these neoantigens could facilitate the development of minimally invasive TCR-based therapies for treating patients with various types of cancer.

In this thesis, a method has been developed to identify candidate public neoantigens that can be targeted by T cells. The identified TCRs, which recognize three different public neoantigens, represent new promising off-the-shelf TCRs that could be used for treating multiple patients with different types of tumors.

Conclusions

Mass spectrometry screening of purified HLA-I peptides from monoallelic cells revealed 33 novel peptide-HLA combinations originating from hotspot-derived neoantigens from various driver genes presented on highly prevalent HLA-I alleles. Moreover, we raised T-cell responses and identified TCRs targeting three public neoantigens, which could be exploited to develop off-the-shelf TCR-based T-cell therapies.

1. We prioritized 12 HLA-I alleles highly prevalent in the European Caucasian population and selected 35 recurrent mutations across 13 cancer driver genes, distributed among four HSTMGs.
2. The use of HLA-I monoallelic tumor cells as a source for immunopeptidomics increased the sensitivity for detecting previously reported and novel mutant peptides compared to B cells.
3. MS-based immunopeptidomics performed on cells expressing a total of 37 HSTMG-B2M_HLA combinations enabled the identification and validation of 49 mutant peptide-HLA pairs derived from 23 different hotspot driver mutations across 10 HLA-I alleles.
4. In vitro sensitization of peripheral blood lymphocytes from GOI-01 cancer patient raised two HLA-A*11:01-restricted T cell reactivities specific for $PIK3CA_{p.E545K}$ and $TP53_{p.R248Q}$, as well as an HLA-C*04:01-restricted response targeting $PIK3CA_{p.R88Q}$.
5. Three TCRs targeting the above-mentioned mutations were identified, exhibiting specific recognition and variable functional avidities toward their respective cognate neoantigens.
6. The three reactive TCRs demonstrated *in vitro* recognition of tumor cells overexpressing the relevant antigen and/or HLA-I, underscoring their potential to develop off-the-shelf T-cell therapies.
7. The physiological presentation of the identified peptides by tumor cells and the immunogenicity of 30 newly described shared mutated peptide-HLA pairs remain unexplored and warrant further investigation.

References

1. Alberts Bruce. Molecular Biology of the Cell. 6th ed. 2015.

2. Hanahan D, Weinberg RA. The Hallmarks of Cancer Review evolve progressively from normalcy via a series of pre. Vol. 100, Cell. 2000.

3. Hanahan D. Hallmarks of Cancer: New Dimensions. Vol. 12, Cancer Discovery. American Association for Cancer Research Inc.; 2022. p. 31–46.

4. Hanahan D, Weinberg RA. Hallmarks of cancer: The next generation. Vol. 144, Cell. 2011. p. 646–74.

5. Ehrlich P. Ueber den jetzigen Stand der Karzinomforschung. Deutsche Chemische Gesellschaft. 1909;42(1):17–47.

6. Burnet FM. The Concept of Immunological Surveillance. In: Progr exp Tumor Res. Karger; 1970. p. 1–27.

7. Schreiber RD, Old LJ, Smyth MJ. Cancer Immunoediting: Integrating Immunity's Roles in Cancer Suppression and Promotion. Science (1979). 2011;331(6024):1565–70.

8. V. Shankaran, H. Ikeda, A.T. Bruce, J. M. White, P. E. Swanson, L. J. Old, et al. IFNy and lymphocytes prevent primary tumor development and shape tumor immunogenicity. Nature. 2001;410:1107–11011.

9. Dunn GP, Bruce AT, Ikeda H, Old LJ, Schreiber RD. Cancer immunoediting: from immuno-surveillance to tumor escape [Internet]. 2002. Available from: http://www.nature.com/natureimmunology

10. Dunn GP, Old LJ, Schreiber RD. The Immunobiology of Cancer Immunosurveillance and Immunoediting. Immunity. 2004;21(2):137–48.

11. I. Penn. Posttransplant Malignancies. 1999.

12. Gatti RA, Good RA. Occurrence of malignancy in immunodeficiency diseases: A literature review. Cancer. 1971;28(1):89–98.

13. Boshoff C, Weiss R. AIDS-related malignancies. Nat Rev Cancer [Internet]. 2002;2(5):373–82. Available from: https://doi.org/10.1038/nrc797

14. Street SEA, Cretney E, Smyth MJ. Perforin and interferon-activities independently control tumor initiation, growth, and metastasis [Internet]. 2001. Available from: http://ashpublications.org/blood/article-pdf/97/1/192/1670448/192.pdf

15. Engel AM, Svane IM, Rygaard J, Werdelin O. MCA sarcomas induced in scid mice are more immunogenic than MCA sarcomas induced in congenic, immunocompetent mice. Scand J Immunol. 1997;45(4):463–70.

16. Street SEA, Trapani JA, MacGregor D, Smyth MJ. Suppression of lymphoma and epithelial malignancies effected by interferon-γ. Journal of Experimental Medicine. 2002 Jul 1;196(1):129–34.

17. I M Svane, A-M Engel, M-Br Nielsen, HG Ljunggren, J. Rygaardj, O. Werdelin. Chemically induced sarcomas from nude mice are more immunogenic than similar sarcomas from congenic normal mice. Eur J Immunol. 1996;26(8):1844–50.

18. Ward JP, Gubin MM, Schreiber RD. The Role of Neoantigens in Naturally Occurring and Therapeutically Induced Immune Responses to Cancer. Adv Immunol [Internet]. 2016;130:25–74. Available from: doi:10.1016/bs.ai.2016.01.001.

19. Gubin MM, Vesely MD. Cancer Immunoediting in the Era of Immuno-oncology. Vol. 28, Clinical Cancer Research. American Association for Cancer Research Inc.; 2022. p. 3917–28.

20. Strominger JL. Human histocompatibility proteins. Immunol Rev [Internet]. 2002;185:69–77. Available from: https://doi.org/10.1034/j.1600-065X.2002.18508.x

21. Kloetzel P. Antigen Processing by the proteasome. Nature Reviews [Internet]. 2001;179–87. Available from: www.nature.com/reviews/molcellbio

22. Joffre OP, Segura E, Savina A, Amigorena S. Cross-presentation by dendritic cells. Vol. 12, Nature Reviews Immunology. 2012. p. 557–69.

23. Neefjes J, Jongsma MLM, Paul P, Bakke O. Towards a systems understanding of MHC class i and MHC class II antigen presentation [Internet]. Vol. 11, Nature Reviews Immunology. 2011. p. 823–36. Available from: https://doi.org/10.1038/nri3084

24. Kumar B V., Connors TJ, Farber DL. Human T Cell Development, Localization, and Function throughout Life. Immunity [Internet]. 2018 Feb 20;48(2):202–13. Available from: https://doi.org/10.1016/j.immuni.2018.01.007

25. Golstein P, Griffiths GM. An early history of T cell-mediated cytotoxicity. Nat Rev Immunol [Internet]. 2018 Aug 1;18(8):527–35. Available from: https://doi.org/10.1038/s41577-018-0009-3

26. Oh DY, Kwek SS, Raju SS, Li T, McCarthy E, Chow E, et al. Intratumoral CD4+ T Cells Mediate Anti-tumor Cytotoxicity in Human Bladder Cancer. Cell [Internet]. 2020 Jun 25;181(7):1612-1625.e13. Available from: doi: 10.1016/j.cell.2020.05.017.

27. Ozato Y, Kojima Y, Kobayashi Y, Hisamatsu Y, Toshima T, Yonemura Y, et al. Spatial and single-cell transcriptomics decipher the cellular environment containing HLA-G+ cancer cells and SPP1+ macrophages in colorectal cancer. Cell Rep. 2023 Jan 31;42(1).

28. Malmberg KJ, Levitsky V, Norell H, Matos CT de, Carlsten M, Schedvins K, et al. IFN-γ protects short-term ovarian carcinoma cell lines from CTL lysis via a CD94/NKG2A-dependent mechanism. Journal of Clinical Investigation. 2002 Nov 15;110(10):1515–23.

29. P.J. Bjorkman, M.A. Saper, B. Samraoui, W.S. Bennett, J.L.Strominger, D.C Wiley. Structure of the human class I histocompatibility antigen, HLA-A2. Nature. 1987;329:506–11.

30. Kaufman J. Generalists and Specialists: A New View of How MHC Class I Molecules Fight Infectious Pathogens. Trends Immunol. 2018 May 1;39(5):367–79.

31. Lee Schlosstein, Paul I Terasaki, Rodney Bluestone, Carl M Pearson. High Association of an HL-A Antigen, W27, with Ankylosing Spondylitis. N Engl J Med. 1973;288(14):704–6.

32. A. Diepsrea, M. Niens, GJ. Meerman, S. Poppema, A. van den Berg. Genetic susceptibility to Hodgkin's lymphoma associated with the human leukocyte antigen region. Eur J Haematol. 2005;75:34–41.

33. Manczinger M, Koncz B, Balogh GM, Papp BT, Asztalos L, Kemény L, et al. Negative trade-off between neoantigen repertoire breadth and the specificity of HLA-I molecules shapes antitumor immunity. Nat Cancer. 2021 Sep 1;2(9):950–61.

34. van Deutekom HWM, Keşmir C. Zooming into the binding groove of HLA molecules: which positions and which substitutions change peptide binding most? Immunogenetics [Internet]. 2015 Aug 22;67(8):425–36. Available from: 10.1007/s00251-015-0849-y

35. Kubo R T, Sette A, Grey H M, Appella E, Sakaguchi K, Zhu N Z, et al. Definition of specific peptide motifs for four major HLA-A alleles. The Journal of Immunology [Internet]. 1994;152(8):3913–24. Available from: http://www.jimmunol.org/content/152/8/3913

36. Sidney J, Peters B, Frahm N, Brander C, Sette A. HLA class I supertypes: A revised and updated classification. BMC Immunol [Internet]. 2008 Jan 22;9. Available from: 10.1186/1471-2172-9-1

37. Pishesha N, Harmand TJ, Ploegh HL. A guide to antigen processing and presentation. Nat Rev Immunol. 2022 Dec 1;22(12):751–64.

38. Habib JA, Lesenfants J, Vigneron N, Van den Eynde BJ. Functional Differences between Proteasome Subtypes. Cells [Internet]. 2022 Feb 1;11(3). Available from: 10.3390/cells11030421

39. Aki M, Shimbara N, Takashina M, Akiyama K, Kagawa S, Tamura T, et al. Interferon-y Induces Different Subunit Organizations and Functional Diversity of Proteasomes 1. J Biochem. 1994;115:257–69.

40. Guillaume B, Chapiro J, Stroobant V, Colau D, Van Holle B, Parvizi G, et al. Two abundant proteasome subtypes that uniquely process some antigens presented by HLA class I molecules. Proc Natl Acad Sci U S A. 2010 Oct 26;107(43):18599–604.

41. Chapiro J, Claverol S, Piette F, Ma W, Stroobant V, Guillaume BB, et al. Destructive Cleavage of Antigenic Peptides Either by the Immunoproteasome or by the Standard Proteasome Results in Differential Antigen Presentation 1. The Journal of Immunology [Internet]. 2006;176:1053–61. Available from: http://journals.aai.org/jimmunol/article-pdf/176/2/1053/1213777/1053.pdf

42. Irla M. Instructive Cues of Thymic T Cell Selection. Annu Rev Immunol [Internet]. 2022;40:95–119. Available from: https://doi.org/10.1146/annurev-immunol-101320-

43. Bluestone JA. Mechanisms of tolerance. Immunol Rev. 2011 May;241(1):5–19.

44. Van Der Bruggen P, Traversari C, Chomez P, Lurquin C, De Plaen E, Van Den Eynde B, et al. A Gene Encoding an Antigen Recognized by Cytolytic T Lymphocytes on a Human Melanoma. Science (1979) [Internet]. 1991;13(5038):1643–7. Available from: https://www.jstor.org/stable/2879499

45. Coulie PG, Van Den Eynde BJ, Van Der Bruggen P, Boon T. Tumour antigens recognized by T lymphocytes: At the core of cancer immunotherapy. Nat Rev Cancer. 2014 Feb;14(2):135–46.

46. Laumont CM, Perreault C. Exploiting non-canonical translation to identify new targets for T cell-based cancer immunotherapy. Cellular and Molecular Life Sciences. 2018 Feb 1;75(4):607–21.

47. Khurana E, Fu Y, Chakravarty D, Demichelis F, Rubin MA, Gerstein M. Role of non-coding sequence variants in cancer. Nat Rev Genet. 2016 Feb 1;17(2):93–108.

48. Garcia-Garijo A, Fajardo CA, Gros A. Determinants for neoantigen identification. Front Immunol. 2019;10.

49. Lozano-Rabella M, Garcia-Garijo A, Palomero J, Yuste-Estevanez A, Erhard F, Farriol-Duran R, et al. Exploring the Immunogenicity of Noncanonical HLA-I Tumor Ligands Identified through Proteogenomics. Clinical Cancer Research. 2023 Jun 15;29(12):2250–65.

50. Fisk B, Blevins TL, Wharton JT, Ioannides CG. Identification of an Immunodominant Peptide of HER-2/neu Protooncogene Recognized by Ovarian Tumor-specific Cytotoxic T Lymphocyte Lines. J Exp Med. 1995;181:2109–17.

51. Rezvani K, Brenchley JM, Price DA, Kilical Y, Gostick E, Sewell AK, et al. T-cell responses directed against multiple HLA-A*0201-restricted epitopes derived from Wilms' tumor 1 protein in patients with leukemia and healthy donors: Identification, quantification, and characterization. Clinical Cancer Research. 2005 Dec 15;11(24):8799–807.

52. Brichard V, Pel A Van, W6lfel T, W61fel C, De Plaen E, Leth6 B, et al. The Tyrosinase Gene Codes for an Antigen Recognized by Autologous Cytolytic T Lymphocytes on HLA-A2 Melanomas. J Exp Med. 1993;178:489–95.

53. Coulie PG, Brichard V, Pel A Van, W61fel T, Schneider J, Traversari C, et al. A New Gene Coding for a Differentiation Antigen Recognized by Autologous Cytolytic T Lymphocytes on HLA-A2 Melanomas. JExpMed. 1994;180:35–42.

54. Bakker AB, Schreurs MW, Tafazzul G, De Boer AJ, Kawakami Y, Adema GJ, et al. Identification of a novel peptide derived from the melanocyte-specific gp100 antigen as the dominant epitope recognized by an HLA-A2.1-restricted anti-melanoma CTL line. Int J Cancer. 1995;62:97–102.

55. Olson BM, Frye TP, Johnson LE, Fong L, Knutson KL, Disis ML, et al. HLA-A2-restricted T-cell epitopes specific for prostatic acid phosphatase. Cancer Immunology, Immunotherapy. 2010 Jun;59(6):943–53.

56. Correale P, Walmsley K, Nieroda C, Zaremba S, Zhu M, Schlom J, et al. In Vitro Generation of Human Cytotoxic T Lymphocytes Specific for Peptides Derived From Prostate-Specific Antigen. J Natl Cancer Inst [Internet]. 1997;89(4):293–300. Available from: https://academic.oup.com/jnci/article/89/4/293/2526832

57. Aleksic M, Liddy N, Molloy PE, Pumphrey N, Vuidepot A, Chang KM, et al. Different affinity windows for virus and cancer-specific T-cell receptors: Implications for therapeutic strategies. Eur J Immunol. 2012 Dec;42(12):3174–9.

58. Eberhardt CS, Kissick HT, Patel MR, Cardenas MA, Prokhnevska N, Obeng RC, et al. Functional HPV-specific PD-1+ stem-like CD8 T cells in head and neck cancer. Nature. 2021 Sep 9;597(7875):279–84.

59. Iyer JG, Afanasiev OK, McClurkan C, Paulson K, Nagase K, Jing L, et al. Merkel cell polyomavirus-specific CD8+and CD4+ T-cell responses identified in Merkel cell carcinomas and blood. Clinical Cancer Research. 2011 Nov 1;17(21):6671–80.

60. Lee SP, Chan ATC, Cheung ST, Thomas WA, CroomCarter D, Dawson CW, et al. CTL Control of EBV in Nasopharyngeal Carcinoma (NPC): EBV-Specific CTL Responses in the Blood and Tumors of NPC Patients and the Antigen-Processing Function of the Tumor Cells. The Journal of Immunology. 2000 Jul 1;165(1):573–82.

61. Akers SN, Odunsi K, Karpf AR. Regulation of cancer germline antigen gene expression: Implications for cancer immunotherapy. Future Oncology. 2010 May;6(5):717–32.

62. Almeida LG, Sakabe NJ, de Oliveira AR, Silva MCC, Mundstein AS, Cohen T, et al. CTdatabase: A knowledge-base of high-throughput and curated data on cancer-testis antigens. Nucleic Acids Res. 2009;37(SUPPL. 1).

63. Xie N, Shen G, Gao W, Huang Z, Huang C, Fu L. Neoantigens: promising targets for cancer therapy. Signal Transduct Target Ther. 2023 Dec 1;8(1).

64. Ostroverkhova D, Przytycka TM, Panchenko AR. Cancer driver mutations: predictions and reality. Trends Mol Med. 2023 Jul 1;29(7):554–66.

65. Cook JH, Melloni GEM, Gulhan DC, Park PJ, Haigis KM. The origins and genetic interactions of KRAS mutations are allele- and tissue-specific. Nat Commun. 2021 Dec 1;12(1):1–14.

66. Li S, Balmain A, Counter CM. A model for RAS mutation patterns in cancers: finding the sweet spot. Nat Rev Cancer. 2018 Dec 1;18(12):767–77.

67. Dennis W. Stacey, Hsiang-Fu Kung. Transformation of NIH 3T3 cells by microinjection of HA-ras p21 protein. Nature. 1984;310:508–11.

68. Feramisco JR, Gross+ M, Kamata T, Rosenberg+ M, Sweet+ RW. Microinjection of the Oncogene Form of the Human H-ras (T-24) Protein Results in Rapid Proliferation of Quiescent Cells. Cell. 1984;38:105–22.

69. Gerstung M, Jolly C, Leshchiner I, Dentro SC, Gonzalez S, Rosebrock D, et al. The evolutionary history of 2,658 cancers. Nature. 2020 Feb 6;578(7793):122–8.

70. Makohon-Moore AP, Zhang M, Reiter JG, Bozic I, Allen B, Kundu D, et al. Limited heterogeneity of known driver gene mutations among the metastases of individual patients with pancreatic cancer. Nat Genet. 2017 Mar 1;49(3):358–66.

71. Pearlman AH, Hwang MS, Konig MF, Hsiue EHC, Douglass J, DiNapoli SR, et al. Targeting public neoantigens for cancer immunotherapy. Nat Cancer. 2021 May 1;2(5):487–97.

72. Parkhurst MR, Robbins PF, Tran E, Prickett TD, Gartner JJ, Li J, et al. Unique neoantigens arise from somatic mutations in patients with gastrointestinal cancers. Cancer Discov. 2019 Aug 1;9(8):1022–35.

73. Zacharakis N, Chinnasamy H, Black M, Xu H, Lu YC, Zheng Z, et al. Immune recognition of somatic mutations leading to complete durable regression in metastatic breast cancer. Nat Med. 2018 Jun 1;24(6):724–30.

74. Deniger DC, Pasetto A, Robbins PF, Gartner JJ, Prickett TD, Paria BC, et al. T-cell responses to TP53 "Hotspot" Mutations and unique neoantigens expressed by human ovarian cancers. Clinical Cancer Research. 2018 Nov 15;24(22):5562–73.

75. Malekzadeh P, Pasetto A, Robbins PF, Parkhurst MR, Paria BC, Jia L, et al. Neoantigen screening identifies broad TP53 mutant immunogenicity in patients with epithelial cancers. Journal of Clinical Investigation. 2019 Mar 1;129(3):1109–14.

76. Tran E, Robbins PF, Lu YC, Prickett TD, Gartner JJ, Jia L, et al. T-Cell Transfer Therapy Targeting Mutant KRAS in Cancer. New England Journal of Medicine. 2016 Dec 8;375(23):2255–62.

77. Bobisse S, Genolet R, Roberti A, Tanyi JL, Racle J, Stevenson BJ, et al. Sensitive and frequent identification of high avidity neo-epitope specific CD8 + T cells in immunotherapy-naive ovarian cancer. Nat Commun. 2018 Dec 1;9(1):1–10.

78. Chen DS, Mellman I. Oncology meets immunology: The cancer-immunity cycle. Immunity. 2013 Jul 25;39(1):1–10.

79. Cruz FM, Colbert JD, Merino E, Kriegsman BA, Rock KL. The biology and underlying mechanisms of cross-presentation of exogenous antigens on MHC-I molecules. Annu Rev Immunol. 2017 Apr 26;35:149–76.

80. Lenschow DJ, Walunas TL, Bluestone JA. CD28/B7 System of T cell costimulation. Annu Rev Immunol. 1996;14:233–58.

81. Rosenberg SA. IL-2: The First Effective Immunotherapy for Human Cancer. The Journal of Immunology. 2014 Jun 15;192(12):5451–8.

82. Anne Morgan D, Ruscetti FW, Gallo R, Proni JR, Newman Ronald L Sellers FC, Parker C, et al. Selective in vitro Growth of T Lymphocytes from Normal Human Bone Marrows. Science (1979) [Internet]. 1976;193(4257):1007–8. Available from: https://www.jstor.org/stable/1742642

83. Yang JC, Sherry RM, Steinberg SM, Topalian SL, Schwartzentruber DJ, Hwu P, et al. Randomized Study of High - Dose and Low - Dose Inter leukin - 2 in Patients With Metastatic Renal Cancer. J Clin Oncol. 2008;21(16):3127–32.

84. Rosenberg SA, Yang JC, Topalian SL, Schwartzentruber DJ, Weber JS, Parkinson DR, et al. Treatment of 283 Consecutive Patients With Metastatic Melanoma or Renal Cell Cancer Using High-Dose Bolus Interleukin 2. JAMA [Internet]. 1994 Mar 23;271(12):907–13. Available from: https://doi.org/10.1001/jama.1994.03510360033032

85. Mclane LM, Abdel-Hakeem MS, Wherry EJ. CD8 T Cell Exhaustion During Chronic Viral Infection and Cancer. Annu Rev Immunol [Internet]. 2019;37:457–95. Available from: https://doi.org/10.1146/annurev-immunol-041015-

86. Sharma P, Siddiqui BA, Anandhan S, Yadav SS, Subudhi SK, Gao J, et al. The next decade of immune checkpoint therapy. Cancer Discov. 2021;11(4):838–57.

87. Sharpe AH, Pauken KE. The diverse functions of the PD1 inhibitory pathway. Nat Rev Immunol. 2018 Mar 1;18(3):153–67.

88. Wei SC, Duffy CR, Allison JP. Fundamental mechanisms of immune checkpoint blockade therapy. Cancer Discov. 2018 Sep 1;8(9):1069–86.

89. Khair DO, Bax HJ, Mele S, Crescioli S, Pellizzari G, Khiabany A, et al. Combining immune checkpoint inhibitors: Established and emerging targets and strategies to improve outcomes in melanoma. Front Immunol. 2019;10(453).

90. Topp MS, Gökbuget N, Stein AS, Zugmaier G, O'Brien S, Bargou RC, et al. Safety and activity of blinatumomab for adult patients with relapsed or refractory B-precursor acute lymphoblastic leukaemia: A multicentre, single-arm, phase 2 study. Lancet Oncol. 2015 Jan 1;16(1):57–66.

91. Liang M. Oncorine, the World First Oncolytic Virus Medicine and its Update in China. Curr Cancer Drug Targets. 2018 Jan 17;18(2):171–6.

92. Boorjian SA, Alemozaffar M, Konety BR, Shore ND, Gomella LG, Kamat AM, et al. Intravesical nadofaragene firadenovec gene therapy for BCG-unresponsive non-muscle-invasive bladder cancer: a single-arm, open-label, repeat-dose clinical trial. Lancet Oncol. 2021 Jan 1;22(1):107–17.

93. Todo T, Ito H, Ino Y, Ohtsu H, Ota Y, Shibahara J, et al. Intratumoral oncolytic herpes virus G47Δ for residual or recurrent glioblastoma: a phase 2 trial. Nat Med. 2022 Aug 1;28(8):1630–9.

94. Doniņa S, Strele I, Proboka G, Auziņš J, Alberts P, Jonsson B, et al. Adapted ECHO-7 virus Rigvir immunotherapy (oncolytic virotherapy) prolongs survival in melanoma patients after surgical excision of the tumour in a retrospective study. Melanoma Res. 2015 Sep 18;25(5):421–6.

95. Andtbacka RHI, Kaufman HL, Collichio F, Amatruda T, Senzer N, Chesney J, et al. Talimogene laherparepvec improves durable response rate in patients with advanced melanoma. Journal of Clinical Oncology. 2015 Sep 1;33(25):2780–8.

96. Sugawara K, Iwai M, Ito H, Tanaka M, Seto Y, Todo T. Oncolytic herpes virus G47Δ works synergistically with CTLA-4 inhibition via dynamic intratumoral immune modulation. Mol Ther Oncolytics. 2021 Sep 24;22:129–42.

97. Smith HG, Mansfield D, Roulstone V, Kyula-Currie JN, McLaughlin M, Patel RR, et al. PD-1 blockade following isolated limb perfusion with vaccinia virus prevents local and distant relapse of soft-tissue sarcoma. Clinical Cancer Research. 2019 Jun 1;25(11):3443–54.

98. Park AK, Fong Y, Kim SI, Yang J, Murad JP, Lu J, et al. Effective combination immunotherapy using oncolytic viruses to deliver CAR targets to solid tumors. Sci Transl Med. 2020;12(559).

99. Tang X, Li Y, Ma J, Wang X, Zhao W, Hossain MA, et al. Adenovirus-mediated specific tumor tagging facilitates CAR-T therapy against antigen-mismatched solid tumors. Cancer Lett. 2020 Sep 1;487:1–9.

100. Blass E, Ott PA. Advances in the development of personalized neoantigen-based therapeutic cancer vaccines. Nat Rev Clin Oncol. 2021 Apr 1;18(4):215–29.

101. Tanyi JL, Bobisse S, Ophir E, Tuyaerts S, Roberti A, Genolet R, et al. Personalized cancer vaccine effectively mobilizes antitumor T cell immunity in ovarian cancer. Sci Transl Med [Internet]. 2018;10:5931. Available from: https://www.science.org

102. Schwartzentruber DJ, Lawson DH, Richards JM, Conry RM, Miller DM, Treisman J, et al. gp100 Peptide Vaccine and Interleukin-2 in Patients with Advanced Melanoma. New England Journal of Medicine. 2011 Jun 2;364(22):2119–27.

103. Karbach J, Neumann A, Atmaca A, Wahle C, Brand K, Von Boehmer L, et al. Efficient in vivo priming by vaccination with recombinant NY-ESO-1 protein and CpG in antigen naïve prostate cancer patients. Clinical Cancer Research. 2011 Feb 15;17(4):861–70.

104. Disis ML, Wallace DR, Gooley TA, Dang Y, Slota M, Lu H, et al. Concurrent trastuzumab and HER2/neu-specific vaccination in patients with metastatic breast cancer. Journal of Clinical Oncology. 2009 Oct 1;27(28):4685–92.

105. Svane IM, Pedersen AE, Johansen JS, Johnsen HE, Nielsen D, Kamby C, et al. Vaccination with p53 peptide-pulsed dendritic cells is associated with disease stabilization in patients with p53 expressing advanced breast cancer; monitoring of serum YKL-40 and IL-6 as response biomarkers. Cancer Immunology, Immunotherapy. 2007 Jul;56(9):1485–99.

106. Gardner TA, Elzey BD, Hahn NM. Sipuleucel-T (Provenge) autologous vaccine approved for treatment of men with asymptomatic or minimally symptomatic castrate-resistant metastatic prostate cancer. Hum Vaccin Immunother. 2012;8(4):534–9.

107. Pedersen SR, Sørensen MR, Buus S, Christensen JP, Thomsen AR. Comparison of Vaccine-Induced Effector CD8 T Cell Responses Directed against Self- and Non–Self-Tumor Antigens: Implications for Cancer Immunotherapy. The Journal of Immunology. 2013 Oct 1;191(7):3955–67.

108. Ott PA, Hu-Lieskovan S, Chmielowski B, Govindan R, Naing A, Bhardwaj N, et al. A Phase Ib Trial of Personalized Neoantigen Therapy Plus Anti-PD-1 in Patients with Advanced Melanoma, Non-small Cell Lung Cancer, or Bladder Cancer. Cell. 2020 Oct 15;183(2):347-362.e24.

109. Sahin U, Oehm P, Derhovanessian E, Jabulowsky RA, Vormehr M, Gold M, et al. An RNA vaccine drives immunity in checkpoint-inhibitor-treated melanoma. Nature. 2020 Sep 3;585(7823):107–12.

110. Rojas LA, Sethna Z, Soares KC, Olcese C, Pang N, Patterson E, et al. Personalized RNA neoantigen vaccines stimulate T cells in pancreatic cancer. Nature. 2023 Jun 1;618(7963):144–50.

111. Shemesh CS, Hsu JC, Hosseini I, Shen BQ, Rotte A, Twomey P, et al. Personalized Cancer Vaccines: Clinical Landscape, Challenges, and Opportunities. Molecular Therapy. 2021 Feb 3;29(2):555–70.

112. Steven A. Rosenberg, Beverly S. Packard, Paul D. Aebersold, Diane Solomon, Suzanne L. Topalian, Stephen T. Toy, et al. Use of Tumor-infiltrating lymphocytes and interleukin-2 in the immunotherapy of patients with metastatic melanoma. N Engl J Med. 1988;319(25):1676–80.

113. Rosenberg SA, Restifo NP. Adoptive cell transfer as personalized immunotherapy for human cancer. Science (1979). 2015 Apr 3;348(6230):62–8.

114. Kristensen NP, Heeke C, Tvingsholm SA, Borch A, Draghi A, Crowther MD, et al. Neoantigen-reactive CD8+ T cells affect clinical outcome of adoptive cell therapy with tumor-infiltrating lymphocytes in melanoma. Journal of Clinical Investigation. 2022 Jan 18;132(2):1–16.

115. Robbins PF, Lu YC, El-Gamil M, Li YF, Gross C, Gartner J, et al. Mining exomic sequencing data to identify mutated antigens recognized by adoptively transferred tumor-reactive T cells. Nat Med. 2013 Jun;19(6):747–52.

116. Lu YC, Yao X, Crystal JS, Li YF, El-Gamil M, Gross C, et al. Efficient identification of mutated cancer antigens recognized by T cells associated with durable tumor regressions. Clinical Cancer Research. 2014 Jul 1;20(13):3401–10.

117. Tran E, Turcotte S, Gros A, Robbins PF, Lu YC, Dudley ME, et al. Cancer immunotherapy based on mutation-specific CD4+ T cells in a patient with epithelial cancer. Science (1979). 2014;344(6184):641–5.

118. Chesney J, Lewis KD, Kluger H, Hamid O, Whitman E, Thomas S, et al. Efficacy and safety of lifileucel, a one-time autologous tumor-infiltrating lymphocyte (TIL) cell therapy, in patients with advanced melanoma after progression on immune checkpoint inhibitors and targeted therapies: Pooled analysis of consecutive cohorts of the C-144-01 study. J Immunother Cancer. 2022 Dec 13;10(12).

119. Monberg TJ, Borch TH, Svane IM, Donia M. TIL Therapy: Facts and Hopes. Clinical Cancer Research. 2023 Sep 1;29(17):3275–83.

120. Sterner RC, Sterner RM. CAR-T cell therapy: current limitations and potential strategies. Vol. 11, Blood Cancer Journal. Springer Nature; 2021.

121. Maus M V., June CH. Making better chimeric antigen receptors for adoptive T-cell therapy. Clinical Cancer Research. 2016 Apr 15;22(8):1875–84.

122. Fagerberg L, Jonasson K, Von Heijne G, Uhlén M, Berglund L. Prediction of the human membrane proteome. Proteomics. 2010 Mar;10(6):1141–9.

123. Thul PJ, Akesson L, Wiking M, Mahdessian D, Geladaki A, Ait Blal H, et al. A subcellular map of the human proteome. Science (1979). 2017 May 26;356(6340).

124. Kochenderfer JN, Yu Z, Frasheri D, Restifo NP, Rosenberg SA. Adoptive transfer of syngeneic T cells transduced with a chimeric antigen receptor that recognizes murine CD19 can eradicate lymphoma and normal B cells. Blood. 2010 Nov 11;116(19):3875–86.

125. Neelapu SS, Locke FL, Bartlett NL, Lekakis LJ, Miklos DB, Jacobson CA, et al. Axicabtagene Ciloleucel CAR T-Cell Therapy in Refractory Large B-Cell Lymphoma. New England Journal of Medicine. 2017 Dec 28;377(26):2531–44.

126. Schuster SJ, Svoboda J, Chong EA, Nasta SD, Mato AR, Anak Ö, et al. Chimeric Antigen Receptor T Cells in Refractory B-Cell Lymphomas. New England Journal of Medicine. 2017 Dec 28;377(26):2545–54.

127. Raje N, Berdeja J, Lin Y, Siegel D, Jagannath S, Madduri D, et al. Anti-BCMA CAR T-Cell Therapy bb2121 in Relapsed or Refractory Multiple Myeloma. New England Journal of Medicine. 2019 May 2;380(18):1726–37.

128. Smith EL, Staehr M, Masakayan R, Tatake IJ, Purdon TJ, Wang X, et al. Development and Evaluation of an Optimal Human Single-Chain Variable Fragment-Derived BCMA-Targeted CAR T Cell Vector. Molecular Therapy. 2018 Jun 6;26(6):1447–56.

129. Liu X, Jiang S, Fang C, Yang S, Olalere D, Pequignot EC, et al. Affinity-tuned ErbB2 or EGFR chimeric antigen receptor T cells exhibit an increased therapeutic index against tumors in mice. Cancer Res. 2015 Sep 1;75(17):3596–607.

130. Cole DK, Pumphrey NJ, Boulter JM, Sami M, Bell JI, Gostick E, et al. Human TCR-Binding Affinity is Governed by MHC Class Restriction. The Journal of Immunology. 2007 May 1;178(9):5727–34.

131. Watanabe K, Terakura S, Martens AC, van Meerten T, Uchiyama S, Imai M, et al. Target Antigen Density Governs the Efficacy of Anti–CD20-CD28-CD3 ζ Chimeric Antigen Receptor–Modified Effector CD8+ T Cells. The Journal of Immunology. 2015 Feb 1;194(3):911–20.

132. Walker AJ, Majzner RG, Zhang L, Wanhainen K, Long AH, Nguyen SM, et al. Tumor Antigen and Receptor Densities Regulate Efficacy of a Chimeric Antigen Receptor Targeting Anaplastic Lymphoma Kinase. Molecular Therapy. 2017 Sep 6;25(9):2189–201.

133. Huang J, Brameshuber M, Zeng X, Xie J, Li Q jing, Chien Y hsiu, et al. A Single peptide-major histocompatibility complex ligand triggers digital cytokine secretion in CD4+ T Cells. Immunity. 2013 Nov 14;39(5):846–57.

134. Christinick ER, Luscher MA, Barber BH, Williams DB. Peptide Binding to Class I MHC on Living Cells and Quantitation of Complexes Required for CTL Lysis. Nature Letters. 1991;352:67–70.

135. Morgan RA, Dudley ME, Wunderlich JR, Hughes MS, Yang JC, Sherry RM, et al. Cancer Regression in Patients After Transfer of Genetically Engineered Lymphocytes NIH Public Access. Science (1979) [Internet]. 2006;314(5796):126–9. Available from: www.sciencemag.org/cgi/content/full/1129003/DC1

136. Johnson LA, Morgan RA, Dudley ME, Cassard L, Yang JC, Hughes MS, et al. Gene therapy with human and mouse T-cell receptors mediates cancer regression and targets normal tissues expressing cognate antigen. Blood. 2009;114(3):535–46.

137. Moore T, Wagner CR, Scurti GM, Hutchens KA, Godellas C, Clark AL, et al. Clinical and immunologic evaluation of three metastatic melanoma patients treated with autologous melanoma-reactive TCR-transduced T cells. Cancer Immunology, Immunotherapy. 2018 Feb 1;67(2):311–25.

138. Parkhurst MR, Yang JC, Langan RC, Dudley ME, Nathan DAN, Feldman SA, et al. T cells targeting carcinoembryonic antigen can mediate regression of metastatic colorectal cancer but induce severe transient colitis. Molecular Therapy. 2011;19(3):620–6.

139. Tawara I, Kageyama S, Miyahara Y, Fujiwara H, Nishida T, Akatsuka Y, et al. Safety and persistence of WT1-specific T-cell receptor gene2transduced lymphocytes in patients with AML and MDS. Blood [Internet]. 2017;130(18):1985–94. Available from: www.umin.ac.jpas#UMIN000011519

140. Chapuis AG, Egan DN, Bar M, Schmitt TM, McAfee MS, Paulson KG, et al. T cell receptor gene therapy targeting WT1 prevents acute myeloid leukemia relapse post-transplant. Nat Med. 2019 Jul 1;25(7):1064–72.

141. Robbins PF, Kassim SH, Tran TLN, Crystal JS, Morgan RA, Feldman SA, et al. A pilot trial using lymphocytes genetically engineered with an NY-ESO-1-reactive T-cell receptor: Long-term follow-up and correlates with response. Clinical Cancer Research. 2015 Mar 1;21(5):1019–27.

142. D'angelo SP, Melchiori L, Merchant MS, Bernstein D, Glod J, Kaplan R, et al. Antitumor activity associated with prolonged persistence of adoptively transferred NY-ESO-1c259T cells in synovial sarcoma. Cancer Discov. 2018 Aug 1;8(8):944–57.

143. Morgan RA, Chinnasamy N, Abate-Daga D, Gros A, Robbins PF, Zheng Z, et al. Cancer regression and neurological toxicity following anti-MAGE-A3 TCR gene therapy. Journal of Immunotherapy. 2013 Feb;36(2):133–51.

144. Linette GP, Stadtmauer EA, Maus M V, Rapoport AP, Levine BL, Emery L, et al. Cardiovascular toxicity and titin cross-reactivity of affinity-enhanced T cells in myeloma and melanoma. Blood [Internet]. 2013;122(6):863–71. Available from: http://ashpublications.org/blood/article-pdf/122/6/863/1374971/863.pdf

145. Lu YC, Parker LL, Lu T, Zheng Z, Toomey MA, White DE, et al. JOURNAL OF CLINICAL ONCOLOGY Treatment of Patients With Metastatic Cancer Using a Major Histocompatibility Complex Class II-Restricted T-Cell Receptor Targeting the Cancer Germline Antigen MAGE-A3. J Clin Oncol [Internet]. 2017;35:3322–9. Available from: https://doi.org/10.1200/JCO.2017.

146. Kageyama S, Ikeda H, Miyahara Y, Imai N, Ishihara M, Saito K, et al. Adoptive transfer of MAGE-A4 T-cell receptor gene-transduced lymphocytes in patients with recurrent esophageal cancer. Clinical Cancer Research. 2015 May 15;21(10):2268–77.

147. Hong DS, Van Tine BA, Biswas S, McAlpine C, Johnson ML, Olszanski AJ, et al. Autologous T cell therapy for MAGE-A4+ solid cancers in HLA-A*02+ patients: a phase 1 trial. Nat Med. 2023 Jan 1;29(1):104–14.

148. Blumenschein GR, Devarakonda S, Johnson M, Moreno V, Gainor J, Edelman MJ, et al. Phase I clinical trial evaluating the safety and efficacy of ADP-A2M10 SPEAR T cells in patients with MAGE-A10+ advanced non-small cell lung cancer. J Immunother Cancer. 2022 Jan 27;10(1).

149. Doran SL, Stevanoví S, Adhikary S, Gartner JJ, Jia L, Li Kwong MM, et al. T-Cell Receptor Gene Therapy for Human Papillomavirus-Associated Epithelial Cancers: A First-in-Human, Phase I/II Study. J Clin Oncol [Internet]. 2019;37:2759–68. Available from: https://doi.

150. Nagarsheth NB, Norberg SM, Sinkoe AL, Adhikary S, Meyer TJ, Lack JB, et al. TCR-engineered T cells targeting E7 for patients with metastatic HPV-associated epithelial cancers. Nat Med. 2021 Mar 1;27(3):419–25.

151. Foy SP, Jacoby K, Bota DA, Hunter T, Pan Z, Stawiski E, et al. Non-viral precision T cell receptor replacement for personalized cell therapy. Nature. 2023 Mar 23;615(7953):687–96.

152. Leidner R, Sanjuan Silva N, Huang H, Sprott D, Zheng C, Shih YP, et al. Neoantigen T-Cell Receptor Gene Therapy in Pancreatic Cancer. New England Journal of Medicine. 2022 Jun 2;386(22):2112–9.

153. Kim SP, Vale NR, Zacharakis N, Krishna S, Yu Z, Gasmi B, et al. Adoptive Cellular Therapy with Autologous Tumor-Infiltrating Lymphocytes and T-cell Receptor- Engineered T Cells Targeting Common p53 Neoantigens in Human Solid Tumors. Cancer Immunol Res. 2022 Aug 1;10(8):932–46.

154. Vanhaver C, Gordon-Alonso M, Bayard A, Catanese MT, Colau D, van der Bruggen P, et al. Reverse immunology: From peptide sequence to tumor-killing human T-cell clones. In: Methods in Enzymology. Academic Press Inc.; 2020. p. 159–94.

155. Viatte S, Alves PM, Romero P. Reverse immunology approach for the identification of CD8 T-cell-defined antigens: Advantages and hurdles. Immunol Cell Biol. 2006 Jun;84(3):318–30.

156. Riley TP, Keller GLJ, Smith AR, Davancaze LM, Arbuiso AG, Devlin JR, et al. Structure based prediction of neoantigen immunogenicity. Front Immunol. 2019;10(2047).

157. Wells DK, van Buuren MM, Dang KK, Hubbard-Lucey VM, Sheehan KCF, Campbell KM, et al. Key Parameters of Tumor Epitope Immunogenicity Revealed Through a Consortium Approach Improve Neoantigen Prediction. Cell. 2020 Oct 29;183(3):818–34.

158. Schmidt J, Smith AR, Magnin M, Racle J, Devlin JR, Bobisse S, et al. Prediction of neo-epitope immunogenicity reveals TCR recognition determinants and provides insight into immunoediting. Cell Rep Med. 2021 Feb 16;2(2).

159. Saxová P, Buus S, Brunak S, Keşmir C. Predicting proteasomal cleavage sites: A comparison of available methods. Int Immunol. 2003 Jul 1;15(7):781–7.

160. Mei S, Li F, Leier A, Marquez-Lago TT, Giam K, Croft NP, et al. A comprehensive review and performance evaluation of bioinformatics tools for HLA class I peptide-binding prediction. Brief Bioinform. 2019 Jul 10;21(4):1119–35.

161. Reynisson B, Alvarez B, Paul S, Peters B, Nielsen M. NetMHCpan-4.1 and NetMHCIIpan-4.0: Improved predictions of MHC antigen presentation by concurrent motif deconvolution and integration of MS MHC eluted ligand data. Nucleic Acids Res. 2021;48(W1):W449–54.

162. Becker JP, Helm D, Rettel M, Stein F, Hernandez-Sanchez A, Urban K, et al. NMD inhibition by 5-azacytidine augments presentation of immunogenic frameshift-derived neoepitopes. iScience CellPress. 2021 Apr 23;24(4).

163. Bonsack M, Hoppe S, Winter J, Tichy D, Zeller C, Kupper MD, et al. Performance evaluation of MHC class-I binding prediction tools based on an experimentally validated MHC–peptide binding data set. Cancer Immunol Res. 2019 May 1;7(5):719–36.

164. Tubb VM, Schrikkema DS, Croft NP, Purcell AW, Linnemann C, Freriks MR, et al. Isolation of T cell receptors targeting recurrent neoantigens in hematological malignancies. J Immunother Cancer. 2018 Jul 13;6(1).

165. Chen F, Zou Z, Du J, Su S, Shao J, Meng F, et al. Neoantigen identification strategies enable personalized immunotherapy in refractory solid tumors. Journal of Clinical Investigation. 2019 May 1;129(5):2056–70.

166. Chheda ZS, Kohanbash G, Okada K, Jahan N, Sidney J, Pecoraro M, et al. Novel and shared neoantigen derived from histone 3 variant H3.3K27M mutation for glioma T cell therapy. Journal of Experimental Medicine. 2018 Jan 1;215(1):141–57.

167. Nielsen JS, Sedgwick CG, Shahid A, Zong Z, Brumme ZL, Yu S, et al. Toward Personalized Lymphoma Immunotherapy: Identification of Common Driver Mutations Recognized by Patient CD8+ T Cells. Clinical Cancer Research. 2016 May 1;22(9):2226–36.

168. Freudenmann LK, Marcu A, Stevanović S. Mapping the tumour human leukocyte antigen (HLA) ligandome by mass spectrometry. Immunology. 2018 Jul 1;154(3):331–45.

169. Cox AL, Skipper J, Chen Y, Henderson RA, Darrow TL, Shabanowitz J, et al. Identification of a Peptide Recognized by Five Melanoma-Specific Human Cytotoxic T Cell Lines. Source: Science. 1994;264(5159).

170. Bassani-Sternberg M, Bräunlein E, Klar R, Engleitner T, Sinitcyn P, Audehm S, et al. Direct identification of clinically relevant neoepitopes presented on native human melanoma tissue by mass spectrometry. Nat Commun. 2016 Nov 21;7.

171. Kalaora S, Barnea E, Merhavi-Shoham E, Qutob N, Teer JK, Shimony N, et al. Use of HLA peptidomics and whole exome sequencing to identify human immunogenic neo-antigens. Oncotarget [Internet]. 2016;7(5):5110–7. Available from: www.impactjournals.com/oncotarget

172. Newey A, Griffiths B, Michaux J, Pak HS, Stevenson BJ, Woolston A, et al. Immunopeptidomics of colorectal cancer organoids reveals a sparse HLA class i neoantigen landscape and no increase in neoantigens with interferon or MEK-inhibitor treatment. J Immunother Cancer. 2019 Nov 18;7(1).

173. Bruno PM, Timms RT, Abdelfattah NS, Leng Y, Lelis FJN, Wesemann DR, et al. High-throughput, targeted MHC class I immunopeptidomics using a functional genetics screening platform. Nat Biotechnol. 2023 Jul 1;41(7):980–92.

174. Kalaora S, Wolf Y, Feferman T, Barnea E, Greenstein E, Reshef D, et al. Combined analysis of antigen presentation and T-cell recognition reveals restricted immune responses in melanoma. Cancer Discov. 2018 Nov 1;8(11):1366–75.

175. Van Der Lee DI, Reijmers RM, Honders MW, Hagedoorn RS, De Jong RCM, Kester MGD, et al. Mutated nucleophosmin 1 as immunotherapy target in acute myeloid leukemia. Journal of Clinical Investigation. 2019 Feb 1;129(2):774–85.

176. Abelin JG, Keskin DB, Sarkizova S, Hartigan CR, Zhang W, Sidney J, et al. Mass Spectrometry Profiling of HLA-Associated Peptidomes in Mono-allelic Cells Enables More Accurate Epitope Prediction. Immunity. 2017 Feb 21;46(2):315–26.

177. Sarkizova S, Klaeger S, Le PM, Li LW, Oliveira G, Keshishian H, et al. A large peptidome dataset improves HLA class I epitope prediction across most of the human population. Nat Biotechnol. 2020 Feb 1;38(2):199–209.

178. Choi J, Goulding SP, Conn BP, McGann CD, Dietze JL, Kohler J, et al. Systematic discovery and validation of T cell targets directed against oncogenic KRAS mutations. Cell Reports Methods. 2021 Sep 27;1(5).

179. Bear AS, Blanchard T, Cesare J, Ford MJ, Richman LP, Xu C, et al. Biochemical and functional characterization of mutant KRAS epitopes validates this oncoprotein for immunological targeting. Nat Commun. 2021 Dec 1;12(1).

180. Ade CM, Sporn MJ, Das S, Yu Z, Hanada KI, Qi YA, et al. Identification of neoepitope reactive T-cell receptors guided by HLA-A∗03:01 and HLA-A∗11:01 immunopeptidomics. J Immunother Cancer. 2023 Sep 27;11(9).

181. Gurung HR, Heidersbach AJ, Darwish M, Chan PPF, Li J, Beresini M, et al. Systematic discovery of neoepitope–HLA pairs for neoantigens shared among patients and tumor types. Nat Biotechnol. 2023;42(7):1107–17.

182. Wang Q, Douglass J, Hwang MS, Hsiue EHC, Mog BJ, Zhang M, et al. Direct detection and quantification of neoantigens. Cancer Immunol Res. 2019;7(11):1748–54.

183. Wang QJ, Yu Z, Griffith K, Hanada KI, Restifo NP, Yang JC. Identification of T-cell receptors targeting KRAS-mutated human tumors. Cancer Immunol Res. 2016 Mar 1;4(3):204–14.

184. Davis JL, Theoret MR, Zheng Z, Lamers CHJ, Rosenberg SA, Morgan RA. Development of human anti-murine T-cell receptor antibodies in both responding and nonresponding patients enrolled in TCR gene therapy trials. Clinical Cancer Research. 2010 Dec 1;16(23):5852–61.

185. Li LP, Lampert JC, Chen X, Leitao C, Popović J, Müller W, et al. Transgenic mice with a diverse human T cell antigen receptor repertoire. Nat Med. 2010 Sep;16(9):1029–34.

186. Moore MJ, Zhong M, Hansen J, Gartner H, Grant C, Huang M, et al. Humanization of T cell-mediated immunity in mice. Sci Immunol [Internet]. 2021;6:4026. Available from: https://www.science.org

187. Obenaus M, Leitão C, Leisegang M, Chen X, Gavvovidis I, Van Der Bruggen P, et al. Identification of human T-cell receptors with optimal affinity to cancer antigens using antigen-negative humanized mice. Nat Biotechnol. 2015 Apr 1;33(4):402–7.

188. Poncette L, Chen X, Lorenz FKM, Blankenstein T. Effective NY-ESO-1-specific MHC II-restricted T cell receptors from antigen-negative hosts enhance tumor regression. Journal of Clinical Investigation. 2019 Jan 2;129(1).

189. Creelan BC, Wang C, Teer JK, Toloza EM, Yao J, Kim S, et al. Tumor-infiltrating lymphocyte treatment for anti-PD-1-resistant metastatic lung cancer: a phase 1 trial. Nat Med. 2021 Aug 1;27(8):1410–8.

190. Stevanović S, Pasetto A, Helman SR, Gartner JJ, Prickett TD, Howie B, et al. Landscape of immunogenic tumor antigens in successful immunotherapy of virally induced epithelial cancer. Science (1979). 2017;356(6334):200–5.

191. Tran E, Ahmadzadeh M, Lu YC, Gros A, Turcotte S, Robbins PF, et al. Immunogenicity of somatic mutations in human gastrointestinal cancers. Science (1979). 2015 Dec 11;350(6266):1387–90.

192. Strønen E, Toebes M, Kelderman S, Van Buuren MM, Yang W, Van Rooij N, et al. Targeting of cancer neoantigens with donor-derived T cell receptor repertoires. Science (1979). 2016 Jun 10;352(6291):1337–41.

193. Pasetto A, Gros A, Robbins PF, Deniger DC, Prickett TD, Matus-Nicodemos R, et al. Tumor- and neoantigen-reactive T-cell receptors can be identified based on their frequency in fresh tumor. Cancer Immunol Res. 2016 Sep 1;4(9):734–43.

194. Gros A, Robbins PF, Yao X, Li YF, Turcotte S, Tran E, et al. PD-1 identifies the patient-specific CD8+ tumor-reactive repertoire infiltrating human tumors. Journal of Clinical Investigation. 2014;124(5):2246–59.

195. Inozume T, Hanada KI, Wang QJ, Ahmadzadeh M, Wunderlich JR, Rosenberg SA, et al. Selection of CD8++PD-1+ lymphocytes in fresh human melanomas enriches for tumor-reactive T cells. Journal of Immunotherapy. 2010 Nov;33(9):956–64.

196. Palomero J, Panisello C, Lozano-Rabella M, Tirtakasuma R, Díaz-Gómez J, Grases D, et al. Biomarkers of tumor-reactive CD4 + and CD8 + TILs associate with improved prognosis in endometrial cancer. J Immunother Cancer. 2022 Dec 29;10(12).

197. Duhen T, Duhen R, Montler R, Moses J, Moudgil T, De Miranda NF, et al. Co-expression of CD39 and CD103 identifies tumor-reactive CD8 T cells in human solid tumors. Nat Commun. 2018 Dec 1;9(1).

198. Gros A, Parkhurst MR, Tran E, Pasetto A, Robbins PF, Ilyas S, et al. Prospective identification of neoantigen-specific lymphocytes in the peripheral blood of melanoma patients. Nat Med. 2016 Apr 1;22(4):433–8.

199. Gros A, Tran E, Parkhurst MR, Ilyas S, Pasetto A, Groh EM, et al. Recognition of human gastrointestinal cancer neoantigens by circulating PD-1+ lymphocytes. Journal of Clinical Investigation. 2019 Nov 1;129(11):4992–5004.

200. Dolton G, Lissina A, Skowera A, Ladell K, Tungatt K, Jones E, et al. Comparison of peptide-major histocompatibility complex tetramers and dextramers for the identification of antigen-specific T cells. Clin Exp Immunol. 2014 Jul;177(1):47–63.

201. Rodenko B, Toebes M, Hadrup SR, van Esch WJE, Molenaar AM, Schumacher TNM, et al. Generation of peptide-MHC class I complexes through UV-mediated ligand exchange. Nat Protoc. 2006 Aug;1(3):1120–32.

202. Luimstra JJ, Garstka MA, Roex MCJ, Redeker A, Janssen GMC, van Veelen PA, et al. A flexible MHC class I multimer loading system for large-scale detection of antigen-specific T cells. Journal of Experimental Medicine. 2018 May 1;215(5):1493–504.

203. Saini SK, Tamhane T, Anjanappa R, Saikia A, Ramskov S, Donia M, et al. Empty peptide-receptive MHC class I molecules for efficient detection of antigen-specific T cells. Sci Immunol [Internet]. 2019;4:9039. Available from: https://www.science.org

204. Newell EW, Klein LO, Yu W, Davis MM. Simultaneous detection of many T-cell specificities using combinatorial tetramer staining. Nat Methods. 2009;6(7):497–9.

205. Hadrup SR, Bakker AH, Shu CJ, Andersen RS, van Veluw J, Hombrink P, et al. Parallel detection of antigen-specific T-cell responses by multidimensional encoding of MHC multimers. Nat Methods. 2009;6(7):520–6.

206. Perumal D, Imai N, Lagana A, Finnigan J, Melnekoff D, Leshchenko V V., et al. Mutation-derived Neoantigen-specific T-cell Responses in Multiple Myeloma. Clinical Cancer Research. 2020 Jan 15;26(2):450–64.

207. Cohen CJ, Gartner JJ, Horovitz-Fried M, Shamalov K, Trebska-McGowan K, Bliskovsky V V., et al. Isolation of neoantigen-specific T cells from tumor and peripheral lymphocytes. Journal of Clinical Investigation. 2015 Oct 1;125(10):3981–91.

208. Bentzen AK, Marquard AM, Lyngaa R, Saini SK, Ramskov S, Donia M, et al. Large-scale detection of antigen-specific T cells using peptide-MHC-I multimers labeled with DNA barcodes. Nat Biotechnol. 2016 Oct 1;34(10):1037–45.

209. Zhang SQ, Ma KY, Schonnesen AA, Zhang M, He C, Sun E, et al. High-throughput determination of the antigen specificities of T cell receptors in single cells. Nat Biotechnol. 2018 Dec 1;36(12):1156–9.

210. Wölfl M, Merker K, Morbach H, Van Gool SW, Eyrich M, Greenberg PD, et al. Primed tumor-reactive multifunctional CD62L+ human CD8 + T cells for immunotherapy. Cancer Immunology, Immunotherapy. 2011 Feb;60(2):173–86.

211. Cafri G, Yossef R, Pasetto A, Deniger DC, Lu YC, Parkhurst M, et al. Memory T cells targeting oncogenic mutations detected in peripheral blood of epithelial cancer patients. Nat Commun. 2019 Dec 1;10(1).

212. Herin' M, Lemoine' C, Weynants' P, Vessiere' F, Van Pel' A, Knljth~ A, et al. Production of stable cytolytic T-cell clones directed against autologous human melanoma. Int J Cancer. 1987;39(3):390–6.

213. Ali M, Foldvari Z, Giannakopoulou E, Böschen ML, Strønen E, Yang W, et al. Induction of neoantigen-reactive T cells from healthy donors. Nat Protoc. 2019 Jun 1;14(6):1926–43.

214. Lissina A, Briceño O, Afonso G, Larsen M, Gostick E, Price DA, et al. Priming of Qualitatively Superior Human Effector CD8+ T Cells Using TLR8 Ligand Combined with FLT3 Ligand. The Journal of Immunology. 2016 Jan 1;196(1):256–63.

215. Maus M V, Thomas AK, Leonard DGB, Allman D, Addya K, Schlienger K, et al. Ex vivo expansion of polyclonal and antigen-specific cytotoxic T lymphocytes by artificial APCs expressing ligands for the T-cell receptor, CD28 and 4-1BB. Nat Biotechnol [Internet]. 2002;20(2):143–8. Available from: http://biotech.nature.com

216. Arnaud M, Chiffelle J, Genolet R, Navarro Rodrigo B, Perez MAS, Huber F, et al. Sensitive identification of neoantigens and cognate TCRs in human solid tumors. Nat Biotechnol. 2022 May 1;40(5):656–60.

217. Wang S, Zhang X, Zou X, Wen M, Gan C, Jiang X, et al. Expansion of KRAS hotspot mutations reactive T cells from human pancreatic tumors using autologous T cells as the antigen-presenting cells. Cancer Immunology, Immunotherapy. 2023 May 1;72(5):1301–13.

218. Hoyos D, Zappasodi R, Schulze I, Sethna Z, de Andrade KC, Bajorin DF, et al. Fundamental immune–oncogenicity trade-offs define driver mutation fitness. Nature. 2022 Jun 2;606(7912):172–9.

219. Chevalier MF, Bobisse S, Costa-Nunes C, Cesson V, Jichlinski P, Speiser DE, et al. High-throughput monitoring of human tumor-specific T-cell responses with large peptide pools. Oncoimmunology. 2015 Oct 3;4(10).

220. Bethune MT, Li XH, Yu J, McLaughlin J, Cheng D, Mathis C, et al. Isolation and characterization of NY-ESO-1-specific T cell receptors restricted on various MHC molecules. PNAS. 2018 Nov 6;115(45):E10702–11.

221. Gerdemann U, Katari U, Christin AS, Cruz CR, Tripic T, Rousseau A, et al. Cytotoxic T lymphocytes simultaneously targeting multiple tumor-associated antigens to treat ebv negative lymphoma. Molecular Therapy. 2011;19(12):2258–68.

222. Fossum B, Gedde-dahl Iiii T, Breivik J, Amund ERIK SEN J, Spurkland A, Thorsby E. p21-ras-PEPTIDE-SPECIFIC T-CELL RESPONSES IN A PATIENT WITH COLORECTAL CANCER. CD4+ AND CD8+ T CELLS RECOGNIZE A PEPTIDE CORRESPONDING TO A COMMON MUTATION (13Gly+Asp). Int J Cancer. 1994;56:40–5.

223. Chandran SS, Ma J, Klatt MG, Dündar F, Bandlamudi C, Razavi P, et al. Immunogenicity and therapeutic targeting of a public neoantigen derived from mutated PIK3CA. Nat Med. 2022 May 1;28(5):946–57.

224. Malekzadeh P, Yossef R, Cafri G, Paria BC, Lowery FJ, Jafferji M, et al. Antigen experienced T cells from peripheral blood recognize p53 neoantigens. Clinical Cancer Research. 2020 Mar 15;26(6):1267–76.

225. Levin N, Kim SP, Marquardt CA, Vale NR, Yu Z, Sindiri S, et al. Neoantigen-specific stimulation of tumor-infiltrating lymphocytes enables effective TCR isolation and expansion while preserving stem-like memory phenotypes. J Immunother Cancer. 2024 May 30;12(5).

226. Li Y, Bleakley M, Yee C. IL-21 Influences the Frequency, Phenotype, and Affinity of the Antigen-Specific CD8 T Cell Response 1. The Journal of Immunology [Internet]. 2005;175:2261–9. Available from: http://journals.aai.org/jimmunol/article-pdf/175/4/2261/1206651/2261.pdf

227. Murphy K& WC. The Generation of Lymphocyte Antigen Receptors. In: Immunobiology Janeway's. 9th ed. 2017. p. 187–91.

228. Howie B, Sherwood AM, Berkebile AD, Berka J, Emerson RO, Williamson DW, et al. High-throughput pairing of T cell receptor α and β sequences. Sci Transl Med [Internet]. 2015;7(301). Available from: www.ScienceTranslationalMedicine.org

229. Mcdaniel JR, DeKosky BJ, Tanno H, Ellington AD, Georgiou G. Ultra-high-throughput sequencing of the immune receptor repertoire from millions of lymphocytes. Nat Protoc. 2016 Mar 1;11(3):429–42.

230. Spindler MJ, Nelson AL, Wagner EK, Oppermans N, Bridgeman JS, Heather JM, et al. Massively parallel interrogation and mining of natively paired human TCRαβ repertoires. Nat Biotechnol. 2020 May 1;38(5):609–19.

231. Peri A, Greenstein E, Alon M, Pai JA, Dingjan T, Reich-Zeliger S, et al. Combined presentation and immunogenicity analysis reveals a recurrent RAS.Q61K neoantigen in melanoma. Journal of Clinical Investigation. 2021;131(20).

232. Fast E, Dhar M, Chen B. TAPIR: a T-cell receptor language model for predicting rare and novel targets. BioRxiv [Internet]. 2023; Available from: https://doi.org/10.1101/2023.09.12.557285

233. Croce G, Bobisse S, Moreno DL, Schmidt J, Guillame P, Harari A, et al. Deep learning predictions of TCR-epitope interactions reveal epitope-specific chains in dual alpha T cells. Nat Commun. 2024 Dec 1;15(1).

234. Chandran SS, Klebanoff CA. T cell receptor-based cancer immunotherapy: Emerging efficacy and pathways of resistance. Immunol Rev. 2019 Jul 1;290(1):127–47.

235. Klebanoff CA, Chandran SS, Baker BM, Quezada SA, Ribas A. T cell receptor therapeutics: immunological targeting of the intracellular cancer proteome. Nat Rev Drug Discov. 2023 Dec 1;22(12):996–1017.

236. Nauerth M, Weißbrich B, Knall R, Franz T, Dössinger G, Bet J, et al. TCR-ligand koff rate correlates with the protective capacity of antigen-specific CD8+ T cells for adoptive transfer. Sci Transl Med. 2013 Jul 3;5(192).

237. Allard M, Couturaud B, Carretero-Iglesia L, Duong MN, Schmidt J, Monnot GC, et al. TCR-ligand dissociation rate is a robust and stable biomarker of CD8+ T cell potency. JCI Insight. 2017 Jul 20;2(14).

238. Huang J, Zarnitsyna VI, Liu B, Edwards LJ, Jiang N, Evavold BD, et al. The kinetics of two-dimensional TCR and pMHC interactions determine T-cell responsiveness. Nature. 2010 Apr 8;464(7290):932–6.

239. Margulies DH, Plaksin D, Khilko SN, Jelonek MT. Studying interactions involving the T-cell antigen receptor by surface plasmon resonance. Curr Opin Immunol. 1996;8:262–70.

240. Border EC, Sanderson JP, Weissensteiner T, Gerry AB, Pumphrey NJ. Affinity-enhanced T-cell receptors for adoptive T-cell therapy targeting MAGE-A10: strategy for selection of an optimal candidate. Oncoimmunology. 2019 Feb 1;8(2).

241. Cameron BJ, Gerry AB, Dukes J, Harper J V., Kannan V, Bianchi FC, et al. Identification of a titin-derived HLA-A1-presented peptide as a cross-reactive target for engineered MAGE A3-directed T cells. Sci Transl Med. 2013 Aug 7;5(197).

242. Birnbaum ME, Mendoza JL, Sethi DK, Dong S, Glanville J, Dobbins J, et al. Deconstructing the peptide-MHC specificity of t cell recognition. Cell. 2014 May 22;157(5):1073–87.

243. Levin N, Paria BC, Vale NR, Yossef R, Lowery FJ, Parkhurst MR, et al. Identification and validation of T-cell receptors targeting RAS hotspot mutations in human cancers for use in cell-based immunotherapy. Clinical Cancer Research. 2021 Sep 15;27(18).

244. Rive CM, Yung E, Hughes CS, Brown SD, Sharma G, Dreolini L, et al. Recombinant T cell receptors specific for HLA-A*02:01-restricted neoepitopes containing KRAS codon 12 hotspot mutations. BioRxiv [Internet]. 2020; Available from: https://doi.org/10.1101/2020.06.15.149021

245. Lo W, Parkhurst M, Robbins PF, Tran E, Lu YC, Jia L, et al. Immunologic recognition of a shared p53 mutated neoantigen in a patient with metastatic colorectal cancer. Cancer Immunol Res. 2019 Apr 1;7(4):534–43.

246. Matthias Leisegang, Thomas Kammertoens, Wolfgang Uckert, Thomas Blankenstein. Targeting human melanoma neoantigens by T cell receptor gene therapy. J Clin Invest [Internet]. 2016;126:854–8. Available from: http://www.cbs.dtu.dk/services/NetMHC/

247. Inderberg EM, Wälchli S, Myhre MR, Trachsel S, Almåsbak H, Kvalheim G, et al. T cell therapy targeting a public neoantigen in microsatellite instable colon cancer reduces in vivo tumor growth. Oncoimmunology. 2017 Apr 3;6(4).

248. Linard B, Bézieau S, Benlalam H, Labarrière N, Guilloux Y, Diez E, et al. A ras-Mutated Peptide Targeted by CTL Infiltrating a Human Melanoma Lesion . The Journal of Immunology. 2002 May 1;168(9):4802–8.

249. Somasundaram R, Swoboda R, Caputo L, Otvos L, Weber B, Volpe P, et al. Human leukocyte antigen-A2-restricted CTL responses to mutated BRAF peptides in melanoma patients. Cancer Res. 2006 Mar 15;66(6):3287–93.

250. Andersen MH, Fensterle J, Ugurel S, Reker S, Houben R, Guldberg P, et al. Immunogenicity of Constitutively Active V599E BRaf. Cancer Res [Internet]. 2004;64:5456–60. Available from: http://www.mpiib-berlin.mpg.de/MAPPP/.

251. Lu D, Chen Y, Jiang M, Wang J, Li Y, Ma K, et al. KRAS G12V neoantigen specific T cell receptor for adoptive T cell therapy against tumors. Nat Commun. 2023 Dec 1;14(1).

252. Douglass J, Hsiue EHC, Mog BJ, Hwang MS, DiNapoli SR, Pearlman AH, et al. Bispecific antibodies targeting mutant RAS neoantigens. Sci Immunol. 2021 Mar 25;6(57).

253. Iizumi S, Ohtake J, Murakami N, Kouro T, Kawahara M, Isoda F, et al. Identification of novel HLA class II-restricted neoantigens derived from driver mutations. Cancers (Basel). 2019 Feb 1;11(2).

254. Veatch JR, Jesernig BL, Kargl J, Fitzgibbon M, Lee SM, Baik C, et al. Endogenous CD4+ T cells recognize neoantigens in lung cancer patients, including recurrent oncogenic KRAS and ERBB2 (Her2) driver mutations. Cancer Immunol Res. 2019 Jun 1;7(6):910–22.

255. Yossef R, Tran E, Deniger DC, Gros A, Pasetto A, Parkhurst MR, et al. Enhanced detection of neoantigen-reactive T cells targeting unique and shared oncogenes for personalized cancer immunotherapy. JCI Insight. 2018 Oct 4;3(19).

256. Veatch JR, Lee SM, Fitzgibbon M, Chow IT, Jesernig B, Schmitt T, et al. Tumor-infiltrating BRAFV600E-specific CD4+ T cells correlated with complete clinical response in melanoma. Journal of Clinical Investigation. 2018 Apr 2;128(4):1563–8.

257. Platten M, Bunse L, Wick A, Bunse T, Le Cornet L, Harting I, et al. A vaccine targeting mutant IDH1 in newly diagnosed glioma. Nature. 2021 Apr 15;592(7854):463–8.

258. Martínez-Jiménez F, Muiños F, Sentís I, Deu-Pons J, Reyes-Salazar I, Arnedo-Pac C, et al. A compendium of mutational cancer driver genes. Nat Rev Cancer. 2020 Oct 1;20(10):555–72.

259. Castle JC, Uduman M, Pabla S, Stein RB, Buell JS. Mutation-derived neoantigens for cancer immunotherapy. Front Immunol. 2019;10(1856).

260. Bailey MH, Tokheim C, Porta-Pardo E, Sengupta S, Bertrand D, Weerasinghe A, et al. Comprehensive Characterization of Cancer Driver Genes and Mutations. Cell. 2018 Apr 5;173(2):371-385.e18.

261. Toshitanit K, Braudt V, Browningt MJ, Murrayt N, Mcmichaelt AJ, Bodmertl WF. Expression of a single-chain HLA class I molecule in a human cell line: Presentation of exogenous peptide and processed antigen to cytotoxic T lymphocytes. Immunology. 1996;93:236–40.

262. Chong C, Marino F, Pak H, Racle J, Daniel RT, Mü Ller M, et al. High-throughput and sensitive immunopeptidomics platform reveals profound interferon γ-mediated remodeling of the human leukocyte antigen (HLA) ligandome. Molecular and Cellular Proteomics. 2018 Mar 1;17(3):533–48.

263. Cohen CJ, Zhao Y, Zheng Z, Rosenberg SA, Morgan RA. Enhanced antitumor activity of murine-human hybrid T-cell receptor (TCR) in human lymphocytes is associated with improved pairing and TCR/CD3 stability. Cancer Res. 2006 Sep 1;66(17):8878–86.

264. Cohen CJ, Li YF, El-Gamil M, Robbins PF, Rosenberg SA, Morgan RA. Enhanced Antitumor Activity of T Cells Engineered to Express T-Cell Receptors with a Second Disulfide Bond. Cancer Res. 2007;67(8):3898–903.

265. Haga-Friedman A, Horovitz-Fried M, Cohen CJ. Incorporation of Transmembrane Hydrophobic Mutations in the TCR Enhance Its Surface Expression and T Cell Functional Avidity. The Journal of Immunology. 2012 Jun 1;188(11):5538–46.

266. Chang MT, Bhattarai TS, Schram AM, Bielski CM, Donoghue MTA, Jonsson P, et al. Accelerating discovery of functional mutant alleles in cancer. Cancer Discov. 2018 Feb 1;8(2):174–83.

267. Chang MT, Asthana S, Gao SP, Lee BH, Chapman JS, Kandoth C, et al. Identifying recurrent mutations in cancer reveals widespread lineage diversity and mutational specificity. Nat Biotechnol. 2016 Feb 1;34(2):155–63.

268. Garrido F, Ruiz-Cabello F, Cabrera T, Perez-Villar JJ, L6pez-Botet M, Duggan-Keen M, et al. Implications for immunosurveillance of altered HLA class I phenotypes in human tumours. Immunol Today. 1997;18(2):89–95.

269. Sahin U, Derhovanessian E, Miller M, Kloke BP, Simon P, Löwer M, et al. Personalized RNA mutanome vaccines mobilize poly-specific therapeutic immunity against cancer. Nature. 2017 Jul 13;547(7662):222–6.

270. Müller M, Gfeller D, Coukos G, Bassani-Sternberg M. "Hotspots" of antigen presentation revealed by human leukocyte antigen ligandomics for neoantigen prioritization. Front Immunol. 2017 Oct 20;8(1367).

271. Pearson H, Daouda T, Granados DP, Durette C, Bonneil E, Courcelles M, et al. MHC class I-associated peptides derive from selective regions of the human genome. Journal of Clinical Investigation. 2016 Dec 1;126(12):4690–701.

272. Bassani-Sternberg M, Pletscher-Frankild S, Jensen LJ, Mann M. Mass spectrometry of human leukocyte antigen class i peptidomes reveals strong effects of protein abundance and turnover on antigen presentation. Molecular and Cellular Proteomics. 2015 Mar 1;14(3):658–73.

273. Zhang W, Hawkins PG, He J, Gupta NT, Liu J, Choonoo G, et al. A framework for highly multiplexed dextramer mapping and prediction of T cell receptor sequences to antigen specificity. Sci Adv. 2021;7:5835–49.

274. Lanoix J, Durette C, Courcelles M, Cossette É, Comtois-Marotte S, Hardy MP, et al. Comparison of the MHC I Immunopeptidome Repertoire of B-Cell Lymphoblasts Using Two Isolation Methods. Proteomics. 2018 Jun 1;18(12).

275. Hassan C, Kester MGD, De Ru AH, Hombrink P, Drijfhout JW, Nijveen H, et al. The human leukocyte antigen-presented ligandome of B lymphocytes. Molecular and Cellular Proteomics. 2013;12(7):1829–43.

276. Marino F, Semilietof A, Michaux J, Pak HS, Coukos G, Müller M, et al. Biogenesis of HLA Ligand Presentation in Immune Cells Upon Activation Reveals Changes in Peptide Length Preference. Front Immunol. 2020 Aug 28;11.

277. Bassani-Sternberg M, Gfeller D. Unsupervised HLA Peptidome Deconvolution Improves Ligand Prediction Accuracy and Predicts Cooperative Effects in Peptide–HLA Interactions. The Journal of Immunology. 2016 Sep 15;197(6):2492–9.

278. Bassani-Sternberg M, Chong C, Guillaume P, Solleder M, Pak HS, Gannon PO, et al. Deciphering HLA-I motifs across HLA peptidomes improves neo-antigen predictions and identifies allostery regulating HLA specificity. PLoS Comput Biol. 2017 Aug 1;13(8):e1005725.

279. Rasmussen M, Harndahl M, Stryhn A, Boucherma R, Nielsen LL, Lemonnier FA, et al. Uncovering the Peptide-Binding Specificities of HLA-C: A General Strategy To Determine the Specificity of Any MHC Class I Molecule. The Journal of Immunology. 2014 Nov 15;193(10):4790–802.

280. Kaur G, Gras S, Mobbs JI, Vivian JP, Cortes A, Barber T, et al. Structural and regulatory diversity shape HLA-C protein expression levels. Nat Commun. 2017 Jun 26;8.

281. Bettens F, Ongen H, Rey G, Buhler S, Sollet ZC, Dermitzakis E, et al. Regulation of HLA class I expression by non-coding gene variations. PLoS Genet. 2022 Jun 6;18(6).

282. Apps R, Meng Z, Del Prete GQ, Lifson JD, Zhou M, Carrington M. Relative Expression Levels of the HLA Class-I Proteins in Normal and HIV-Infected Cells. The Journal of Immunology. 2015 Apr 15;194(8):3594–600.

283. Pyke RM, Mellacheruvu D, Dea S, Abbott CW, Zhang S V., Phillips NA, et al. Precision neoantigen discovery using large-scale immunopeptidomes and composite modeling of MHC peptide presentation. Molecular and Cellular Proteomics. 2021 Jun 1;20.

284. Abelin JG, Harjanto D, Malloy M, Suri P, Colson T, Goulding SP, et al. Defining HLA-II Ligand Processing and Binding Rules with Mass Spectrometry Enhances Cancer Epitope Prediction. Immunity. 2019 Oct 15;51(4):766-779.e17.

285. Lee L, Loftus D, Appella E, Margulies DH, Mage M. A Recombinant Single-Chain HLA-A2.1 Molecule, with a cis Active f3-2-Microglobulin Domain, is Biologically Active in Peptide Binding and Antigen Presentation. Hum Immunol. 1996;49(1):28–37.

286. Lee L, McHugh L, Kibaudov RK, Kozlowski S, Margulies DH, Mage MG. Functional cell surface expression by a recombinant single-chain class I major histocompatibility complex molecule with a cis-active Pz-microglobulin domain. Eur J Immunol. 1994;24:2633–9.

287. Guillaume B, Stroobant V, Bousquet-Dubouch MP, Colau D, Chapiro J, Parmentier N, et al. Analysis of the Processing of Seven Human Tumor Antigens by Intermediate Proteasomes. The Journal of Immunology. 2012 Oct 1;189(7):3538–47.

288. Woods K, Knights AJ, Anaka M, Schittenhelm RB, Purcell AW, Behren A, et al. Mismatch in epitope specificities between IFNγ inflamed and uninflamed conditions leads to escape from T lymphocyte killing in melanoma. J Immunother Cancer. 2016 Feb 16;4(1).

289. Chapatte L, Ayyoub M, Morel S, Peitrequin AL, Lévy N, Servis C, et al. Processing of tumor-associated antigen by the proteasomes of dendritic cells controls in vivo T-cell responses. Cancer Res. 2006 May 15;66(10):5461–8.

290. Schultz ES, Chapiro J, Lurquin C, Claverol S, Burlet-Schiltz O, Warnier G, et al. The Production of a New MAGE-3 Peptide Presented to Cytolytic T Lymphocytes by HLA-B40 Requires the Immunoproteasome. J Exp Med [Internet]. 2002;195(4):391–9. Available from: http://www.jem.org/cgi/content/full/195/4/391

291. Larson AC, Knoche SM, Brumfield GL, Doty KR, Gephart BD, Moore-Saufley PR, et al. Gemcitabine Modulates HLA-I Regulation to Improve Tumor Antigen Presentation by Pancreatic Cancer Cells. Int J Mol Sci. 2024 Mar 11;25(6):3211.

292. Kalaora S, Lee JS, Barnea E, Levy R, Greenberg P, Alon M, et al. Immunoproteasome expression is associated with better prognosis and response to checkpoint therapies in melanoma. Nat Commun. 2020 Dec 1;11(1).

293. Tan CT, Croft NP, Dudek NL, Williamson NA, Purcell AW. Direct quantitation of MHC-bound peptide epitopes by selected reaction monitoring. Proteomics. 2011 Jun;11(11):2336–40.

294. Hassan C, Kester MGD, Oudgenoeg G, de Ru AH, Janssen GMC, Drijfhout JW, et al. Accurate quantitation of MHC-bound peptides by application of isotopically labeled peptide MHC complexes. J Proteomics. 2014 Sep 23;109:240–4.

295. Duan F, Duitama J, Al Seesi S, Ayres CM, Corcelli SA, Pawashe AP, et al. Genomic and bioinformatic profiling of mutational neoepitopes reveals new rules to predict anticancer immunogenicity. Journal of Experimental Medicine. 2014;211(11):2231–48.

296. Harndahl M, Rasmussen M, Roder G, Dalgaard Pedersen I, Sørensen M, Nielsen M, et al. Peptide-MHC class I stability is a better predictor than peptide affinity of CTL immunogenicity. Eur J Immunol. 2012 Jun;42(6):1405–16.

297. Sette A, Vitiello A, Reherman B, Fowler P, Nayersina R, Kast WM, et al. The relationship between class I binding affinity and immunogenicity of potential cytotoxic T cell epitopes. The Journal of Immunology. 1994 Dec 15;153(12):5586–92.

298. Hsiue EHC, Wright KM, Douglass J, Hwang MS, Mog BJ, Pearlman AH, et al. Targeting a neoantigen derived from a common TP53 mutation. Science (1979). 2021 Mar 5;371(6533).

299. Kuznetsov A, Voronina A, Govorun V, Arapidi G. Critical Review of Existing MHC I Immunopeptidome Isolation Methods. Molecules. 2020 Nov 1;25(22).

300. Faridi P, Purcell AW, Croft NP. In Immunopeptidomics We Need a Sniper Instead of a Shotgun. Proteomics. 2018 Jun 1;18(12).

301. Kuznetsova KG, Levitsky LI, Pyatnitskiy MA, Ilina IY, Bubis JA, Solovyeva EM, et al. Cysteine alkylation methods in shotgun proteomics and their possible effects on methionine residues. J Proteomics. 2021 Jan 16;231.

302. Partridge T, Nicastri A, Kliszczak AE, Yindom LM, Kessler BM, Ternette N, et al. Discrimination between human leukocyte antigen class I-Bound and co-purified HIV-derived peptides in immunopeptidomics workflows. Front Immunol. 2018 Apr 27;9(912).

303. Schittenhelm RB, Dudek NL, Croft NP, Ramarathinam SH, Purcell AW. A comprehensive analysis of constitutive naturally processed and presented HLA-C*04:01 (Cw4) - specific peptides. Tissue Antigens. 2014 Mar;83(3):174–9.

304. Zemmour J, Little AM, Schendel DJ, Parham P. The HLA-A,B "negative" mutant cell line C1R expresses a novel HLA-B35 allele, which also has a point mutation in the translation initiation codon. The Journal of Immunology. 1992 Mar 15;148(6):1941–8.

305. Moldovan I, Targoni O, Zhang W, Sundararaman S, Lehmann P V. How frequently are predicted peptides actually recognized by CD8 cells? Cancer Immunology, Immunotherapy. 2016 Jul 1;65(7):847–55.

306. Zhang W, Moldovan I, Targoni OS, Subbramanian RA, Lehmann P V. How much of virus-specific CD8 T cell reactivity is detected with a peptide pool when compared to individual peptides? Viruses. 2012 Nov;4(11):2636–49.

307. Berard M, Tough DF. Qualitative differences between naïve and memory T cells. Immunology. 2022;106:127–38.

308. Geiger R, Duhen T, Lanzavecchia A, Sallusto F. Human naive and memory CD4+ T cell repertoires specific for naturally processed antigens analyzed using libraries of amplified T cells. Journal of Experimental Medicine. 2009 Jul 6;206(7):1525–34.

309. Pant S, Wainberg ZA, Weekes CD, Furqan M, Kasi PM, Devoe CE, et al. Lymph-node-targeted, mKRAS-specific amphiphile vaccine in pancreatic and colorectal cancer: the phase 1 AMPLIFY-201 trial. Nat Med. 2024 Feb 1;30(2):531–42.

310. Yewdell JW, Bennink JR. IMMUNODOMINANCE IN MAJOR HISTOCOMPATIBILITY COMPLEX CLASS I-RESTRICTED T LYMPHOCYTE RESPONSES 1. Annu Rev Immunol. 1999;17:51–88.

311. Derby MA, Wang J, Margulies DH, Berzofsky JA. Two intermediate-avidity cytotoxic T lymphocyte clones with a disparity between functional avidity and MHC tetramer staining. Int Immunol. 2001;13(6):817–24.

312. Lyons GE, Roszkowski JJ, Man S, Yee C, Kast WM, Nishimura MI. T-cell receptor tetramer binding or the lack there of does not necessitate antigen reactivity in T-cell receptor transduced T cells. Cancer Immunology, Immunotherapy. 2006 Sep;55(9):1142–50.

313. Jørgensen KW, Rasmussen M, Buus S, Nielsen M. NetMHCstab - Predicting stability of peptide-MHC-I complexes; impacts for cytotoxic T lymphocyte epitope discovery. Immunology. 2014 Jan;141(1):18–26.

314. Rasmussen M, Fenoy E, Harndahl M, Kristensen AB, Nielsen IK, Nielsen M, et al. Pan-Specific Prediction of Peptide–MHC Class I Complex Stability, a Correlate of T Cell Immunogenicity. The Journal of Immunology. 2016 Aug 15;197(4):1517–24.

315. Qi Q, Liu Y, Cheng Y, Glanville J, Zhang D, Lee JY, et al. Diversity and clonal selection in the human T-cell repertoire. Proc Natl Acad Sci U S A. 2014;111(36):13139–44.

316. Goldrath AW, Bevan MJ. Selecting and maintaining a diverse T-cell repertoire. Nat Immunol. 1999;402(6759).

317. Blank CU, Haining WN, Held W, Hogan PG, Kallies A, Lugli E, et al. Defining 'T cell exhaustion.' Nat Rev Immunol. 2019 Nov 1;19(11):665–74.

318. Kuchroo JR, Hafler DA, Sharpe AH, Lucca LE. The double-edged sword: Harnessing PD-1 blockade in tumor and autoimmunity. Sci Immunol [Internet]. 2021;6. Available from: https://www.science.org

319. Andersen RS, Thrue CA, Junker N, Lyngaa R, Donia M, Ellebæk E, et al. Dissection of T-cell antigen specificity in human melanoma. Cancer Res. 2012 Apr 1;72(7):1642–50.

320. Moravec Z, Zhao Y, Voogd R, Cook DR, Kinrot S, Capra B, et al. Discovery of tumor-reactive T cell receptors by massively parallel library synthesis and screening. Nat Biotechnol [Internet]. 2024 Apr 23; Available from: https://www.nature.com/articles/s41587-024-02210-6

321. Zeh HJ, Perry-Lalley D, Dudley ME, Rosenberg SA, Yang JC. High Avidity CTLs for Two Self-Antigens Demonstrate Superior In Vitro and In Vivo Antitumor Efficacy. The Journal of Immunology. 1999 Jan 15;162(2):989–94.

322. Dutoit V, Rubio-Godoy V, Dietrich PY, Quiqueres AL, Schnuriger V, Rimoldi D, et al. Heterogeneous T-Cell Response to MAGE-A10 254-262 : High Avidity-specific Cytolytic T Lymphocytes Show Superior Antitumor Activity 1. Cancer Res [Internet]. 2001;61:5850–6. Available from: http://aacrjournals.org/cancerres/article-pdf/61/15/5850/2486077/5850.pdf

323. Laugel B, Van Den Berg HA, Gostick E, Cole DK, Wooldridge L, Boulter J, et al. Different T cell receptor affinity thresholds and CD8 coreceptor dependence govern cytotoxic T lymphocyte activation and tetramer binding properties. Journal of Biological Chemistry. 2007 Aug 17;282(33):23799–810.

324. Corse E, Gottschalk RA, Krogsgaard M, Allison JP. Attenuated T cell responses to a high-potency ligand in vivo. PLoS Biol. 2010 Sep;8(9).

325. Schmid DA, Irving MB, Posevitz V, Hebeisen M, Posevitz-Fejfar A, Sarria JCF, et al. Evidence for a TCR Affinity Threshold Delimiting Maximal CD8 T Cell Function. The Journal of Immunology. 2010 May 1;184(9):4936–46.

326. Malcolm J.W. Sim, Jinghua Lu, Matthew Spencer, Francis Hopkins, Eric Tran, Steven A. Rosenberg, et al. High-affinity oligoclonal TCRs define effective adoptive T cell therapy targeting mutant KRAS-G12D. PNAS. 2020;117(23):12826–35.

327. Hay ZLZ, Knapp JR, Magallon RE, O'Connor BP, Slansky JE. Low TCR Binding Strength Results in Increased Progenitor-like CD8+ Tumor-Infiltrating Lymphocytes. Cancer Immunol Res. 2023 May 1;11(5):570–82.

328. Gattinoni L, Lugli E, Ji Y, Pos Z, Paulos CM, Quigley MF, et al. A human memory T cell subset with stem cell-like properties. Nat Med. 2011 Oct;17(10):1290–7.

329. Klebanoff CA, Gattinoni L, Torabi-Parizi P, Kerstann K, Cardones AR, Finkelstein SE, et al. Central memory selftumor-reactive CD8 T cells confer superior antitumor immunity compared with effector memory T cells. PNAS [Internet]. 2005;102(27):9571–6. Available from: www.pnas.orgcgidoi10.1073pnas.0503726102

330. Bronkhorst AJ, Ungerer V, Holdenrieder S. The emerging role of cell-free DNA as a molecular marker for cancer management. Biomol Detect Quantif. 2019 Mar 1;17.

331. Gormally E, Caboux E, Vineis P, Hainaut P. Circulating free DNA in plasma or serum as biomarker of carcinogenesis: Practical aspects and biological significance. Mutat Res. 2007 May;635:105–17.

332. Vitale SR, Groenendijk FH, van Marion R, Beaufort CM, Helmijr JC, Dubbink HJ, et al. TP53 mutations in serum circulating cell-free tumor DNA as longitudinal biomarker for high-grade serous ovarian cancer. Biomolecules. 2020 Mar 1;10(415).

333. Chen TWW, Hsiao W, Dai MS, Lin CH, Chang DY, Chen IC, et al. Plasma cell-free tumor DNA, PIK3CA and TP53 mutations predicted inferior endocrine-based treatment outcome in endocrine receptor-positive metastatic breast cancer. Breast Cancer Res Treat. 2023 Oct 1;201(3):377–85.

334. Calapre L, Giardina T, Beasley AB, Reid AL, Stewart C, Amanuel B, et al. Identification of TP53 mutations in circulating tumour DNA in high grade serous ovarian carcinoma using next generation sequencing technologies. Sci Rep. 2023 Dec 1;13(1).

335. Tzanikou E, Markou A, Politaki E, Koutsopoulos A, Psyrri A, Mavroudis D, et al. PIK3CA hotspot mutations in circulating tumor cells and paired circulating tumor DNA in breast cancer: a direct comparison study. Mol Oncol. 2019 Dec 1;13(12):2515–30.

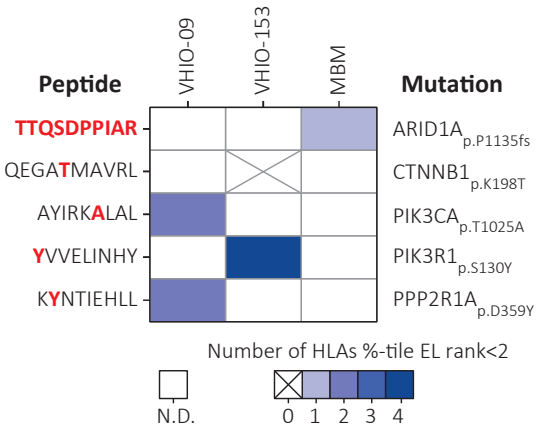
336. Moynahan ME, Chen D, He W, Sung P, Samoila A, You D, et al. Correlation between PIK3CA mutations in cell-free DNA and everolimus efficacy in HR+, HER2-advanced breast cancer: Results from BOLERO-2. Br J Cancer. 2017 Mar 14;116(6):726–30.

337. Dhatchinamoorthy K, Colbert JD, Rock KL. Cancer Immune Evasion Through Loss of MHC Class I Antigen Presentation. Front Immunol. 2021 Mar 9;12.

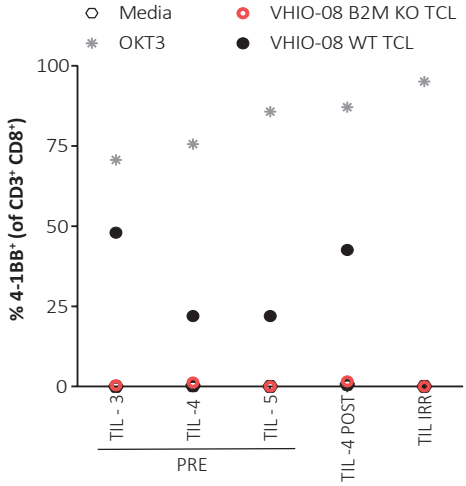
Appendix

Abbreviations tumor type

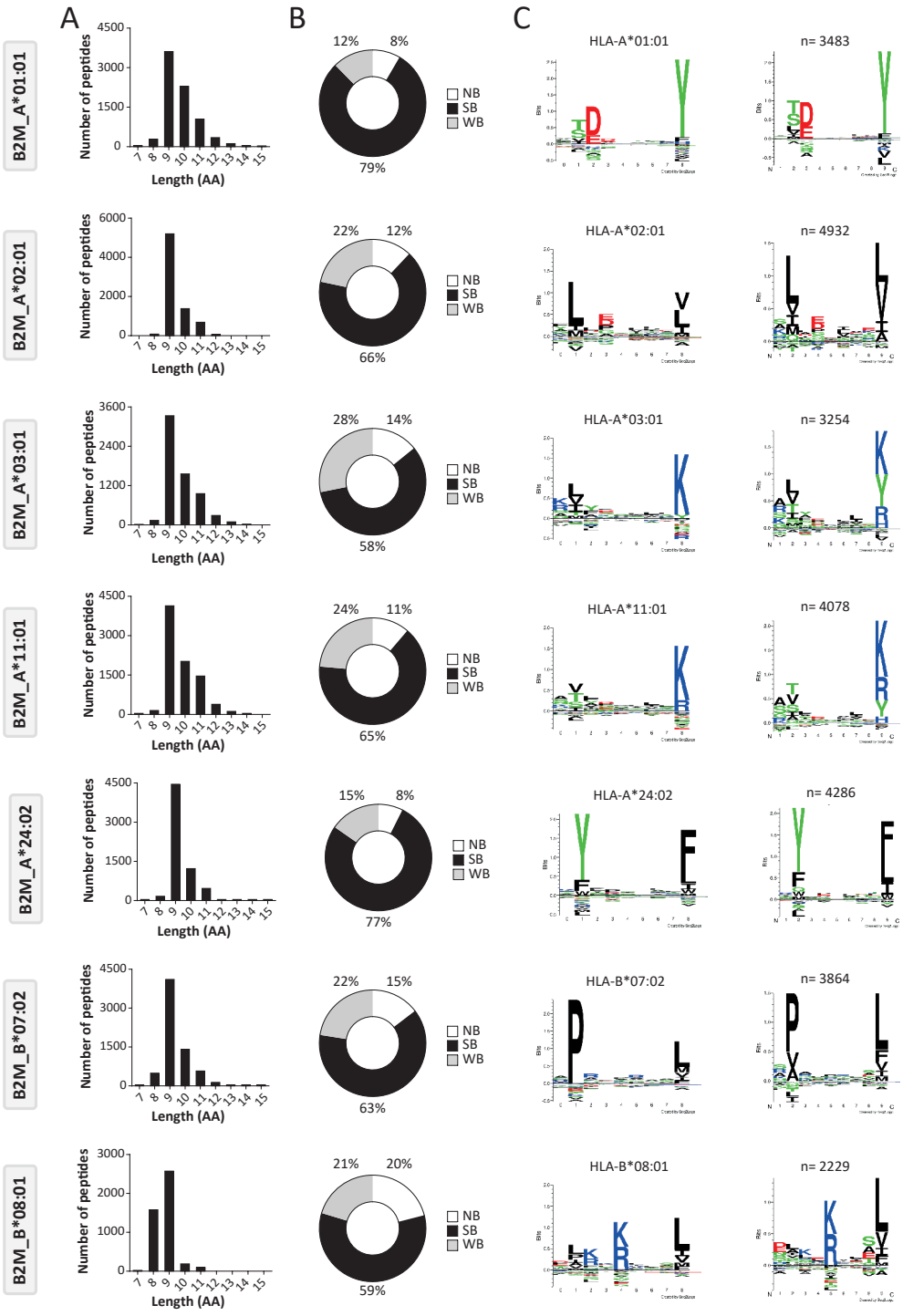
BLCA	Bladder urothelial carcinoma
BRCA	Breast invasive carcinoma
CESC	Cervical squamous cell carcinoma and endocervical Adenocarcinoma
CHOL	Cholangio carcinoma
COAD	Colon adenocarcinoma
ESCA	Esophageal carcinoma
GBM	Glioblastoma multiforme
HNSC	Head and neck squamous cell carcinoma
KIRC	Kidney renal clear cell carcinoma
LAML	Acute myeloid leukemia
LGG	Bran lower grade glioma
LIHC	Liver hepatocellular carcinoma
LUAD	Lung adenocarcinoma
LUSC	Lung squamous cell carcinoma
OV	Ovarian serous cystadenocarcinoma
PAAD	Pancreatic adenocarcinoma
PRAD	Prostate adenocarcinoma
READ	Rectum adenocarcinoma
SARC	Sarcoma
SKCM	Skin cutaneous melanoma
STAD	Stomach adenocarcinoma
TGCT	Testicular germ cell tumors
UCEC	Uterine corpus endometrial carcinoma
UCS	Uterine carcinosarcoma

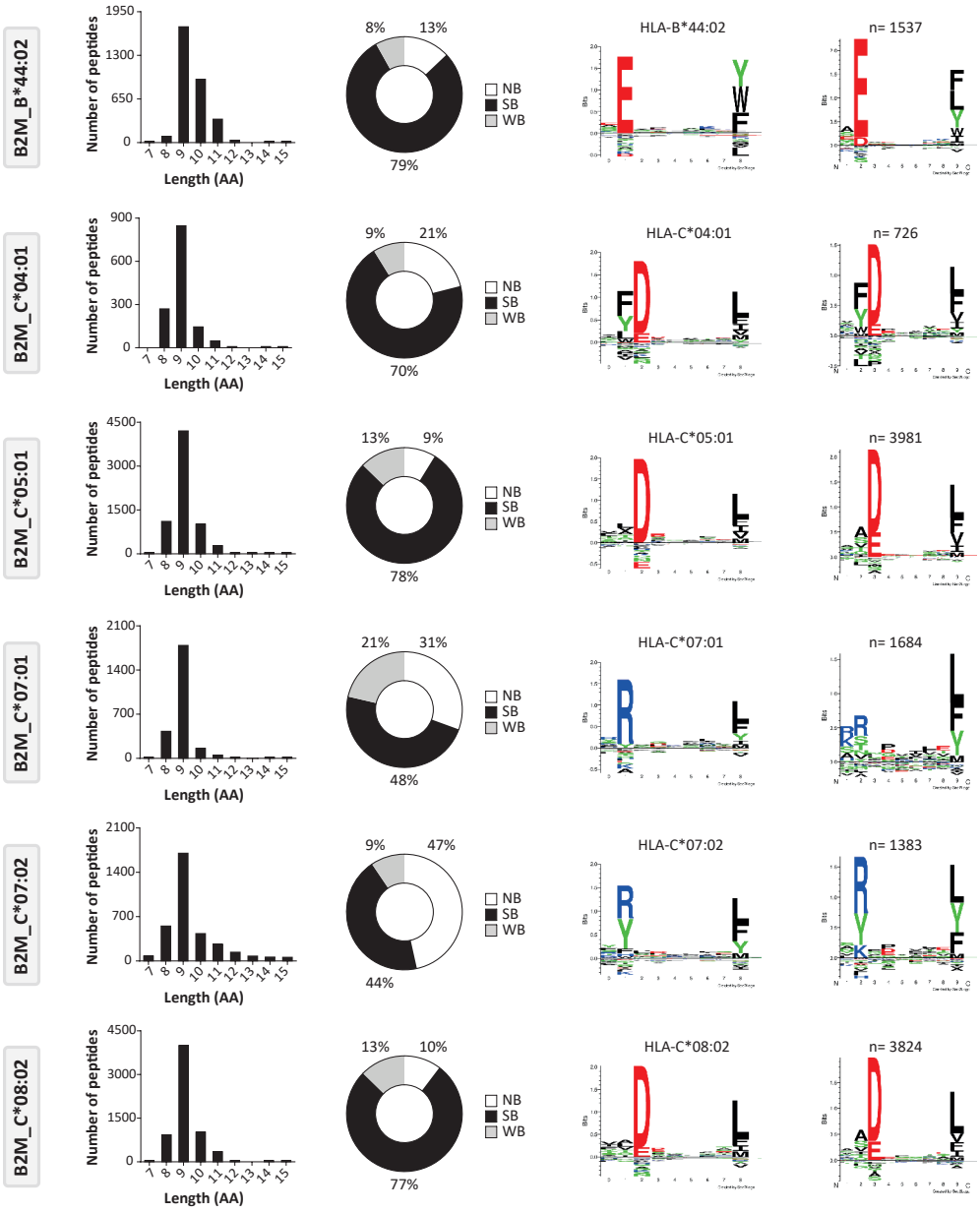


Appendix Figure 1. Mutant peptides derived from patient-specific neoantigens encoded in HSTMGs were identified in HSTMG-expressing B cells from three patients. The specific peptide sequence (left) and the mutation from which they derive (right) are annotated. The mutated AA is highlighted in red. Cells filled in blue indicate peptides detected in B cells derived from a particular patient, while blank cells indicate that the peptide was not detected (N.D.). For presented peptides, the number of HLA-I alleles from the patient for which it can be considered as a binder according to NetMHCPan 4.1 (%-tile EL rank <2) is specified in the corresponding cell from pale blue (n = 1) to dark blue (n = 4). White crossed cells indicate peptides detected by mass spectrometry that were not classified as binders for any of the patient's HLA-I alleles according to NetMHCPan4.1.



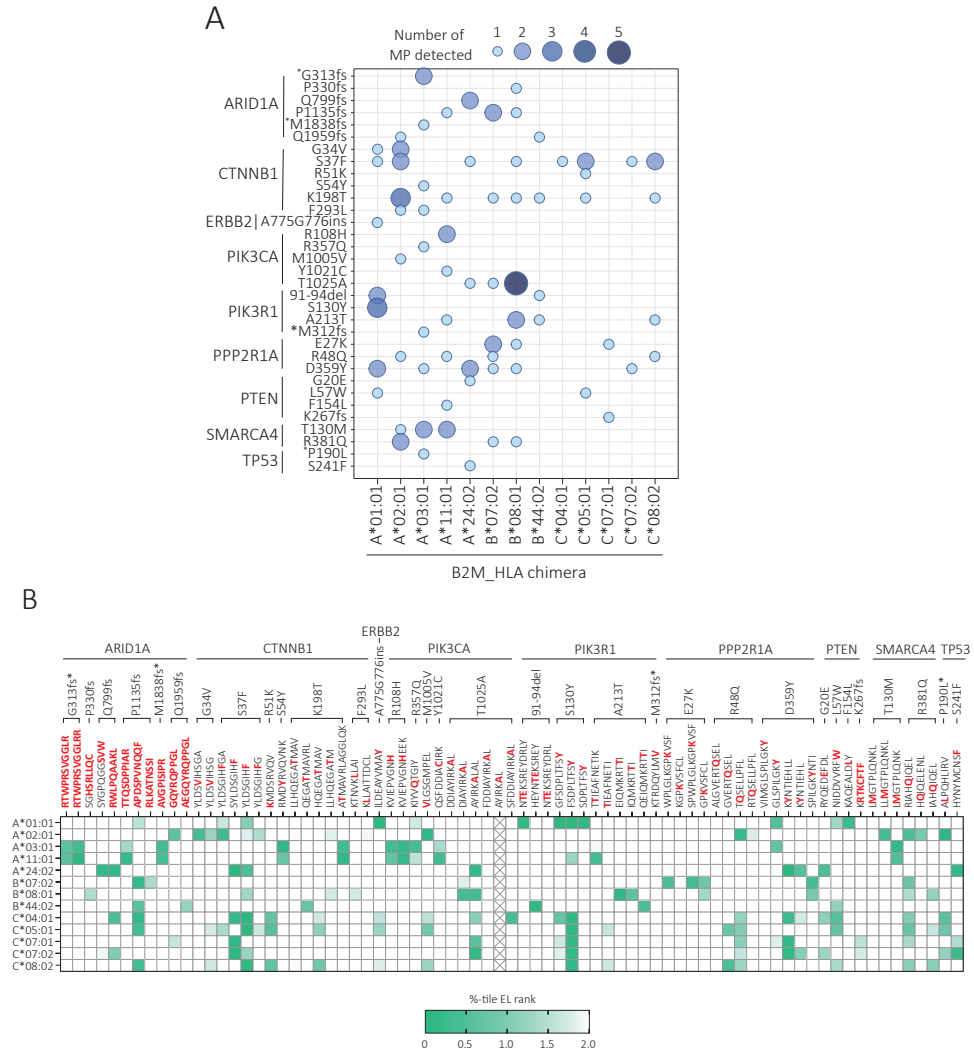
Appendix Figure 2. Autologous TCL recognition by VHIO-08 TIL. The frequency of 4-1BB$^+$ ex vivo expanded TIL gated on CD3$^+$CD8$^+$ cells after 20h co-culture with either autologous wild-type (VHIO-08 TCL) or the B2M KO (VHIO-08 B2M KO TCL) patient-derived tumor cell lines (TCL). Three and one TIL lines expanded ex vivo from a pre- and post-treatment biopsy of patient VHIO-08, respectively, were co-cultured independently with the two tumor cell lines. The patient was treated with anti-PD1 and anti-LAG-3. An irrelevant TIL population from a different patient (HLA-I mismatched) was included as a control (TIL IRR). Media and anti-CD3 (OKT3) were used as negative and positive controls, respectively. Data is representative of at least two independent experiments.


A
B
C
B2M_A*01:01
B2M_A*02:01
B2M_A*03:01
B2M_A*11:01
B2M_A*24:02
B2M_B*07:02
B2M_B*08:01
Number of peptides
Length (AA)
NB
SB
WB
12%
8%
79%
22%
12%
66%
28%
14%
58%
24%
11%
65%
15%
8%
77%
22%
15%
63%
21%
20%
59%
HLA-A*01:01
n= 3483
HLA-A*02:01
n= 4932
HLA-A*03:01
n= 3254
HLA-A*11:01
n= 4078
HLA-A*24:02
n= 4286
HLA-B*07:02
n= 3864
HLA-B*08:01
n= 2229

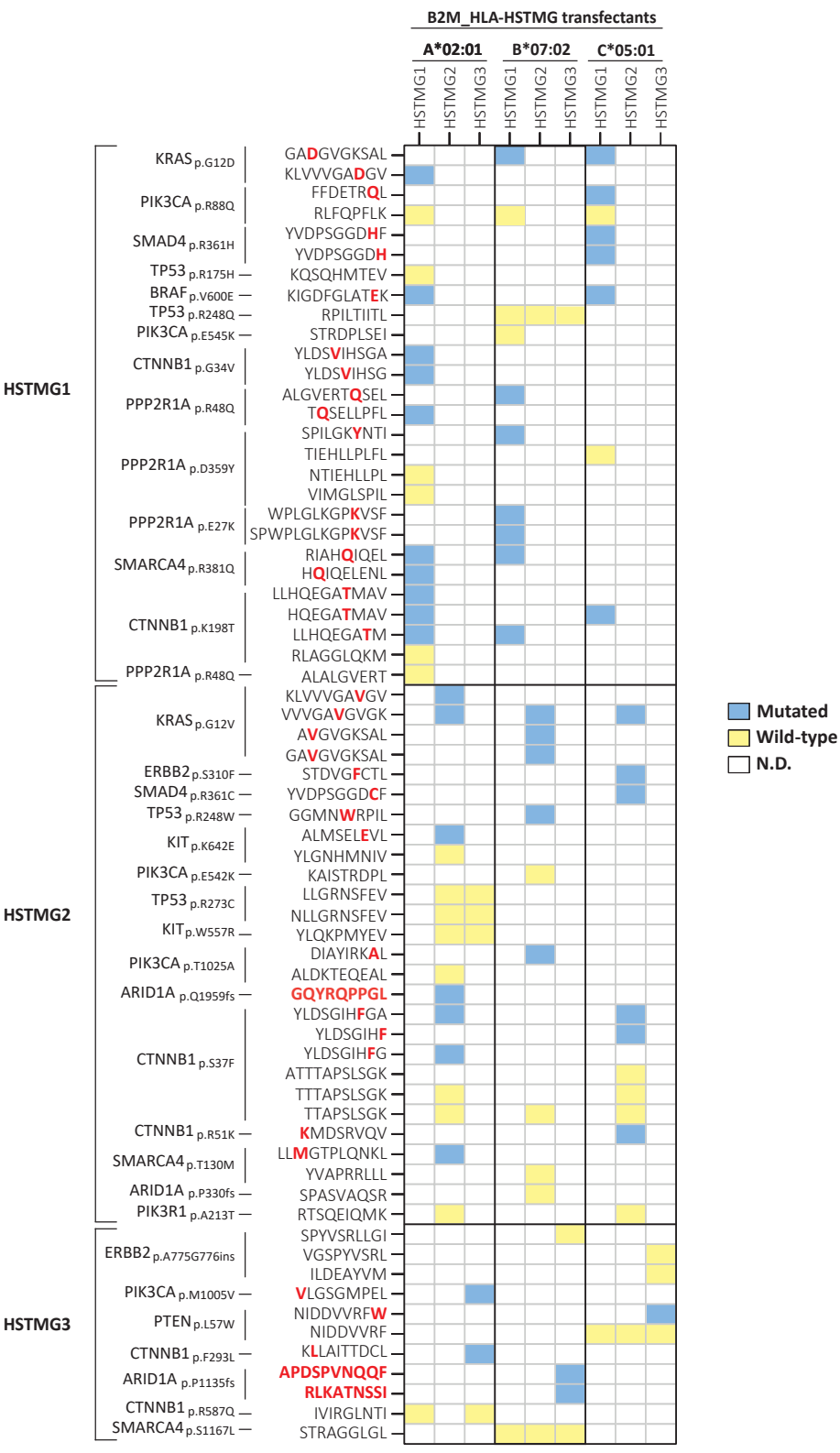


Appendix Figure 3. Peptides presented by the 13 studied B2M_HLA chimeras in electroporated B2M KO TCL display the expected HLA-I characteristics. For each B2M_HLA chimera, all unique peptides recovered from transfectants with HTMG1-3 were pooled together for the analysis. For B2M_A*03:01, unique peptides recovered from transfectants with HSMTG1-4 were also pooled. A) Peptide length distribution of the total unique HLA-I peptide sequences identified for transfectants with the indicated B2M_HLA chimeras. Only peptides <15Aa are plotted. B) The percentage of unique peptides (ranging from 8 to 15 Aa) predicted to bind to the introduced B2M_HLA chimera. Peptides are classified as strong binders (SB, %-tile EL rank <0.5), weak binders (WB, %-tile EL rank 0.5-2), and non-binders (NB, %-tile EL rank >2). C) Comparison of HLA-I binding motif from the introduced HLA-I alleles defined by NetMHCPan4.1-EL to the one defined by GibbsCluster2.0.

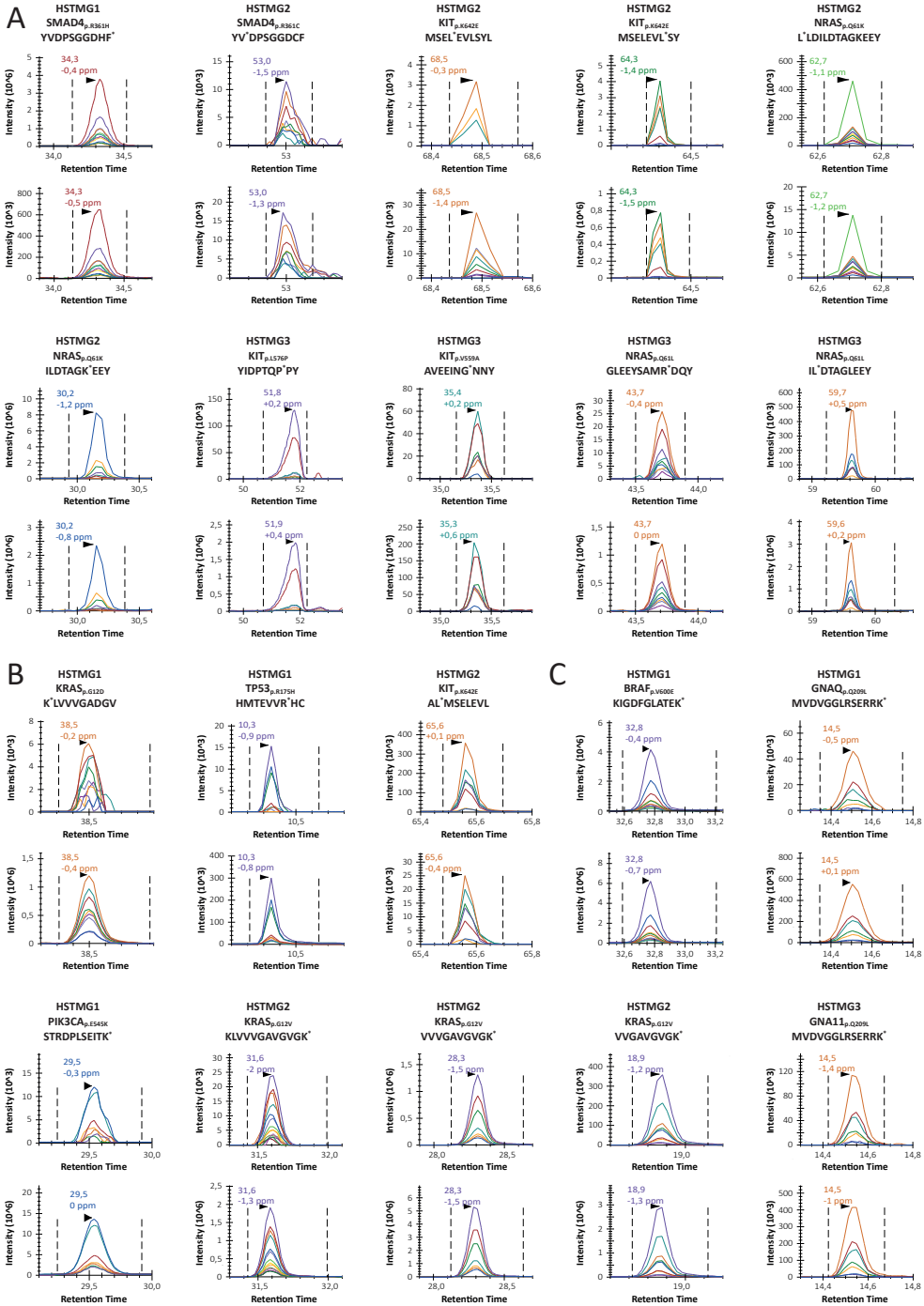
Unique 9-mers identified in each of the generated transfectants were used for the analysis. The solution, according to GibsCluster2.0, analyzed by default settings when allowing for a single group is depicted. The number of sequences (n=) is indicated in each case.

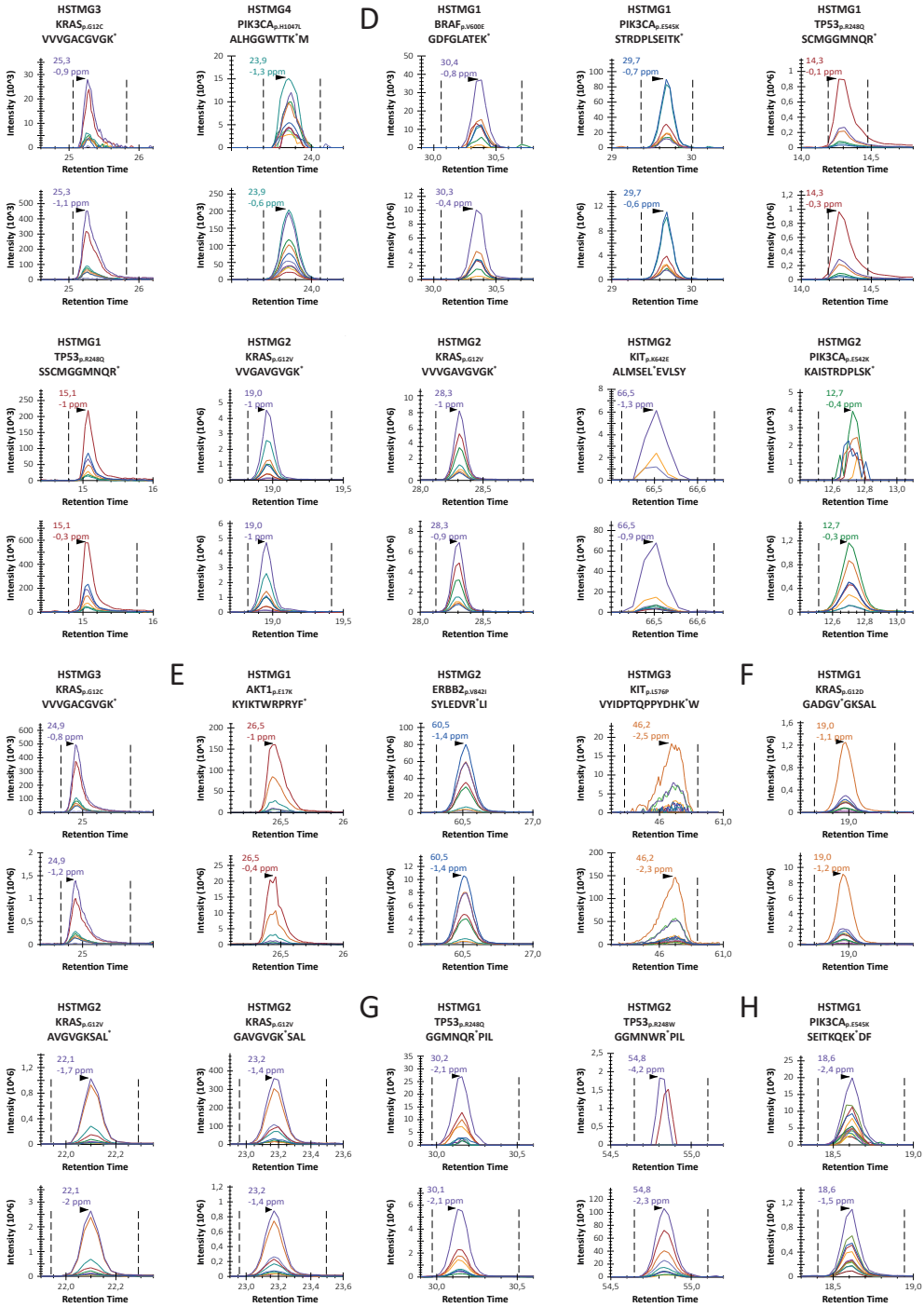


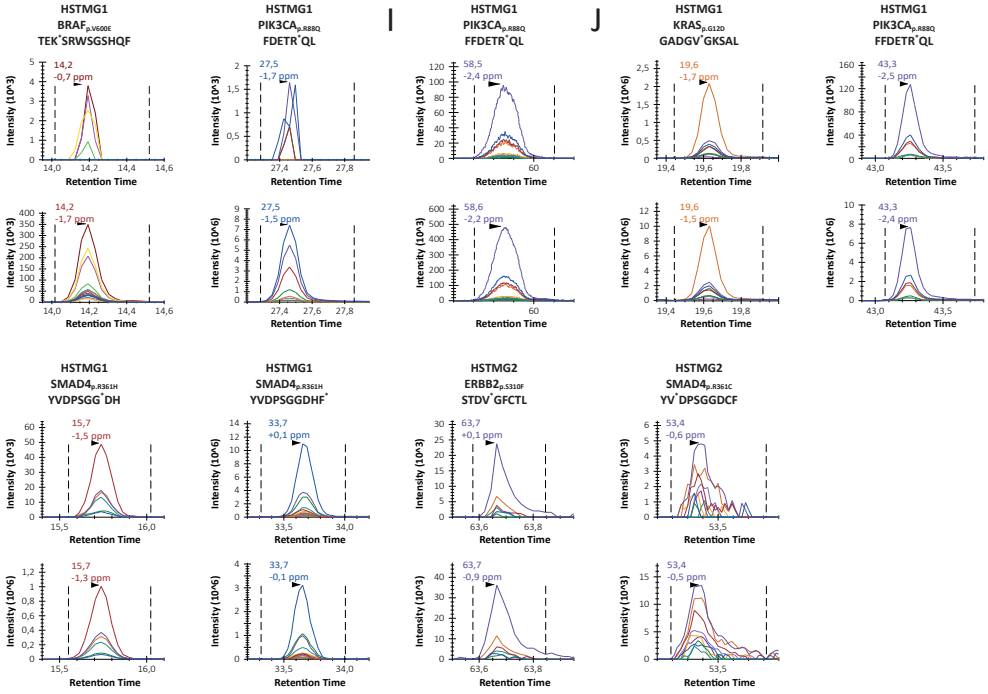
Appendix Figure 4. Shotgun HLA-I immunopeptidomics on HLA-I monoallelic tumor cells detected more than 90 mutant peptide-HLA pairs derived from 22 patient-specific neoantigens presented across 13 HLA-I alleles. A) The number of mutated peptides (MP) detected by shotgun MS screenings is displayed for each of the B2M_HLA chimeras studied. The gene name, the position, and the specific AA change are specified. The mutations labeled as (*), were encoded in HSTMG4 that was used only in combination with B2M_A*03:01. B) Heatmap displaying the predicted %-tile EL rank of identified mutant peptides to the evaluated HLA-I alleles, as determined by NetMHCPan4.1. Crossed cells indicate an identified mutant peptide of 7 AA in length for which the %-tile EL rank could not be evaluated by NetMHCPan4.1. Blank cells indicate peptides predicted as non-binders for each allele according to NetMHCPan4.1 (%-tile EL rank >2). The specific mutation and gene name from which each peptide originates are annotated.


B2M_HLA-HSTMG transfectants
A*02:01
B*07:02
C*05:01
HSTMG1
HSTMG2
HSTMG3
HSTMG1
HSTMG2
HSTMG3
KRAS p.G12D
PIK3CA p.R88Q
SMAD4 p.R361H
TP53 p.R175H
BRAF p.V600E
TP53 p.R248Q
PIK3CA p.E545K
CTNNB1 p.G34V
PPP2R1A p.R48Q
PPP2R1A p.D359Y
PPP2R1A p.E27K
SMARCA4 p.R381Q
CTNNB1 p.K198T
PPP2R1A p.R48Q
KRAS p.G12V
ERBB2 p.S310F
SMAD4 p.R361C
TP53 p.R248W
KIT p.K642E
PIK3CA p.E542K
TP53 p.R273C
KIT p.W557R
PIK3CA p.T1025A
ARID1A p.Q1959fs
CTNNB1 p.S37F
CTNNB1 p.R51K
SMARCA4 p.T130M
ARID1A p.P330fs
PIK3R1 p.A213T
ERBB2 p.A775G776ins
PIK3CA p.M1005V
PTEN p.L57W
CTNNB1 p.F293L
ARID1A p.P1135fs
CTNNB1 p.R587Q
SMARCA4 p.S1167L
GADGVGKSAL
KLVVVGADGV
FFDETRQL
RLFQPFLK
YVDPSGGDHF
YVDPSGGDH
KQSQHMTEV
KIGDFGLATEK
RPILTIITL
STRDPLSEI
YLDSVIHSGA
YLDSVIHSG
ALGVERTQSEL
TQSELLPFL
SPILGKYNTI
TIEHLLPLFL
NTIEHLLPL
VIMGLSPIL
WPLGLKGPKVSF
SPWPLGLKGPKVSF
RIAHQIQEL
HQIQELENL
LLHQEGATMAV
HQEGATMAV
LLHQEGATM
RLAGGLQKM
ALALGVERT
KLVVVGAVGV
VVVGAVGVGK
AVGVGKSAL
GAVGVGKSAL
STDVGFCTL
YVDPSGGDCF
GGMNWRPIL
ALMSELEVL
YLGNHMNIV
KAISTRDPL
LLGRNSFEV
NLLGRNSFEV
YLQKPMYEV
DIAYIRKAL
ALDKTEQEAL
GQYRQPPGL
YLDSGIHFGA
YLDSGIHF
YLDSGIHFG
ATTTAPSLSGK
TTTAPSLSGK
TTAPSLSGK
KMDSRVQV
LLMGTPLQNKL
YVAPRRLLL
SPASVAQSR
RTSQEIQMK
SPYVSRLLGI
VGSPYVSRL
ILDEAYVM
VLGSGMPEL
NIDDVVRFW
NIDDVVRF
KLLAITTDCL
APDSPVNQQF
RLKATNSSI
IVIRGLNTI
STRAGGLGL
Mutated
Wild-type
N.D.

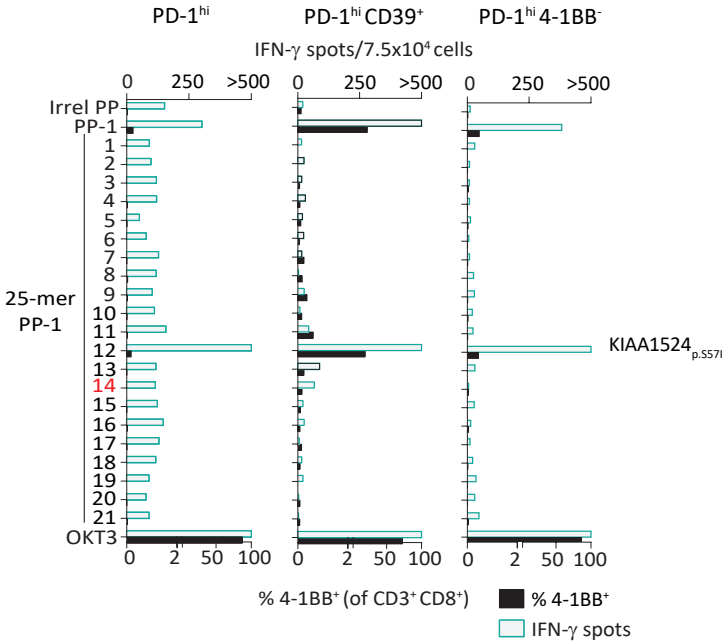
Appendix Figure 5. Peptide identifications of HLA-I monoallelic cells mapped specifically to the transfected HSTMG constructs. Heat map showing peptides identified in each transfectant through HLA-I immunopeptidomics. The peptide sequence with the mutated AA is highlighted in red, and the neoantigen from which they are derived is specified. The HSTMG construct encoding the listed neoantigens is specified on the far left. Cells filled in blue depict mutant peptides mapping to shared or patient-specific mutations detected through shotgun MS in the corresponding B2M_HLA + HSTMG transfectants. Wild-type peptides mapping to minigenes encoding for shared or patient-specific mutations detected in the corresponding transfectants are depicted in yellow. The withe cells denote that the specified peptides were not detected (N.D.). Only transfectants resulting from combinations of B2M_A*02:01, B2M_B*07:02, and B2M_C*05:01 with HSTMG1-3 are shown as representative examples. Artificial junction or peptides mapping to P2A-ZSG detected in each of the transfectants are not shown.


A
HSTMG1
SMAD4p.R361H
YVDPSGGDHF*
HSTMG2
SMAD4p.R361C
YV*DPSGGDCF
HSTMG2
KITp.K642E
MSEL*EVLSYL
HSTMG2
KITp.K642E
MSELEVL*SY
HSTMG2
NRASp.Q61K
L*LDILDTAGKEEY
HSTMG2
NRASp.Q61K
ILDTAGK*EEY
HSTMG3
KITp.L576P
YIDPTQP*PY
HSTMG3
KITp.V559A
AVEEING*NNY
HSTMG3
NRASp.Q61L
GLEEYSAMR*DQY
HSTMG3
NRASp.Q61L
IL*DTAGLEEY
B
HSTMG1
KRASp.G12D
K*LVVVGADGV
HSTMG1
TP53p.R175H
HMTEVVR*HC
HSTMG2
KITp.K642E
AL*MSELEVL
C
HSTMG1
BRAFp.V600E
KIGDFGLATEK*
HSTMG1
GNAQp.Q209L
MVDVGGLRSERRK*
HSTMG1
PIK3CAp.E545K
STRDPLSEITK*
HSTMG2
KRASp.G12V
KLVVVGAVGVGK*
HSTMG2
KRASp.G12V
VVGAVGVGK*
HSTMG2
KRASp.G12V
VVGAVGVGK*
HSTMG3
GNA11p.Q209L
MVDVGGLRSERRK*
Intensity (10^3)
Intensity (10^6)
Retention Time


HSTMG3
KRAS p.G12C
VVVGACGVGK*
HSTMG4
PIK3CA p.H1047L
ALHGGWTTK*M
D
HSTMG1
BRAF p.V600E
GDFGLATEK*
HSTMG1
PIK3CA p.E545K
STRDPLSEITK*
HSTMG1
TP53 p.R248Q
SCMGGMNQR*
HSTMG1
TP53 p.R248Q
SSCMGGMNQR*
HSTMG2
KRAS p.G12V
VVGAVGVGK*
HSTMG2
KRAS p.G12V
VVVGAVGVGK*
HSTMG2
KIT p.K642E
ALMSEL*EVLSY
HSTMG2
PIK3CA p.E542K
KAISTRDPLSK*
E
HSTMG3
KRAS p.G12C
VVVGACGVGK*
HSTMG1
AKT1 p.E17K
KYIKTWRPRYF*
HSTMG2
ERBB2 p.V842I
SYLEDVR*LI
HSTMG3
KIT p.L576P
VYIDPTQPPYDHK*W
F
HSTMG1
KRAS p.G12D
GADGV*GKSAL
HSTMG2
KRAS p.G12V
AVGVGKSAL*
HSTMG2
KRAS p.G12V
GAVGVGK*SAL
G
HSTMG1
TP53 p.R248Q
GGMNQR*PIL
HSTMG2
TP53 p.R248W
GGMNWR*PIL
H
HSTMG1
PIK3CA p.E545K
SEITKQEK*DF
Intensity (10^3)
Intensity (10^6)
Retention Time



Appendix Figure 6. Co-elution profiles of the forty-nine candidate public neoantigens validated by PRM-MS. Co-elution profiles of transitions of endogenous (top) and isotope-labeled (bottom) peptides, analyzed using Skyline software, are displayed for the neoantigens validated to be presented in A) B2M_A*01:01, B) B2M_A*02:01, C) B2M_A*03:01, D) B2M_A*11:01, E) B2M_A*24:02, F) B2M_B*07:02, G) B2M_B*08:01, H) B2M_B*44:02, I) B2M_C*04:01, J) B2M_C*05:01. The specific amino acid sequence of the validated peptides, the name of the driver gene and protein alteration, and the HSTMG construct encoding each neoantigen are specified. Isotope-labeled amino acids are marked with *.



Appendix Figure 7. Enriched CD8$^+$ PBL T-cell subsets from GOI-01 recognize a neoantigen derived from KIAA1524$_{p.S57I}$ identified by tumor WES. CD8$^+$ and CD4$^+$ PBL subsets from patient GOI-01 either expressing PD-1 alone or in combination with other co-stimulatory and co-inhibitory markers were sorted using FACS. Three PD-1 populations were defined: PD-1neg, PD-1dim, and PD-1hi cells, comprising the top 1.5% of cells expressing PD-1. Within each PD-1 population, cells were classified as positive or negative for the other analyzed markers. Following cell sorting, subsets were ex vivo expanded via a REP. A personalized screening of the enriched CD8$^+$ and CD4$^+$ populations was performed using autologous B cells electroporated with tandem minigenes (TMG) TMG1-12. Each TMG contained up to 22 different minigenes encoding for NSMs detected in the patient tumor by WES. The screening identified that different CD8$^+$ subsets (PD-1^{hi}; PD-1^{hi}CD39$^+$ and PD-1^{hi}4-1BB$^-$) recognized TMG1. To determine the mutation specifically recognized by these CD8$^+$ T-cell subsets, 25-mer peptides encompassing the individual NSM contained in TMG1 were independently pulsed onto autologous B cells at 5ug/mL overnight. A pool of 25-mers (PP-1), containing all the NSM encoded in TMG1, was also pulsed onto autologous B cells. After 20h, T-cell responses were evaluated by measuring IFN-γ production and upregulation of 4-1BB gated on CD3$^+$CD8$^+$ cells by flow cytometry as indicated below. The specific mutated protein and amino acid changes are annotated. Autologous B cells pulsed with an Irrelevant peptide pool (Irrel PP) and OKT3 (anti-CD3) were used as negative and positive controls, respectively. Data are representative of two independent experiments. Notably, the PIK3CA$_{p.E545K}$ hotspot mutation represented by the 25-mer number 14, highlighted in red, showed no recognition by these enriched CD8$^+$ subsets. All findings shown in the figure are derived from prior experiments conducted in our laboratory.

Appendix Table 1. Candidate public neoantigens validated through PRM-MS in transfectants expressing B2M_HLA chimera and HSTMG constructs.

Peptide sequence	Length	Shared neoantigen	Validated in B2M_HLA chimera	Previous reports
KYIKTWRPRYF	11mer	AKT1 $_{p.E17K}$	A*24:02	Novel
KIGDFGLAT**E**K	11mer	BRAF $_{p.V600E}$	A*03:01	181
GDFGLAT**E**K	9mer		A*11:01	Novel
T**E**KSRWSGSHQF	12mer		B*44:02	Novel
MVDVGG**L**RSERRK	13mer	GNA11 $_{p.Q209L}$	A*03:01	Novel
MVDVGG**L**RSERRK	13mer	GNAQ $_{p.Q209L}$	A*03:01	Novel
STDVG**F**CTL	9mer	ERBB2 $_{p.S310F}$	C*05:01	181
SYLEDVRL**I**	9mer	ERBB2 $_{p.V842I}$	A*24:02	Novel
VYIDPTQ**P**PYDHKW	14mer	KIT $_{p.L576P}$	A*24:02	Novel
YIDPTQ**P**PY	9mer		A*01:01	Novel
AVEEINGNNY	10mer	KIT $_{p.V559A}$	A*01:01	Novel
ALMSEL**E**VLSY	11mer	KIT $_{p.K642E}$	A*11:01	Novel
MSEL**E**VLSYL	10mer		A*01:01	Novel
MSEL**E**VLSY	9mer		A*01:01	Novel
ALMSEL**E**VL	9mer		A*02:01	Novel
VVVGA**C**GVGK	10mer	KRAS $_{p.G12C}$	A*03:01	178
			A*11:01	178
GA**D**GVGKSAL	10mer	KRAS $_{p.G12D}$	B*07:02	179
			C*05:01	181
KLVVVGA**D**GV	10mer		A*02:01	244
VVVGA**V**GVGK	10mer	KRAS $_{p.G12V}$	A*03:01	252
			A*11:01	183
VVGA**V**GVGK	9mer		A*03:01	252
			A*11:01	183
A**V**GVGKSAL	9mer		B*07:02	Novel
GA**V**GVGKSAL	10mer		B*07:02	Novel
KLVVVGA**V**GVGK	12mer		A*03:01	Novel
ILDTAG**K**EEY	10mer	NRAS $_{p.Q61K}$	A*01:01	231
LLDILDTAG**K**EEY	13mer		A*01:01	Novel
ILDTAG**L**EEY	10mer	NRAS $_{p.Q61L}$	A*01:01	182
G**L**EEYSAMRDQY	12mer		A*01:01	Novel
FFDETR**Q**L	8mer	PIK3CA $_{p.R88Q}$	C*04:01	Novel
			C*05:01	Novel
FDETR**Q**L	7mer		B*44:02	Novel
KAISTRDPLS**K**	11mer	PIK3CA $_{p.E542K}$	A*11:01	Novel
STRDPLSEIT**K**	11mer	PIK3CA $_{p.E545K}$	A*11:01	181
			A*03:01	Novel
SEIT**K**QEKDF	10mer		B*44:02	Novel
A**L**HGGWTTKM	10mer	PIK3CA $_{p.H1047L}$ *	A*03:01	Novel
YVDPSGGD**C**F	10mer	SMAD4 $_{p.R361C}$	A*01:01	Novel
			C*05:01	Novel
YVDPSGGD**H**F	10mer	SMAD4 $_{p.R361H}$	A*01:01	Novel
			C*05:01	Novel
YVDPSGGD**H**	9mer		C*05:01	Novel
HMTEVVR**H**C	9mer	TP53 $_{p.R175H}$	A*02:01	75
SSCMGGMN**Q**R	10mer	TP53 $_{p.R248Q}$	A*11:01	Novel
SCMGGMN**Q**R	9mer		A*11:01	181
GGMN**Q**RPIL	9mer		B*08:01	Novel
GGMN**W**RPIL	9mer	TP53 $_{p.R248W}$	B*08:01	Novel

Peptide sequence with the mutant AA highlighted in red, length, and shared neoantigen from which they derive are listed. The specific chimera where each peptide was validated is specified. The neoantigen highlighted with (*) was only interrogated with B2M_A*03:01 chimera. Reference to the first previous report detecting the pepide-HLA pairs validated are specified.